

The pre-nucleation of aluminosilicate zeolites:
a theoretical approach

Chao Shiang Yang

Centre for Theoretical and Computational Chemistry
Department of Chemistry,

University College London

London, January 2013

A thesis submitted for the degree of Doctor of Philosophy

I, Chao Shiang Yang, confirm that the work presented in this thesis is my own. Where information has been derived from other sources, I confirm that this has been indicated in the thesis.

London, January 2013

ACKNOWLEDGMENTS

I want to thank to the following people for their support during my PhD in UCL:
Dr. José Miguel Mora Fonz, Dr. Hsin-Yi Chen, Dr. Mohamed Matar, Dr. Vladimir Martis, Dr. Martin Martis, Dr. Rozie Sarip, Dr. Nazarudin, Tom Daley, Husna Islam, David Mora Fonz, Daniel Deacon-Smith.

To my supervisors, Prof. Richard Catlow and Prof Gopinathan Sankar my deepest gratitude for all the advise, guidance and inspire me to enter the field of zeolites.

Finally I would also like to thank my family who give me all love.

CONTENTS

ACKNOWLEDGMENTS.....	2
CONTENTS.....	3-7
LIST OF FIGURES	8-11
LIST OF TABLES	12-14
ABSTRACT.....	15
Chapter 1 Introduction	16
1.1 Objective.....	16-17
1.2 Zeolites.....	17
1.2.1 The Nature of zeolites.....	17-19
1.2.2 Hydrothermal synthesis	19-23
1.2.3 Lowenstein’s rule	23
1.2.4 Dempsey’s rule	24
1.2.5 Experimental aluminosilicate zeolite nucleation and crystal growth	24-25
1.2.6 Proposed condensation mechanisms in aluminosilicates.....	26
1.2.7 Modelling aluminosilicate species and nucleation	26-27
1.2.7.1 The effect of solvent	27-28
Chapter 2 Computational Methodology	33
2.1 Introduction.....	33
2.2 Electronic structure methods	33-35
2.2.1 Hartree-Fock method	36-39
2.2.2 Density Functional Theory (DFT)	39-43
2.2.3 Basis set	43-44
2.3 Geometry optimisation (minimisation).....	44-45
2.4 Statistical mechanics.....	45-47
2.5 COnductor-like Screening MOdel (COSMO)	47-49
2.6 Methodology of modelling aluminosilicate clusters.....	49
2.6.1 Geometry optimisation and thermodynamic property	50-51
2.6.2 Modelling the solvent	52
2.6.3 The counterions: cation.....	52
Chapter 3 The Stability and Structures of Aluminosilicate Clusters	55
3.1 Introduction.....	55-56
3.2 Methodology.....	57

3.3 Results and Discussion	57-58
3.3.1 Geometry analysis for open clusters	58
3.3.1.1 Structures of the $\text{Al}(\text{OH})_4\text{Na}$ monomer and the $\text{AlSiO}(\text{OH})_6\text{Na}$ and $\text{Al}_2\text{O}(\text{OH})_6\text{Na}_2$ dimers.....	58-62
3.3.1.2 Structures of trimers.....	62
3.3.1.2.1 One Al atom substitution in trimers.....	62-64
3.3.1.2.2 Two Al atom substitutions in trimers	65-66
3.3.1.3 Structures of tetramers	67
3.3.1.3.1 One Al atom substitution in tetramers	67-69
3.3.1.3.2 Two Al atom substitutions in tetramers	70-73
3.3.1.4 Structures of pentamers.....	74
3.3.1.4.1 One Al atom substitution in pentamers.....	74-76
3.3.1.4.2 Two Al atom substitutions in pentamers.....	77-81
3.3.1.4.3 Three Al substitutions in pentamers.....	82-87
3.3.1.5 Structures of hexamers.....	87
3.3.1.5.1 One Al substitution in hexamers	87-89
3.3.1.5.2 Two Al substitutions in hexamers	90-96
3.3.1.5.3 Three Al substitutions in hexamers.....	96-103
3.3.2 Geometry analysis for cyclic clusters (rings)	104
3.3.2.1 The three rings	104-106
3.3.2.2 The four rings.....	106-109
3.3.2.3 The five rings	109-113
3.3.2.4 The six rings.....	114-121
3.3.3 Relative energies of open clusters.....	121-122
3.3.3.1 Dimers.....	122-123
3.3.3.2 One Al substitution in trimers, tetramers, pentamers and hexamers	123
3.3.3.2.1 Trimers	123
3.3.3.2.2 Tetramers.....	123-124
3.3.3.2.3 Pentamers.....	125
3.3.3.2.4 Hexamers	125-126
3.3.3.3 Two Al substitutions in trimers, tetramers, pentamers and hexamers.....	126
3.3.3.3.1 Trimers	126-127
3.3.3.3.2 Tetramers.....	127-128

3.3.3.3.3 Pentamers.....	128-129
3.3.3.3.4 Hexamers	130-131
3.3.3.4 Three Al substitutions in pentamers and hexamers.....	131
3.3.3.4.1 Pentamers	131-132
3.3.3.4.2 Hexamers	132-133
3.3.4 Relative energies of rings.....	133
3.3.4.1 Two Al substitutions in the four, five and six rings	133-134
3.3.4.2 Three Al substitutions in the five and six rings.....	134-135
3.4 Conclusion	135-136
Chapter 4 Modelling the Polymerisation of Aluminosilicate Clusters.....	139
4.1 Introduction.....	139-141
4.2 Methodology	141
4.3 Results and Discussion	141-142
4.3.1 Geometry analysis.....	142
4.3.1.1 Cages: the double four and double six rings.....	142-143
4.3.1.2 Ring structures with “hanging” monomers or dimers	143-152
4.3.2 Condensation reactions of open clusters and rings	153
4.3.2.1 Condensation reactions of open clusters.....	153
4.3.2.1.1 Trimerisation reactions	153-154
4.3.2.1.2 Tetramerisation reactions	154-155
4.3.2.1.2.1 Tetramerisation reactions with the Si(OH) ₄ or Al(OH) ₄ Na monomers	155-156
4.3.2.1.2.2 Tetramerisation reactions with the AlSiO(OH) ₆ Na dimer	156-158
4.3.2.2 Condensation reaction of the four, six, double four and double six rings	158
4.3.2.2.1 Condensation reactions of the four ring with the Si(OH) ₄ or Al(OH) ₄ Na monomers.....	159-160
4.3.2.2.2 Condensation reactions of the six, double four and double six ring with the Si(OH) ₄ or Al(OH) ₄ Na monomers	161-162
4.3.2.3 Condensation reactions of the Al-(Si) fused four, six and double four rings. 163	
4.3.2.3.1 Condensation reactions of the Al-(Si) fused four rings with the Si(OH) ₄ or Al(OH) ₄ Na monomers or the AlSiO(OH) ₆ Na dimer	163-164
4.3.2.3.2 Condensation reactions of the Al-(Si) fused six, double four rings with the Si(OH) ₄ or Al(OH) ₄ Na monomers or the AlSiO(OH) ₆ Na dimer	165-166

4.3.2.4 Condensation reactions of the four, six, double four and double six rings with the $\text{AlSiO}(\text{OH})_6\text{Na}$ dimer.....	167
4.3.2.4.1 Condensation reactions of the four ring with the $\text{AlSiO}(\text{OH})_6\text{Na}$ dimer	167-168
4.3.2.4.2 Condensation reactions of the six, double four and double six rings with the $\text{AlSiO}(\text{OH})_6\text{Na}$ dimer	169-171
4.4 Conclusion	171-172
Chapter 5 Modelling the Nucleation of Zeolite A	175
5.1 Introduction.....	175-177
5.2 Methodology.....	177
5.3 Results and Discussion	177-178
5.3.1 Geometry analysis of the multiple ring structures	179-183
5.3.2 Polymerisation and cyclisation reactions.....	183
5.3.3 Polymerisation reactions.....	184
5.3.3.1 Dimer	184-186
5.3.3.2 Tetramer	186-187
5.3.4 Cyclisation	187
5.3.4.1 Hexamer, the four ring and three ring with one dangling monomer...187-192	
5.3.4.2 The six ring, five ring with a dangling monomer and four ring with a dangling dimer	192-194
5.3.5 Dimer or the four ring addition to the four ring species	194
5.3.5.1 The four ring with a dangling dimer and four ring with a dangling four ring	194-196
5.3.5.2 The four ring with two dangling dimers and four ring with a dangling tetramer	197-198
5.3.5.3 The bi-four and tri-four rings.....	198-200
5.3.5.4 The open double four and double four ring.....	200-202
5.4 Conclusion	203-204
Chapter 6 Modelling the Polymerisation of Aluminosilicate Clusters in Alkali Media	206
6.1 Introduction.....	206-208
6.2 Methodology.....	208
6.3 Results and Discussion	208-209

6.3.1 Geometric analysis of deprotonated clusters	209-211
6.3.2 Deprotonation reactions	212-214
6.3.3 Condensation reactions of the open deprotonated clusters and four rings	214
6.3.3.1 Condensation reaction of the deprotonated open clusters	215
6.3.3.1.1 Dimerisation reactions	215-216
6.3.3.1.2 Trimerisation reactions	216-218
6.3.3.1.3 Tetramerisation reactions	218
6.3.3.1.3.1 Condensation reactions of the trimer with the Si(OH)_4 , $\text{Si(OH)}_3\text{ONa}$ or $\text{Al(OH)}_4\text{Na}$ monomers	218-220
6.3.3.1.3.2 Condensation reactions of the $\text{AlSiO(OH)}_6\text{Na}$ and $\text{AlSiO}_2(\text{OH})_5\text{Na}_2$ dimers	220-221
6.3.3.2 Condensation reactions of the deprotonated rings	221
6.3.3.2.1 Condensation reactions of the four ring with the Si(OH)_4 , $\text{Si(OH)}_3\text{ONa}$ and $\text{Al(OH)}_4\text{Na}$ monomers	221-223
6.3.3.2.2 Condensation reactions of the four ring and $\text{AlSiO(OH)}_6\text{Na}$ or $\text{AlSiO}_2(\text{OH})_5\text{Na}_2$ dimer	223-224
6.4 Conclusion	225
Chapter 7 Conclusion.....	227
7.1 Summary	227
7.1.1 The stability and structures of aluminosilicate clusters	227
7.1.2 The polymerisation of aluminosilicate clusters	227-228
7.1.3 The nucleation mechanism of zeolite A.....	228
7.1.4 The polymerisation of aluminosilicate clusters in alkali media.....	228
7.1.5 Future work.....	229

LIST OF FIGURES

Figure 1.1 Aluminosilicate zeolitic structures, (a) zeolite A and (b) zeolite X. Si atoms are represented by yellow colour; the Al atoms are represented by pink colour.....	18
Figure 1.2 Brønsted acids changed to Lewis acid sites under high temperature.....	19
Figure 1.3 Hydrothermal zeolite synthesis: the starting materials are mixed in aqueous media containing base sources (OH^- ion) to produce the crystalline structure ²	20
Figure 1.4 The processes for building up structures of three selected zeolites.....	20
Figure 1.5 Conceptional illustration for the change of crystallization and crystallinity with time on hydrothermal treatment at a constant temperature in conventional slow Crystallization method ²²	21
Figure 1.6 Conceptional illustration for the change of crystallization rate with time on hydrothermal treatment in rapid-crystallization method with a programmed temperature rise ²²	22
Figure 1.7 Interrelationship between the metastable phases with changing synthesis conditions ²³ . CAN, LTA, GIS and SOD as framework types of zeolites.....	23
Figure 2.1 The Hartree-Fock self-consistent iteration ⁸	38
Figure 3.1 Aqueous aluminosilicate species have been presented by ²⁹ Si NMR and ²⁷ Al NMR spectroscopy ¹⁻⁸ . Open circles representing Al atoms.....	56
Figure 3.2 $\text{Al}(\text{OH})_4\text{Na}$. Optimised isomers of aluminosilicate species in COSMO solvation: monomer, dimers, trimers, and tetramers. In all Figures, colour coding as follows: purple spheres represent the Na^+ ion, pink, Al; red, O; and white H atoms. The dashed line represent hydrogen bonds.....	61
Figure 3.3 $\text{AlSiO}(\text{OH})_6\text{Na}$	61
Figure 3.4 $\text{Al}_2\text{O}(\text{OH})_6\text{Na}_2$	62
Figure 3.5 Trimer A1.....	64
Figure 3.6 Trimer A2.....	64
Figure 3.7 Trimer B1.....	66
Figure 3.8 Trimer B2.....	66
Figure 3.9 Tetramer A1.....	69
Figure 3.10 Tetramer A2.....	69
Figure 3.11 Tetramer B1.....	71
Figure 3.12 Tetramer B2.....	71

Figure 3.13 Tetramer B3	73
Figure 3.14 Tetramer B4	73
Figure 3.15 Pentamer A1	75
Figure 3.16 Pentamer A2	76
Figure 3.17 Pentamer A3	76
Figure 3.18 Pentamer B1	78
Figure 3.19 Pentamer B2	79
Figure 3.20 Pentamer B3	79
Figure 3.21 Pentamer B4	80
Figure 3.22 Pentamer B5	81
Figure 3.23 Pentamer B6	81
Figure 3.24 Pentamer C1	83
Figure 3.25 Pentamer C2	85
Figure 3.26 Pentamer C3	85
Figure 3.27 Pentamer C4	86
Figure 3.28 Pentamer C5	86
Figure 3.29 Pentamer C6	87
Figure 3.30 Hexamer A1	88
Figure 3.31 Hexamer A2.....	89
Figure 3.32 Hexamer A3.....	89
Figure 3.33 Hexamer B1.....	91
Figure 3.34 Hexamer B2.....	92
Figure 3.35 Hexamer B3.....	92
Figure 3.36 Hexamer B4.....	93
Figure 3.37 Hexamer B5.....	93
Figure 3.38 Hexamer B6.....	94
Figure 3.39 Hexamer B7.....	95
Figure 3.40 Hexamer B8.....	95
Figure 3.41 Hexamer B9.....	96
Figure 3.42 Hexamer C1.....	97
Figure 3.43 Hexamer C2.....	98
Figure 3.44 Hexamer C3.....	99
Figure 3.45 Hexamer C4.....	100

Figure 3.46 Hexamer C5.....	100
Figure 3.47 Hexamer C6.....	101
Figure 3.48 Hexamer C7.....	101
Figure 3.49 Hexamer C8.....	102
Figure 3.50 Hexamer C9.....	102
Figure 3.51 Hexamer C10.....	103
Figure 3.52 3-ring A.....	105
Figure 3.53 3-ring B.....	106
Figure 3.54 4-ring A.....	108
Figure 3.55 4-ring B1.....	108
Figure 3.56 4-ring B2.....	109
Figure 3.57 5-ring A.....	110
Figure 3.58 5-ring B1.....	111
Figure 3.59 5-ring B2.....	112
Figure 3.60 5-ring C1.....	113
Figure 3.61 5-ring C2.....	113
Figure 3.62 6-ring A.....	114
Figure 3.63 6-ring B1.....	116
Figure 3.64 6-ring B2.....	117
Figure 3.65 6-ring B3.....	117
Figure 3.66 6-ring C1.....	119
Figure 3.67 6-ring C2.....	120
Figure 3.68 6-ring C3.....	120
Figure 4. 1 Optimised aluminosilicate rings: the double four and double six rings. The abbreviations and line diagrams illustrating connectivity are also shown here. In all Figures, colour coding as follows: purple Na ⁺ ion, yellow Si, pink Al, red O and white H atoms.	143
Figure 4.2 Optimised aluminosilicate fused four rings. In the abbreviation, “()” indicates the active atom at which the condensation with other species	145
Figure 4.3 Optimised aluminosilicate fused six rings.....	146
Figure 4.4 Optimised aluminosilicate fused double four rings.	147
Figure 4.5 Optimised aluminosilicate fused double six rings.....	148
Figure 4.6 Optimised aluminosilicate fused four rings.....	149

Figure 4.7 Optimised aluminosilicate fused six rings.....	150
Figure 4.8 Optimised aluminosilicate fused double four rings.....	151
Figure 4.9 Optimised aluminosilicate fused double six rings.....	152
Figure 5.1 Clusters reactions, silicon in each line corner and oxygen in the middle of each line.	178
Figure 5.2 Optimised aluminosilicate four ring species. In the abbreviation, “()” indicates the active atom at which the condensation with other species	180
Figure 5.3 Optimised aluminosilicate four ring species.	181
Figure 5.4 A proposed nucleation mechanism for the formation of a double four ring.	204
Figure 6.1 The most important participants are shown in each axe in zeolite syntheses. Triangles and diamonds mean the Si/T ratio and the OH ⁻ /T ratio, respectively, where “T” is the sum of Al and Si content. The line is drawn for the OH ⁻ /T ratio ^{2,3}	207
Figure 6.2 Optimised deprotonated aluminosilicate clusters: the open clusters. “(-H)” indicates the singly deprotonated clusters at which the condensation with other species occurs.	210
Figure 6.3 Optimised deprotonated aluminosilicate clusters: the four ring species. “(-H)” indicates the singly deprotonated clusters and “()” indicates the the active atom at which the condensation with other species occurs.	211

LIST OF TABLES

Table 3.1 Free energy (ΔG , kJmol^{-1}) changes in the gas phase and COSMO solvation at 298 and 450 K in dimerisation reactions.....	123
Table 3.2 Relative energies (kJmol^{-1}) of aluminosilicate isomers: one Al substitution in trimers and tetramers in the gas phase and COSMO solvation.....	124
Table 3.3 Relative energies (kJmol^{-1}) of aluminosilicate isomers: one Al substitution in pentamers and hexamers in the gas phase and COSMO solvation.....	126
Table 3.4 Relative energies (kJmol^{-1}) of aluminosilicate isomers: two Al substitutions in trimers and tetramers in the gas phase and COSMO solvation.....	128
Table 3.5 Relative energies (kJmol^{-1}) of aluminosilicate isomers: two Al substitutions in pentamers in the gas phase and COSMO solvation.....	129
Table 3.6 Relative energies (kJmol^{-1}) of aluminosilicate isomers: two Al substitutions in hexamers in the gas phase and COSMO solvation.....	131
Table 3.7 Relative energies (kJmol^{-1}) of aluminosilicate isomers: three Al substitutions in pentamers in the gas phase and COSMO solvation.....	132
Table 3.8 Relative energies (kJmol^{-1}) of aluminosilicate isomers: three Al substitutions in hexamers in the gas phase and COSMO solvation.....	133
Table 3.9 Relative energies (kJmol^{-1}) of aluminosilicate isomers: two Al substitutions in the four, five and six rings in the gas phase and COSMO solvation.....	134
Table 3.10 Relative energies (kJmol^{-1}) of aluminosilicate isomers: three Al substitutions in the five and six rings in the gas phase and COSMO solvation.....	135
Table 4.1 Calculated free energy (ΔG , kJmol^{-1}) change in the gas phase and COSMO solvation at 298K and 450K in polymerisations..	154
Table 4.2 Calculated free energy (ΔG , kJmol^{-1}) changes in the gas phase and COSMO solvation at 298 and 450K in polymerisations.....	158
Table 4.3 Calculated free energy (ΔG , kJmol^{-1}) change in the gas phase and in COSMO solvation at 298 and 450K in polymerisations. The reaction: $R + M \rightarrow FR + H_2O$	160
Table 4.4 Calculated free energy (ΔG , kJmol^{-1}) change in the gas phase and COSMO solvation at 298 and 450K in polymerisations.....	162
Table 4.5 Calculated free energy (ΔG , kJmol^{-1}) change in the gas phase and COSMO solvation at 298 and 450K in polymerisations. The reaction: $FR + M \text{ or } D \rightarrow FR + H_2O$	164

Table 4.6 Calculated free energy (ΔG , kJmol^{-1}) change in the gas phase and COSMO solvation at 298 and 450K in polymerisations. The reaction: $\text{FR} + \text{M or D} \rightarrow \text{FR} + \text{H}_2\text{O}$	166
Table 4.7 Calculated free energy (ΔG , kJmol^{-1}) change in the gas phase and COSMO solvation at 298 and 450K in polymerisations. The reaction: $\text{R} + \text{D} \rightarrow \text{FR} + \text{H}_2\text{O}$	168
Table 4.8 Calculated free energy (ΔG , kJmol^{-1}) change in the gas phase and COSMO solvation at 298 and 450K in polymerisations. The reaction: $\text{R} + \text{D} \rightarrow \text{FR} + \text{H}_2\text{O}$..	171
Table 5.1 Calculated free energy (ΔG , kJmol^{-1}) change, associated with the enthalpy (ΔH) and entropy ($T\Delta S$) change for the formation of dimers in the gas phase and COSMO solvation at 298 and 450K in polymerisations.....	185
Table 5.2 Calculated free energy (ΔG , kJmol^{-1}) change, associated with the enthalpy (ΔH) and entropy ($T\Delta S$) change for the formation of trimers in the gas phase and COSMO solvation at 298 and 450K in polymerisations.....	187
Table 5.3 Calculated free energy (ΔG , kJmol^{-1}) change, associated with the enthalpy (ΔH) and entropy ($T\Delta S$) change in the gas phase and COSMO solvation at 298 and 450K in polymerisations and cyclisations.....	188
Table 5.4 Calculated free energy (ΔG , kJmol^{-1}) change, associated with the enthalpy (ΔH) and entropy ($T\Delta S$) change in the gas phase and COSMO solvation at 298 and 450K in polymerisations and cyclisations.....	193
Table 5.5 Calculated free energy (ΔG , kJmol^{-1}) change, associated with the enthalpy (ΔH) and entropy ($T\Delta S$) change in the gas phase and COSMO solvation at 298 and 450K in polymerisations and cyclisations.....	196
Table 5.6 Calculated free energy (ΔG , kJmol^{-1}) change, associated with the enthalpy (ΔH) and entropy ($T\Delta S$) change in the gas phase and COSMO solvation at 298 and 450K in polymerisations.....	198
Table 5.7 Calculated free energy (ΔG , kJmol^{-1}) change, associated with the enthalpy (ΔH) and entropy ($T\Delta S$) change in the gas phase and COSMO solvation at 298 and 450K in cyclisations.....	200
Table 5.8 Calculated free energy (ΔG , kJmol^{-1}) change, associated with the enthalpy (ΔH) and entropy ($T\Delta S$) change in the gas phase and COSMO solvation at 298 and 450K in cyclisations.....	201

Table 6.1 Calculated free energy (ΔG , kJmol^{-1}) change in the gas phase and COSMO solvation at 298 and 450 K for the deprotonated open clusters. The reaction is $M + \text{OH}^- \rightarrow M^- + \text{H}_2\text{O}$	212
Table 6.2 Calculated free energy (ΔG , kJmol^{-1}) change in the gas phase and COSMO solvation at 298 and 450 K for the deprotonated rings. The reaction is $R + \text{OH}^- \rightarrow R^- + \text{H}_2\text{O}$	213
Table 6.3 Calculated free energy (ΔG , kJmol^{-1}) change in the gas phase and COSMO solvation at 298 and 450 K for polymerisations via deprotonated clusters.....	215
Table 6.4 Calculated free energy (ΔG , kJmol^{-1}) change in the gas phase and COSMO solvation at 298 and 450 K for polymerisations via deprotonated clusters.....	217
Table 6.5 Calculated free energy (ΔG , kJmol^{-1}) change in the gas phase and COSMO solvation at 298 and 450 K for polymerisations via deprotonated clusters.....	219
Table 6.6 Calculated free energy (ΔG , kJmol^{-1}) change in the gas phase and COSMO solvation at 298 and 450 K for polymerisations via deprotonated clusters.....	221
Table 6.7 Calculated free energy (ΔG , kJmol^{-1}) change in the gas phase and COSMO solvation at 298 and 450 K for polymerisations via deprotonated clusters.....	222
Table 6.8 Calculated free energy (ΔG , kJmol^{-1}) change in the gas phase and COSMO solvation at 298 and 450 K for polymerisations via deprotonated clusters.....	224

ABSTRACT

Density Functional Theory (DFT) and the Conductor-like Screening Model (COSMO) have been employed to investigate the structural geometry and thermodynamical properties for the condensation reactions of aluminosilicates in the prenucleation of forming aluminosilicate zeolites.

We report the relative structures and energies of clusters containing between one and six Si/Al atoms and the effect on them of the interplay of the Na^+ ions and intramolecular hydrogen bonds. Our result reveals that with the exception of the dimer, “Lowensteinian” clusters (without the Al-O-Al linkage) are more energetically favourable than “non-Lowensteinian” clusters (which contain such bridges) in the gas phase. The stability of aluminosilicate clusters is strongly affected by the COSMO solvation, with the solvent influencing their conformations. In COSMO solvation, all the most stable clusters follow not only Lowenstein’s rule, but also Dempsey’s rule.

The condensation reactions are involved key aluminosilicate species: the $\text{Si}(\text{OH})_4$ or $\text{Al}(\text{OH})_4\text{Na}$ monomers and $\text{AlSiO}(\text{OH})_6\text{Na}$ dimer, where we investigate reactions with the four, six, double four and double six rings to form a series of fused rings in both the gas phase and COSMO solvation. Our calculations suggests that the $\text{Al}(\text{OH})_4\text{Na}$ monomer does not participate in these condensation reactions as such participation would generate structures that contradict Lowenstein’s rule; in contrast, on the basis of our results we propose that the condensation reactions occur via the $\text{AlSiO}(\text{OH})_6\text{Na}$ dimer. As a result, employing the $\text{AlSiO}(\text{OH})_6\text{Na}$ dimer, which could be responsible for forming aluminosilicate aggregates studies the nucleation mechanism of zeolite A. the rational mechanism for nucleated self-assembly for zeolite A is that the double four ring, which is probably the main initial ring in the nucleation stage could be formed by the successive condensation reactions of the $\text{AlSiO}(\text{OH})_6\text{Na}$ dimer, tetramer, four ring, four-four ring, tri-four ring, and open double four ring.

Furthermore, to consider the alkalinity in the nucleation and crystal growth of aluminosilicate zeolites, our supposition is that the $\text{AlSiO}_2(\text{OH})_5\text{Na}_2$ dimer would play the key role in the relative condensation reactions for deprotonated open clusters (the dimers, trimers and tetramers) and rings (the four rings).

Chapter 1 Introduction

1.1 Objective

A complete understanding of the growth mechanism of zeolites is critically important because processes highly control the formation of more than a hundred zeolite structures with specific chemical and physical properties, which have been widely applied in several industries¹. Unfortunately, for aluminosilicate zeolites, given that internal and external factors such as pH, reaction time, temperature and Si/Al ratio have a strong influence over the formation process, identifying the aluminosilicate clusters that probably participate in the nucleation process and the details of the growth mechanism is very elusive²⁻⁵. In this thesis, by using molecular simulations employing density functional theory (DFT) and the Conductor-like Screening Model (COSMO)⁶⁻⁷, we investigate several problems relating to the nucleation of aluminosilicate zeolites. The aim of this work is to identify not only related key aluminosilicate clusters involved in the nucleation but also a sequence of possible nucleation reactions that occur in aluminosilicate zeolites.

Both Lowenstein's⁸ and Dempsey's rule⁹ are key principles in the structural chemistry of aluminosilicate zeolites, so discussion how these rules influence the structures and formation of aluminosilicate zeolites is vitally necessary. Central objectives are to:

- Consideration of the four main factors involved in the formation of the structures of aluminosilicate clusters: the cationic arrangement, distribution of the Si and Al atoms, effect of solvent and pH.
- Analysis of a range of key aluminosilicate clusters that are both consistent and inconsistent with Lowenstein's and Dempsey's rules.
- Identification of the most stable aluminosilicate clusters both in the gas phase as well as in solution while the nucleation proceeds.
- Evaluation of the energetic of aluminosilicate polymerisation reactions and identification the favourable condensation mechanisms that proceed in the nucleation processes including polymerisations and cyclisations.

- Study of the effect of pH involving the energetics of different deprotonations in aluminosilicate polymerisation reactions.

All detailed contents are discussed in depth in later chapters.

1.2 Zeolites

Zeolites are well-known microporous minerals that have been widely investigated for several decades because of their specific chemical and physical properties including ion-exchanging, catalysis, and sorption, which have been widely applied in several industries³. This section reviews not only the frameworks, properties and applications of zeolites, but also our present understanding of their nucleation and growth.

1.2.1 The Nature of zeolites

Zeolites are crystalline aluminosilicates with various pores and cavities of molecular dimension in their framework¹⁰. The elemental structural composition of zeolites usually consists of silicon, aluminium, oxygen, and counter cations eg. alkali or alkaline earth cations. The general formula of aluminosilicate zeolites $M_{x/n}[(AlO_2)_x(SiO_2)_y]_z \cdot H_2O$, where M is a metallic cation and n is its valence. The TO_4 tetrahedron unit (T= Si, Al) is well-known to be the basic structural unit of aluminosilicate zeolites and is used to build a variety of clusters (second building units) including the four, five, six rings and so on, which are combined together to construct different 3D channel frameworks¹¹. Because of the replacement of Si atoms by Al atoms at tetrahedral sites, aluminosilicate zeolites form the negatively charged frameworks with the compensating extra-framework cations such as Na^+ ions (or in the case of acid zeolites, a proton bonded to a bridging oxygen).

The first natural zeolite was discovered in 1756 by Axel Fredrick Cronstedt who was a Swedish chemist and mineralogist¹². In the middle of 20th century, zeolite chemistry had a major breakthrough. Barrer used the hydrothermal method to prepare the first synthetic zeolites ($(Na_2O, BaO), Al_2O_3, 4SiO_2, xBaCl_2, yH_2O$) successfully¹³. Then, Milton¹⁴ synthesized zeolites A and X, which had already been used in industrial gas and liquid separation and purification for the decades. The structures of these zeolites are shown in Figure 1.1. Empirical knowledge and extensive development of synthetic techniques have led the way to both tailoring the size and shape of zeolites

and design of novel zeolites. Moreover, not only do a variety of isomorphous zeolites¹⁵ have been formed such as: AlPO₄s (aluminophosphates) and GaPOs (gallophosphates), modifying their chemical and physic properties but also refined zeolites have been formed by incorporating several metal elements such as Mn, Cr, and Zn, expanding possible applications in industry^{4,16}.

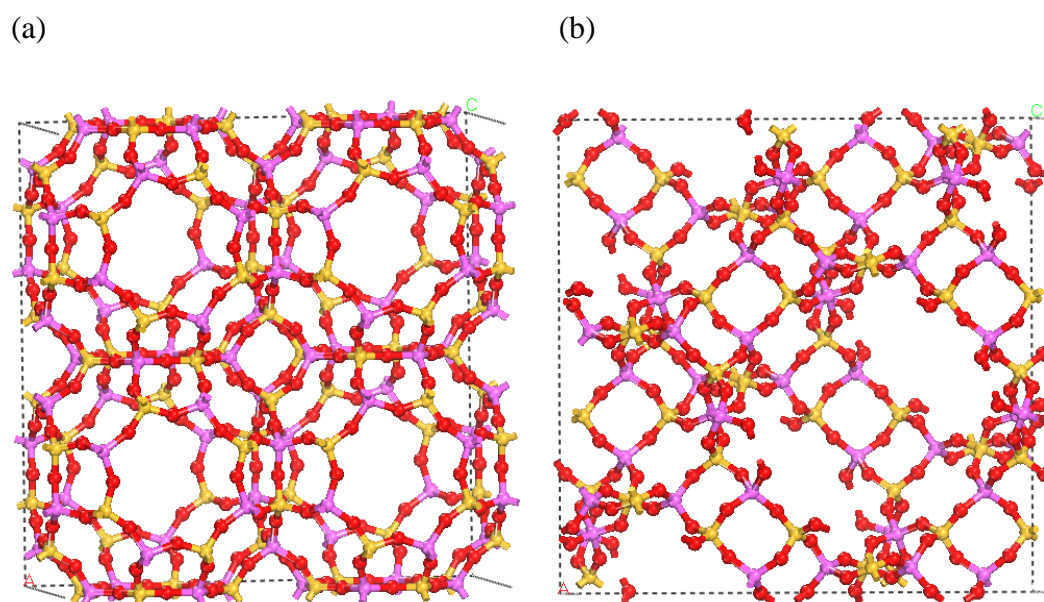


Figure 1.1 Aluminosilicate zeolitic structures, (a) zeolite A and (b) zeolite X. Si atoms are represented by yellow colour; the Al atoms are represented by pink colour.

In general, zeolites have several important characteristics¹⁷. The acidity is among the most important properties of aluminosilicate zeolites. Their acid strength and distribution are determined by the location of distribution of aluminium sites (the acid sites). Both Brønsted and Lewis acid sites occur in zeolite frameworks. Moreover, Brønsted acids can be changed to Lewis acid under high temperature (Figure 1.2). This unique property of zeolites is beneficial to be used in a large variety of industrial applications such as catalytic cracking and catalytic reforming. On the other hand, zeolites can also be used as ion exchangers to purify metallic substances in water or as adsorbents to sieve toxic gas in air and a large variety of novel applications of zeolites still continue to be developed, for example, as insulators for microchip devices, medical diagnosis and templates for porous carbons.

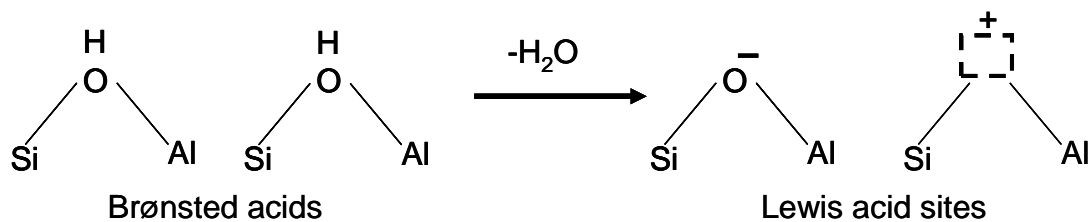


Figure 1.2 Brønsted acids changed to Lewis acid sites under high temperature.

1.2.2 Hydrothermal synthesis

Hydrothermal synthesis¹⁸⁻²⁰ is involved synthesis under controlled high temperature (100 and 200°C) or pressure in aqueous media in a sealed autoclave. The hydrothermal method is widely used in zeolite synthesis because of its advantages especially in the controlled temperature or pressure, avoidance air pollution, and the high reactivity for mixed reactants. Figure 1.3 shows a generalized schematic for zeolite synthesis conducted by the hydrothermal method.

Source materials of silica and alumina, base sources and aqueous media, usually H₂O, are mixed and react at controlled temperature or pressure in the sealed autoclave. All the source materials are essentially crystallized to form zeolite structures. The hydrothermal method for synthesizing zeolites is a solution-mediated and inhomogeneous process involving the initial formation of the hydrated aluminosilicate gel and crystallization process of the gel; there are four crucial stages to be occurred in the formation of zeolites (i) the condensation reactions of polysilicate and aluminate species (ii) nucleation (iii) growth of the nuclei (iv) the subsequent crystal growth²¹, as shown in Figure 1.4.

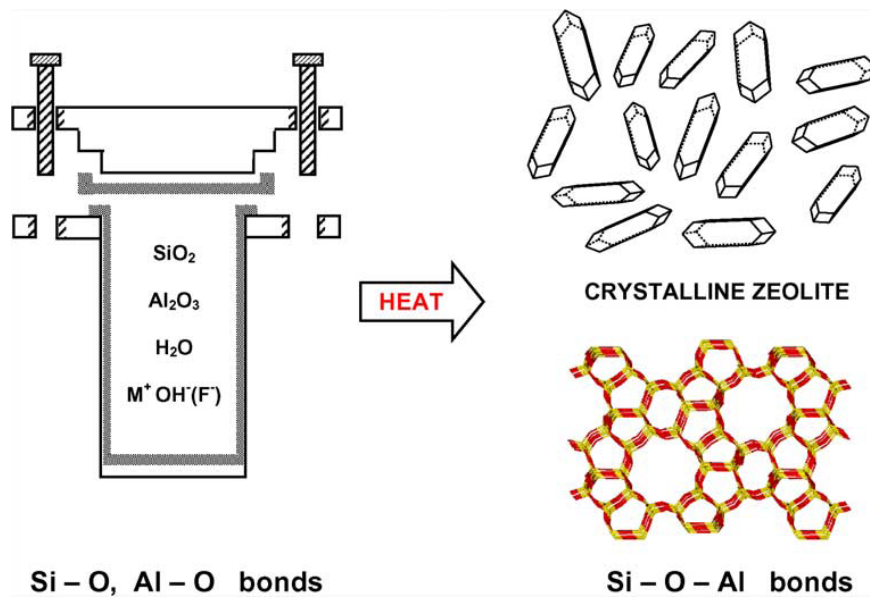


Figure 1.3 Hydrothermal zeolite synthesis: the starting materials are mixed in aqueous media containing base sources (OH^- ion) to produce the crystalline structures².

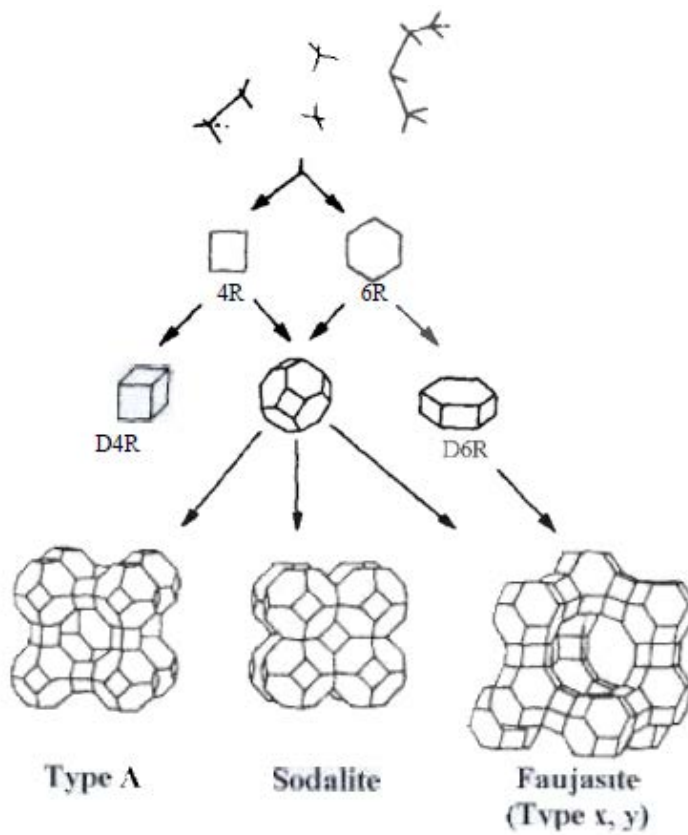


Figure 1.4 The processes for building up structures of three selected zeolites²¹.

Moreover, according to Figure 1.5²² that contains schematic crystal growth curves for zeolites at constant temperature. During hydrothermal synthesis, there is no appreciable nucleation during an initial crystallization period, followed by onset of crystallization; a rapid crystal growth occurs while crystallization reaches a maximum and in turn decreases dramatically during a later crystallization period.

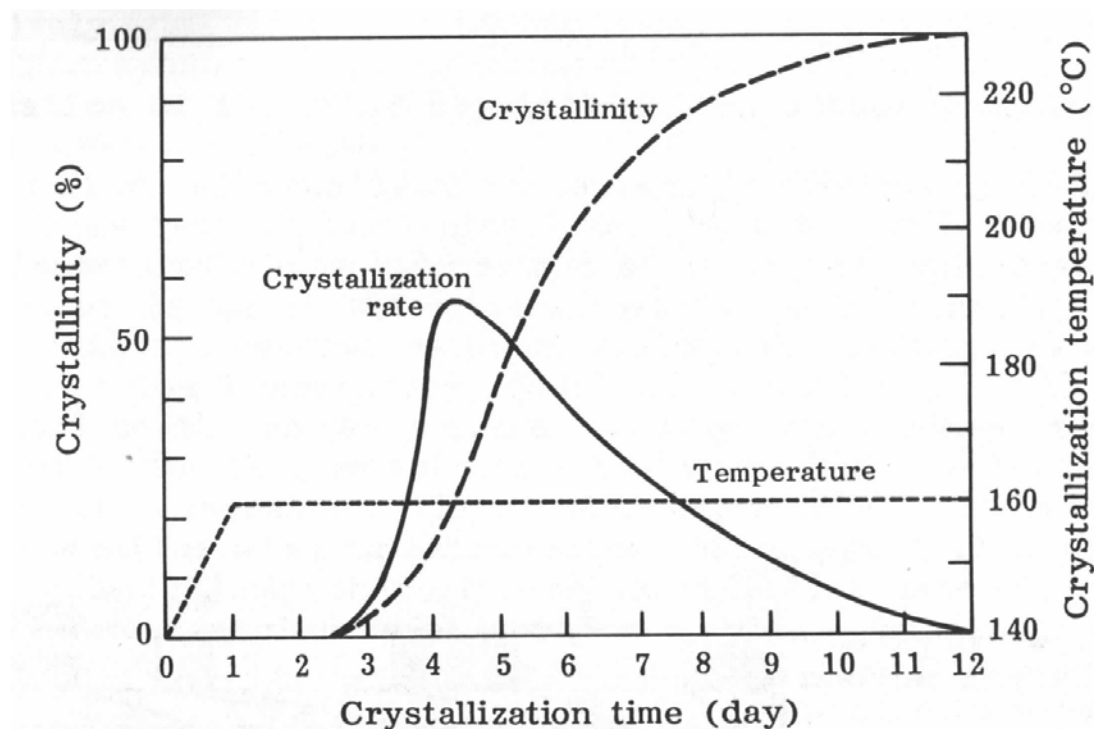


Figure 1.5 Conceptual illustration for the change of crystallization and crystallinity with time on hydrothermal treatment at a constant temperature in conventional slow crystallization method²².

In hydrothermal zeolite synthesis, a variety of factors such as the source materials, gel composition (the Si/Al ratio), pH, temperature and time influence not only the nature and rate of nucleation and crystal growth but also the type of zeolite that is produced. It is relatively easy to observe the change of crystallization with temperature. Compared with the crystallization at constant temperature, as shown in Figure 1.5²², obviously, Figure 1.6 shows that the crystallization reaches a higher level with the variation of temperature.

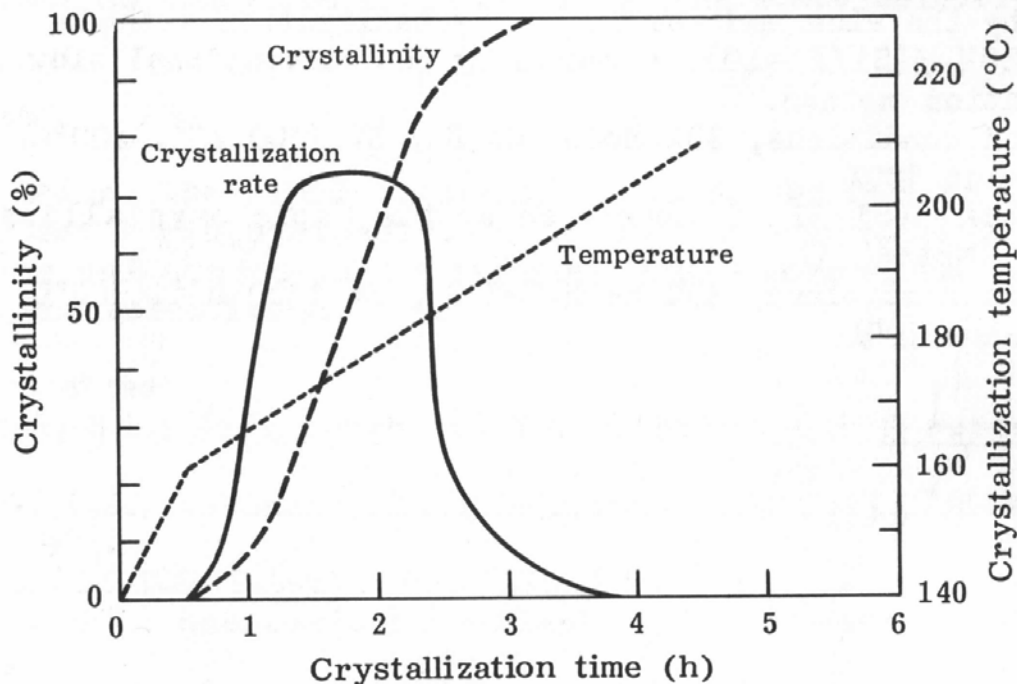


Figure 1.6 Conceptual illustration for the change of crystallization rate with time on hydrothermal treatment in rapid-crystallization method with a programmed temperature rise²².

On the other hand, certain zeolite types can be obtained by controlling the hydrothermal synthesis conditions²³. For example, zeolite A (LTA), sodalite (SOD) and zeolite P (GIS) can all be produced by varying the synthesis conditions as shown in Figure 1.7. The interrelationship between them shows that increasing OH^- , temperature and time favours formation of sodalite (SOD) instead of zeolite A (LTA); zeolite A (LTA) transforms to zeolite P(GIS) by decreasing OH^- ; with increasing time, sodalite (SOD) can be formed from zeolite P(GIS). Indeed, the process of zeolite synthesis is particularly complicated because of a variety of factors, complex species and reactions that influence in these processes.

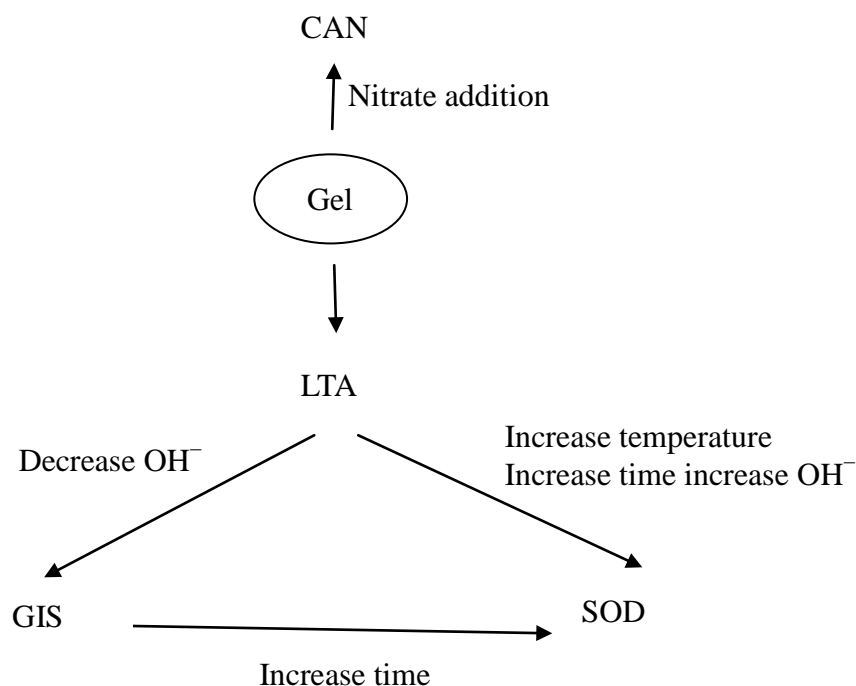


Figure 1.7 Interrelationship between the metastable phases with changing synthesis conditions²³. CAN, LTA, GIS and SOD as framework types of zeolites.

1.2.3 Lowenstein's rule

In aluminosilicate zeolite systems, both Lowenstein's rule⁸ and Dempsey's rule⁹ are the basic principles at constraining the distribution of aluminum to form aluminosilicate zeolitic frameworks. First, Lowenstein has proposed that the distribution of the silica and alumina tetrahedra linking together through oxygen is not entirely random in aluminosilicate zeolites' frameworks. In particular, Lowenstein's rule states that the Al-O-Al linkage is forbidden in the framework of aluminosilicates. Previous computational studies have also suggested that the large angle (180°) of the Al-O-Al linkage is not easily accommodated in aluminosilicate structures and small clusters of the type that is postulated to form during the synthesis of aluminosilicate zeolites have the lower energies for "Lowensteinian" distributions of aluminum.

1.2.4 Dempsey's rule

Dempsey's rule, moreover, is based on simple electrostatic arguments is postulated that, the distance between each aluminum atom (with the effective charge) is maximized in aluminosilicate zeolites to stabilize their frameworks. ^{29}Si MAS NMR studies have shown that as the Si/Al ratio increases, the number of the Al-O-Si-O-Al chains therefore moderately decrease²⁴. Similarly, the result of *ab initio* calculations supposed that the Al-O-Si-O-Si-O-Al chain seems to have an energy minimum in aluminosilicate systems. However, the *ab initio* calculations for the high-silica zeolite²⁵, contrary to Dempsey's rule, found the possibility that the Al-O-Si-O-Al chains would exist in structures. The results described above, suggest that Dempsey's rule is worth further examination.

1.2.5 Experimental aluminosilicate zeolite nucleation and crystal growth

Given that several factors such as pH, reaction time, temperature and Si/Al ratio have a strong influence over the formation process of zeolites, obtaining direct and exact proof of the nucleation is very elusive. Unlike pure silica zeolites²⁶⁻³¹ that have been studying widely, the complexity of aluminosilicate zeolites structural compositions (Si/Al ratio) makes it much more difficult to gain detailed information on the nucleation of these materials. Be that as it may, several techniques still have been applied to this study.

In general, NMR spectroscopy is well suited for investigating aluminosilicate species at the early nucleation stage in solution of zeolites. The evidence for the existence of some aluminosilicate species is revealed in ^{29}Si NMR and ^{27}Al NMR spectroscopy³²⁻³⁴. Besides using NMR spectroscopy for proving the presence of possible aluminosilicate species at the prenucleation stage of zeolite synthesis, understanding the nucleation and crystal growth of zeolites has been accomplished by other techniques, as will be discussed in greater detail below.

Mintova et al.^{35,36} used transmission electron microscopy (TEM) to determine the proposed nucleation of zeolites A or Y and thus suggested that the crystal nuclei could be produced from a clear solution containing aluminosilicate species. Quasi-elastic light scattering, SAXS³⁷, and dynamic light scattering (DLS)^{38,39} have provided

some evidence that the formation of zeolite A is related to the presence of amorphous aluminosilicate species. High energy X-ray diffraction (HEXRD)⁴⁰ and the small angle and wide angle X-ray scattering (SAXS/WAXS)^{41,42} clearly revealed that the presence of small aluminosilicate rings containing the four, five and six rings in the early nucleation stage of different types of aluminosilicate zeolites. UV Raman spectroscopy combined with NMR or X-ray diffraction⁴³⁻⁴⁵ suggested that most amorphous aluminosilicate species contained the four ring species in the early stage of nucleation of zeolites X or A. The double four ring unit has been proposed to be the key building block for crystal growth of zeolite A from atomic force microscopy (AFM)^{46,47}. The kinetic study of Ciric⁴⁸ has shown that small aluminosilicate species: a $(\text{OH})_3\text{AlOSiO}_x(\text{OH})_{3-x}^{(x+1)-}$ dimer or a tetramer are likely to participate in the formation of zeolite A and Carr⁴⁹ has obtained the similar result by X-ray diffraction techniques i.e. in the formation of zeolite A, the basic building block is $(\text{OH})_3\text{AlOSiO}_x(\text{OH})_{3-x}^{(x+1)-}$ dimer. In addition, by solid-state ³¹Si and ²⁷Al NMR. North et al.⁵⁰ have observed the appearance of the small aluminosilicate species such as the $(\text{OH})_3\text{AlOSiO}_x(\text{OH})_{3-x}^{(x+1)-}$ dimer can be rapid to grow aluminosilicates for forming zeolite structures under alkaline solution.

These methods have undoubtedly given useful information on the nucleation and crystal growth of aluminosilicate zeolites. It is, however, still a challenge to elucidate the specific and localized information concerning discrete stages of the formation of aluminosilicate zeolites by the use of the experimental studies due to the simultaneous involvements of several factors such as the charge state (the effect of pH), the cation location, and the key role of templates with the interplay of thermodynamic versus kinetics control causing additional complexity. Given these experimental difficulties, an alternative approach is required. Using computational methods can give considerable insight into probing the nucleation and crystal growth of aluminosilicate zeolites, as described in the section 1.2.6.

1.2.6 Proposed condensation mechanisms in aluminosilicates

In general, two different monomeric reactants: $(\text{OH})_{4-x}\text{SiO}_x^{x-}$ that is readily deprotonated from $\text{Si}(\text{OH})_4$, and $\text{Al}(\text{OH})_4^-$ species are the main sources that directly involve in aluminosilicate zeolite synthesis under alkaline solution³². Furthermore, due to these monomeric reactants, which are negatively charged, the condensation reactions must be balanced by counter ions such alkali metals or alkaline earth metals. The proposed initial reactions under hydrothermal conditions can be described as follows:



Experimental techniques, however, such as NMR spectroscopy cannot distinguish neutral and anionic species during the condensation reaction processes, because the above reactions happen very rapidly. Hence, the presumed condensation reaction is:



Here, the counter ion is ignored in Eq. (1.4), but must be considered when formulating the condensation reactions. Counter ions are arranged with suitable coordinations around the aluminosilicate species in the condensation reactions. Consequently, through the mechanism of counter ions assembly, these aluminosilicate species can become regular periodically and thus assist the propagation. It should be noted that the quantitative treatment of the formation of aluminosilicate species is still difficult especially as different Si/Al ratios, would produce variable degrees of polymerisations.

1.2.7 Modelling aluminosilicate species and nucleation

The above experimental techniques have provided information on the formation of aluminosilicate species and the proposed mechanism of nucleation and crystal growth of aluminosilicate zeolites. However, as mentioned already, identification of the species and of the mechanism of the formation of aluminosilicate zeolites still is difficult to study via experimental techniques. Hence, molecular modelling is

an alternative method that provides further understanding of what kinds of aluminosilicate species being involved and of the mechanisms being proceeded in the formation processes of aluminosilicate zeolites.

Most previous computational studies focused on simulating pure silica species⁵¹⁻⁵⁵, due to their simple structures rather than aluminosilicate species, which give rise to much greater complexity. Over the past few years, there were few papers to study the structures of aluminosilicate species. For the simple aluminosilicate species: $\text{Al}(\text{OH})_4^-$, $\text{AlSiO}(\text{OH})_6^-$ by Pereira et al, employed a local Density Functional Theory (DFT) to study the relative structural and energetic properties of small aluminosilicate species. Moreover, the analysis of the geometry and energy of a variety of calculated aluminosilicate four and double four rings has already been reported by Tossell^{56,57}. These works have indicated that the electrostatic interaction between cations such as H^+ or Na^+ ions and aluminosilicate structures greatly stabilizes the aluminosilicate clusters.

Turning now to primary condensation reactions, the formation of small clusters up to four rings, has been modelled by Catlow et al.⁵⁸ but the energy calculation for the condensation reactions produced a significant error due to the lack of the inclusion of cations, which can effectively stabilize the aluminosilicate structures. To date, a detailed description of the energetics of the key aluminosilicate dimerisations⁵⁹ that directly condense from $(\text{OH})_{4-x}\text{SiO}_x^{x-}$ and $\text{Al}(\text{OH})_4\text{Na}$ has been reported via a solvent model (the COSMO approach) based on DFT methods, but the question of further polymerisations of open clusters as well as rings is still a big challenge.

1.2.7.1 The effect of solvent

As discussed earlier, the raw materials are mixed in a clear solution at the beginning of zeolite synthesis. The nucleation and growth of zeolites is of course effected hydrothermally and cluster properties are strongly influenced by the aqueous solution; the inclusion of solvent effect will be essential if reliable thermodynamic parameters are to be calculated. Mora-Fonz et al.⁶⁰ suggested that using the COSMO approach to model water in pure silicate clusters, the relative strength of the interactions between pure silicate clusters and water would be in order: silicate-silicate > silicate-water > water-water and the accuracy of the reaction of the initial solvated neutral and charge silicate clusters has been enhanced by the inclusion

of sodium ions and the addition of some explicit water molecules under the COSMO method. Such behaviour should also influence the formation of aluminosilicate clusters. Thus, it is evident that to investigate accurately aluminosilicate clusters and the mechanisms of nucleation or crystal growth of aluminosilicate zeolite in solution; we must consider the role of water.

In this work, we will use Density Functional Theory (DFT) and the Conductor-like Screening Model (COSMO) to investigate the structural geometry and thermodynamical properties for the condensation reactions of aluminosilicates in the prenucleation of forming aluminosilicate zeolites.

References:

1. Davis, M. E. *Nature*, **2002**, *417*, 813.
2. C. S. Cundy and P. A. Cox, *Microporous and Mesoporous Materials*, **2005**, *82*, 1.
3. C. S. Cundy and P. A. Cox, *Chemical Reviews*, **2003**, *103*, 663.
4. D. P. Serrano and R. van Grieken, *Journal of Materials Chemistry*, **2001**, *11*, 2391.
5. P. W. Atkins, J. De Paula, *Atkins' Physical chemistry*, 7th ed., Oxford University Press, Oxford, **2002**.
6. A. Klamt and G. Schuurmann, *Journal of the Chemical Society-Perkin Transactions 2*, **1993**, 799.
7. J. Tomasi and M. Persico, *Chemical Reviews*, **1994**, *94*, 2027.
8. W. Loewenstein, *American Mineralogist*, **1954**, *39*, 92.
9. W. Dempsey, G. H. Kuhl and D. H. Olson, *Journal of Physical Chemistry*, **1969**, *73*, 387.
10. C. Baerlocher, W. M. Meier, D. H. Olson, *Atlas of Zeolite Structure Types*, 5th edition, Elsevier, London, **2001**.
11. A. Dyer, *Introduction to Zeolite Molecular Sieves*, Wiley, Chichester, 1988.
12. A. F. Cronstedt, *Akad. Handl* **1756**, *18*, 120-30.
13. R. M. Barrer, *Journal of the Chemical Society*, **1948**, 127.
14. R. M. Milton, U.S. Patent 2,882,243 (**1959**); R. M. Milton, U.S. Patent 2,882,244 (**1959**).
15. H. van Bekkum, E.M. Flanigen, P.A. Jacobs, J.C. Jansen, *Introduction to Zeolite Science and Practice*, 2nd edition, Elsevier, Amsterdam, **2001**.
16. A. Corma, *Chemical Reviews*, **1997**, *97*, 2373.
17. D. W. Breck, *Zeolite molecular sieves : structure, chemistry and use*, Wiley, Interscience 1974, New York ; London, **1974**.
18. R. M. Barrer, *Hydrothermal chemistry of zeolites*, Academic Press **1982**, London, **1982**.
19. H. Robson, *Verified Syntheses of Zeolitic Materials*, 2nd ed., Elsevier-International Zeolite Association, Amsterdam, **2001**.
20. R. Xu, W. Pang, J. Yu, Q. Huo and J. Chen, *Chemistry of Zeolites and Related Porous Materials: Synthesis and Structure*, Wiley, Singapore, **2007**.
21. K. Byrappa, M. Yoshimura, *Handbook of Hydrothermal Technology*, Elsevier, USA, 2012.

22. M. L. Occelli, H. E. Robson, *Zeolite Synthesis*, ACS Symposium Series No. 398. Washington, DC, American Chemical Society, **1989**.
23. R. Szostak, *Molecular Sieves: Principles of Synthesis and Identification*, Blackie Academic & Professional, London, **1998**.
24. J. Dedecek, S. Sklenak, C. Li, B. Wichterlova, V. Gabova, J. Brus, M. Sierka and J. Sauer, *Journal of Physical Chemistry C*, **2009**, *113*, 1447.
25. K. P. Schroeder, J. Sauer, *Journal of Physical Chemistry*, **1993**, *97*, 6579.
26. C. T. G. Knight and S. D. Kinrade, *Journal of Physical Chemistry B*, **2002**, *106*, 3329.
27. M. Haouas and F. Taulelle, *Journal of Physical Chemistry B*, **2006**, *110*, 3007.
28. S. D. Kinrade, J. C. H. Donovan, A. S. Schach and C. T. G. Knight, *Journal of the Chemical Society-Dalton Transactions*, **2002**, 1250.
29. S. D. Kinrade, C. T. G. Knight, D. L. Pole and R. T. Syvitski, *Inorganic Chemistry*, **1998**, *37*, 4278.
30. S. D. Kinrade, C. T. G. Knight, D. L. Pole and R. T. Syvitski, *Inorganic Chemistry*, **1998**, *37*, 4272.
31. F. Schuth, *Current Opinion in Solid State & Materials Science*, **2001**, *5*, 389.
32. T. W. Swaddle, *Coordination Chemistry Reviews*, **2001**, *219*, 665.
33. S. D. Kinrade and T. W. Swaddle, *Inorganic Chemistry*, **1989**, *28*, 1952.
34. A. Samadi-Maybodi, N. Goudarzi and H. Naderi-Manesh, *Bulletin of the Chemical Society of Japan*, **2006**, *79*, 276.
35. S. Mintova, N. H. Olson, V. Valtchev and T. Bein, *Science*, **1999**, *283*, 958.
36. S. Mintova, N. H. Olson and T. Bein, *Angewandte Chemie-International Edition*, **1999**, *38*, 3201.
37. P. S. Singh, T. L. Dowling, J. N. Watson and J. W. White, *Physical Chemistry Chemical Physics*, **1999**, *1*, 4125.
38. L. Gora, K. Streltzky, R. W. Thompson and G. D. J. Phillies, *Zeolites*, **1997**, *18*, 119.
39. B. J. Schoeman, O. Regev, *Zeolites*, **1996**, *17*, 447.
40. T. Wakihara, S. Kohara, G. Sankar, S. Saito, M. Sanchez-Sanchez, A. R. Overweg, W. Fan, M. Ogura and T. Okubo, *Physical Chemistry Chemical Physics*, **2006**, *8*, 224.
41. W. Fan, M. Ogura, G. Sankar and T. Okubo, *Chemistry of Materials*, **2007**, *19*, 1906.

42. W. Fan, M. O'Brien, M. Ogura, M. Sanchez-Sanchez, C. Martin, F. Meneau, K. Kurumada, G. Sankar and T. Okubo, *Physical Chemistry Chemical Physics*, **2006**, *8*, 1335.
43. F. T. Fan, Z. C. Feng, G. N. Li, K. J. Sun, P. F. Ying and C. Li, *Chemistry-a European Journal*, **2008**, *14*, 5125.
44. L. M. Ren, C. J. Li, F. T. Fan, Q. Guo, D. S. Liang, Z. C. Feng, C. Li, S. G. Li and F. S. Xiao, *Chemistry-a European Journal*, **2011**, *17*, 6162.
45. A. Depla, E. Verheyen, A. Veyfeyken, E. Gobechiya, T. Hartmann, R. Schaefer, J. A. Martens and C. E. A. Kirschhock, *Physical Chemistry Chemical Physics*, **2011**, *13*, 13730.
46. J. R. Agger, N. Pervaiz, A. K. Cheetham and M. W. Anderson, *Journal of the American Chemical Society*, **1998**, *120*, 10754.
47. S. Sugiyama, S. Yamamoto, O. Matsuoka, H. Nozoye, J. Yu, G. Zhu, S. Qiu and T. I, *Microporous and Mesoporous Materials*, **1999**, *28*, 1.
48. J. Ciric, *Journal of Colloid and Interface Science*, **1968**, *28*, 315.
49. J. M. Shi, M. W. Anderson and S. W. Carr, *Chemistry of Materials*, **1996**, *8*, 369.
50. M. R. North and T. W. Swaddle, *Inorganic Chemistry*, **2000**, *39*, 2661.
51. M. J. Mora-Fonz, C. R. A. Catlow and D. W. Lewis, *Angewandte Chemie-International Edition*, **2005**, *44*, 3082.
52. J. C. G. Pereira, C. R. A. Catlow and G. D. Price, *Journal of Physical Chemistry A*, **1999**, *103*, 3252.
53. J. C. G. Pereira, C. R. A. Catlow and G. D. Price, *Journal of Physical Chemistry A*, **1999**, *103*, 3268.
54. T. T. Trinh, A. P. J. Jansen and R. A. van Santen, *Journal of Physical Chemistry B*, **2006**, *110*, 23099.
55. X. Q. Zhang, T. T. Trinh, R. A. van Santen and A. P. J. Jansen, *Journal of the American Chemical Society*, **2011**, *133*, 6613.
56. J. A. Tossell, *Journal of Physical Chemistry*, **1996**, *100*, 14828.
57. J. A. Tossell and G. SaggiSzabo, *Geochimica Et Cosmochimica Acta*, **1997**, *61*, 1171.
58. C. R. A. Catlow, A. R. George and C. M. Freeman, *Chemical Communications*, **1996**, 1311.

59. C. E. White, J. L. Provis, G. J. Kearley, D. P. Riley and J. S. J. van Deventer, *Dalton Transactions*, **2011**, *40*, 1348.
60. M. J. Mora-Fonz, C. R. A. Catlow and D. W. Lewis, *Physical Chemistry Chemical Physics*, **2008**, *10*, 6571.

Chapter 2 Computational Methodology

2.1 Introduction

One of the most important recent developments has been the use of computational chemistry derived from quantum mechanics to investigate structural properties in the study of materials. In general, the fundamental purpose of computational chemistry is to model and predict the behaviour of atoms and molecules that relate to macroscopic properties or phenomena. It means that many chemical and physical properties such as transition states, vibrational frequencies, NMR properties or thermodynamical properties and so on can be obtained via the calculation of computational modelling.

Of course, as for the chemistry of zeolites, a number of notable successes of predictive modelling in the past two decades have been published and often been used as complements to experimental results¹⁻⁵. In this work, density functional theory (DFT) based on quantum mechanics is the main method to be employed to investigate aluminosilicate zeolites. In this chapter, the relative computational methods based on classical and quantum mechanical, the approaches for modelling solvation and the principles of statistical mechanics will be outlined⁶⁻¹², following which the detailed features of modelling work used in this thesis will also be described.

2.2 Electronic structure methods

Electronic structure methods based on quantum mechanics study the behaviour of electrons in atoms and molecules, and aim to predict the physical and chemical properties of macroscopic phenomena from atomic scales model^{6,8,10}. At the basis of quantum mechanics is the Schrödinger equation. In other words, electronic structure methods involve solving the Schrödinger equation, but the exact solution, except that of the hydrogen atom, of the Schrödinger equation is very difficult to obtain in many-atoms system. To overcome the fundamental problem, various approximations have also been suggested, which we will discuss in detail in this section. First, however, let us consider the Schrödinger equation: in its time independent form (Eq. 2.1).

$$H\Psi = E\Psi \quad (2.1)$$

$$H\Psi = \frac{i\hbar}{2\pi} \frac{\partial \Psi(r,t)}{\partial t} \quad (2.2)$$

where H is the Hamiltonian operator of the system, Ψ is the wave function to describe the state of a system, and E is the total energy of the system that we can obtain from the solution of equation (2.3), which on substitutability in for the Hamiltonian operator (H) to be written to:

$$-\frac{\hbar^2}{2m} \nabla^2 \psi(r) + V(r)\psi(r) = E\psi(r) \quad (2.3)$$

where the Hamiltonian operator (H) is expanded into kinetic and potential energies of a system, total energy of E -the eigenvalue, with the wavefunction is the eigenfunction. Full expansion of the Hamiltonian operator gives:

$$H = -\sum_{i=1}^N \frac{\hbar^2}{2m_n} \nabla_i^2 - \sum_{i=1}^n \frac{\hbar^2}{2m_e} \nabla_i^2 - \sum_{i=1}^n \sum_{a=1}^N \frac{Z_a}{|r_i - R_a|} e^2 + \sum_{i=1}^n \sum_{j>i}^n \frac{1}{|r_i - r_j|} e^2 + \sum_{a=1}^N \sum_{b>a}^N \frac{Z_a Z_b}{|R_a - R_b|} e^2 \quad (2.4)$$

$$H = T_n(R) + T_e(r) + V_{en}(r) + V_{ee}(r) + V_{nn}(R) \quad (2.5)$$

Here, R and r are the coordinates of the nucleus and electron and T_n and T_e are the kinetic energy of nuclei and electrons, respectively. V comprises three items: the potential energy of nuclei (V_{nn}), the electrostatic interaction between nuclei and electrons (V_{en}), and electrostatic repulsion between electrons (V_{ee}). However, with such complexity it is difficult to obtain the exact solution of the Schrödinger equation; the Born-Oppenheimer approximation first has been put forward for simplifying the Schrödinger equation.

The Born-Oppenheimer approximation states that because of the mass of the nucleus being much larger than that of the electron, the motion of the nuclei and electrons can be considered to be separated in the whole system. In other words, the Born-Oppenheimer approximation regards the nuclei as fixed in solving the Schrödinger equation, which means the electronic wavefunction only relies on the positions of the nuclei but not their momenta. The kinetic energy of the nuclei is

thereby omitted and the repulsion between nuclei becomes a constant. As a result, the Schrödinger equation only corresponding to electronic motion is represented as:

$$H_e(R)\Psi_e(r, R) = E_e(R)\Psi_e(r, R) \quad (2.6)$$

The Hamiltonian operator from equation (2.7) that ignore terms T_n and V_{nn} can also be reduced:

$$H = T_e(r) + V_{ee}(r) + V_{en}(r, R) \quad (2.7)$$

The wavefunction is subject to two constants for normalization condition:

$$\int_{-\infty}^{\infty} |\Psi|^2 dx = 1 \quad (2.8)$$

where the square of the wavefunction gives the probability density.

The second is that the electronic wavefunction must be antisymmetric, which means the spin must be included in the electronic wavefunction and obey the Pauli exclusion principle which requires that the wavefunction is antisymmetric with respect to particle exchange:

$$\Psi = -\Psi \quad (2.9)$$

For satisfying the antisymmetric property in the electronic wavefunction, the Slater determinant, which is a wavefunction, consisting of one spin orbital per electron, which can solve the many-electronic Schrödinger equation consistently is given as:

$$\Psi = \frac{1}{\sqrt{N!}} \begin{vmatrix} \psi_1(x_1) & \psi_2(x_1) & \cdots & \psi_N(x_1) \\ \psi_1(x_2) & \psi_2(x_2) & \cdots & \psi_N(x_2) \\ \vdots & \vdots & \ddots & \vdots \\ \psi_1(x_N) & \psi_2(x_N) & \cdots & \psi_N(x_N) \end{vmatrix} \quad (2.10)$$

There is no exact solution for the Schrödinger equation for polyelectronic systems owing to molecules being electron-electron repulsions. Hence, there have been several approximations for solving this problem, most calculation being the Hartree-Fock (HF) and DFT (Density Functional Theory) methods, which are outlined as below.

2.2.1 Hartree-Fock method

The Hartree-Fock method is a mean field approximation following the postulate proposed by Fock which simplifies the electron-electron interaction form by assuming that each electron interacts with the average field of the rest of the electrons instead of each electron interacting with other electrons one by one^{6,12,13}.

The Hartree-Fock method uses the Slater determinant (2.10) discussed above and the Hartree-Fock equation is given as follows:

$$E = \langle \Psi | H | \Psi \rangle = \sum_{i=1}^N H_i + \frac{1}{2} \sum_{i=1}^N \sum_{j=1}^N (J_{ij} - K_{ij}) \quad (2.11)$$

$$H_i = \int \phi_i^*(r) \left[-\frac{1}{2} \nabla_i^2 + \mathcal{U}_i \right] \phi_i(r) d(r) \quad (2.12)$$

$$J_{ij} = \iint \phi_i^*(r_1) \phi_j^*(r_2) \frac{1}{|r_1 - r_2|} \phi_i(r_1) \phi_j(r_2) dr_1 dr_2 \quad (2.13)$$

$$K_{ij} = \iint \phi_i^*(r_1) \phi_j^*(r_1) \frac{1}{|r_1 - r_2|} \phi_i(r_2) \phi_j(r_2) dr_1 dr_2 \quad (2.14)$$

Here, H_i is the contribution of kinetic energy and the electron potential. J_{ij} represents the Coulomb interaction of electron i and j . K_{ij} represents the exchange function of i and j .

To solve the Hartree-Fock equation, a widely used approach is to employ a basis set in which the molecular orbitals can be described by a linear combination of atomic orbitals:

$$\psi_i = \sum_k^M C_{ik} \phi_k \quad (2.15)$$

where ϕ is a series of basis functions and C is a coefficient, which can be derived from variation principles. In the Hartree-Fock Method, the purpose is to find a determinantal function, which corresponds to the lowest energy. Therefore, to introduce the Fock operator, we can obtain the Hartree-Fock eigen equation:

$$f(r_1)\phi_i(r_1) = \varepsilon_i\phi_i(r_1) \quad (2.16)$$

$$f(r_1) = h(r_1) + \sum_{a=1}^N [j_a(r_1) - k_a(r_1)] \quad (2.17)$$

where f is the Fock operator, which is an one-electron operator on the atomic orbitals. Then, the Hartree-Fock eigen equation can be led to the matrix form (the Roothan-Hall equations):

$$FC = SC\varepsilon \quad (2.18)$$

$$\det |F - \varepsilon_a S| = 0 \quad (2.19)$$

with the Fock matrix(F) and overlap matrix(S) defined as:

$$F_{ij} = \int \chi_i^*(1) f_1 \chi_j(1) dv \quad (2.20)$$

$$S_{ij} = \int \chi_i^*(1) \chi_j(1) dv \quad (2.21)$$

We can obtain the numerical solution of the Roothan-Hall equations iteratively (self-consistent) by using the Hartree-Fock Method, as shown in Figure 2.1. Determination of the energy of this system is achieved by finding a set of spin orbitals that minimises the electronic energy, in accordance with the variation principle.

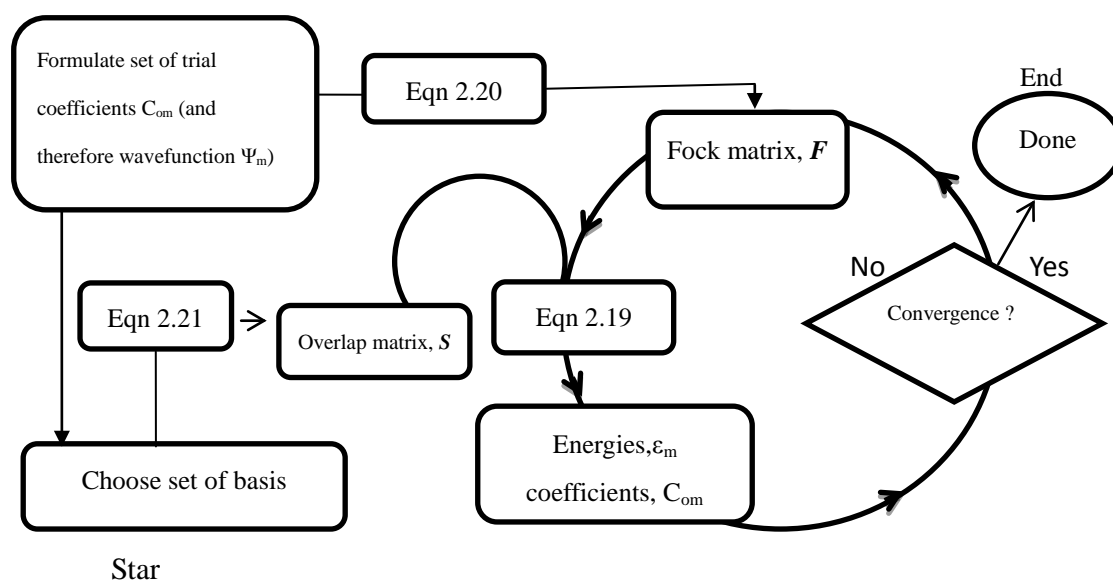


Figure 2.1 The Hartree-Fock self-consistent iteration⁸.

The Hartree-Fock Method has given a good description of the electronic wavefunction, by means of the average field, but the main obstacle of the method, which derives from the neglect of instantaneous electron-electron repulsions, is the lack of representation of electron correlation, leading to the difference between the exact total energy of a system and energy in the HF limit:

$$E_{corr} = E - E_{HF} \quad (2.22)$$

To correct the limitation of the HF method, three known electron correlation methods: the Configuration Interaction (CI)¹⁴, the Møller-Plesset (MP)¹⁵ perturbation theory and the Coupled-Cluster (CC) method^{16,17} are used. Configuration Interaction goes beyond the HF level and includes excited states of electrons such as singly excited, doubly excited and so on in order to improve the ground state configuration of the electronic wavefunction. This means that the electronic wavefunction is described as a linear combination of the Hartree-Fock determinants and all possible excited determinants.

Unfortunately, a full CI calculation is computationally very expensive and is possible only for the smallest systems. Truncated CI, also referred to as limited CI, is a

practical alternative approach that uses the significant configurations, but discards the trivial ones to reduce space of the basis functions. Among truncated CI approaches, the CISD in which singly and doubly excited states are represented in determinants is the most common approach but the size consistency error is inevitable, which means that in the truncated CI approach, fails to represent the accurate correlation energy for a large system. For this problem of the size consistency error, an advance has been made in the treatment of the Coupled-Cluster (CC) method, which employs the exponential wave function to guarantee the size extensibility instead of the linear wavefunction:

$$\psi = e^C \psi_0 \quad (2.23)$$

where e^C is the exponential operator of the series expansion and C is the cluster operator of the electron excitation on many-body perturbation theory; all determinants are formed by electron excitations, which means that the virtual orbitals are occupied. The perturbation is defined by:

$$H\Psi_n = (H^{(0)} + \lambda \hat{u})\Psi_n = E_n \Psi_n \quad (2.24)$$

where $H^{(0)}$ is the unperturbed Hamiltonian; λ is an arbitrary real parameter and \hat{u} is a perturbation. Furthermore, to obtain an accurate result, the inclusion of the second-order energy correction, referred to as MP2, is necessary in the Møller-Plesset (MP) perturbation theory.

$$E_n^{(2)} = \sum_{m \neq n} \frac{\left| \langle \Psi_m^{(0)} | V | \Psi_n^{(0)} \rangle \right|^2}{E_n^{(0)} - E_m^{(0)}} \quad (2.25)$$

2.2.2 Density Functional Theory (DFT)

It is no doubt that DFT that adopts another approach to the many-body electronic interaction has been extensively applied in modelling the structure and energy of molecules and has had a significant influence on quantum chemistry¹³. Compared with the Hartree-Fock method, DFT is based on the electron density (ρ) instead of the wave function. A cornerstone of DFT is derived from Hohenberg-Kohn theorem¹⁸ that demonstrates that the ground-state energy and all other ground-state electronic

properties of a system are uniquely determined by the electron density. The expression of the total energy of a system is given as:

$$E[\rho] = T[\rho] + V[\rho] + U[\rho] \quad (2.26)$$

where ρ is the electron density, which is derived from the molecular orbitals. In equation (2.26), $T[\rho]$ is the kinetic energy of non-interacting electrons, $V[\rho]$ is the potential energy of the nuclei-electron interaction, and $U[\rho]$ is the potential energy of the electron-electron interaction. A purpose of Hohenberg-Kohn theorem is to obtain the energy of a system as a functional of the electron density, but the exact energy functionals of the kinetic energy of the electrons and the potential energy of the electron-electron interaction is unascertained and to approximate these functionals must be known. Kohn and Sham introduced in concept of an imaginary reference system of N non-interacting electrons with the electron density of the reference system regarded as that of the real system. The Kohn-Sham Hamiltonian is given as follows:

$$h_{ref} = \sum_{i=1}^{N_e} h_i^{ks} \quad (2.27)$$

$$h_i^{KS} = -\frac{\hbar^2}{2m_e} \nabla_i^2 + v_{ref}(r_i) \quad (2.28)$$

where v_{ref} is an external potential. Moreover, the Kohn-Sham ground-state energy of a system can be obtained as a functional of the electron density, which is defined by the equation.

$$E[\rho] = T[\rho] + V[\rho] + U[\rho] + E_{xc}[\rho] \quad (2.29)$$

$$\rho(r) = \sum_{i=1}^N |\Psi_i(r)|^2 \quad (2.30)$$

where the last term $E_{xc}[\rho]$ is defined as the exchange-correlation energy which is the description of the exchange energy from the antisymmetrical properties of wavefunction and the correlation energy from the movement of the electrons. The term E_{xc} can also be written as:

$$E_{xc}[n(r)] = T[n(r)] - T_s[n(r)] + E_{ee}[n(r)] - E_H[n(r)] \quad (2.31)$$

where $T_s[n(r)]$ and $E_{ee}[n(r)]$ are the exact kinetic and electron-electron interaction energies for a real system, respectively. The exchange-correlation potential is given by the functional derivative:

$$v_{xc}(r) = \frac{\delta E_{xc}[\rho(r)]}{\delta \rho(r)} \quad (2.32)$$

Hence, the Kohn-Sham equation is obtained, which can be written as:

$$\left[-\frac{1}{2}\nabla_i^2 + V_{eff}(r)\right]\Psi_i(r) = \varepsilon_i \Psi_i \quad (2.33)$$

$$V_{eff}(r) = V(r) + U(r) + \frac{\delta E_{xc}[\rho(r)]}{\delta \rho(r)} \quad (2.34)$$

The Kohn-Sham equation is found to be analogous to the Hartree-Fock equation, but the Kohn-Sham equation differs greatly from the Hartree-Fock equation in the exchange-correlation potential. To obtain the total energy, it is necessary to solve the Kohn-Sham equation. However, the main error of the solution of Kohn-Sham equation is from the exchange-correlation potential. How do we obtain better practical approximations for the exchange-correlation potential? There are three common approximations in use: the local density approximation (LDA), generalised gradient approximation (GGA) and hybrid exchange correlation functional.

The simplest and most useful method is the local density approximation (LDA), which postulates that the exchange-correlation energy of a system at each given point is identical to that of the uniform homogeneous electron gas; the exchange-correlation functional can be separated into the exchange and correlation contributions:

$$E^{xc}(\rho) = E^x(\rho) + E^c(\rho) \quad (2.35)$$

Note that the local density approximation (LDA) emphasizes the contribution of the exchange functional rather than that of the correlation one. The exchange energy functional can be expressed as:

$$E_x^{LDA} = -C_x \int \rho^{4/3}(r) dr \quad (2.36)$$

The corresponding exchange correlation¹⁹ is defined as:

$$\varepsilon_x(\rho) = \frac{3}{4} \left(\frac{3n}{\pi} \right)^{1/3} \quad (2.37)$$

For example, BHL which developed by von Barth and Hedin²⁰, after Hedin and Lundqvist²¹, and reviewed by Moruzzi et al.²² for both spin-restricted and spin-unrestricted calculations is a functional for calculating the local exchange and correlation energies separately.

Although LDA can predict the ground-state energy of the homogeneous systems accurately, in the inhomogeneous systems, LDA will be inaccurate. Hence, a variety of approaches such as the general gradient approximation (GGA), and hybrid approximations has been successfully developed to reduce the error of LDA. In the generalized gradient approximation (GGA), the exchange-correlation energy can be written as:

$$\varepsilon_{x/c}^{GGA}[n] = \varepsilon_{x/c}^{LDA}[n] + \Delta_{\varepsilon_{x/c}} \left[\frac{|\nabla n(r)|}{n^{3/4}(r)} \right] \quad (2.38)$$

In order to account for the inhomogeneous systems, the exchange-correlation energy of GGA is a function not only of the density at each point but also additionally the gradient of the density.

The hybrid functional introduces a component of the exact exchange energy functional of the Hartree-Fock theory into the exchange-correlation energy of DFT to calculate the exchange-correlation energy. One of the most accurate functional is B3LYP²³⁻²⁵, which is combined with an exchange functional derived from Becke and a correlation functional derived from Lee, Yang, and Parr and three empirical parameters:

$$E_{XC}^{B3LYP} = E_{XC}^{LDA} + a_0(E_X^{HF} - E_X^{LDA}) + a_x(E_X^{GGA} - E_X^{LDA}) + a_c(E_c^{GGA} - E_c^{LDA}) \quad (2.39)$$

where E_X^{HF} , E_X^{GGA} and E_c^{GGA} and E_c^{LDA} are the Hartree-Fock exact exchange energy, the

exchange functional of Becke 88 , the correlation functional of Lee, Yang and Parr and the correlation functional of the VWN local-density approximation respectively; the three empirical parameters $a_0 = 0.20$, $a_x = 0.72$ and $a_c = 0.81$ are determined by fitting to a set of measured atomisation energy. In our work, the measured atomisation energy including the H, Si, Al, O and Na atoms are considered.

2.2.3 Basis set

The basis set is a set of basis functions in which the molecular orbitals can be described commonly by a linear combination of atomic orbitals²⁶. A complete set of basis functions can represent well-behaved molecular orbitals exactly to obtain the exact result, but in practice, the computational requirements for such sets will be very expensive. Incomplete (finite) basis functions are computationally feasible, but will produce the basis set error due to the incomplete description of molecular orbitals. In this context, the choice of the basis functions is particularly important. Two types of basis functions: Slater-Type Orbitals (STOs)²⁷ and Gaussian-Type Orbitals (GTOs)²⁸⁻³⁰ are often used. The construction of Slater-Type Orbitals (STOs) is given by:

$$\chi_{\zeta,n,l,m}(r, \theta, \varphi) = NY_{l,m}(\theta, \varphi)r^{n-1}e^{-\zeta r} \quad (2.40)$$

where N is a normalisation constant, $Y_{l,m}(\theta, \varphi)$ are spherical harmonics, r is the distance from the atomic nucleus, n is the principal quantum number and ζ is a constant involved with the effective nuclear charge. Note that the serious deficiency of STOs is the expense of integrating these functions numerically, which means that to evaluate such a many electrons integral is unfeasible; the use of STOs is limited to a small number of functions.

The other choice of basis functions: Gaussian-Type Orbitals (GTOs), is much more common in current work and adopts Cartesian coordinate to generate a set of solvable basis functions, which can be written:

$$\chi_{\zeta,l_x,l_y,l_z}(x, y, z) = Nx^{l_x}y^{l_y}z^{l_z}e^{-\zeta r^2} \quad (2.41)$$

where x , y and z are integer positive numbers and the type of orbital can be

determined by the sum of l_x , l_y and l_z , ζ is a orbital exponent, N is a normalization constant. The advantage of GTOs related to the treatment of these functions in multicenter integration that the integral can be reduced, reducing the computational expensive. The comparison of the functional behaviour of STOs and GTOs, however, indicates that GTOs provide a poor description of the atomic orbitals, owing to the incorrect behaviour (too smooth) near the nucleus and the asymptotic decay (too fast, due to an exponential in r^2) at large interparticle distances (r). To overcome this problem, *Contracted Gaussian* functions composed of a fixed linear combination of primitive Gaussian functions are constructed. A minimal basis set uses are *contracted Gaussian* functions for each above orbital. A Double Zeta (DZ) basis set³¹⁻³³, referring to as a double-numerical (DN) set, in which each atomic orbital can be represented by two basis functions is used to achieve higher accuracy. Triple Zeta (TZ) basis set³⁴ has each atomic orbital represented by three basis functions; and split valence(SV) basis sets use two basis functions to describe each valence atomic orbitals while a single basis function for each inner-shell atomic orbitals.

The Dmol³ code uses GTOs (the Gaussian type orbitals) with the basis sets including Minimal, DN (Double Numeric), DND and DNP. DNP is based on DN basis sets with the addition of polarization functions, but DND (based on DN basis sets) does not have the addition of polarization functions for hydrogen atoms.

2.3 Geometry optimisation (minimisation)

Geometry optimisation is fundamental procedure in molecular modelling; the objective is to find the lowest energy configurations of a given system. In other words, identifying the minimum points¹¹⁻¹³, which correspond to stable states of a given system on the energy surface is often needed. Here, the energy surface depends on the various arrangement of coordinates of a given system. In principle, the definition of a minimum point in terms of derivatives is:

$$\frac{\partial E}{\partial R_i} = 0, \quad \frac{\partial^2 E}{\partial R_i^2} > 0 \quad (2.42)$$

where the first derivative of energy function with respect to each of the coordinate variables is 0 while the second derivatives of the energy function are all positive.

For real complex systems however finding the minimum with the very lowest energy, also known as the global energy minimum, is a challenging task due to the presence of many possible minima on the energy surface. For the problem of alleviating the minimum, various algorithms have been developed with numerical or analytical methods. Derivative minimisation methods are commonly used in energy minimisation including both the first-derivative and the second-derivative minimisation methods.

In first-derivative minimisation methods, the steepest descent method and conjugate gradients methods are commonly used. The steepest descent method is based on the idea of sliding down the gradient gradually so as to locate the minimum in a zig-zag manner, where the new search direction is orthogonal to the previous one, but the limit of orthogonal directions also causes the convergence to be slow in this method. The conjugate gradients method, in which, for each step, the new search direction relies on all the other directions to locate the minimum achieves more rapid convergence.

In second-derivative minimisation methods, the most popular is the Newton-Raphson method, due to its faster convergence; each step in principle involves calculation at inversion of the matrix of second derivatives of the energy with respect to coordinates. As a result, this procedure is rather time consuming, especially for large molecules. Thus, many variants on the Newton-Raphson method, which attempts to simplify the calculation at inversion of the matrix have been put proposed, such as the block diagonal Newton-Raphson method, which reduces the original Matrix with $(3N-6)^2$ elements to N 3×3 matrices or the quasi-Newton method in which successive iterations update the inverse of the second derivative matrix.

2.4 Statistical mechanics

Having identified the minimum energy configuration of a system, statistical mechanics produces a good tool to describe the thermodynamic properties of a system such as entropy, enthalpy and free energy¹³. In Statistical Mechanics, one of the most important quantity is the partition function, which is given by:

$$q = \sum_i \exp(-\varepsilon_i / k_B T) \quad (2.43)$$

where K_B is the Boltzmann constant from which the entropy (S) and internal energy (U) of molecular gases can be expressed as follows:

$$S = \left(\ln(Q) + T \left(\frac{\partial \ln Q}{\partial T} \right) \right)_V \quad (2.44)$$

$$U = k_B T^2 \left(\frac{\partial \ln Q}{\partial T} \right)_V \quad (2.45)$$

Note that Q that is the ensemble partition function associates with different degrees of freedom in a system:

$$Q = q_{trans} q_{rot} q_{vib} q_{elec} \quad (2.46)$$

giving:

$$\ln Q = \ln q_{trans} + \ln q_{rot} + \ln q_{vib} + \ln q_{elec} \quad (2.47)$$

where q_{trans} , q_{rot} , q_{vib} and q_{elec} are the translational, rotational, vibrational and electronic partition functions. Thus, the Gibbs free energy also is determined from the partition functions:

$$G = H - TS \quad (2.48)$$

$$G = (U + PV) - TS \quad (2.49)$$

$$H = k_B T^2 \left(\frac{\partial \ln Q}{\partial T} \right)_V + K_B T V \left(\frac{\partial \ln Q}{\partial V} \right)_T \quad (2.50)$$

$$G = -k_B T \ln Q + k_B T V \left(\frac{\partial \ln Q}{\partial V} \right)_T \quad (2.51)$$

Moreover, the translational, rotational and vibrational and electronic partition

Functions (q_{trans} , q_{rot} , q_{vib} and q_{elec}) are given by, respectively:

$$q_{trans} = \left(\frac{2\pi m K_B T}{h^2} \right)^{3/2} V \quad (2.52)$$

$$q_{rot} = \left(\frac{\pi^{1/2}}{\sigma} \right) \left(\frac{2I_A K_B T}{h^2} \right) \left(\frac{2I_B K_B T}{h^2} \right) \left(\frac{2I_C K_B T}{h^2} \right) \quad (2.53)$$

where I_A , I_B and I_C are the moments of inertia and σ is the symmetry number.

$$q_{vib} = \frac{1}{1 - \exp(-\hbar\omega / K_B T)} \quad (2.54)$$

where ω is the angular frequency.

$$q_{elec} = \sum g_{ei} e^{-\beta\epsilon_{ei}} \quad (2.55)$$

where g_{ei} is the degeneracy of the i th energy level and q_{elec} is usually the degeneracy of equal or low lying electron states.

Based on the concept of statistical mechanics, the thermodynamic properties of molecular gases can be evaluated in modelling and simulation, but for most chemical reactions, which occur in the solvent, the consideration of the thermodynamic properties of molecular gases is of relatively little interest. As a result, incorporating the effect of solvent into modelling simulation is required. In the next section, we introduce CONductor-like Screening MOdel (COSMO)³⁵ as an approximate method in calculating solution energy.

2.5 CONductor-like Screening MOdel (COSMO)

For molecules in the gas phase, computational chemistry had been able accurately to calculate or predict their atomic structures, energies and physical properties for the past several decades. Modelling solvation, however, is still a challenge, which involves complex interactions of solute-solvent systems. Several approaches for modelling solvent effects have been developed, but are still some technical problems that need to be overcome. For example, molecular dynamics (MD) and Monte Carlo (MC) methods may be used to model solvation explicitly, but their use in the

Continuum solvation models (CSMs)³⁶ are a valuable approach to model the electrostatic component of solvation. The CSMs principle is to regard the solvent as a continuum dielectric medium and the solute as a void cavity removing the need for modelling of explicit solvent. Several CSMs approaches have been developed, such as the polarisable continuum model (PCM), self-consistent reaction field models (SCRF), COSMO.

In this work, we adopt the COSMO approach, of which the basic idea is as follows. The solvation of molecules is treated as the calculation of the dielectric screening charge and energy on a Van der Waals-like molecular surface in a conductor-like environment. In other words, if we put solute in the solvent, the solute will construct a cavity within the finite dielectric continuum of permittivity ϵ , forming as an assembly of atom-centre spheres with radii approximately 20% larger than the Van der Waals radius. The calculation of these dielectric screening charge and energy of the cavity surface can be segmented into hexagons, pentagons, or triangles and then embedded in a Self Consistent Field such as the Hartree-Fock or Density Functional Theory methods. Since the COSMO approach regards the medium as a conductor in which the finite dielectric continuum of permittivity ϵ is changed to ∞ , it means that the screening charge density can be thought of as the constant on surface of the solute. The screening charge, in other words, is calculated in the approximation of an ideal conductor. Hence, under such a dielectric boundary condition, the total potential (V_{tot}) on the surface is zero.

$$\Phi^{tot} = \Phi^{sol} + Aq \quad (2.56)$$

$$0 = \Phi^{sol} + Aq \quad (2.57)$$

$$q = -A^{-1}\Phi^{sol} \quad (2.58)$$

Here, Φ^{tot} is the total electrostatic potential on the surface segments, Φ^{sol} is the solute potential, and Aq is the potential arising from the surface charge q . q^* is the actual screening distribution, which gives an exact expression for the screening charges in a conducting continuum:

$$q^* = f(\varepsilon)q \quad (2.59)$$

$$f(\varepsilon) = \frac{\varepsilon - 1}{\varepsilon + \frac{1}{2}} \quad (2.60)$$

Here $f(\varepsilon)$ is the scaling function to correct electrostatic solute-solvent energy.

2.6 Methodology of modelling aluminosilicate clusters

The early computational studies in modelling pure silica clusters have been performed by Density Function Theory (DFT) code DMOL³, version 2.2³⁷⁻³⁹. Two different numerical basis sets: BHL/DNP within the DMOL³ code have been chosen to predict the geometry and energy of pure silica clusters by Pereira et al. and Mora-Fonz et al. The description of structure of pure silica clusters in Pereira's work (BHL/DNP)^{2,3} showed that the formation of "circular-like" open silicate clusters, due to the effect of the intramolecular hydrogen bonds, has more thermodynamic stability compared to linear ones. Mora-Fonz et al et al.⁴⁰ who applied an alternative basis set: BLYP/DNP with the more accurate, but computational expensive functional accurately predicted not only the conformation of pure silica clusters, which also accounted for the hydrogen bonds well especially in the optimised four, five and six ring clusters giving structures that are in agreement with those in actual zeolite crystals, but also the primary condensation reactions of silicate clusters in an alkaline solution. The results encouraged confidence in the study of silicate chemistry by using these methods.

The present work investigates aluminosilicate clusters, focusing on their self-assembly. Since aluminosilicate clusters are considered as an analogue of silicate clusters, a double numerical basis set plus polarization (DNP) and BLYP exchange-correlation functional has also shown to yield reliable results on the relative structures and energetics of silicate clusters. Based on the reliability of the approach, the BLYP functional is employed to optimise the original aluminosilicate clusters, The next section will focus on a detailed account of the method.

2.6.1 Geometry optimisation and thermodynamic property

The procedure is essentially the same as that adopted by Mora-Fonz et al.⁴ in their study of silica clusters, where the approach has shown the reliability of the approach on the relative energy of clusters studied.

All calculations on aluminosilicate clusters are performed by using the DMol³ code²⁵ based on Density Functional Theory (DFT). A double numerical basis set plus polarization (DNP) and BLYP exchange-correlation functional has been shown to yield reliable results on the relative structures and energetics of silicate, aluminate and aluminosilicate clusters and account for the hydrogen bonds well. Based on the reliability of the approach, the BLYP functional was also employed to optimise the original aluminosilicate clusters, setting an energy of 10^{-5} Hartree and maximum displacement of 5×10^{-3} Hartree \AA^{-1} , the gradient of 2×10^{-3} Hartree \AA^{-1} for geometry optimisation convergence and an SCF convergence of 10^{-6} Hartree, along with an orbital cutoff of 5.2 \AA for all types of atoms.

Moreover, it should be stressed, as with the experimental techniques, that to estimate the value of all geometrical properties and energies, there is a degree of error resulting from the measurement of each variable. However, for DFT calculations, the calculated bond lengths, angles and energies express a quantity with integers and decimals. These two quantities of the calculated bond lengths and angles have been rounded to one decimal place and the quantity of the relative energies has been rounded off to the nearest integer. In other words, rounding of variables will introduce some round-off errors in these results. Such round-off errors will be noticeable, but usually not significant since a thorough appraisal of DFT calculations for pure silica clusters, with the similar round-off errors, has provided reliable information which is comparable to the experimental data.

In the geometry optimisation, there is no complete guarantee that the system will reach a global minimum or to know whether the energy minimum is global or local. Hence, in order to avoid generating local minima and ensure global minima to be achieved in the clusters, choosing the optimum starting configurations is an important procedure as the optimisation is carried out. In an aluminosilicate system, a potential energy surface with many local minima may result from the structural

flexibility, and the number of atoms involved especially Na^+ ions. For the structural flexibility, two types of aluminosilicate clusters are chosen to compare the optimised energy, one being linear and the other being curve. On the other hand, taking the appropriate location of the Na^+ ions is particularly important in aluminosilicate clusters due to the electrostatic attraction between clusters and Na^+ ions and electrostatic repulsion between the Na^+ ions that will cause obvious local minima.

Hence, finding the most effective coordination between clusters and Na^+ ions and the longer cation-cation distance is a primary work; the Na^+ ions can be extended more than three coordinations. As for presenting the structure for the deprotonated aluminosilicate clusters, the deprotonated silica clusters have been referred to by highly complete and well refined models, where explicit water molecules are placed surrounding the clusters. The purpose of adding explicit water molecules is to create a shell around both anion and cation so as to obtain accurate electronic energy of the clusters because in the absence of explicit water molecules in the clusters, the stronger electrostatic interaction of the Na^+ ions and the anionic silica clusters will result in an overestimation of the calculated binding energy. Hence, for refining the deprotonated aluminosilicate clusters, the similar model mentioned above can probably be employed.

To do the geometry optimisation, different starting configurations are used to obtain an energy minimum, which is the electronic energy at 0K. The calculation of the Gibbs free energy with the zero-point energy, and the translational, rotational, and vibrational contributions is achieved by a statistical mechanical approach, using a frequency analysis for the geometry optimised aluminosilicate structures. The results allow a series of standard thermodynamic quantities including enthalpy, entropy, and Gibbs free energy at a range of different temperatures to be obtained. In this work, we study the thermodynamic quantities of structures at 298 (room temperature) and 450K that is the typical reaction temperature in zeolite synthesis. Furthermore, given that all calculations for the structures via the above operations are carried out without any kind of outside interaction on them such as solvent, the structures generated can be thought as the “gas phase” clusters in a contrast to the “solvated” ones that are produced in processes of hydrothermal zeolite synthesis.

2.6.2 Modelling the solvent

To model the realistic “solvated” aluminosilicate clusters, COSMO (COnductor-like Screening MOdel) is an inexpensive computational treatment to simulate the effect of solvation on aluminosilicate clusters. As noted above in the COSMO approach, the effect of solvation is simply treated as a dielectric continuum in a self-consistent procedure; but there is no explicit water in aluminosilicate clusters and no chemical interactions such as H-bonding between the aluminosilicate clusters and solvent. The procedure is that the optimised clusters (the “gas phase” clusters) are then re-optimised via the COSMO approach, finally obtaining the optimised structures of the “solvated” aluminosilicate clusters. Here, the Gibbs free energy of the “solvated” aluminosilicate clusters are also calculated by the COSMO approach at 298 and 450K.

2.6.3 The counterions: cation

The structures of aluminosilicate clusters associated with the presence of the cation such as Na^+ ions or a proton bonded to a bridging oxygen can establish more complete and accurate models for the aluminosilicate clusters. For the extra-framework cations, several studies have also indicated that the concentration of the alkali metal indeed influences the formation of clusters in the prenucleation of aluminosilicate zeolites. Thus, arranging the relative location of the counterions (the Na^+ ions) in aluminosilicate structures is clearly of importance. Because of several possibilities for the relative location of cations in the aluminosilicate structures, a comprehensive conformational analysis is not possible for the wide range of clusters studied. The X-ray diffraction analysis for the structures of aluminosilicate zeolites can give us useful information to study plausible locations of the cations. In general, the Na^+ ions have 3 or 4 oxygen neighbours at about 2.3 to 2.7 Å in the structures and their distribution, which has the maximum separation distance in the structures drives them to minimise the electrostatic repulsion between each other.

References:

1. C. R. A. Catlow, D. S. Coombes and J. C. G. Pereira, *Chemistry of Materials*, **1998**, *10*, 3249.
2. J. C. G. Pereira, C. R. A. Catlow and G. D. Price, *Journal of Physical Chemistry A*, **1999**, *103*, 3252.
3. J. C. G. Pereira, C. R. A. Catlow and G. D. Price, *Journal of Physical Chemistry A*, **1999**, *103*, 3268.
4. B. Slater, C. R. A. Catlow, Z. Liu, T. Ohsuna, O. Terasaki and M. A. Camblor, *Angewandte Chemie-International Edition*, **2002**, *41*, 123.
5. A. A. Sokol, C. R. A. Catlow, J. M. Garces and A. Kuperman, *Journal of Physical Chemistry B*, **2002**, *106*, 6163.
6. J. B. Foresman, A. Frisch, *Exploring chemistry with electronic structure methods*, 2nd ed., Gaussian, Pittsburgh, PA, **1996**.
7. P. W. Atkins, J. De Paula, *Atkins' Physical chemistry*, 7th ed., Oxford University Press, Oxford, **2002**.
8. P. W. Atkins, R. S. Friedman, *Molecular quantum mechanics*, 4th ed., Oxford University Press, Oxford, **2004**.
9. I. N. Levine, *Physical chemistry*, 4th ed., McGraw-Hill, New York ; London, **1995**.
10. I. N. Levine, *Quantum chemistry*, 5th ed., Prentice Hall, Upper Saddle River, N.J., **2000**.
11. F. Jensen, *An introduction to computational chemistry*, Wiley, Chichester, **1999**.
12. G. H. Grant, W. G. Richards, *Computational Chemistry*, Oxford University Press, Oxford, **1995**.
13. A. R. Leach, *Molecular Modelling Principles and Applications*, 2nd ed., Prentice Hall, Harlow, **2001**.
14. A. Szabo and N. S. Ostlund. *Modern quantum chemistry: introduction to advanced electronic structure theory*, Now York, Dover Pub. Inc. **1996**.
15. C. Møller and M. S. Plesset, *Physical Review*, **1934**, *46*, 618.
16. J. Čížek, *Journal of Chemical Physics*, **1966**, *45*, 4256.
17. J. Čížek, *Advances in Chemical Physics*, **1966**, *14*, 35.
18. W. Kohn and L. J. Sham, *Physical Review*, **1965**, *140*, 1133.
19. J. VandeVondele and J. Hutter, *Journal of Chemical Physics*, **2007**, *127*, 114105.

20. U. von Barth,; L. Hedin, *Journal of Physics C: Solid State Physics* **1972**, 5, 1629.
21. L. Hedin,; B. I. Lundqvist, *Journal of Physics C: Solid State Physics***1971**, 4, 2064.
22. V. L. Moruzzi,; J. F. Janak,; K. Schwarz, *Physical Review B* **1988**, 37, 2, 790.
23. P. J. Stephens, F. J. Devlin, C. F. Chabalowski and M. J. Frisch, *Journal of Physical Chemistry*, **1994**, 98, 11623.
24. A. D. Becke, *Journal of Chemical Physics*, **1993**, 98, 5648.
25. C. T. Lee, W. T. Yang and R. G. Parr, *Physical Review B*, **1988**, 37, 785.
26. H. Dorsett and A. White. *Overview of molecular modelling and ab initio molecular orbital methods suitable for use with energetic materials*, DSTO Aeronautical and Maritime Research Laboratory **2000**.
27. J. C. Slater, *Physical Review*, **1930**, 36, 57.
28. E. R. Davidson and D. Feller, *Chemical Reviews*, **1986**, 86, 681.
29. J. B. Foresman and A. Frisch. *Exploring chemistry with electronic structure methods*, Gaussian **1996**.
30. R. C. Raffenet, *Journal of Chemical Physics*, **1973**, 58, 4452.
31. A. Schafer, H. Horn and R. Ahlrichs, *Journal of Chemical Physics*, **1992**, 97, 2571.
32. T. H. Dunning, *Journal of Chemical Physics*, **1970**, 53, 2823.
33. T. H. Dunning, *Chemical Physics Letters*, **1970**, 7, 423.
34. A. Schafer, C. Huber and R. Ahlrichs, *Journal of Chemical Physics*, **1994**, 100, 5829.
35. A. Klamt and G. Schuurmann, *Journal of the Chemical Society-Perkin Transactions 2*, **1993**, 799.
36. J. Tomasi and M. Persico, *Chemical Reviews*, **1994**, 94, 2027.
37. B. Delley, *Journal of Chemical Physics*, **1990**, 92, 508.
38. B. Delley, *Journal of Chemical Physics*, **2000**, 113, 7756.
39. Biosym/MSI, DMol USER GUIDE, San Diego, **1995**.
40. M. J. Mora-Fonz, C. R. A. Catlow and D. W. Lewis, *Angewandte Chemie-International Edition*, **2005**, 44, 3082.

Chapter 3

The Stability and Structures of Aluminosilicate Clusters

3.1 Introduction

As discussed in chapter 1, several experimental studies have been attempted to clarify the processes involved in zeolite nucleation. Among them, the definition of the relevant aluminosilicate clusters in zeolite nucleation is the subject of many experimental studies and is generally considered as key information for understanding zeolite nucleation due to the fact that zeolite synthesis is a self-assembly process via various small molecules and clusters. Often-used experimental techniques to investigate the relevant characteristic of the aluminosilicate clusters are NMR spectroscopy¹⁻⁸, mass spectrometry⁹, high-energy X-ray diffraction (HEXRD)¹⁰, extended X-ray absorption spectroscopic (EXAFS)^{11,12} or other scattering techniques such as dynamic light scattering (DLS)¹³ or *in situ* small angle and wide angle X-ray scattering (SAXS/WAXS)^{14,15}. One of the most important experimental technique is NMR spectroscopy, which has provided solid evidence for the presence of a variety of clusters leading to the suggestion that zeolite formation proceeds by the participation of various clusters rather than only one type of cluster.

Relevant aluminosilicate clusters are shown in Figure 3.1. Not all are necessarily involved in the prenucleation and subsequent growth processes. On the other hand, it is noted with interest that according to experimental crystallographic results, some key clusters such as five or six rings that are common units in many known zeolite frameworks are not detected in the synthesis gel¹⁶. Hence, the nature of key aluminosilicate clusters that are involved in aluminosilicate zeolite nucleation remains poorly understood. Therefore, to investigate further the actual nucleation mechanism will be particularly difficult due to the lack of direct evidence of these aluminosilicate clusters. As described in chapter 2, DFT is a powerful tool to define these key aluminosilicate clusters. Indeed, some aluminosilicate clusters have been studied by means of DFT methods¹⁷⁻¹⁹, but the previous work was limited and suffered from the lack of the inclusion of cations or solvation process. Thus, in this chapter, the primary

task is to analyse which are the key aluminosilicate clusters and consider what factors control the presence of these aluminosilicate clusters in the nucleation processes by using molecular simulations employing density functional theory (DFT)²⁰ and Conductor-like Screening Model (COSMO)^{21,22}. The results give considerable insight into the question of aluminosilicate zeolite nucleation.

The structures of the chapter are as follows. First we will present the detailed analysis of the geometric features of the key aluminosilicate clusters such as open clusters and rings that are both consistent and inconsistent with Lowenstein's²³ and Dempsey's rule²⁴. Next, we compare the relative energies of the aluminosilicate clusters to identify which clusters are likely to exist both in the gas phase as well as in COSMO solvation. Moreover, in each case, we will also discuss the factors which influence the cluster structures and energies.

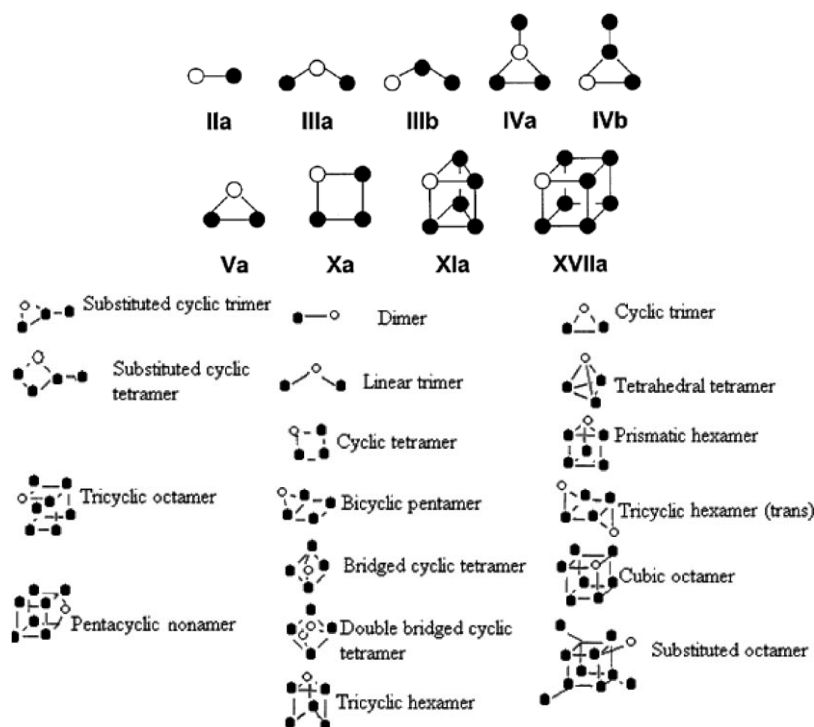


Figure 3.1 Aqueous aluminosilicate species have been presented by ²⁹Si NMR and ²⁷Al NMR spectroscopy¹⁻⁸. Open circles representing Al atoms.

3.2 Methodology

We construct clusters with various Si/Al ratios and arrangements of the extra-framework Na^+ ions used to neutralise the negative frameworks of the aluminosilicate clusters. Clusters also have isomers that are identified by atomic arrangements of Si and Al atoms. More detail of the structures investigated is given below. All calculations on aluminosilicate clusters were performed using the DMol³ code²⁵ based on Density Functional Theory (DFT), as discussed in chapter 2, a double numerical basis set plus polarization (DNP) and BLYP exchange-correlation functional is employed to optimise the original clusters in the gas phase.

These optimised clusters are then re-optimised including Conductor-like Screening Model (COSMO)^{21, 22} used to simulate the solvation of the aluminosilicate clusters. In COSMO approach, the effect of solvation is simply treated as a dielectric continuum in a self-consistent procedure; but there is no explicit water in aluminosilicate clusters during the DFT calculation. The Gibbs free energy, including the zero point energy, the translational, rotational, and vibrational contributions to the energy is calculated with a statistical mechanical approach for the temperatures 298 and 450K.

3.3 Results and Discussion

Our calculation has yielded both energies and structures for the clusters investigated in this work. Hence, in this section, we focus on analysing the detailed geometric features of the bond lengths and angles for the range of aluminosilicate clusters and structural and energetic comparison between the relative isomers. The optimised structures for aluminosilicate clusters in the gas phase and COSMO solvation are obtained from the two types of calculation: BLYP/DNP for the gas phase and BLYP/DNP (COSMO) for solution. However, there is no substantial geometrical difference between the optimised “gas phase” and “solvated” aluminosilicate structures.

In this study, we examine two types of aluminosilicate clusters: open clusters and rings. A range of key aluminosilicate open clusters containing dimers, trimers, tetramers, pentamers and hexamers and rings containing the three, four, five, and six rings are constructed. We consider all possible open clusters and rings containing

between 1 and 6 Si/Al atoms, which are identified with different Si/Al ratios and atomic arrangements of Si and Al atoms, and which both do and do not accord with Lowenstein's and Dempsey's rule. Moreover, we concentrate on the structures obtained by the COSMO method, as we are mainly concerned with the properties of the clusters in solution. A detailed structural description of all optimised aluminosilicate isomers for calculations of COSMO solvation is shown in Figures 3.2-3.68. Moreover, the letters of "A", "B", and "C" are labeled with the Al numbers in these aluminosilicate clusters; the letters of "A", "B", and "C" represent one, two three Al atoms, respectively. The relevant structural parameters (only minimum and maximum values) for aluminosilicate clusters including the calculated Si-O, Al-O and OH bond lengths, the distances between the Na⁺ ions and nearest oxygens, T-O-T angles, O-T-O angles and the hydrogen bonds are shown in Figures 3.2-3.68. In addition, the relative energies of these isomers are also compared in Tables 3.1-3.10. A detailed discussion of the results for the different clusters now follows.

3.3.1 Geometry analysis for open clusters

In this section, we consider the structures and energies of open clusters, with special attention to the effects of Al distribution. Charge neutrality is ensured for all clusters by including the appropriate number of the Na⁺ ions. With an analysis of open cluster, it can explain why open clusters usually serve as nutrient to form cyclic rings.

3.3.1.1 Structures of the Al(OH)₄Na monomer and the AlSiO(OH)₆Na and Al₂O(OH)₆Na₂ dimers

Al(OH)₄Na, AlSiO(OH)₆Na and Al₂O(OH)₆Na₂ are the smallest basic clusters in aluminosilicate zeolites. The relevant structures of Al(OH)₄⁻, AlSiO(OH)₆⁻ and Al₂O(OH)₆²⁻ have been reported in a previous study²⁶. Here we add the counterion (the Na⁺ ions) to neutralise these clusters and analyse the resulting structures of the solvated clusters.

To begin with Al(OH)₄Na (Figure 3.2), we find that the Na⁺ ion is coordinated to the O atoms of the structure, generating an electrostatic attraction between the Na⁺ ion and O atoms; the Na⁺ ion is close to a pair of oxygen atoms (Na-O: 2.29 Å). In general, while an electrostatic attraction forms between the opposite electrically charged bodies, it has a significant effect on bond lengths or bond angles of the

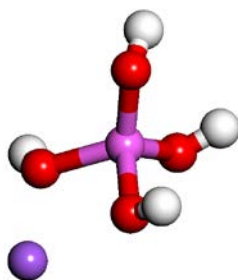
structure. In $\text{Al}(\text{OH})_4\text{Na}$, the strong electrostatic attraction between the Na^+ ion and O atom causes the two $\text{Al}-\text{O}_t$ bonds (where t refers to the terminal-OH) to weaken, varying from 1.79 to 1.82 Å and the $\text{O}_t-\text{Al}-\text{O}_t$ angle decreases remarkably, varying from 118° to 94°.

Both $\text{AlSiO}(\text{OH})_6^-$ and $\text{Al}_2\text{O}(\text{OH})_6^{2-}$ originally contain two hydrogen bonds in each cluster²⁶. However, with the inclusion of the Na^+ ions, there is the competition of the interplay of the Na^+ ions and intramolecular hydrogen bonds in both $\text{AlSiO}(\text{OH})_6\text{Na}$ and $\text{Al}_2\text{O}(\text{OH})_6\text{Na}_2$. Considering first $\text{AlSiO}(\text{OH})_6\text{Na}$ (Figure 3.3), the Na^+ ion is coordinated to the three O atoms in the tetrahedral position by the electrostatic attraction, whereas an intramolecular hydrogen bond forms opposite. Because of the electrostatic attraction between the Na^+ ion and O atom, some geometric features for $\text{AlSiO}(\text{OH})_6\text{Na}$ show the similar trend to $\text{Al}(\text{OH})_4\text{Na}$. The $\text{Si}-\text{O}_t$ and $\text{Al}-\text{O}_t$ bond lengths increase to 1.70 Å and 1.80 Å, respectively; the $\text{O}_t-\text{Al}-\text{O}_b$ bond angle decreases considerably to 96°: much more than the change in the $\text{O}_t-\text{Si}-\text{O}_b$ bond angle (101°). This calculated difference between the $\text{O}_t-\text{Al}-\text{O}_b$ and the $\text{O}_t-\text{Si}-\text{O}_b$ bond angles can be explained by a comparison of the Na-O bond lengths, revealing that the distance of the Na^+ ion bonding to the O atom that is bonded to the Al atom (2.24 Å) is shorter than that to the Si atom (2.33 Å). In other words, the Na^+ ion is more strongly bonded to the O atom that bonds to the Al atom owing to the stronger electrostatic force in comparison with that to the Si atom; thus pulling the $\text{O}_t-\text{Al}-\text{O}_b$ linkage closer so that the bond angle falls to a smaller value. We also find that the $\text{Al}-\text{O}_b-\text{Si}$ angle in $\text{AlSiO}(\text{OH})_6^-$, of 115° (where b refers to the bridging oxygen), increases to 131° in $\text{AlSiO}(\text{OH})_6\text{Na}$ because of the Na^+ ion that produces the electrostatic interaction with the O atoms.

In $\text{AlSiO}(\text{OH})_6\text{Na}$, there is an intramolecular hydrogen bond to be formed. Because the charge on the oxygen bonded to aluminum is larger than on the oxygen bonded to silicon, this hydrogen bond is expected to be stronger, which is confirmed by the smaller O-H distance of 1.77 Å, the typical of hydrogen bonds. It is also worth noting that the bond lengths of the atoms, which are involved in forming the intramolecular hydrogen bond, will change. Indeed, the $\text{Al}-\text{O}_t$ bond acting as the hydrogen bond acceptor becomes longer (1.79 Å) and the $\text{Si}-\text{O}_t$ bond acting as the hydrogen bond donor become shorter (1.67 Å) while the O-H bond acting as the hydrogen bond

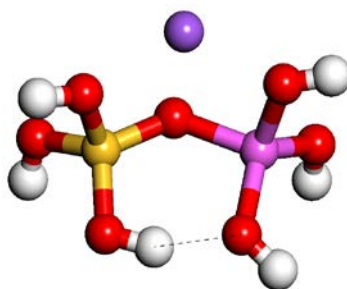
acceptor is similar to the expected value (0.98 Å) and the other one acting as the hydrogen bond donor become longer (1.01 Å). Such changes in the bond lengths can be attributed to the charge redistribution of oxygen or hydrogen atoms. In addition, the difference in valence for Si and Al atoms results in an unequal charge distribution and, as a consequence, a large difference in bond lengths to the bridging oxygen can be found (Si-O_b: 1.65 Å, Al-O_b: 1.83 Å). This change in bond lengths to the bridging oxygen can also be observed in the latter clusters regarding open clusters and rings.

Turning now to Al₂O(OH)₆Na₂ (Figure 3.4), this has the two Na⁺ ions, where each Na⁺ ion is also coordinated to the three O atoms, both in the tetrahedral positions and stronger framework-cation electrostatic attraction, constraining the Al-O_b-Al angle to be close to 180°. The bond elongation and angle reduction caused by the Na⁺ ions is also noted in Al₂O(OH)₆Na₂; the Al-O_t bond lengths are elongated to about 1.81-1.82 Å and the O_t-Al-O_b angles are reduced to about 99-100°. Hence, on comparing with the structures of Al(OH)₄⁻, AlSiO(OH)₆⁻ and Al₂O(OH)₆²⁻, it is clear that the structural conformations of Al(OH)₄Na, AlSiO(OH)₆Na and Al₂O(OH)₆Na₂ are strongly influenced by the Na⁺ ions rather than the intramolecular hydrogen bonds.



Bond angle (°)	COSMO sol.
O_tAlO_t	94-118
Bond length (Å)	
AlO_t	1.79-1.82
NaO	2.29
OH	0.98

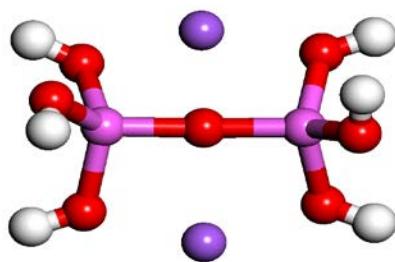
Figure 3.2 $Al(OH)_4Na$. Optimised isomers of aluminosilicate species in COSMO solvation: monomer, dimers, trimers, and tetramers. In all Figures, colour coding as follows: purple spheres represent the Na^+ ion, pink, Al; red, O; and white H atoms. The dashed line represent hydrogen bonds.



Bond angle (°)	COSMO sol.
SiO_bAl	131
O_tSiO_t	104
O_tSiO_b	101-116
O_tAlO_t	107
O_tAlO_b	96-118

Bond length (Å)	COSMO sol.
AlO_b	1.83
AlO_t	1.77-1.80
SiO_b	1.65
SiO_t	1.67-1.70
OH	0.98-1.02
Na-O	2.24-2.33
O-H	1.77

Figure 3.3 $AlSiO(OH)_6Na$



Bond angle (°)	COSMO sol.
O _t AlO _t	176
O _t AlO _t	104
O _t AlO _b	99-123

Bond length (Å)	COSMO sol.
AlO _b	1.77
AlO _t	1.77-1.82
OH	0.98
NaO	2.23-2.44

Figure 3.4 Al₂O(OH)₆Na₂

3.3.1.2 Structures of trimers

We now extend our study to trimers. In trimers (Figures 3.5-3.8), we consider the two types of isomer formed. First, those in which only one Al atom is substituted: trimers A1 and A2 and second, those in which two Al atoms are substituted: trimers B1 and B2.

3.3.1.2.1 One Al atom substitution in trimers

The structures of trimers A1 and A2 are shown in Figures 3.5 and 3.6. In these trimers, the Na⁺ ion is located at the similar position i.e. coordinated to the axial O atoms to form the almost triangular pyramid, but remarkably, the variation of the Na-O bond lengths in trimer A1 (2.29-2.50 Å) is larger than that in trimer A2 (2.23-2.36 Å), which further confirms that in trimer A1, the Na⁺ ion is bonded to the extra bridging O atom to form the fourth coordination with the Na-O distance, of 2.50 Å. Clearly, the strong electrostatic force between the Na⁺ ions and O atoms also causes the change of bond lengths and angles in trimers A1 and A2. The axial bond lengths including the one Al-O_t (trimer A1: 1.80 Å; trimer A2: 1.80 Å) and two Si-O_t bond lengths (trimer A1: 1.69 Å; trimer A2: 1.69-1.70 Å) are longer than the other equatorial Al-O_t or Si-O_t bond lengths; the smallest O_t-Al-O_b bond angle, of 97° is found in trimer A1, but not found in trimer A2. In this case, we find that the change in the O-Al-O angles is related to the nature of the coordination between the Na⁺ ion and O atoms. In trimer A1, the Na⁺ ion coordinating to a pair of oxygen atoms adjacent to the same Al atom, can displace a pair of oxygen atoms to closer, thus reducing the

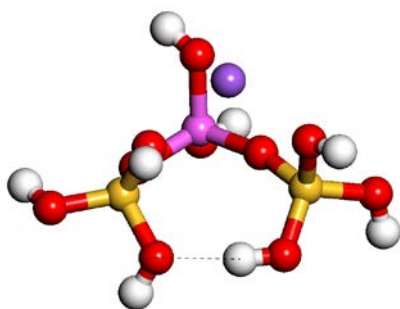
O-Al-O bond angle; in contrast, in trimer A2, the Na⁺ ion coordinating to different isolated oxygen atoms has no change in the O-Al-O bond angle. More evidence can be obtained to confirm this statement by the observation of the later clusters.

As we noted earlier, the hydrogen bonds will affect bond lengths. In trimer A1, the outer Si-O_t bond acting as the hydrogen bond acceptor is longer (1.69 Å) whereas the other acting as the hydrogen bond donor is shorter (1.67 Å). Similarly, in trimer A2, the outer Al-O_t bond acts as the hydrogen bond acceptor that produces the longer Al-O_t bond of 1.80 Å and the outer Si-O_t bond acts as the hydrogen bond donor that produces the shorter Si-O_t bond of 1.65 Å. On the other hand, the hydrogen bond (O--H) formed by the aluminum-bonded oxygen of trimer A2 is much stronger (1.60 Å) than the silica-bonded oxygen of trimer A1 (1.91 Å), which can also be confirmed by the corresponding OH donors, with the OH bond lengths of 1.03 Å and 0.99 Å, respectively.

Since trimer A1 is the symmetrical structure, we expect that when the Al atom occupies the centre of the structure, the Si-O_b bond lengths and the Al-O_b-Si angles would remain constant. Indeed, the Si-O_b bond lengths of trimer A1, with the central Al atom remain constant but the Si-O_b bond lengths of trimer A2, which has a the terminal Al atom, vary considerably (1.62 to 1.67 Å), reflecting its asymmetrical structure. However, the range of Al-O_b-Si angles in trimer A1 is generally larger (132-166°) while the range of T-O_b-T angles (the Al-O_b-Si or Si-O_b-Si angles) in trimer A2 remain constant (141°-144°). To explain the question of the large variation of Al-O_b-Si angles in trimer A1, the effect of the hydrogen bond is considered.

As mentioned earlier, trimer A2 has the stronger hydrogen bond; such a strong driving force could effectively make the adjacent distance of the Al-O_t and Si-O_t bonds much closer, which helps reinforce the formation of the almost cyclic structure, owing to the smaller variation of the Al-O_b-Si and Si-O_b-Si angles. The hydrogen bond formed by the two adjacent Si-O_t bonds found in trimer A1 is much weaker in driving formation of the cyclic structure, thus resulting to the large degree, the change of the Al-O_b-Si angles. The effect of the hydrogen bonds, therefore, probably gives us the rationalisation for the difference of the T-O_b-T angles in trimers A1 and A2. As discussed above, the considerable variation of bond lengths and angles observed in

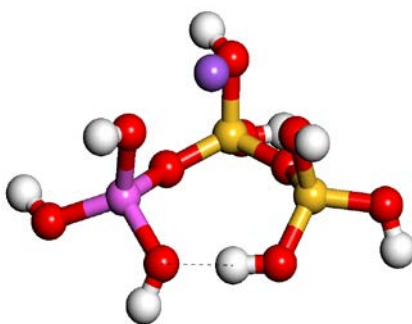
trimers A1 and A2 indicates that the interplay of the Na^+ ions and hydrogen bonds indeed impacts on the cluster structures. The similar behaviour can also be found in the following large clusters.



Bond angle ($^\circ$)	COSMO sol.
SiO_bAl	132-166
O_tSiO_t	102-113
O_tSiO_b	101-117
O_tAlO_t	119
O_tAlO_b	97-119
O_bAlO_b	106

Bond length (\AA)	COSMO sol.
AlO_b	1.79-1.80
AlO_t	1.76-1.80
SiO_b	1.62
SiO_t	1.67-1.69
OH	0.99-1.00
NaO	2.29-2.50
O--H	1.91

Figure 3.5 Trimer A1



Bond angle ($^\circ$)	COSMO sol.
SiO_bAl	141
SiO_bSi	144
O_tSiO_t	106-114
O_tSiO_b	101-114
O_bSiO_b	114
O_tAlO_t	107-115
O_tAlO_b	103-116

Bond length (\AA)	COSMO sol.
AlO_b	1.79
AlO_t	1.77-1.81
SiO_b	1.62-1.67
SiO_t	1.65-1.70
OH	0.98-1.03
NaO	2.23-2.37
O--H	1.60

Figure 3.6 Trimer A2

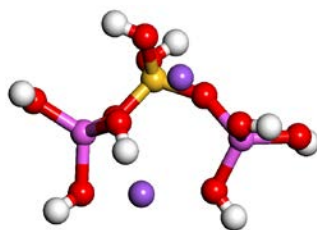
3.3.1.2.2 Two Al atom substitutions in trimers

Trimer B1 with the Al-Al separation and trimer B2 with the Al-O-Al linkage, as shown in Figures 3.7 and 3.8, are now considered. The position of the Na^+ ions in trimer B1 is significantly different to that in trimer B2. In trimer B1, one Na^+ ion is bonded to the three axial O atoms and the other is bonded to the two equatorial and one bridging O atoms, with the distances of 2.27-2.73 Å; whereas in trimer B2, one Na^+ ion is bonded to the four outer terminal O atoms and the other Na^+ ion is bonded to the two equatorial and one bridging O atoms with the distances of 2.26-2.48 Å.

On examining the variation of bond lengths and angles of trimers B1 and B2, the electrostatic attraction between the Na^+ ions and O atoms apparently causes not only the elongation of the Si-O_t and Al-O_t bond lengths, of respectively, to 1.70 and 1.82 Å in trimer B1 and 1.70 and 1.81 Å in trimer B2 but also the smallest angles of O_t-Al-O_b (96°) in trimer B1 and of the O_t-Si-O_t (99°) and O_t-Al-O_t (93°) in trimer B2, again illustrating the nature of the coordination between the Na^+ ions and O atoms, where the Na^+ ion is coordinated to a pair of oxygen atoms adjacent to the same Al atom. Moreover, as mentioned earlier, the change in the Si-O_b and Al-O_b bond lengths mainly results from the unequal charge distribution between Al and Si atoms, but the Na^+ ions probably results in the small increase in the Si-O_b and Al-O_b bond lengths. The analysis of the Si-O_b and Al-O_b bond lengths for trimer B1 reveals that the value of the Si-O_b and Al-O_b bond lengths, due to the Na^+ ion slightly increases about 0.01-0.03 Å. To explain this we note that in trimer B1, because the Na^+ ion is located within the ring and coordinates to the bridging O atom, the bridging O atom will donate charge to the Na^+ ion, thus making the Si-O_b and Al-O_b bond lengths increase slightly. This phenomenon can also be observed in the larger clusters.

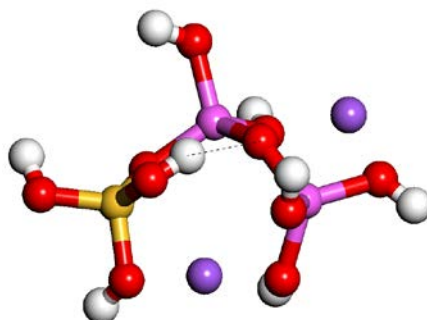
On the other hand, the comparison of the T-O_b-T angles in trimers B1 and B2 reveals that the variation of T-O_b-T angles, trimer B1 (129-150°) and B2 (128-145°) are similar, varying over the large range. According to the case of $\text{Al}_2\text{O}(\text{OH})_6\text{Na}_2$, the stronger framework-cation electrostatic attraction will lead to the larger Al-O_b-Al angle, which is confirmed by the Al-O_b-Al angle of trimer B2, calculated as 145°. However, the large T-O_b-T angle range is also presented in trimer B1. This result may be explained by the fact that in trimer B1, the almost cyclic conformation formed due to the stronger framework-cation electrostatic attraction is strained, resulting in the

structural deformation. Overall, the structural features of trimers B1 and B2 are clearly affected by the Na^+ ions.



Bond angle ($^\circ$)	COSMO sol.	Bond length (\AA)	COSMO sol.
SiO_bAl	129-150	AlO_b	1.79-1.82
O_tSiO_t	112	AlO_t	1.76-1.81
O_tSiO_b	102-113	SiO_b	1.63-1.64
O_bSiO_b	109	SiO_t	1.67-1.70
O_tAlO_t	107-120	OH	0.98-0.99
O_tAlO_b	96-119	NaO	2.27-2.73

Figure 3.7 Trimer B1



Bond angle ($^\circ$)	COSMO sol.	Bond length (\AA)	COSMO sol.
SiO_bAl	128	AlO_b	1.78-1.81
AlO_bAl	145	AlO_t	1.79-1.81
O_tSiO_t	99-112	SiO_b	1.63
O_tSiO_b	111-117	SiO_t	1.68-1.70
O_tAlO_t	93-120	OH	0.98-1.00
O_tAlO_b	101-115	NaO	2.26-2.48
		O--H	2.01

Figure 3.8 Trimer B2

3.3.1.3 Structures of tetramers

Moving to tetramers, there are six different isomers that form almost cyclic structures: two isomers with one Al atom substitutional are tetramers A1 and A2 and four isomers with two Al atoms substitutionals are tetramers B1, B2, B3 and B4.

3.3.1.3.1 One Al atom substitution in tetramers

Let us now consider tetramers A1 and A2. Figures 3.9 and 3.10 show that in tetramer A1, the Al atom is arranged at the terminal site of tetramer A1 and at the interior site of tetramer A2; the two tetramers have almost cyclic conformations. The structural features are affected not only by the Na⁺ ion, but also by the hydrogen bonds.

In tetramer A1, the Na⁺ ion is located among the four outer terminal O atoms, with the calculated Na-O distances of 2.23-2.68 Å; in tetramer A2, the Na⁺ ion is located among the three axial O and one bridging O atoms, with the calculated Na-O distances of 2.36-2.63 Å. Apparently, the Na⁺ ions of tetramers A1 and A2 are positioned at different locations.

Again, while the Na⁺ ion coordinating to the O atoms generates a strong electrostatic force, the significant variation in bond lengths as well as bond angles is observed in tetramers A1 and A2. The Al-O_t and Si-O_t bond lengths of tetramer A1 are weaker and longer, at 1.83 Å and 1.68 Å and those of tetramer A2, are 1.82 Å and 1.70 Å. As for the change in the O-T-O angles, while the Na⁺ ion coordinates to a pair of O atoms in tetramer A1, the O_t-Al-O_t angle (95°) is much smaller than that of the O_t-Si-O_t angle (104°), showing the tendency of the Na⁺ ion to coordinate to a pair of O atoms adjacent to the same Al atom (2.23-2.41 Å) rather than to the Si atom (the Na-O: 2.38-2.67 Å). However, tetramer A2 shows a typical change in the O_t-Al-O_b angle (102°) although the Na⁺ ion coordinates to a pair of O atoms. Probably, the O atom of the Al-O_t bond acting as the hydrogen bond acceptor influences the change in the O-Al-O angle in tetramer A2.

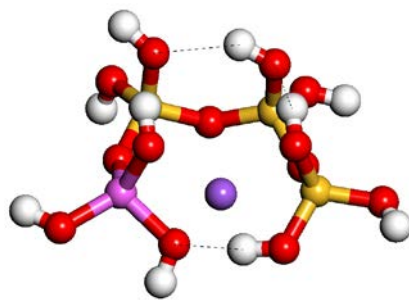
To summarise, the observation of the change in the O-T-O angle from dimers, trimers and tetramers, therefore, reveals two important features: (i) The Na⁺ ion tends to coordinate to the aluminum-bonded oxygens to form the stronger electrostatic force rather than that to the silica-bonded oxygens. (ii) When the Na⁺ ion is coordinated to a pair of O atoms adjacent to the same Al/Si atom, with the consequent reinforce the

electrostatic force between the Na^+ ion and O atoms, the considerable reduction of the O-T-O bond angle, especially in the $\text{O}_t\text{-Al-O}_t$ bond angle, can be observed.

As in tetramers A1 and A2, there are several intramolecular hydrogen bonds to be formed. First, in tetramer A1, the three hydroxyl groups in the axial positions form a system of two hydrogen bonds, with O--H distances of 2.02-2.14 Å, showing the Si-O_t bonds of 1.67-1.68 Å whereas in the isolated hydrogen bond, the outer Al-O_t bond acting as the hydrogen bond acceptor is 1.83 Å and the outer Si-O_t bond acting as the hydrogen bond donor is 1.66 Å. It is worth noting that owing to the hydrogen bonds, the Si-O_t bond acting as the hydrogen bond donor would be a little shorter than normal Si-O bond lengths (1.66-1.67 Å). However, such a change is only observed with the isolated hydrogen bond, but with a system of two hydrogen bonds. This can be explained by two factors: first, in a system of two hydrogen bonds, the hydroxyl group acts as both the donor and acceptor simultaneously, showing the intermediate Si-O_t bond; second, the electrostatic attraction between the Na^+ ion and O atoms impacts on the Si-O_t bond (the hydrogen bond donor), elongating the bond length. The interplay between the Na^+ ion and hydrogen bonds could rationalise the change in the Si-O_t bond length.

For tetramer A2, there are two different systems of hydrogen bonds: one is from the three axial hydroxyl groups (O--H:1.72-2.59 Å) to form a system of two hydrogen bonds, with distances of Al-O_t 1.83 Å and Si-O_t 1.69 Å and the other is from the three outer terminal hydroxyl groups (O--H:1.88-2.10 Å) to form a system of three hydrogen bonds, with 1.66-1.70 Å in Si-O_t bonds. The change in the bond lengths also shows the similar behaviour to tetramer A1 due to the interplay between the Na^+ ion and the hydrogen bonds. In addition to the hydrogen bonds causing significant variation in the bond lengths, the observation of the change in T-O_b-T angles in tetramers A1 and A2 reveals that the T-O_b-T angles in tetramer A1 remains very close (136°) as well as in tetramer A2 (132-136°), which probably are modified by the appearance of a system of hydrogen bonds.

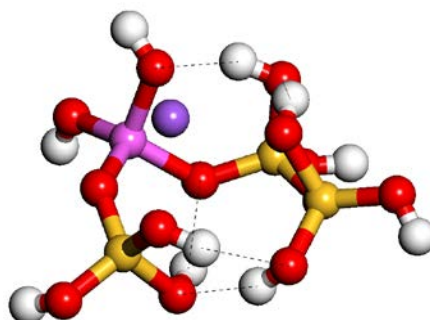
Overall, the geometrical analysis of tetramers A1 and A2 indicates that the variation of bond lengths and angles depends on the interplay of the Na^+ ion and hydrogen bonds.



Bond angle (°)	COSMO sol.
SiO _b Al	136
O _t SiO _t	104-114
O _t SiO _b	105-115
O _b SiO _b	110-113
O _t AlO _t	95-118
O _t AlO _b	109-115

Bond length (Å)	COSMO sol.
AlO _b	1.78
AlO _t	1.77-1.83
SiO _b	1.62-1.68
SiO _t	1.66-1.68
OH	0.98-1.02
NaO	2.23-2.68
O--H	1.72-2.14

Figure 3.9 Tetramer A1



Bond angle (°)	COSMO sol.
SiO _b Al	132-136
SiO _b Si	128
O _t SiO _t	104-113
O _t SiO _b	105-114
O _b SiO _b	112
O _t AlO _t	108
O _t AlO _b	102-120
O _b AlO _b	104

Bond length (Å)	COSMO sol.
AlO _b	1.79-1.80
AlO _t	1.75-1.82
SiO _b	1.63-1.68
SiO _t	1.66-1.70
OH	0.98-1.01
NaO	2.36-2.63
O--H	1.72-2.59

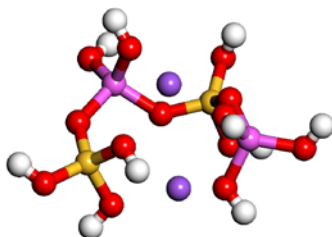
Figure 3.10 Tetramer A2

3.3.1.3.2 Two Al atom substitutions in tetramers

Considering now cluster in which two Al atoms are employed to substitute for two Si atoms in tetramers, four different isomers are formed, as shown in Figures 3.11-3.14; tetramers B1 and B2 are “Lowensteinian” structures and tetramers B3 and B4 are “non-Lowensteinian” structures. First, we consider two Lowensteinian structures: tetramer B1 with alternating Al atoms and tetramer B2 with the maximum Al-Al separation (Figures 3.11-3.12). We find that each Na^+ ion is coordinated to the nearest four O atoms to form an almost cyclic structure in these tetramers. To begin with tetramer B1, one Na^+ ion is located above the plane to coordinate to the three axial O and one bridging O atoms, with bond lengths of 2.26 and 2.54 Å while the other is located below the opposite plane to coordinate to the three equatorial O and one bridging O atoms, with bond lengths of 2.31 and 2.49 Å. As for tetramer B2, one Na^+ ion is located above the plane to coordinate to the three axial O and one bridging O atoms, with bond lengths of 2.32-2.52 Å while the other is located below the opposite plane to coordinate to the two equatorial O and two bridging O atoms, with bond lengths of 2.26-2.57 Å. As a result, the Na^+ ions are located in the similar position in tetramers B1 and B2; but the interesting aspect of the geometry shows that the magnitude of the structural distortion differs from tetramers B1 and B2, which is probably due to the different arrangement of Al atoms in these tetramers.

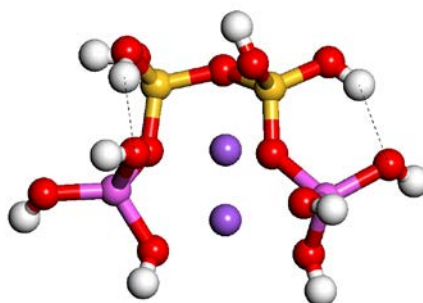
The main structural distortion can be explained by the electrostatic interaction between the Na^+ ions and aluminum-bonded O atoms. We recall from our analysis of the trimer structures, that the Na^+ ion tends to coordinate to the aluminum-bonded oxygens. Hence, we find that in tetramer B1, the strong electrostatic force drives the interior aluminum-bonded O atom to displace so as to coordinate to the Na^+ ion, resulting in the significant structural distortion, but the structural distortion is very weak in tetramer B2. The Na^+ ion, of course, makes the clear change in the relative structural parameters in tetramers B1 and B2. The Al-O_t and Si-O_t bond lengths extend to 1.80 and 1.69 Å in tetramer B1 and 1.82 and 1.69 Å in tetramer B2; the $\text{O}_t\text{-Si-O}_b$ and $\text{O}_t\text{-Al-O}_b$ angles reduce to 99° and 96° in tetramer B1 and the $\text{O}_t\text{-Al-O}_b$ angle reduces to 95° in tetramer B2 due to the way in which the Na^+ ion is coordinated to a pair of O atoms bonded to the same Al atom. However, for the change in the $\text{T-O}_b\text{-T}$ angles of tetramers B1 and B2, the range of the $\text{T-O}_b\text{-T}$ change in tetramer B1 (129-134°) is very close to that in tetramer B2 (126-132°), which reflects the

similarity of the location of Na⁺ ions. Certainly, the Na⁺ ions is the major factor in influencing the conformation of tetramers B1 and B2.



Bond angle (°)	COSMO sol.	Bond length (Å)	COSMO sol.
SiO _b Al	129-134	AlO _b	1.80-1.81
O _t SiO _t	103-113	AlO _t	1.77-1.80
O _t SiO _b	99-116	SiO _b	1.63-1.65
O _b SiO _b	112	SiO _t	1.68-1.69
O _t AlO _t	106-118	OH	0.98-0.99
O _t AlO _b	96-118	NaO	2.26-2.54
O _b AlO _b	103	Al-Al	5.22

Figure 3.11 Tetramer B1



Bond angle (°)	COSMO sol.	Bond length (Å)	COSMO sol.
SiO _b Al	130-132	AlO _b	1.82-1.83
SiO _b Si	126	AlO _t	1.77-1.82
O _t SiO _t	109-113	SiO _b	1.64-1.69
O _t SiO _b	102-115	SiO _t	1.67-1.69
O _b SiO _b	110-112	OH	0.98-1.00
O _t AlO _t	104-120	NaO	2.26-2.57
O _t AlO _b	95-120	O--H	2.08-2.26
		Al-Al	5.23

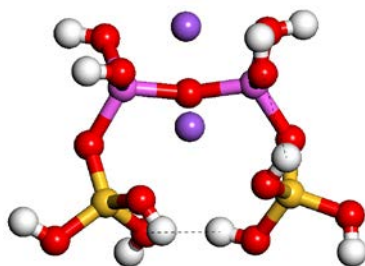
Figure 3.12 Tetramer B2

Moving now to tetramers B3 and B4 (Figures 3.13 and 3.14). Here, the distinct structural feature is that there is an interior Al-O_b-Al linkage in tetramer B3 and a terminal Al-O_b-Al one in tetramer B4. The comparison of the location of the Na⁺ ions in their structures reveals that they have the similar geometrical feature: one Na⁺ ion is coordinated to the three aluminium-bonded O atoms in the tetrahedral position outside the plane and the other is located in the centre among the four axial oxygen atoms, calculated at 2.28-2.70 Å in tetramer B3 and 2.28-2.80 Å in tetramer B4.

With the interplay of the Na⁺ ions and hydrogen bonds, the bond lengths in tetramers B3 and B4 again vary considerably. The Al-O_t and Si-O_t bond lengths elongate to 1.81 Å and 1.70 Å in tetramer B3 and 1.81 Å and 1.69 Å in tetramer B4, showing the similar trend. An important distinction between tetramers B3 and B4 is the formation of the hydrogen bonds. The former with two outer terminal Si-O_t bonds forms a weaker hydrogen bond (O--H) of 1.98 Å whereas the latter through the outer terminal Si-O_t and Al-O_t bonds forms stronger hydrogen bond (O--H) of 1.67 Å.

Moreover, owing to the close proximity of the Na⁺ ions that form the symmetrical electrostatic attraction with the O atoms, the T-O_b-T angle in tetramers B3 and B4 shows a wider range of about 30° to 40° comparable to other tetramers. The Al-O_b-Al angles of tetramer B3, with 156° and tetramer B4, with 161° are much larger than the other T-O_b-T angles, which explains why, in tetramers B3 and B4, the two Na⁺ ions are symmetrically located at tetrahedral sites to coordinate with the aluminum-bonded O atoms of the Al-O_b-Al linkage.

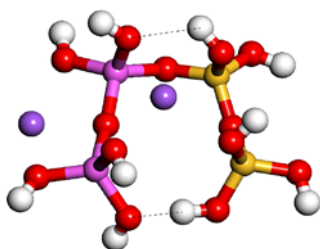
The detailed analysis of the structures of trimers and tetramers has revealed the competition between the interplay of the Na⁺ ions and hydrogen bonds. The similar behaviour will be noted in the larger clusters discussed below.



Bond angle (°)	COSMO sol.
SiO _b Al	127-129
AlO _b Al	156
O _t SiO _t	102-113
O _t SiO _b	108-117
O _t AlO _t	117-118
O _t AlO _b	102-112
O _b AlO _b	112

Bond length (Å)	COSMO sol.
AlO _b	1.76-1.80
AlO _t	1.79-1.81
SiO _b	1.62
SiO _t	1.67-1.70
OH	0.98-0.99
NaO	2.28-2.70
O--H	1.98-2.38

Figure 3.13 Tetramer B3



Bond angle (°)	COSMO sol.
SiO _b Al	125
SiO _b Si	143
AlO _b Al	161
O _t SiO _t	109-113
O _t SiO _b	104-114
O _b SiO _b	115
O _t AlO _t	104-119
O _t AlO _b	100-116
O _b AlO _b	110

Bond length (Å)	COSMO sol.
AlO _b	1.76-1.80
AlO _t	1.78-1.81
SiO _b	1.63-1.67
SiO _t	1.65-1.69
OH	0.98-1.03
NaO	2.28-2.80
O--H	1.67-2.21

Figure 3.14 Tetramer B4

3.3.1.4 Structures of pentamers

In this section, there are 15 isomers in pentamers to be investigated. Note that no more than three Al atoms can be accommodated in such clusters without violating Lowenstein's rule, and that a large number of isomers are possible. It is also more difficult to achieve the Na^+ coordination that avoids substantial framework distortion or collapse, especially in the asymmetrical clusters. Moreover, as for the smaller clusters, the Na^+ ion is more stable when binding with three or four O atoms when they are bonded to Al atoms rather than Si atoms. As expected, we find that the Na^+ coordination of all pentamers and hexamers has the similar features.

3.3.1.4.1 One Al atom substitution in pentamers

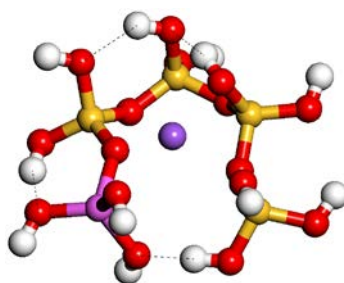
Pentamers in which only one Al atom is substituted in pentamers, form three isomers: pentamer A1 with a terminal Al atom, pentamer A2 with an interior asymmetrical Al atom, and pentamer A3 with an interior symmetrical Al atom. Inspection of Figures 3.15, 3.16 and 3.17 shows that there is clear difference in the conformations for pentamers A1, A2 and A3, exhibiting the "open chair", "open like-chair" and "open crown" forms, respectively. To clarify this, it is necessary to compare the structural parameters of all pentamers.

In pentamer A1, the Na^+ ion locates above the cluster plane to bond to the three axial O and one bridging O atoms (Na-O bond: 2.35-2.45 Å) while the other axial hydroxyl groups form a system of two hydrogen bonds, with the O--H distances of 1.98-2.01 Å. In pentamer A2, the Na^+ ion lies below the cluster plane to bond to the two equatorial and two bridging O atoms (2.38-2.82 Å) whereas a system of three hydrogen bonds through the participation of the four axial hydroxyl groups is formed on the opposite side (1.63-2.17 Å). As for pentamer A3, the Na^+ ion locates at the centre of the cluster plane to coordinate with the two equatorial and two bridging O atoms with an Na-O distance of 2.36-2.46 Å. According to these descriptions, the different conformations formed can be attributed to the distinct site of Al atoms in the frameworks of these pentamers that produce the varying degrees of competition of the interplay between the Na^+ ion and hydrogen bonds.

Due to the cooperation of the Na^+ ion and hydrogen bonds, the similar behaviour is found in these pentamers, where the bond lengths and angles change considerably. The range in the Al-O_t and Si-O_t bond lengths of pentamers A1, A2 and A3 is

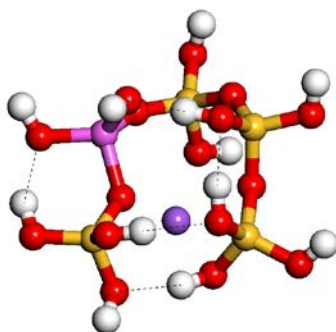
1.78-1.80 Å and 1.65-1.69 Å, 1.77-1.80 Å and 1.66-1.69 Å and 1.77-1.78 Å and 1.65-1.68 Å, respectively. The shortest Si-O_t bond formed acts as the hydrogen bond donor. Similarly, as noted for the trimer, the manner in which the Na⁺ ion bonds to a pair of O atoms adjacent to the same Al atom causes reduction in the O-Al-O angles in pentamers A1 and A3, calculated at 95° and 99° respectively.

For these pentamers, we also consider the variation of the T-O_b bond lengths and T-O_b-T bond angles when the Al atom is located at different sites in the frameworks. In all cases, the Si-O_b bond adjacent to the Al-O_b bond is about 1.62-1.64 Å shorter than to the other Si-O_b bonds due to the unequal charge of Si and Al atoms. Moreover, as for pentamer A3, the Si-O_b-Al and Si-O_b-Si bond angles are to be found in the range of 130-132° and 136-139° (almost constant), which are less wide than found in pentamers A1 and A2. This difference can be explained by the fact that the location of the Al atom at the middle interior site generates the high-symmetry structure in pentamer A3, thus causing the small distortion in pentamer A3. It is, of course, evident that having the highly symmetrical geometry in pentamer A3, the Al-O_b and Si-O_b bond lengths as well as the Si-O-Al and Si-O-Si bond angles can be regularly distributed, but not in pentamers A1 and A2.



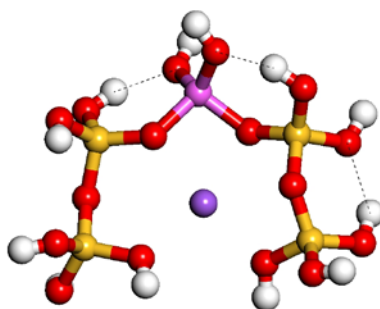
Bond angle (°)	COSMO sol.	Bond length (Å)	COSMO sol.
SiO _b Al	131	AlO _b	1.83
SiO _b Si	130-137	AlO _t	1.78-1.80
O _t SiO _t	106-114	SiO _b	1.64-1.69
O _t SiO _b	103-113	SiO _t	1.65-1.69
O _b SiO _b	109-114	OH	0.98-1.03
O _t AlO _t	106-124	NaO	2.35-2.45
O _t AlO _b	95-114	O--H	1.64-2.01

Figure 3.15 Pentamer A1



Bond angle (°)	COSMO sol.	Bond length (Å)	COSMO sol.
SiO _b Al	131-137	AlO _b	1.77-1.83
SiO _b Si	125-145	AlO _t	1.77-1.80
O _t SiO _t	106-114	SiO _b	1.62-1.68
O _t SiO _b	104-116	SiO _t	1.66-1.69
O _b SiO _b	107-113	OH	0.98-1.00
O _t AlO _t	117	NaO	2.38-2.82
O _t AlO _b	102-116	O--H	1.62-2.00
O _b AlO _b	104		

Figure 3.16 Pentamer A2



Bond angle (°)	COSMO sol.	Bond length (Å)	COSMO sol.
SiO _b Al	130-132	AlO _b	1.80-1.81
SiO _b Si	136-139	AlO _t	1.77-1.78
O _t SiO _t	105-114	SiO _b	1.62-1.69
O _t SiO _b	102-116	SiO _t	1.65-1.68
O _b SiO _b	105-106	OH	0.97-1.00
O _t AlO _t	117	NaO	2.36-2.46
O _t AlO _b	102-118	O--H	1.81-2.10
O _b AlO _b	99		

Figure 3.17 Pentamer A3

3.3.1.4.2 Two Al atom substitutions in pentamers

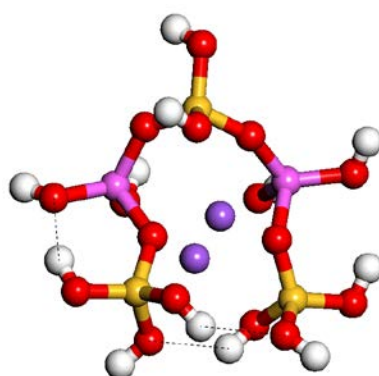
As pentamers contain two Al atoms, there are six isomers to be formed including four Lowensteinian structures: pentamers B1, B2, B3 and B4 and two non-Lowensteinian structures: pentamers B5 and B6. Let us first consider four Lowensteinian structures, as presented in Figures 3.18-3.21: pentamer B1 with two interior alternate Al atoms, pentamer B2 with two terminal Al atoms, pentamers B3 and B4 with two types of arrangements with one interior and one terminal Al atoms.

In contrast to pentamers A1, A2 and A3, the conformation of pentamers B1, B2, B3 and B4 exhibit the geometrical similarity, giving the “open chair” form. A rationale for the structural similarity in these pentamers is that there is the similar framework-cation electrostatic attraction. As can be seen in Figures 3.18-3.21, the two Na⁺ ions are placed at the similar position (on opposite sides of the structure) in each framework where one Na⁺ ion is located above the plane and the other is located below the plane; the two Na⁺ ions bond to two types of oxygen atoms: the axial and bridging O atoms and as a result form the similar Na-O distances in pentamers B1, B2, B3 and B4, calculated as 2.36-2.86 Å, 2.31-2.79 Å, 2.38-2.87 Å and 2.35-2.79 Å, respectively.

Moreover, in each pentamer, the range of Na-O bond distances are wider than in the other clusters discussed above, which is due to the increase in the Na⁺ coordination number from four to five. This is especially true for pentamer B2, which is the highly symmetrical structure with each Na⁺ ion bonding to up to the five O atoms. With regards to charge distribution, such a coordination will decrease the negative charges of structures more effectively. We also find that due to the structural similarity, the symmetrical distribution of the hydrogen bonds is formed in pentamers B1, B2 and B4 although the strength and number of hydrogen bonds is not identical. The interplay of the Na⁺ ions and hydrogen bonds, without exception, gives rise to the change in bond lengths and angles in the structures, showing the typical variation of the Si-O_t and Al-O_t bonds in pentamers. The O-Al-O angle in pentamers B2, B3, and B4 shows the large reduction (95-96°) for the same reason as for the previously discussed clusters.

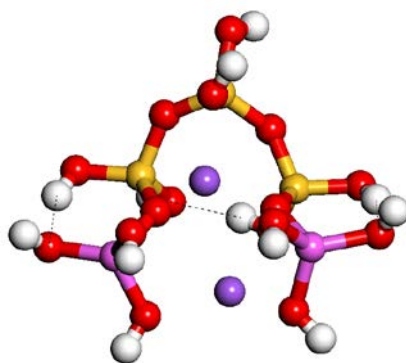
Moreover, clusters with the highly symmetrical distribution of Al atoms such as pentamers B1 or B2 usually impose the symmetry constraint and their conformations

suffer very little distortion. Pentamer B2, as expected, has almost the same Si-O_b-Al and Si-O_b-Si angles, of 129-130° and 132-136°, respectively. However, in pentamer A1, the Si-O_b-Al angles of pentamer B1 have the surprisingly large range (130-154°). Such behaviour is unexpected when pentamer B1 is the symmetrical structure. To investigate this question, we find that the Al-Al distance in pentamer B1 is very close at 4.51 Å causing the stronger electrostatic repulsion between Al atoms in pentamer B1 than in other pentamers (5.13-5.66 Å). Such a strong electrostatic repulsion probably leads to the large structural strain in pentamer B1, with the Si-O_b-Al angle extending to 154°.



Bond angle (°)	COSMO sol.	Bond length (Å)	COSMO sol.
SiO _b Al	130-154	AlO _b	1.77-1.84
O _t SiO _t	106-112	AlO _t	1.77-1.79
O _t SiO _b	100-112	SiO _b	1.64
O _b SiO _b	117	SiO _t	1.66-1.70
O _t AlO _t	112-118	OH	0.98-1.01
O _t AlO _b	100-113	NaO	2.36-2.86
O _b AlO _b	101-106	O--H	1.85-2.38
		Al-Al	4.51

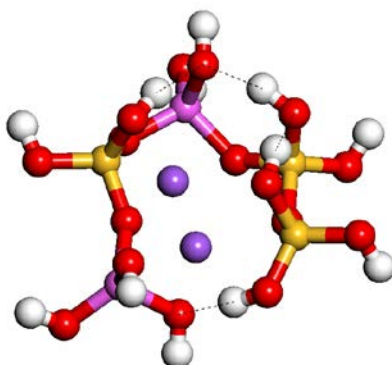
Figure 3.18 Pentamer B1



Bond angle (°)	COSMO sol.
SiO _b Al	129-130
SiO _b Si	132-136
O _t SiO _t	107-110
O _t SiO _b	106-115
O _b SiO _b	110-112
O _t AlO _t	112-121
O _t AlO _b	95-118

Bond length (Å)	COSMO sol.
AlO _b	1.83
AlO _t	1.78-1.79
SiO _b	1.64-1.68
SiO _t	1.66-1.69
OH	0.98-1.00
NaO	2.31-2.79
O--H	1.88-2.03
Al-Al	5.13

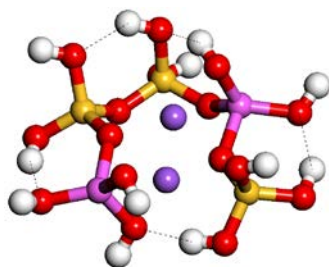
Figure 3.19 Pentamer B2



Bond angle (°)	COSMO sol.
SiO _b Al	129-151
SiO _b Si	129
O _t SiO _t	106-111
O _t SiO _b	104-114
O _b SiO _b	105-112
O _t AlO _t	108-119
O _t AlO _b	95-118
O _b AlO _b	104

Bond length (Å)	COSMO sol.
AlO _b	1.78-1.82
AlO _t	1.76-1.82
SiO _b	1.64-1.70
SiO _t	1.65-1.70
OH	0.98-1.02
NaO	2.38-2.87
O--H	1.66-1.98
Al-Al	5.66

Figure 3.20 Pentamer B3

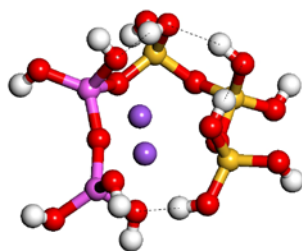


Bond angle (°)	COSMO sol.	Bond length (Å)	COSMO sol.
SiO _b Al	129-132	AlO _b	1.79-1.84
SiO _b Si	131	AlO _t	1.78-1.81
O _t SiO _t	108-113	SiO _b	1.64-1.69
O _t SiO _b	103-114	SiO _t	1.67-1.70
O _b SiO _b	107-110	OH	0.98-1.01
O _t AlO _t	110-126	NaO	2.35-2.79
O _t AlO _b	96-114	O--H	1.88-2.40
O _b AlO _b	99	Al-Al	5.17

Figure 3.21 Pentamer B4

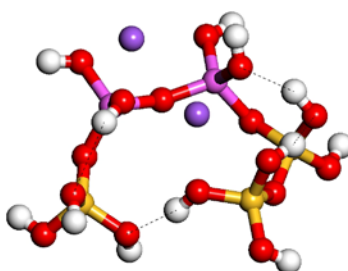
We consider now non-Lowensteinian structures: pentamer B5 with the terminal Al-O-Al linkage and pentamer B6 with the interior Al-O-Al linkage, as shown in Figures 3.22 and 3.23. Again when the Al-O-Al linkage is formed in the structures, the two Na⁺ ions are symmetrically close to the Al-O-Al linkage and coordinate with the aluminum-bonded O atoms, calculated as 2.37-2.57 Å in pentamer B5 and 2.34-2.66 Å in pentamer B6. The difference between pentamers B5 and B6 is the Na⁺ location, where in the former, the Na⁺ ion is located within the cluster plane whereas in the latter, it is located outside the cluster plane. Given the distortion of the structure, pentamer B6 probably lacks available space for any Na⁺ ion to be situated within the structure.

The considerable variation of bond lengths and angles is still observed in pentamers B5 and B6, because of the interplay of the Na⁺ ions and hydrogen bonds. It is notable that the calculated Al-O_t bond lengths of pentamers B5 and B6 increase to 1.83-1.84 Å longer than others, which is due to the fact that the O atoms not only donate charge to the Na⁺ ions but also are bonded to the hydrogen atom forming the hydrogen bonds. Moreover, the significant change in the Al-O_b-Al angle is much larger (pentamer B5: 165°; pentamer B6: 157°) than in the other T-O_b-T angles (pentamer B5: 127-130°; pentamer B6: 130-136°) owing to the strong electrostatic attraction between the closely located Na⁺ ions and aluminum-bonded O atoms.



Bond angle (°)	COSMO sol.	Bond length (Å)	COSMO sol.
SiO _b Al	130	AlO _b	1.75-1.82
SiO _b Si	127-130	AlO _t	1.78-1.84
AlO _b Al	165	SiO _b	1.64-1.70
O _t SiO _t	105-112	SiO _t	1.66-1.68
O _t SiO _b	105-114	OH	0.98-1.03
O _b SiO _b	106-108	NaO	2.37-2.57
O _t AlO _t	105-112	O--H	1.61-2.46
O _t AlO _b	101-112		
O _b AlO _b	102		

Figure 3.22 Pentamer B5



Bond angle (°)	COSMO sol.	Bond length (Å)	COSMO sol.
SiO _b Al	131-136	AlO _b	1.75-1.80
SiO _b Si	130	AlO _t	1.80-1.83
AlO _b Al	157	SiO _b	1.63-1.69
O _t SiO _t	99-114	SiO _t	1.66-1.70
O _t SiO _b	101-116	OH	0.99-1.01
O _b SiO _b	112	NaO	2.34-2.66
O _t AlO _t	115-114	O--H	1.80-2.46
O _t AlO _b	102-114		
O _b AlO _b	114		

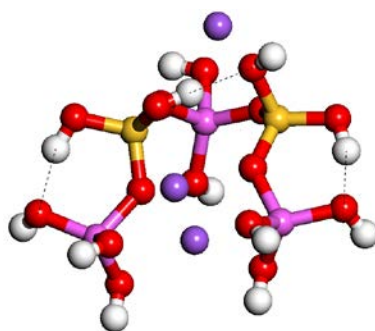
Figure 3.23 Pentamer B6

3.3.1.4.3 Three Al substitutions in pentamers

The substitution of three Al atoms for three Si atoms in pentamers will form six isomers including one Lowensteinian structure: pentamer C1 and five non-Lowensteinian structures: pentamers C2, C3, C4, C5 and C6.

Figure 3.24 shows pentamer C1, which is the only structure with the Si/Al alternation. Due to the presence of the three Na^+ ions that will produce the strong electrostatic interaction with the framework, the O atoms must be taken in locating the Na^+ ions. According to our optimisation, in pentamer C1, the two Na^+ ions are located on opposite sides of the plane, where one bonds to the five O atoms and the other bonds to the four O atoms, calculated as 2.33-2.98 and 2.40-2.49 Å, respectively; the remaining Na^+ ion is located away from the above two Na^+ ions to bond to the four O atoms, calculated as 2.45-2.67 Å. Clearly, such an arrangement of the Na^+ ions in pentamer C1 enables the Na^+ ions to maximise their coordination with the O atoms and avoid the significant excess of the electrostatic repulsion with each other. Moreover, the hydrogen bonds are arranged to be symmetrical in the equatorial positions.

Further analysis of bond lengths and angles shows that due to the symmetry constraint of pentamer C1 imposed by the interplay of the Na^+ ions and hydrogen bonds, most of the relative bond lengths and angles are equal, especially for the T- O_b bond lengths and Si- O_b -Al angles. In particular, for pentamer C1, the stronger electrostatic force of the Na^+ ions causes the significant distortion in the Si-O-Al angles, Al- O_b and Si- O_b bond lengths, as shown by the increase of the maximum Si- O_b -Al angle of 137° and of the maximum Al- O_b and Si- O_b bond lengths of 1.83 Å and 1.66 Å, respectively. Further, the variation of the axial Si- O_t bond length to 1.73 Å occurs because the O atom acts as the donor for the Na^+ ion and hydrogen bond simultaneously.



Bond angle (°)	COSMO sol.	Bond length (Å)	COSMO sol.
SiO _b Al	128-137	AlO _b	1.80-1.83
O _t SiO _t	106-109	AlO _t	1.79-1.80
O _t SiO _b	100-112	SiO _b	1.64-1.66
O _b SiO _b	114	SiO _t	1.68-1.73
O _t AlO _t	113-122	OH	0.98-1.01
O _t AlO _b	97-116	NaO	2.33-2.98
O _b AlO _b	104	O--H	1.76-2.01

Figure 3.24 Pentamer C1

Turning our attention to pentamers C2, C3, C4, C5 and C6 with the Al-O-Al or Al-O-Al-O-Al linkages, the more pronounced deformation of the frameworks is found, as shown in Figures 3.25-3.29.

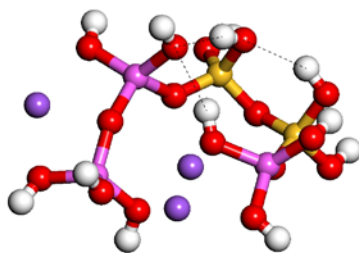
In the case of pentamers C2, C3 and C4 with the Al-O_b-Al linkage, the main structural effect of the presence of the Al-O_b-Al linkage in these pentamers is that all the closely spaced Na⁺ ions preferentially bond to the Al-O_b-Al linkage, thus making the Al-O_b-Al angle enlarge and directionality of the hydrogen bonds is irregular. There is the large increase in the Al-O_b-Al angles of 163°, 179° and 142°, respectively. The significantly larger angles of the former two implies that the Al-O_b-Al linkage positioned at the terminal site of the framework does not encounter the ring strain, which probably enlarges the Al-O_b-Al angle.

The same feature, namely that all the Na⁺ ions closely coordinate to the Al-O_b-Al linkages are also seen when the Al-O_b-Al-O_b-Al linkage forms in pentamers C5 and C6. Surprisingly, the Al-O_b-Al angles, which are found in pentamers C5 and C6 hold in the smaller angles of 136° and 147° in pentamer C5 and of 126° and 130° in pentamer C6. This result reveals that only one Al-O_b-Al angle range reaches the

maximum value of 147° , but others have no appreciable difference between the Si-O_b-Al and Si-O_b-Si angles. The formation of three smaller Al-O_b-Al angles referring 126° , 130° and 136° can be explained by the presence of the hydrogen bonds between the adjacent hydroxyl groups of the Al-O_b-Al linkages, which moves the hydroxyl groups closer, leading to the smaller angle in the Al-O_b-Al linkage. Indeed, the O--H distance in three Al-O_b-Al angles is calculated at 2.08-2.20 Å, the typical of the hydrogen bonds, which is shorter than 3.66 Å in the Al-O_b-Al angle of 147° .

As with tetramers mentioned in section 3.3.1.3.2, the two O atoms adjacent to the same Al atom bonding to the Na⁺ ion will move the O-Al-O bond angles to the minimum value. The reduction of the O_t-Al-O_t bond angle in these cases is found in pentamers C2 and C4, with 95° and 101° , respectively; the latter is significantly larger than the former by 6° , which can be attributed to the cooperative effect of the hydrogen bond in which the hydroxyl group acts as the hydrogen bond donor to drive the O_t-Al-O_t bond to enlarge.

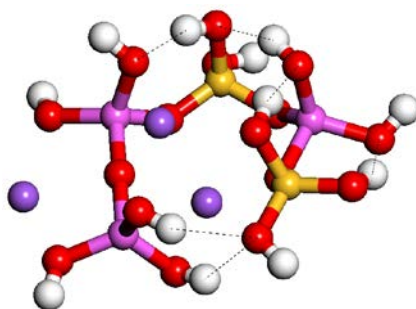
It is notable that in all pentamers, the cooperative effect of the Na⁺ ions and hydrogen bonds causes the considerable variation in the T-O bond lengths, which is consistent with other clusters, as mentioned above. Moreover, in the case of pentamer C6, the particularly strong hydrogen bond is formed, with the smallest O--H distance of 1.50 Å. The explanation for the shortening of the O--H distance is the large-scale charge separation between the Al-O_b-Al-O_b-Al and Si-O_b-Si linkages in the structure.



Bond angle (°)	COSMO sol.
SiO _b Al	131-134
SiO _b Si	130
AlO _b Al	163
O _t SiO _t	109-113
O _t SiO _b	107-114
O _b SiO _b	109-110
O _t AlO _t	95-118
O _t AlO _b	99-118
O _b AlO _b	109

Bond length (Å)	COSMO sol.
AlO _b	1.74-1.83
AlO _t	1.77-1.82
SiO _b	1.64-1.69
SiO _t	1.67-1.69
OH	0.98-1.01
NaO	2.29-2.62
O--H	1.81-2.31

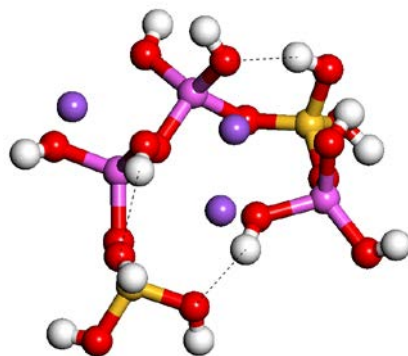
Figure 3.25 Pentamer C2



Bond angle (°)	COSMO sol.
SiO _b Al	116-133
AlO _b Al	179
O _t SiO _t	105-112
O _t SiO _b	107-115
O _b SiO _b	111
O _t AlO _t	112-117
O _t AlO _b	100-121
O _b AlO _b	103-106

Bond length (Å)	COSMO sol.
AlO _b	1.76-1.84
AlO _t	1.78-1.81
SiO _b	1.65
SiO _t	1.68-1.70
OH	0.98-1.01
NaO	2.30-2.62
O--H	1.86-2.40

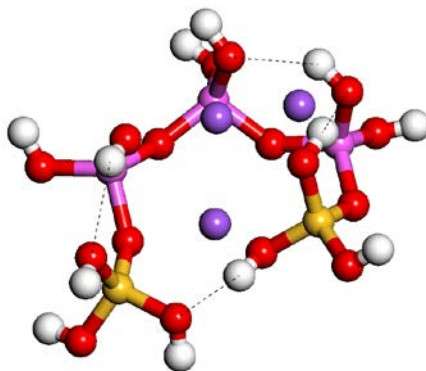
Figure 3.26 Pentamer C3



Bond angle (°)	COSMO sol.
SiO _b Al	131-135
AlO _b Al	142
O _t SiO _t	103-113
O _t SiO _b	107-117
O _b SiO _b	111
O _t AlO _t	101-119
O _t AlO _b	100-116
O _b AlO _b	105-111

Bond length (Å)	COSMO sol.
AlO _b	1.77-1.80
AlO _t	1.78-1.81
SiO _b	1.63-1.66
SiO _t	1.69
OH	0.98-1.00
NaO	2.31-2.76
O--H	1.96-2.27

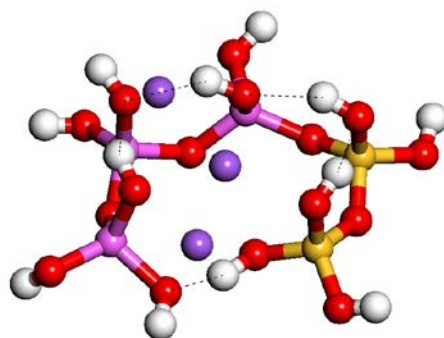
Figure 3.27 Pentamer C4



Bond angle (°)	COSMO sol.
SiO _b Al	120-132
AlO _b Al	136-147
O _t SiO _t	103-113
O _t SiO _b	107-116
O _t AlO _t	114-116
O _t AlO _b	102-118
O _b AlO _b	102-111

Bond length (Å)	COSMO sol.
AlO _b	1.76-1.83
AlO _t	1.79-1.82
SiO _b	1.63-1.64
SiO _t	1.68-1.70
OH	0.98-1.03
NaO	2.31-2.52
O--H	1.72-2.42

Figure 3.28 Pentamer C5



Bond angle (°)	COSMO sol.	Bond length (Å)	COSMO sol.
SiO _b Al	132	AlO _b	1.77-1.81
SiO _b Si	129	AlO _t	1.78-1.84
AlO _b Al	126-130	SiO _b	1.63-1.68
O _t SiO _t	108-112	SiO _t	1.65-1.69
O _t SiO _b	101-112	OH	0.98-1.06
O _b SiO _b	113	NaO	2.31-2.76
O _t AlO _t	103-116	O--H	1.50-2.21
O _t AlO _b	99-119		
O _b AlO _b	104-116		

Figure 3.29 Pentamer C6

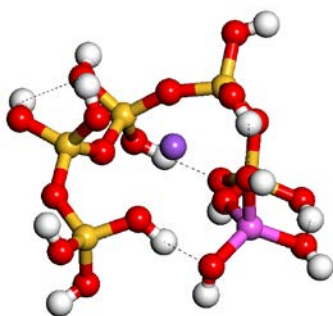
3.3.1.5 Structures of hexamers

Hexamers are the largest linear aluminosilicate clusters to be discussed in this study; total 22 isomers are formed with no more than three Al atoms.

3.3.1.5.1 One Al substitution in hexamers

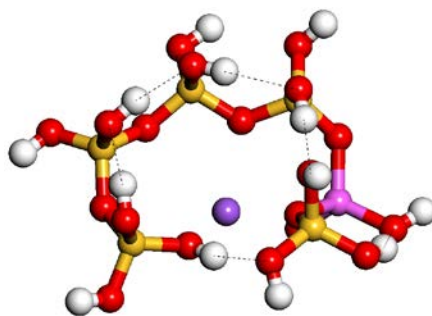
Hexamers with only one Al atom substituted are: hexamers A1, A2 and A3 as presented in Figures 3.30-3.32. In hexamer A1, the Na⁺ ion is bonded to the four “almost equidistant” axial O atoms calculated as 2.40-2.47 Å and most hydrogen bonds are formed by the equatorial hydroxyl groups. As for hexamers A2 and A3, the conformations have the similar feature that the Na⁺ ions are located in the plane bonding to the two equatorial and two bridging O atoms, calculated as 2.38-2.56 and 2.37-2.56 Å while the axial hydroxyl groups form a system of four hydrogen bonds. As can be observed in these hexamers, the variation of bond lengths shows typical change in each hexamer, but there is the large change in the T-O_b-T angles: the Si-O_b-Si angles in hexamer A1 (129-155°), Si-O_b-Si angles in hexamer A2 (124-136°) and Si-O_b-Al angles in hexamer A3 (137-156°). This is a result of the formation of

hydrogen bonds, whose different directionalities drive the general deformation. Related to the above result, the previous study has indicated that there are certain intramolecular hydrogen bonds in different pure silica clusters which strongly influence their conformations²⁷. Presumably, the conformations with the high Si/Al ratio should also be affected by the intramolecular hydrogen bonds instead of the Na⁺ ions.



Bond angle (°)	COSMO sol.	Bond length (Å)	COSMO sol.
SiO _b Al	129	AlO _b	1.81
SiO _b Si	129-155	AlO _t	1.78-1.81
O _t SiO _t	107-115	SiO _b	1.63-1.68
O _t SiO _b	101-115	SiO _t	1.66-1.69
O _b SiO _b	108-113	OH	0.98-1.03
O _t AlO _t	105-120	NaO	2.40-2.47
O _t AlO _b	99-111	O--H	1.62-2.37

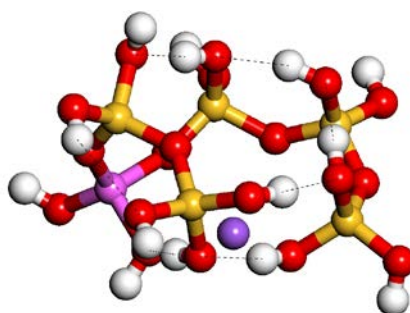
Figure 3.30 Hexamer Al



Bond angle (°)	COSMO sol.
SiO _b Al	129-130
SiO _b Si	124-136
O _t SiO _t	105-114
O _t SiO _b	104-115
O _b SiO _b	106-111
O _t AlO _t	120
O _t AlO _b	95-115
O _b AlO _b	103

Bond length (Å)	COSMO sol.
AlO _b	1.79-1.83
AlO _t	1.77-1.78
SiO _b	1.62-1.71
SiO _t	1.66-1.69
OH	0.98-1.01
NaO	2.38-2.56
O--H	1.87-2.11

Figure 3.31 Hexamer A2



Bond angle (°)	COSMO sol.
SiO _b Al	137-156
SiO _b Si	130-135
O _t SiO _t	106-114
O _t SiO _b	103-116
O _b SiO _b	105-113
O _t AlO _t	107
O _t AlO _b	97-117
O _b AlO _b	110

Bond length (Å)	COSMO sol.
AlO _b	1.78-1.81
AlO _t	1.77-1.84
SiO _b	1.63-1.70
SiO _t	1.65-1.69
OH	0.98-1.02
NaO	2.37-2.56
O--H	1.70-2.42

Figure 3.32 Hexamer A3

3.3.1.5.2 Two Al substitutions in hexamers

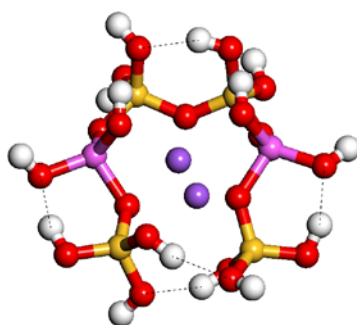
Hexamers with distinct four Si and two Al atoms are shown in Figures 3.33-3.41, including two groups with six Lowensteinian structures: hexamers B1, B2, B3, B4, B5 and B6 and three non-Lowensteinian structures: hexamers B7, B8 and B9.

Focusing first on six different Lowensteinian structures (Figures 3.33-3.38): hexamers B1, B2, B3, B4, B5 and B6, the two Na⁺ ions present in each hexamer show the similar behaviour in that one is located opposite the other within the structure; one is positioned above the cluster plane and the other is positioned below the cluster plane. An analysis of the coordination of the Na⁺ ions reveals that they are arranged so as to have four-fold or five-fold coordination with the O atoms and as a result forms the Na-O distances of 2.38-2.74 Å, 2.36-2.74 Å, 2.33-2.76 Å, 2.28-2.59 Å, 2.37-2.65 Å and 2.30-2.65 Å in hexamers B1, B2, B3, B4, B5 and B6. The former three have the increase in the Na-O distances by as much as 0.17 Å due to the formation of the fifth coordination with the O atom. The similar situation is also found for these hexamers, where the variation of bond lengths shows the typical range of bond lengths when the interplay of the Na⁺ ions and hydrogen bonds are involved in the structures. Moreover, the hydrogen bonds influence the variation of the Si-O_b-Al angles, decreasing them by more than 10°. For example, in hexamer B6, the Si-O_b-Al angles (139°) are larger than others (124-127°), which is due to the absence of the hydrogen bond between the Si-O_b-Al linkage. On the whole, the Si-O_b-Al angles drastically decrease to 124-127° in these hexamers.

As mentioned earlier, when the clusters are symmetrical structures, the conformations usually impose the symmetry constraint, making the distribution of bond lengths and angles symmetrically. Considering the Si-O_b-Al angles of hexamers B1 and B2, the outer Si-O_b-Al and interior Si-O_b-Al angles are 124-130° and 130-135° in hexamer B1; the Si-O_b-Al angles of 127° are found in hexamer B2. In particular, the highly symmetric framework of hexamer B2 also has the similar behaviour to that of tetramer B2 and pentamer B2 discussed previously. Hence, the location of the two Al atoms at each terminal site generates the high symmetry structure, which appears to assist the effective neutralization of the negative electronic density of Al atoms by the symmetrically distributed Na⁺ ions which will lessen the structural distortion.

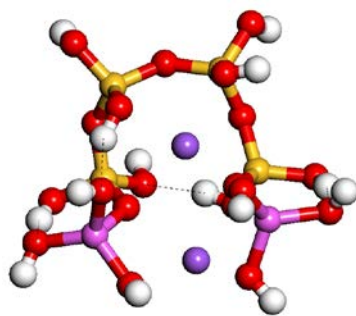
Incidentally, more than four hydrogen bonds, whose distribution is irregular are found

in most hexamers, which suggests that the result corresponds to their asymmetrical geometry. Conversely, considering hexamers B1 and B2, with the symmetrical structures, hexamers B1 and B2 reveal that the symmetrical distribution in hydrogen bonds is found in hexamer B1, but not hexamer B2, which explains why, in hexamer B2, the electrostatic attraction between the O atoms and Na⁺ ions is stronger than the hydrogen bonds.



Bond angle (°)	COSMO sol.	Bond length (Å)	COSMO sol.
SiO _b Al	124-135	AlO _b	1.78-1.84
SiO _b Si	134	AlO _t	1.78-1.79
O _t SiO _t	104-112	SiO _b	1.63-1.69
O _t SiO _b	104-115	SiO _t	1.66-1.69
O _b SiO _b	105-107	OH	0.98-1.01
O _t AlO _t	108-120	NaO	2.38-2.74
O _t AlO _b	98-122	O--H	1.78-1.97
O _b AlO _b	102-107	Al-Al	5.52

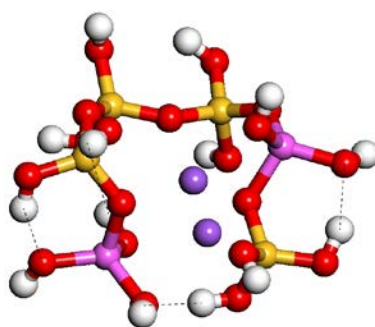
Figure 3.33 Hexamer B1



Bond angle (°)	COSMO sol.
SiO _b Al	127
SiO _b Si	136-139
O _t SiO _t	107-111
O _t SiO _b	105-115
O _b SiO _b	110-112
O _t AlO _t	112-118
O _t AlO _b	97-107

Bond length (Å)	COSMO sol.
AlO _b	1.83-1.84
AlO _t	1.78-1.80
SiO _b	1.63-1.68
SiO _t	1.66-1.69
OH	0.98-1.01
NaO	2.36-2.74
O--H	1.64-1.90
Al-Al	5.10

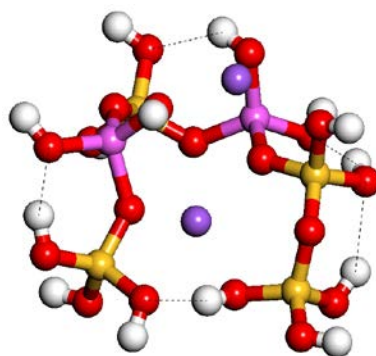
Figure 3.34 Hexamer B2



Bond angle (°)	COSMO sol.
SiO _b Al	124-131
SiO _b Si	136-141
O _t SiO _t	107-112
O _t SiO _b	102-113
O _b SiO _b	109-112
O _t AlO _t	103-118
O _t AlO _b	98-116
O _b AlO _b	105

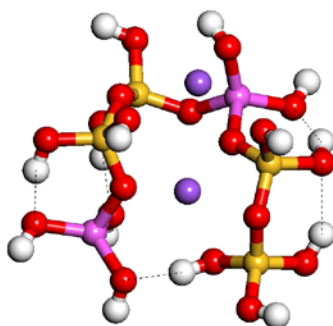
Bond length (Å)	COSMO sol.
AlO _b	1.78-1.83
AlO _t	1.78-1.80
SiO _b	1.62-1.68
SiO _t	1.66-1.70
OH	0.98-1.03
NaO	2.33-2.76
O--H	1.63-2.08
Al-Al	5.72

Figure 3.35 Hexamer B3



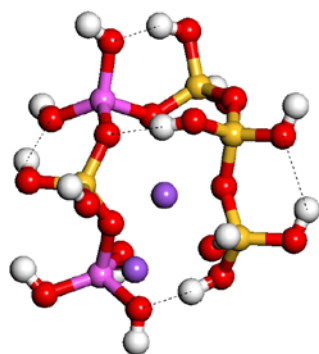
Bond angle (°)	COSMO sol.	Bond length (Å)	COSMO sol.
SiO _b Al	125-146	AlO _b	1.77-1.84
SiO _b Si	128	AlO _t	1.78-1.80
O _t SiO _t	104-115	SiO _b	1.64-1.67
O _t SiO _b	104-113	SiO _t	1.66-1.69
O _b SiO _b	113-115	OH	0.98-1.01
O _t AlO _t	113-120	NaO	2.28-2.59
O _t AlO _b	100-119	O--H	1.77-2.34
O _b AlO _b	100-107	Al-Al	4.61

Figure 3.36 Hexamer B4



Bond angle (°)	COSMO sol.	Bond length (Å)	COSMO sol.
SiO _b Al	127-132	AlO _b	1.80-1.83
SiO _b Si	129	AlO _t	1.77-1.81
O _t SiO _t	107-114	SiO _b	1.64-1.68
O _t SiO _b	104-113	SiO _t	1.66-1.69
O _b SiO _b	110-113	OH	0.98-1.02
O _t AlO _t	115-121	NaO	2.37-2.65
O _t AlO _b	95-117	O--H	1.74-2.22
O _b AlO _b	98	Al-Al	5.85

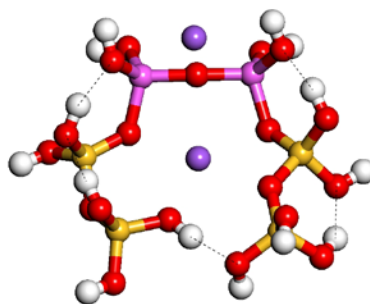
Figure 3.37 Hexamer B5



Bond angle (°)	COSMO sol.	Bond length (Å)	COSMO sol.
SiO _b Al	124-139	AlO _b	1.82-1.83
SiO _b Si	132-135	AlO _t	1.77-1.83
O _t SiO _t	107-112	SiO _b	1.64-1.69
O _t SiO _b	102-115	SiO _t	1.65-1.69
O _b SiO _b	108-110	OH	0.98-1.02
O _t AlO _t	112-120	NaO	2.30-2.65
O _t AlO _b	94-119	O--H	1.68-2.35
O _b AlO _b	103	Al-Al	5.16

Figure 3.38 Hexamer B6

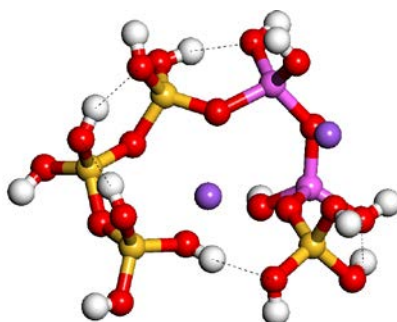
Turning to non-Lowensteinian structures: hexamers B7, B8, and B9 (Figures 3.39-3.41), the presence of the Al-O_b-Al linkage generates an Al-O_b-Al angle with a larger value of 174° for hexamer B7 and 147° for hexamer B9 when the two Na⁺ ions are symmetrically bonded to the Al-O_b-Al linkage. In contrast, the Al-O_b-Al linkage for hexamer B8 is much smaller than the above two, calculated as 132° owing to the distinct ordering of the Al-O_b-Al linkage, which arises from the excess angular strain required to move the Na⁺ ion away from the Al-O_b-Al linkage. Similarly, the distribution of the irregular hydrogen bonds found in the three hexamers drives distortion in the structures.



Bond angle (°)	COSMO sol.
SiO _b Al	127-130
SiO _b Si	127-133
AlO _b Al	174
O _t SiO _t	106-115
O _t SiO _b	103-115
O _b SiO _b	105-111
O _t AlO _t	114-116
O _t AlO _b	104-119
O _b AlO _b	104-106

Bond length (Å)	COSMO sol.
AlO _b	1.74-1.84
AlO _t	1.79-1.80
SiO _b	1.64-1.69
SiO _t	1.66-1.69
OH	0.98-1.01
NaO	2.30-2.76
O--H	1.74-2.08

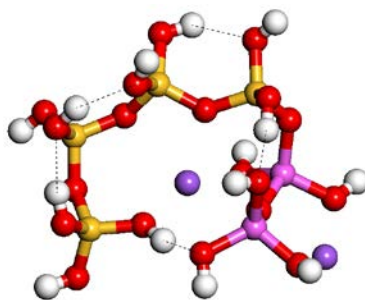
Figure 3.39 Hexamer B7



Bond angle (°)	COSMO sol.
SiO _b Al	131
SiO _b Si	132-135
AlO _b Al	132
O _t SiO _t	106-116
O _t SiO _b	102-114
O _b SiO _b	105-111
O _t AlO _t	115-117
O _t AlO _b	96-121
O _b AlO _b	106-110

Bond length (Å)	COSMO sol.
AlO _b	1.75-1.83
AlO _t	1.79-1.80
SiO _b	1.63-1.69
SiO _t	1.66-1.70
OH	0.98-1.01
NaO	2.34-2.65
O--H	1.85-2.11

Figure 3.40 Hexamer B8



Bond angle (°)	COSMO sol.	Bond length (Å)	COSMO sol.
SiO _b Al	129	AlO _b	1.77-1.80
SiO _b Si	128-136	AlO _t	1.79-1.81
AlO _b Al	147	SiO _b	1.63-1.71
O _t SiO _t	107-117	SiO _t	1.66-1.69
O _t SiO _b	103-115	OH	0.98-1.04
O _b SiO _b	103-110	NaO	2.25-2.55
O _t AlO _t	107-117	O--H	1.56-2.21
O _t AlO _b	100-113		
O _b AlO _b	112		

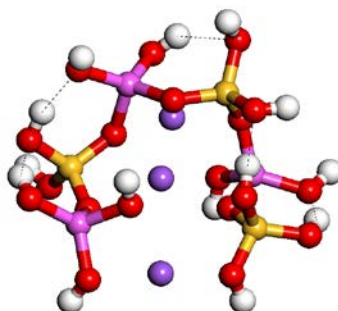
Figure 3.41 Hexamer B9

3.3.1.5.3 Three Al substitutions in hexamers

Finally, hexamers with three Si atoms substituted by three Al atoms have two types of configurations: two Lowensteinian structures including hexamers C1, C2 and seven non-Lowensteinian structures including hexamers C3, C4, C5, C6, C7, C8, C9 and C10.

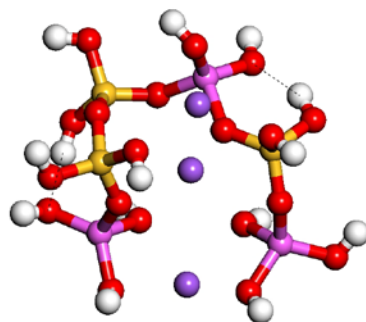
The Lowensteinian structures: hexamers C1 and C2 are discussed first (Figures 3.42 and 3.43). Due to the similarity in the Si/Al distribution, the coordination between the Na⁺ ions and O atoms in hexamers C1 and C2 are also similar. One Na⁺ ion is located among the four outside terminal O atoms, another is located at the central point so as to bond with the five O atoms and the final Na⁺ ion is located away from the remaining two Na⁺ ions and bonded with the four O atoms, calculated as 2.32-2.84 and 2.29-2.59 Å, respectively. The Na⁺ ions maximize the coordination to the O atoms, which appears to be the most significant factor influencing the conformation rather than hydrogen bonds. The analysis of the bond length of hexamers C1 and C2, shows an increase in the Al-O and Si-O bond lengths arising primarily from the Na⁺ ions. The analysis of the T-O_b-T angles reveals the small range

(132-139°) occurring in hexamer C2, due to its almost symmetrical structure that effectively drives the Na⁺ ions in the symmetrical coordination and reduces the structural distortion; in contrast, the large range of T-O_b-T angles (122-137°) found in hexamer C1, arises from its alternating structure that results in the asymmetrical coordination of the Na⁺ ions, thus inducing the large structural distortion.



Bond angle (°)	COSMO sol.	Bond length (Å)	COSMO sol.
SiO _b Al	122-137	AlO _b	1.80-1.82
O _t SiO _t	99-115	AlO _t	1.77-1.83
O _t SiO _b	104-113	SiO _b	1.65-1.67
O _b SiO _b	107-113	SiO _t	1.67-1.71
O _t AlO _t	94-123	OH	0.98-1.01
O _t AlO _b	99-118	NaO	2.32-2.84
O _b AlO _b	104-107	O--H	1.74-2.10

Figure 3.42 Hexamer C1



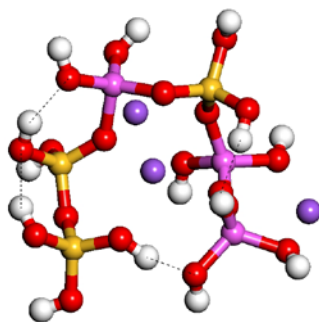
Bond angle (°)	COSMO sol.	Bond length (Å)	COSMO sol.
SiO _b Al	132-139	AlO _b	1.80-1.82
SiO _b Si	136	AlO _t	1.77-1.82
O _t SiO _t	108-110	SiO _b	1.63-1.68
O _t SiO _b	101-111	SiO _t	1.66-1.70
O _b SiO _b	110-115	OH	0.98-1.01
O _t AlO _t	96-125	NaO	2.29-2.59
O _t AlO _b	105-115	O--H	1.80-1.97
O _b AlO _b	110		

Figure 3.43 Hexamer C2

Non-Lowensteinian hexamers C3, C4, C5, C6, C7, C8, C9, and C10 (Figures 3.44-3.51) can be further categorized into two groups: one with the Al-O_b-Al linkage and the other containing the Al-O_b-Al-O_b-Al linkage, which reflect the highly asymmetrical conformations. For such complex conformations, the previous comparison of pentamers, with the Al-O_b-Al or Al-O_b-Al-O_b-Al linkages, provided the general idea that the Na⁺ ions will coordinate to the Al-O_b-Al linkage more strongly than to other T-O_b-T linkages, resulting in the significant variation in structural parameters such as the Al-O bond lengths or the Al-O_b-Al angles. The similar trend is also found in these hexamers. First, a remarkable feature is the variation of the Al-O_b-Al or Al-O_b-Al-O_b-Al linkages that is the primary driving force for the structural distortion. As observed, when most hexamers have much larger Al-O_b-Al angles (between 144° and 176°) than other T-O_b-T linkages, it is not surprising that the Na⁺ ions are so closely bonded to the Al-O_b-Al linkages. Moreover, it is worth noting that when the Al-O_b-Al-O_b-Al linkage forms in hexamers C9 and C10, the Al-O_b-Al angles are more extended than others, being in the range of 119-176° for hexamer C9 and of 120-165° for hexamer C10, owing to the formation of the hydrogen bonds between the Al-O_b-Al linkages that tends to move the linkage closer

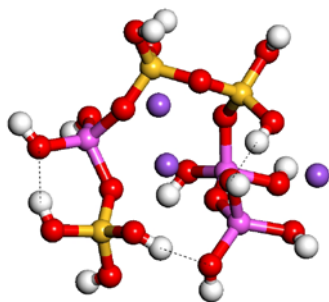
(the smaller Al-O_b-Al angles).

Consequently, the comparison of the Al-O_b-Al angles in several open clusters containing the Al-O_b-Al or Al-O_b-Al-O_b-Al linkages reveals that when the Na⁺ ions are symmetrically located in both tetrahedral positions of the Al-O_b-Al linkage, in which the Na⁺ ions are separately coordinated to the three aluminum-bonded O atoms, the stronger electrostatic attraction of the Na⁺ ions causes the Al-O_b-Al angle to enlarge. This does not occur in other ways of the coordination between the O atoms and Na⁺ ions, which is why the Al-O_b-Al linkage displays the large variation within the clusters. Clearly, the difference in the Na⁺ coordination plays the important factor in determining conformations.



Bond angle (°)	COSMO sol.	Bond length (Å)	COSMO sol.
SiO _b Al	125-138	AlO _b	1.75-1.84
SiO _b Si	129	AlO _t	1.78-1.82
AlO _b Al	156	SiO _b	1.64-1.68
O _t SiO _t	106-114	SiO _t	1.66-1.69
O _t SiO _b	105-115	OH	0.98-1.03
O _b SiO _b	108-112	NaO	2.29-2.65
O _t AlO _t	102-120	O--H	1.62-2.20
O _t AlO _b	98-117		
O _b AlO _b	99-115		

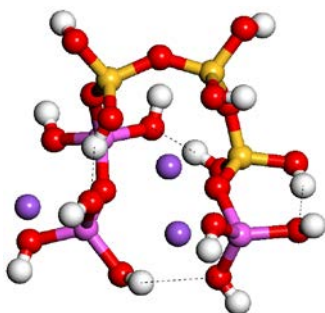
Figure 3.44 Hexamer C3



Bond angle (°)	COSMO sol.
SiO _b Al	127-146
SiO _b Si	130
AlO _b Al	144
O _t SiO _t	105-119
O _t SiO _b	107-116
O _b SiO _b	109-110
O _t AlO _t	105-120
O _t AlO _b	97-117
O _b AlO _b	101-110

Bond length (Å)	COSMO sol.
AlO _b	1.75-1.84
AlO _t	1.77-1.83
SiO _b	1.64-1.69
SiO _t	1.67-1.68
OH	0.98-1.02
NaO	2.33-2.60
O--H	1.67-1.87

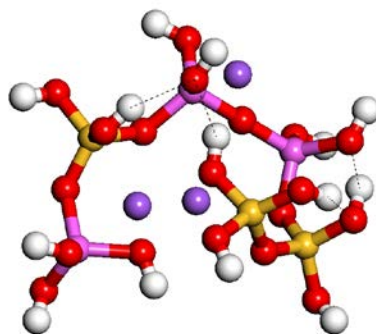
Figure 3.45 Hexamer C4



Bond angle (°)	COSMO sol.
SiO _b Al	130-141
SiO _b Si	137-139
AlO _b Al	148
O _t SiO _t	105-108
O _t SiO _b	106-115
O _b SiO _b	111-112
O _t AlO _t	111-119
O _t AlO _b	98-109
O _b AlO _b	116

Bond length (Å)	COSMO sol.
AlO _b	1.76-1.83
AlO _t	1.78-1.82
SiO _b	1.62-1.68
SiO _t	1.67-1.68
OH	0.98-1.02
NaO	2.28-2.75
O--H	1.600-2.36

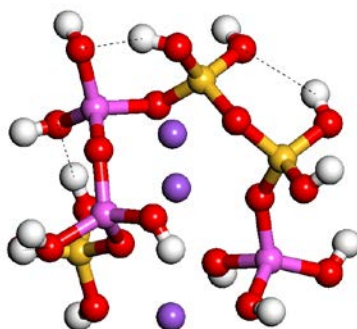
Figure 3.46 Hexamer C5



Bond angle (°)	COSMO sol.
SiO _b Al	129-134
SiO _b Si	128
AlO _b Al	176
O _t SiO _t	99-116
O _t SiO _b	106-113
O _b SiO _b	110-115
O _t AlO _t	101-119
O _t AlO _b	101-117
O _b AlO _b	105

Bond length (Å)	COSMO sol.
AlO _b	1.75-1.82
AlO _t	1.77-1.81
SiO _b	1.64-1.70
SiO _t	1.67-1.71
OH	0.98-1.02
NaO	2.35-2.69
O--H	1.70-2.06

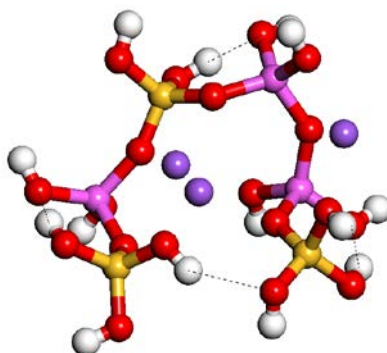
Figure 3.47 Hexamer C6



Bond angle (°)	COSMO sol.
SiO _b Al	119-141
SiO _b Si	133
AlO _b Al	137
O _t SiO _t	107-115
O _t SiO _b	101-115
O _b SiO _b	108-114
O _t AlO _t	98-121
O _t AlO _b	97-118
O _b AlO _b	106-111

Bond length (Å)	COSMO sol.
AlO _b	1.75-1.83
AlO _t	1.77-1.80
SiO _b	1.62-1.69
SiO _t	1.67-1.69
OH	0.98-1.03
NaO	2.30-2.70
O--H	1.67-2.36

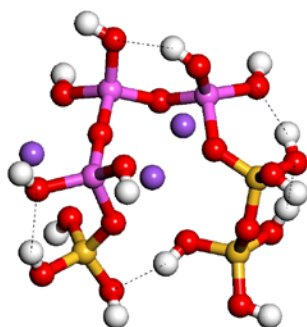
Figure 3.48 Hexamer C7



Bond angle (°)	COSMO sol.
SiO _b Al	127-158
AlO _b Al	137
O _t SiO _t	105-111
O _t SiO _b	1051-115
O _b SiO _b	108
O _t AlO _t	112-122
O _t AlO _b	99-118
O _b AlO _b	101-112

Bond length (Å)	COSMO sol.
AlO _b	1.77-1.85
AlO _t	1.78-1.80
SiO _b	1.64-1.65
SiO _t	1.66-1.69
OH	0.98-1.01
NaO	2.31-2.69
O--H	1.79-2.48

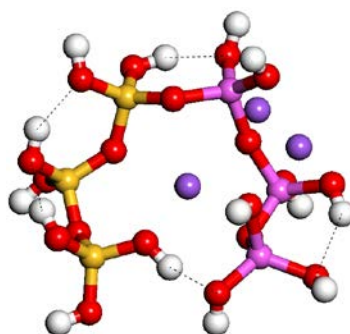
Figure 3.49 Hexamer C8



Bond angle (°)	COSMO sol.
SiO _b Al	124-131
SiO _b Si	129
AlO _b Al	119-176
O _t SiO _t	104-114
O _t SiO _b	103-114
O _b SiO _b	111
O _t AlO _t	112-122
O _t AlO _b	99-116
O _b AlO _b	103-105

Bond length (Å)	COSMO sol.
AlO _b	1.75-1.86
AlO _t	1.78-1.81
SiO _b	1.64-1.68
SiO _t	1.66-1.70
OH	0.98-1.01
NaO	2.32-2.64
O--H	1.78-2.10

Figure 3.50 Hexamer C9



Bond angle (°)	COSMO sol.	Bond length (Å)	COSMO sol.
SiO _b Al	127	AlO _b	1.76-1.81
SiO _b Si	132-135	AlO _t	1.78-1.82
AlO _b Al	120-165	SiO _b	1.64-1.69
O _t SiO _t	109-115	SiO _t	1.66-1.68
O _t SiO _b	106-115	OH	0.98-1.03
O _b SiO _b	106-110	NaO	2.33-2.82
O _t AlO _t	101-120	O--H	1.63-2.33
O _t AlO _b	99-118		
O _b AlO _b	107-108		

Figure 3.51 Hexamer C10

To summarise the main results regarding the geometric parameters of Lowensteinian and non-Lowensteinian open clusters: (i) The range of bond lengths in Lowensteinian and non-Lowensteinian open clusters is similar, with the former having the Si-O bond lengths of 1.62-1.70 Å and the Al-O bond lengths of 1.76-1.83 Å and the latter, the Si-O bond lengths of 1.62-1.70 Å and the Al-O bond lengths of 1.74-1.84 Å. (ii) In non-Lowensteinian open clusters, most of the Al-O_b-Al bond angles are larger than the Si-O_b-Al bond angles, reflecting the fact that when the Na⁺ ions are symmetrically bonded to the Al-O_b-Al linkages, the strong electrostatic attraction will influence on the Al-O_b-Al linkage. (iii) The open clusters form almost cyclic-like frameworks due to the Na⁺ ions or the hydrogen bonds.

3.3.2 Geometry analysis for cyclic clusters (rings)

Open clusters may condense to form more stable and constrained cyclic clusters, which are thought to play an important role in the nucleation processes of aluminosilicate zeolites. Known zeolites are made up of various rings especially the four, five and six rings; understanding their conformations are therefore of considerable importance¹⁶. In this section, possible rings are identified with different Si/Al ratios and atomic arrangements of Si and Al atoms for clusters which both do and do not accord with Lowenstein's and Dempsey's rule. Figures 3.52-3.68 show some geometric parameters for different isomers of the three, four, five and six rings.

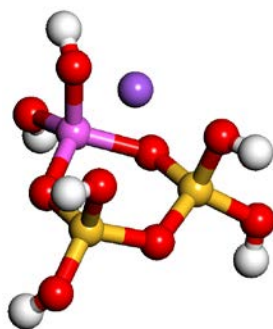
3.3.2.1 The three rings

The three ring is the smallest ring that can be found in the aluminosilicates and the NMR studies have showed the presence of the three rings at the early stage of nucleation. The three ring is, however, rare in aluminosilicate zeolite frameworks, only being presented in the high-silica ZSM-18²⁸. Other zeotype frameworks also have the three rings²⁹ such as the beryllosilicate OSB-1 or zincosilicates but the tetrahedral positions of the frameworks contain other elements. As for pure siliceous zeolite systems, it remains puzzling that no the three ring has been found in the structures even though the evidence of NMR and mass spectrometry indicates that there is the considerable concentration in solution phase of the three rings to be found in reaction processes¹⁻⁸. Hence, the detailed analysis of the three rings is important. The computational simulation for the three rings of ZSM-18 has been studied, but in this case, the counterion, being the proton, neutralises the three ring instead of the Na⁺ ion³⁰. There are two three rings A and B to be studied in this section (Figures 3.52 and 3.53). In three ring A, with one Al atom, the Na⁺ ion that is closer to the three axial O atoms results in nearly triangular coordination with the Na-O distances between 2.25 and 2.40 Å. When comparing with the crystallographic data for the T-O_b-T angle of the three ring in ZSM-18:135°, three ring A has significantly smaller T-O_b-T angles of 122-126°. The difference in value may be due to the fact that the calculated three ring A has the “loose” structure which is constrained as if a component of a crystal.

As discussed already for the open clusters, the enlargement of the Al-O_b-Al angle occurs when the both tetrahedral positions of the Al-O_b-Al linkage are occupied by

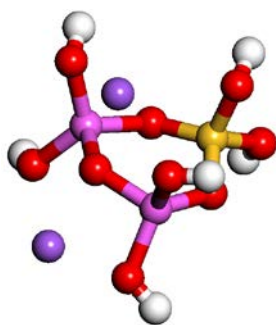
the symmetrically placed Na^+ ions. In contrast, the distribution of the $\text{Al-O}_b\text{-Al}$ angle in three ring B falls in the narrow range of 128° although the Na^+ ions are again symmetrically close to the $\text{Al-O}_b\text{-Al}$ linkage and have almost equidistant three O coordination. We, therefore, suppose that the differences between the three ring B and the previous open clusters is due to the effect of ring strain that necessitates the $\text{Al-O}_b\text{-Al}$ linkage to 128° . Furthermore, comparing the $\text{T-O}_b\text{-T}$ angles of both three rings A and B with those of the four, five and six rings, the distribution of the $\text{T-O}_b\text{-T}$ angles of the three rings are lower and narrower, with substantial reductions of more than 10° from the general $\text{T-O}_b\text{-T}$ angles, of around 140° to 165° . This kind of ring angles will cause structural strain, which might inhibit further combination with other rings during construction of zeolite crystals, or make the three rings readily re-open although we note the presence of the three rings in the synthesis gel has been proven in experimental studies¹⁻⁸.

The variation of bond lengths due to the electrostatic attraction between the Na^+ ions and O atoms and mode of charge distribution (atomic arrangement) is well understood. Thus, the Si-O and Al-O bond lengths are 1.63-1.70 and 1.77-1.81 Å in three ring A and 1.65-1.70 and 1.79-1.80 Å in three ring B.



Bond angle ($^\circ$)	COSMO sol.	Bond length (Å)	COSMO sol.
SiO_bAl	125-126	AlO_b	1.81
SiO_bSi	122	AlO_t	1.77-1.80
O_tSiO_t	104-105	SiO_b	1.63-1.69
O_tSiO_b	102-117	SiO_t	1.67-1.70
O_bSiO_b	111	OH	0.98-0.99
O_tAlO_t	109	NaO	2.25-2.40
O_tAlO_b	103-118		
O_bAlO_b	103		

Figure 3.52 3-ring A



Bond angle (°)	COSMO sol.	Bond length (Å)	COSMO sol.
SiO _b Al	123	AlO _b	1.79-1.80
AlO _b Al	128	AlO _t	1.80
O _t SiO _t	104	SiO _b	1.65
O _t SiO _b	105-113	SiO _t	1.70
O _b SiO _b	114	OH	0.98-0.99
O _t AlO _t	112	NaO	2.35-2.42
O _t AlO _b	99-114		
O _b AlO _b	108		

Figure 3.53 3-ring B

3.3.2.2 The four rings

The four rings are one of the most important cyclic structures and are widely present in known zeolite systems: 61 types of zeolite structures contain the four rings²⁶.

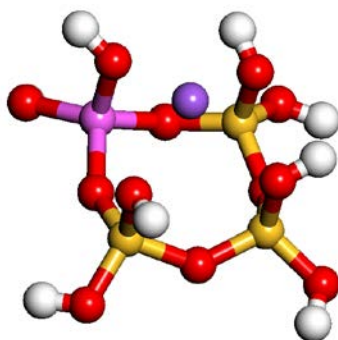
Figures 3.54-3.56 show the relative structural parameters of four rings A, B1 and B2 obtained in this work. In four ring A with one Al atom, the Na⁺ ion is bonded to the four axial O atoms in a range of 2.45-2.61 Å thus forming the square-pyramidal coordination. Four rings B1 and B2 contain two Si atoms and two Al atoms forming alternating and paired conformations, respectively. Four ring B1 is consistent with Lowenstein's rule, but four ring B2 is not. In light of the different distribution of Al atoms, the two Na⁺ ions are present at distinctly varied locations between four rings B1 and B2. First, in four ring B1, each Na⁺ ion forms two shorter equidistant and two longer equidistant Na-O bonds. While one is located at the centre among the four axial O atoms, of 2.33-2.47 Å the other is located below the centre of the ring plane, of 2.45-2.48 Å. We also note that the location of the latter corresponds to the experimental crystallographic data found in aluminosilicate zeolite (zeolite A) although the calculated Na-O distances are shorter than the experimental ones

(2.59-2.61 Å). Turning now to four ring B2, the Na⁺ ions symmetrically locate at both tetrahedral positions of the Al-O_b-Al linkage, but have different Na⁺ coordination numbers, with one Na⁺ ion coordinated by the three O atoms, of 2.33-2.38 Å and the other Na⁺ ion by five O atoms, of 2.43-2.80 Å.

The data refer to the T-O_b-T angles for three the four rings as follows: four ring A 130-147°; four ring B1 134-138°; four ring B2 123-166°. Four ring A shows a reasonable range of the T-O_b-T angles, probably reflecting the modification due to the presence of the Al atom or ring strain. Then, we note that the similar Si-O_b-Al angles are symmetrically distributed in four ring B1, which is in agreement with the experimental angle distribution of the four rings in zeolite A. As for four ring B2, there are the two lower Si-O_b-Al and one higher Al-O_b-Al angles to be found in its framework, exhibiting the large variation of the T-O_b-T angles. This kind of distribution of the T-O_b-T angles could induce stronger strain causing the large structural distortion. Moreover, it is worth mentioning the distribution of the O_b-T-O_b angles of four ring B1. Each corresponding O_b-T-O_b angle represents the highly symmetrical distribution in the structure of four ring B1, which will effectively reduce the structural strain.

Concerning the variation of T-O bond lengths, we observe that in three the four rings, the substitution of one Si atom by one Al atom results in the expected Al-O_b bond lengths of 1.81 Å in four rings A, B1 and B2, but the shortening of the neighbouring Si-O_b bond lengths at 1.62 Å in four ring A, 1.64-1.65 Å in four ring B1, and 1.63 Å in four ring B2. Comparing the value, we can see that the slight increase of the Si-O_b bond lengths in four ring B1 is due to the Na⁺ ions, which also causes the lengthening of the Si-O_t and Al-O_t bond lengths. The Si-O_t bond lengths increase to almost 1.70 Å in three the four rings and the Al-O_t bond lengths increase to 1.80 Å in four ring A, 1.79 Å in four ring B1, and 1.81 Å in four ring B2.

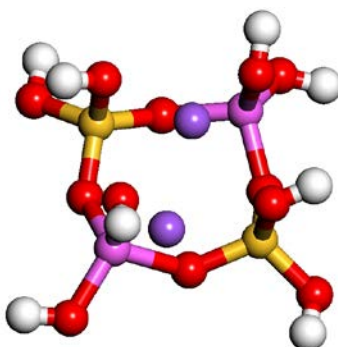
According to the analysis above, the Na⁺ ions dominates in the geometrical parameters of three and four rings. However, with the increase in the Si/Al ratio, the additional force -the emergence of hydrogen bond- will compete with the Na⁺ ions, forming a complex interplay. Subsequently, we will address this phenomenon in the five and six rings.



Bond angle (°)	COSMO sol.
SiO _b Al	130-147
SiO _b Si	133-136
O _t SiO _t	112-114
O _t SiO _b	102-114
O _b SiO _b	113-115
O _t AlO _t	111
O _t AlO _b	104-115
O _b AlO _b	106

Bond length (Å)	COSMO sol.
AlO _b	1.81
AlO _t	1.77-1.80
SiO _b	1.62-1.68
SiO _t	1.66-1.70
OH	0.98-0.99
NaO	2.31-2.61

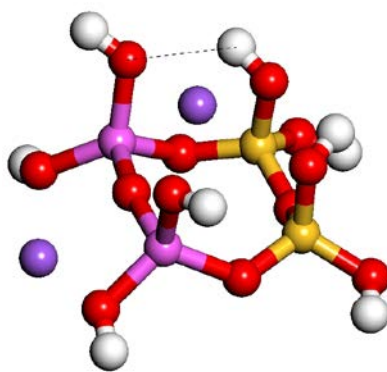
Figure 3.54 4-ring A



Bond angle (°)	COSMO sol.
SiO _b Al	134-138
O _t SiO _t	110-111
O _t SiO _b	106-112
O _b SiO _b	109
O _t AlO _t	118
O _t AlO _b	106-114
O _b AlO _b	102

Bond length (Å)	COSMO sol.
AlO _b	1.81
AlO _t	1.76-1.79
SiO _b	1.64-1.65
SiO _t	1.68-1.70
OH	0.98-0.99
NaO	2.33-2.48

Figure 3.55 4-ring B1



Bond angle (°)	COSMO sol.	Bond length (Å)	COSMO sol.
SiO _b Al	123-126	AlO _b	1.77-1.81
SiO _b Si	136	AlO _t	1.80-1.81
AlO _b Al	166	SiO _b	1.63-1.67
O _t SiO _t	112-113	SiO _t	1.68-1.70
O _t SiO _b	103-111	OH	0.98-0.99
O _b SiO _b	116	NaO	2.33-2.80
O _t AlO _t	120-121	O--H	2.35
O _t AlO _b	101-113		
O _b AlO _b	109-110		

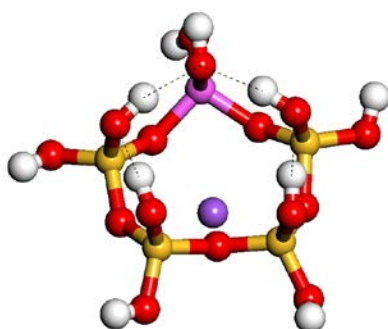
Figure 3.56 4-ring B2

3.3.2.3 The five rings

Unlike the wide presence of the four ring in zeolite frameworks, the five rings are found in only 18 zeolite structures²⁹. Unexpectedly, the NMR evidence suggests the absence of the five rings in solution. Thus, further consideration of the formation mechanism of the five rings, when and how the five rings form, is necessary. In this section, the analysis of the relative structures of the five rings should provide key evidence for understanding the formation of these rings. Considering the substitution of Si atoms by Al atoms in the five rings, there are five the five rings to be formed including five ring A with one Al atom substitution, five rings B1 and B2 with two Al atom substitutions and five rings C1, C2 and C3 with three Al atom substitutions as showed in Figures 3.57-3.61.

Five ring A has the crown conformation, where the Na⁺ ion that coordinates to the five O atoms with the distances between 2.45 and 2.99 Å is located almost at the central point below the ring plane while the five axial hydroxyl groups form a system

of four hydrogen bonds (O--H: 1.82-2.18 Å) above the ring plane. We see that there is the competition of the interplay between the Na⁺ ion and hydrogen bonds in five ring A. Obviously, the hydrogen bonds dominates over the Na⁺ ion; when hydrogen bonds form above the ring plane, they crowd out the Na⁺ ion and make it move below the ring plane; perhaps such almost circular hydrogen bonds in five ring A may provide the extra stabilization energy to the structure. The variation of the T-O bond lengths and T-O_b-T bond angles can also be observed by the fact that the effect of hydrogen bonds results in the increase in the Al-O_t and Si-O_t bond lengths to 1.81 Å and 1.68 Å, which is accompanied by the decrease in the T-O_b-T bond angles to 130°.

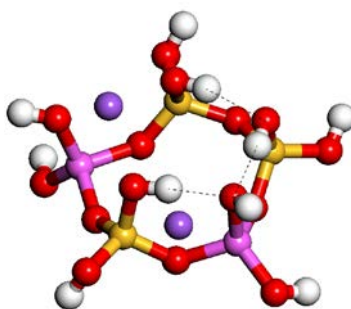


Bond angle (°)	COSMO sol.	Bond length (Å)	COSMO sol.
SiO _b Al	131-132	AlO _b	1.81
SiO _b Si	130-145	AlO _t	1.76-1.81
O _t SiO _t	110-113	SiO _b	1.64-1.69
O _t SiO _b	101-115	SiO _t	1.66-1.68
O _b SiO _b	103-110	OH	0.98-1.01
O _t AlO _t	111	NaO	2.45-2.99
O _t AlO _b	105-118	O--H	1.82-2.18
O _b AlO _b	100		

Figure 3.57 5-ring A

Considering now five rings B1 and B2, in which two Al atoms substitute for two Si atoms. In the alternating five ring B1, one Na⁺ ion and a system of three hydrogen bonds coexist above the ring plane with the other below the plane, with bond lengths of 2.32-2.62 Å; in the paired five ring B2, one Na⁺ ion and a system of two hydrogen bonds coexist above the ring plane with the other outside the plane, calculated as 2.32-2.54 Å. There is again the competition of the interplay between the Na⁺ ions and

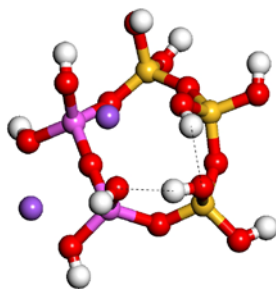
the hydrogen bonds in five rings B1 and B2, where two structures are quite distinct from five ring A. Here, the similar behaviour can be observed as in five rings B1 and B2, the interplay between the Na⁺ ions and hydrogen bonds remains the delicate balance, resulting in the coexistence of the Na⁺ ions and hydrogen bonds above the ring plane. Such an interplay results in the lengthening of the axial T-O_t bonds, with the Al-O_t bond lengths of 1.78-1.81 Å and the Si-O_t bond lengths of 1.69-1.70 Å in five ring B1 and with the Al-O_t bond lengths of 1.81-1.83 Å and Si-O_t bond length of 1.69 Å in five ring B2. Moreover, the formation of the hydrogen bonds, as found in five rings B1 and B2, is the main contributing factor to the decrease in the T-O_b-T bond angles to 128-131°. By contrast, in five ring B2, the increase in the Al-O_b-Al angles to 178° is due to the close proximity of the two symmetrical Na⁺ ions.



Bond angle (°)	COSMO sol.
SiO _b Al	131-140
SiO _b Si	128
O _t SiO _t	104-113
O _t SiO _b	106-114
O _b SiO _b	108-112
O _t AlO _t	116-118
O _t AlO _b	104-115
O _b AlO _b	100-101

Bond length (Å)	COSMO sol.
AlO _b	1.79-1.82
AlO _t	1.76-1.81
SiO _b	1.63-1.69
SiO _t	1.67-1.70
OH	0.98-1.01
NaO	2.32-2.62
O--H	1.75-1.88

Figure 3.58 5-ring B1

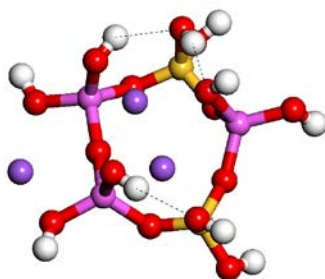


Bond angle (°)	COSMO sol.	Bond length (Å)	COSMO sol.
SiO _b Al	128-134	AlO _b	1.76-1.80
SiO _b Si	131-155	AlO _t	1.79-1.83
AlO _b Al	178	SiO _b	1.63-1.68
O _t SiO _t	106-112	SiO _t	1.67-1.69
O _t SiO _b	104-116	OH	0.98-1.01
O _b SiO _b	113-114	NaO	2.32-2.54
O _t AlO _t	116-118	O--H	1.85-2.01
O _t AlO _b	102-113		
O _b AlO _b	113-115		

Figure 3.59 5-ring B2

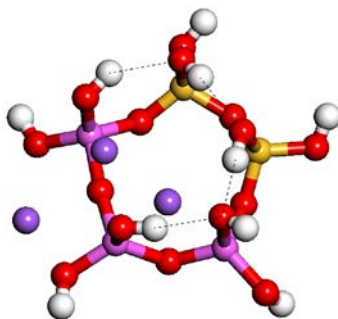
Five rings C1 and C2 with three Al atom substitutionals, which have the Al-O_b-Al and Al-O_b-Al-O_b-Al linkages form typical non-Lowensteinian structures. The comparison of structures of five rings C1 and C2 reveals that the Na⁺ ions of these rings are the similar positions with the Na-O distances of 2.31-2.69 and 2.30-2.71 Å, respectively, where the Na⁺ ion and several hydrogen bonds (five ring C1: a system of four hydrogen bonds; five ring C2: three hydrogen bonds) coexist above the ring plane and the others are symmetrically located within and outside the ring plane. Interestingly, the Na⁺ ions seemingly do not modify the conformations. They still retain the “crown” forms, representing ring constraint. Moreover, according to the interpretation of the variation of structural parameters in five rings B1 and B2, the same feature involving a in the T-O bond lengths and T-O_b-T bond angles can also be observed in five rings C1 and C2. The lengthening in the Al-O_t and Si-O_t bonds in five ring C1, of 1.80-1.83 and 1.69 Å and in five ring C2, of 1.80-1.83 and 1.68 Å is due to the interplay of the Na⁺ ions and hydrogen bonds. The decrease in the T-O_b-T angles in five ring C1, of 128-132° and in five ring C2, of 130-132° is because of the effect of the hydrogen bonds; the increase in the Al-O_b-Al angles in five ring C1, of 159° and

in five ring C2, of 170° is because of the close proximity of the two symmetrical Na^+ ions.



Bond angle ($^\circ$)	COSMO sol.	Bond length (\AA)	COSMO sol.
SiO_bAl	128-151	AlO_b	1.77-1.81
AlO_bAl	159	AlO_t	1.77-1.83
O_tSiO_t	106-107	SiO_b	1.65
O_tSiO_b	105-114	SiO_t	1.68-1.69
O_bSiO_b	109	OH	0.98-1.00
O_tAlO_t	104-116	NaO	2.31-2.69
O_tAlO_b	101-118	O--H	1.94-2.23
O_bAlO_b	101-106		

Figure 3.60 5-ring C1



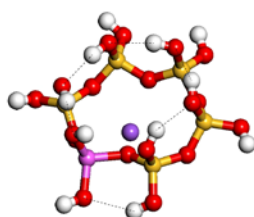
Bond angle ($^\circ$)	COSMO sol.	Bond length (\AA)	COSMO sol.
SiO_bAl	130-131	AlO_b	1.77-1.84
SiO_bSi	132	AlO_t	1.77-1.83
AlO_bAl	128-170	SiO_b	1.64-1.68
O_tSiO_t	106-116	SiO_t	1.67-1.68
O_tSiO_b	107-114	OH	0.98-1.02
O_bSiO_b	109-111	NaO	2.30-2.71
O_tAlO_t	108-112	O--H	1.79-2.23
O_tAlO_b	99-120		
O_bAlO_b	102-107		

Figure 3.61 5-ring C2

3.3.2.4 The six rings

The six rings have been found as structural building units in 39 known zeolites²⁹. However, the six rings are not detected in NMR in solution and as a result it is particularly difficult to probe the geometric features of the six rings. The structural analysis of the six rings is therefore necessary. In this section, seven the distinct six rings formed by the different substitutions of Si atoms by Al atoms are discussed including six ring A with one Al atom substitution, six rings B1, B2, and B3 with two Al atom substitutions and six rings C1, C2 and C3 with three Al atom substitutions, as shown in Figures 3.62-3.68.

The study of six ring A (Figure 3.62) reveals that it is geometrically similar to five ring A. The Na⁺ ion coordinating to the four O atoms locates below the ring plane, with the Na-O distances between 2.34 and 2.66 Å, while the formation of a system of five hydrogen bonds via the axial hydroxyl groups locates above the ring plane, with O--H distances between 1.70 and 2.40 Å. The conformation of six ring A, due to the high Si/Al ratio, is also like the calculated six silicon ring that forms the “extended crown” conformation with a cyclic hydrogen bond system. Obviously, when considering the variation of the T-O bond lengths and T-O_b-T bond angles, the key role is the hydrogen bonds that result in the increase in the Al-O_t and Si-O_t bond lengths to 1.80 and 1.68 Å, respectively and the decrease in the Si-O_b-Al and Si-O_b-Si bond angles to 126° and 131°.



Bond angle (°)	COSMO sol.	Bond length (Å)	COSMO sol.
SiO _b Al	126-128	AlO _b	1.81-1.83
SiO _b Si	131-138	AlO _t	1.77-1.80
O _t SiO _t	107-115	SiO _b	1.64-1.69
O _t SiO _b	102-115	SiO _t	1.65-1.68
O _b SiO _b	103-112	OH	0.98-1.02
O _t AlO _t	119	NaO	2.34-2.66
O _t AlO _b	101-120	O--H	1.70-2.40
O _b AlO _b	98		

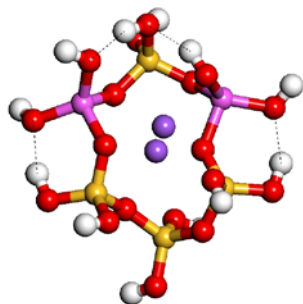
Figure 3.62 6-ring A

In considering the substitution of two Al atoms in the six rings, three cases are studied: six rings B1, B2, and B3 (Figures 3.63-3.65). Here, it is worth noting that the geometry of the rings is greatly modified by the arrangement of Al atoms, forming three distinct conformations. First, the “chair” form is obtained from six ring B1 with the Al-O_b-Si-O_b-Al sequence, in which one Na⁺ ion locates above the ring plane to coordinate to the four O atoms, of 2.36-2.68 Å and the other locates at the opposite to coordinate to the five O atoms, of 2.35-2.78 Å. Second, the “chair like” form is found in six ring B2 with the Al-O_b-(Si-O_b)₂-Al sequence; the location of the Na⁺ ions is similar to that of six ring B1 and each Na⁺ ion is coordinated by the four O atoms, calculated as 2.41-2.62 Å. Finally, the “extended crown” form (as with the six ring A) is, again, found in six ring B3 (the Al-O_b-Al linkage) with a system of four hydrogen bonds above the ring plane; the Na⁺ ions are positioned at both sides of the Al-O_b-Al linkage in the ring plane and have three or four Na-O coordination numbers with the distances of 2.33-2.69 Å.

To illustrate the conformational change in the six rings, an analysis of six rings B1 and B2 reveals that in addition to different aliovalent substitutions that cause local distortion, the accompanying Na⁺ ions that produce the strong electrostatic force with the O atoms probably are the major factor influencing their conformations. Moreover, the deformations also make the hydrogen bonds distribute in axial and equatorial directions in six ring B1 (the symmetrical distribution) and B2 (the asymmetrical distribution). The local geometry in them such as the T-O bond lengths and T-O_b-T bond angles, of course, is significantly affected by both the Na⁺ ions and hydrogen bonds. The interplay between the Na⁺ ions and hydrogen bonds and thus results in the variation range of Al-O_t bond lengths being 1.78-1.79 Å, and Si-O_t bond lengths being 1.67-1.69 Å in six ring B1 and of Al-O_t bond lengths being 1.76-1.81 Å, and Si-O_t bond lengths being 1.67-1.69 Å in six ring B2. Moreover, the reduction of T-O_b-T bond angles is affected by the hydrogen bonds, with 128-130° in six ring B1 and 129-131° in six ring B2.

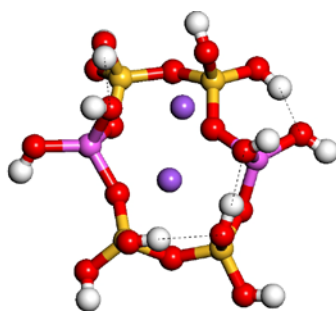
As for six ring B3, the Al-O_t bond lengths of 1.79-1.80 Å is due to the effect of the Na⁺ ions and hydrogen bonds; the variation of the Si-O_t bond lengths of 1.67-1.68 Å and the T-O_b-T angles of 128-135° is due to the effect of the hydrogen bonds. Moreover, the smaller Al-O-Al angle, of 137° is found due to the way of the

asymmetrical coordination between the Na^+ ions and the Al- O_b -Al linkage. Clearly, the study of six rings B1, B2 and B3 provides us the typical example that shows not only the structural deformation depending on the Si/Al distribution but also the competition of the interplay between the Na^+ ions and hydrogen bonds.



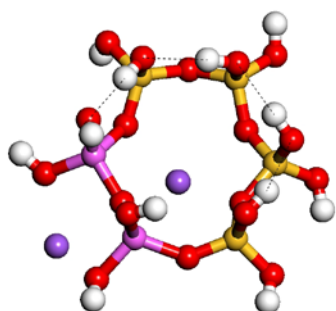
Bond angle (°)	COSMO sol.	Bond length (Å)	COSMO sol.
SiO_bAl	128-130	AlO_b	1.79-1.83
SiO_bSi	128-143	AlO_t	1.78-1.79
O_tSiO_t	110-114	SiO_b	1.64-1.68
O_tSiO_b	104-114	SiO_t	1.66-1.69
O_bSiO_b	107-114	OH	0.98-1.01
O_tAlO_t	119-120	NaO	2.35-2.78
O_tAlO_b	103-118	O--H	1.80-2.22
O_bAlO_b	100-106	Al-Al	4.70

Figure 3.63 6-ring B1



Bond angle (°)	COSMO sol.	Bond length (Å)	COSMO sol.
SiO _b Al	129-151	AlO _b	1.79-1.83
SiO _b Si	129-131	AlO _t	1.76-1.81
O _t SiO _t	109-113	SiO _b	1.65-1.69
O _t SiO _b	102-115	SiO _t	1.67-1.69
O _b SiO _b	107-112	OH	0.98-1.00
O _t AlO _t	107-120	NaO	2.41-2.62
O _t AlO _b	100-122	O--H	1.84-2.01
O _b AlO _b	98-100	Al-Al	5.32

Figure 3.64 6-ring B2



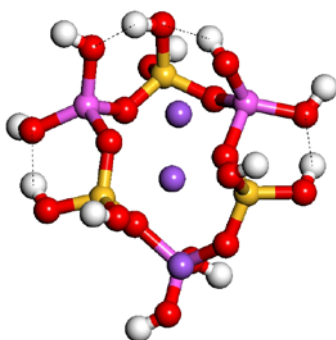
Bond angle (°)	COSMO sol.	Bond length (Å)	COSMO sol.
SiO _b Al	128-138	AlO _b	1.76-1.82
SiO _b Si	131-135	AlO _t	1.79-1.80
AlO _b Al	137	SiO _b	1.62-1.70
O _t SiO _t	108-113	SiO _t	1.66-1.68
O _t SiO _b	102-114	OH	0.98-1.01
O _b SiO _b	103-111	NaO	2.33-2.69
O _t AlO _t	112-116	O--H	1.79-2.35
O _t AlO _b	102-118		
O _b AlO _b	103-108		

Figure 3.65 6-ring B3

Finally, the geometrical analysis ends with a discussion of three Al atom substitutionals in the six rings: the alternating six rings C1 and C2 with the Al-O_b-Al linkage and six ring C3 with the Al-O-Al-O-Al linkage (Figures 3.66-3.68). In six ring C1, each Na⁺ ion is arranged in a suitable position so as to increase the electrostatic attraction between the Na⁺ ion and O atoms and decrease the electrostatic repulsion of the Na⁺ ions with each other. One is located at the almost central point below the ring plane to coordinate to the five O atoms with bond lengths of 2.33-2.69 Å while the others are located above the ring plane to coordinate to the four O atoms with bond lengths of 2.37-2.58 Å. Six ring C1 structure is also similar to the chair conformation, as already observed in six ring B1, as is similar to the most stable carbon six ring structure. In six ring C2, the two Na⁺ ions that have the largest separation are located above the ring plane and the other is below the ring plane; each Na⁺ ion forms the four Na-O coordination numbers with the distances between 2.35 and 2.71 Å. Moreover, the presence of the Al-O_b-Al linkage also arises as a consequence of more distortion, forming the narrower and deformed chair conformation. As for six ring C3, we find that this way of arranging the location of the Al atoms divides its structure into two equal components: one is the Al-O_b-Al-O_b-Al linkage and the other Si-O_b-Si-O_b-Si linkage. The resulting conformation of six ring C3 is slightly distorted because obviously, each Na⁺ ion bonding to the O atoms on the Al-O_b-Al-O_b-Al linkage coordinates to the four O atoms, calculated as 2.27-2.70 Å whereas the Si-O_b-Si-O_b-Si linkage forms a system of two hydrogen bond, with the O-H distances between 1.90 and 2.16 Å.

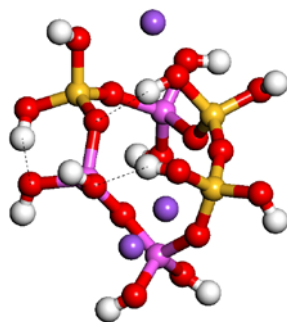
Let us consider further the variation of the bond lengths and bond angles. As usual, the major factors including the electrostatic attraction between the Na⁺ ions and O atoms, the way of Si-Al distribution and the effect of hydrogen bonds impact on the Si-O_t and Al-O_t bond lengths, which are respectively in the range of 1.68-1.70 and 1.78-1.79 Å in six ring C1, 1.67-1.70 and 1.78-1.82 Å in six ring C2, and 1.66-1.70 Å and 1.77-1.82 Å in six ring C3. As regards the variation of the T-O_b-T angle, the hydrogen bonds indeed control the T-O_b-T angle of six rings C1, C2 and C3 to decrease to a certain extent, with 125-132°, 126°, and 126-131°, respectively. But other remaining smaller T-O_b-T angles found in six rings C1, C2 and C3, with 130°, 127°, and 131° result from ring constraint. Additionally, ring constraint also results in the larger T-O_b-T angles in six rings C1 and C2, of 141° and 145-163°. Thus, the large

angular distortion that occurs in the six rings might be due to the closed cyclic rings being particularly constrained structures and the limited steric arrangement of the Na^+ ions. Incidentally, the large range of the Al-O_b-Si angles (125-141°) is found in the highly symmetrical six ring C1 which has the completely alternating conformation, corresponding to the range of the Al-O_b-Si angles (142-164°) of the six ring obtained from crystallographic data for zeolite A³¹.



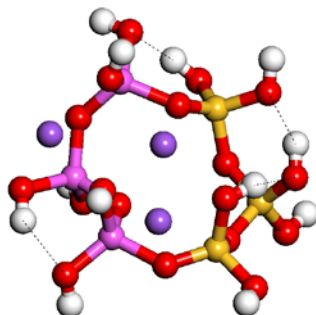
Bond angle (°)	COSMO sol.	Bond length (Å)	COSMO sol.
SiO _b Al	125-141	AlO _b	1.79-1.83
O _t SiO _t	106-110	AlO _t	1.78-1.79
O _t SiO _b	105-114	SiO _b	1.64-1.66
O _b SiO _b	109-112	SiO _t	1.68-1.70
O _t AlO _t	119-129	OH	0.98-1.00
O _t AlO _b	97-115	NaO	2.33-2.69
O _b AlO _b	106-101	O--H	1.82-2.21

Figure 3.66 6-ring C1



Bond angle (°)	COSMO sol.	Bond length (Å)	COSMO sol.
SiO _b Al	126-145	AlO _b	1.76-1.82
SiO _b Si	163	AlO _t	1.78-1.82
AlO _b Al	134	SiO _b	1.63-1.66
O _t SiO _t	103-109	SiO _t	1.67-1.70
O _t SiO _b	100-114	OH	0.98-1.01
O _b SiO _b	110-113	NaO	2.33-2.69
O _t AlO _t	113-124	O--H	1.78-1.85
O _t AlO _b	97-116		
O _b AlO _b	111-115		

Figure 3.67 6-ring C2



Bond angle (°)	COSMO sol.	Bond length (Å)	COSMO sol.
SiO _b Al	129-131	AlO _b	1.74-1.85
SiO _b Si	131	AlO _t	1.77-1.82
AlO _b Al	126-135	SiO _b	1.62-1.70
O _t SiO _t	111-115	SiO _t	1.66-1.70
O _t SiO _b	103-114	OH	0.98-1.01
O _b SiO _b	106-115	NaO	2.27-2.70
O _t AlO _t	108-124	O--H	1.90-2.41
O _t AlO _b	99-119		
O _b AlO _b	104-115		

Figure 3.68 6-ring C3

To summarise the main results regarding the geometric parameters of Lowensteinian and non-Lowensteinian rings. (i) The range of bond lengths in Lowensteinian and non-Lowensteinian rings is similar; the former has the Si-O bond lengths of 1.62-1.70 Å and Al-O bond lengths of 1.76-1.83 Å and the latter has the Si-O bond lengths of 1.62-1.70 Å and Al-O bond lengths of 1.76-1.85 Å. (ii) The Al-O-Al angle in most rings is still nearly as large as that in open ones, reflecting the fact that the Na⁺ ions are close to the Al-O-Al linkage. (iii) The structural distortion can be attributed to the effect of the Na⁺ ions, hydrogen bonds or ring constraint. On the other hand, there are differences in bond lengths and angles in Lowensteinian rings compared with the experimental crystallographic results for zeolites^{31,32}. The range of the T-O bond lengths is 1.62-1.83 Å compared with 1.58 to 1.74 Å for zeolite A and 1.61 to 1.72 Å for zeolite X; the range of the T-O_b-T angles is 125-151° compared with 142-164° for zeolite A and 134-144° for zeolite X. The difference in value is due to the calculated clusters being “loose” structures and not constrained as when a component of a crystal.

Finally, it is worth noting that Wakihara et al. recently employed high-energy X-ray diffraction (HEXRD)¹⁰ to investigate the formation of the four, five, and six rings in the nucleation processes of different aluminosilicate zeolites and found ring structures with sizes in the range of 3.5 and 6 Å between the most distant atoms in the rings. The result corresponds closely to our calculated value of 3.31-5.86 Å for types of the Lowensteinian four, five, and six rings.

3.3.3 Relative energies of open clusters

Following as detailed analysis of the geometry of all relative aluminosilicate clusters, we now analyse the energetics of the calculated clusters to compare the relative energetics in the gas phase and COSMO solvation, with the aim of understanding the relationship between the relative energies and distribution of Al atoms in clusters. These data also provide us with evidence to illustrate what kind of aluminosilicate clusters are involved in the prenucleation processes, which will help us further understand the mechanism of formation of the zeolite. Tables 3.1-3.10 show the calculated relative energies depending on the number of Al atoms in these clusters; the relative energetics data for the gas phase and COSMO solvation are given. In this section, we will discuss the relative energetics of the aluminosilicate clusters on the

basis of the number of Al atoms. We also note that aluminosilicate clusters are studied in aqueous media, but not in the gas phase. The result in the gas phase being the reference, may provide us some useful information to observe what important characteristics are in the non-aqueous condition.

3.3.3.1 Dimers

The dimerisation reactions are the special case owing to the totally distinct conformations of the $\text{AlSiO}(\text{OH})_6\text{Na}$ and $\text{Al}_2\text{O}(\text{OH})_6\text{Na}_2$ dimer. The two dimerisation reactions are:



The calculated free energy in the gas phase and COSMO solvation is given in Table 3.1. In the gas phase, the free energy is -60 kJmol^{-1} and -54 kJmol^{-1} for the $\text{AlSiO}(\text{OH})_6\text{Na}$ dimer and -106 kJmol^{-1} and -100 kJmol^{-1} for the $\text{Al}_2\text{O}(\text{OH})_6\text{Na}_2$ dimer at 298 K and 450K. The formation of the $\text{Al}_2\text{O}(\text{OH})_6\text{Na}_2$ dimer would contradict Lowenstein's rule. But the hydrothermal synthesis of occurs in aqueous media and, in COSMO solvation, the free energy is -21 kJmol^{-1} and -23 kJmol^{-1} for the $\text{AlSiO}(\text{OH})_6\text{Na}$ dimer and -16 kJmol^{-1} and -18 kJmol^{-1} for the $\text{Al}_2\text{O}(\text{OH})_6\text{Na}_2$ dimer at 298 K and 450K. Therefore, when considering the effect of the COSMO solvation, the formation of the $\text{AlSiO}(\text{OH})_6\text{Na}$ dimer is more favorable than the $\text{Al}_2\text{O}(\text{OH})_6\text{Na}_2$ dimer. Such a change can probably be attributed to the assumption that the electrostatic interaction between the "gas phase" clusters and charge-neutralizing Na^+ ions provide a high degree of stability for the $\text{Al}_2\text{O}(\text{OH})_6\text{Na}_2$ dimer, which is greatly reduced in COSMO solvation. Furthermore, our value for the formation of the $\text{AlSiO}(\text{OH})_6\text{Na}$ dimer (298K: -21 kJmol^{-1} , 450K: -23 kJmol^{-1}) is also close to the experimental value that was obtained from the solubility measurement ($-21.56 \pm 0.29 \text{ kJmol}^{-1}$)³³. It is clear that in the dimerisation reactions, the $\text{AlSiO}(\text{OH})_6\text{Na}$ dimer is indeed the key cluster to involved in the nucleation of zeolites, and the Na^+ ion is also needed to present in this dimer.

Table 3.1 Free energy (ΔG , kJmol^{-1}) changes in the gas phase and COSMO solvation at 298 and 450 K in dimerisation reactions.

Dimerisations	Gas		COSMO sol.		Exp.
	298K	450K	298K	450K	
Si + Al \rightarrow Si-Al + H ₂ O	-60	-54	-21	-23	-21.56 \pm 0.29
Al + Al \rightarrow Al-Al + H ₂ O	-106	-100	-16	-18	

3.3.3.2 One Al substitution in trimers, tetramers, pentamers and hexamers

We now discuss the open clusters when only one Al atom substitutes for one Si atom in these open clusters.

3.3.3.2.1 Trimers

First, Table 3.2 shows that in the gas phase, the lowest energy found for trimer A1, which is 12 kJmol^{-1} more stable than trimer A2. From the earlier geometrical analysis of trimers A1 and A2, this result is, however, unexpected, because trimer A1 has the very large T-O_b-T angle distortion (132-166°), which might be accompanied with the energy penalty. In fact, such a result is determined by the charge distribution, which depends on the siting of the Al atom in trimers. In trimer A1, the Al atom is positioned at the centre of the structure, where the charge is distributed evenly, but in trimer A2, the terminal Al atom causes the localized charge distribution. Hence, the average charge distribution in trimer A1 seems to compensate the energy penalty due to the large T-O_b-T angle distortion, making it more stable than trimer A2. Considering now the inclusion of the COSMO solvation, trimer A1 is slightly more stable than trimer A2 by 3 kJmol^{-1} ; the similar energy suggests that trimers A1 and A2 could be found to coexist in COSMO solvation. Indeed, the evidence of the ²⁹Si and ²⁷Al NMR data has indicated the existence of the two different trimers¹⁻⁸.

3.3.3.2.2 Tetramers

Turning now to tetramers, the result for which is presented in Table 3.2, we find that in the gas phase, the most stable structure is tetramer A2 and the energy difference between tetramers A1 and A2 is about 7 kJmol^{-1} . In COSMO solvation, we note the

similar trend, in which tetramer A2 is 19 kJmol^{-1} more stable than tetramer A1. To understand the relative stability for two tetramers, the structural distortion and charge distribution are considered. First, the previous geometrical comparison of tetramers A1 and A2 reveals that the conformation of tetramer A1 is somewhat similar to that of tetramer A2 and thus they could suffer the same degree of structural distortion. As a result, the relative stability of tetramers A1 and A2 seems not to be determined by the structural distortion. On the other hand, the analysis of the charge distribution in tetramers A1 and A2 shows that they both have the localized charge distribution due to their asymmetrical features. Obviously, such a charge distribution is not to be the major factor in influencing their relative stability.

Which factor, therefore, most directly affects the relative stability? It is very possible that the presence of the intramolecular hydrogen bonds is responsible for the relative stability of the two tetramers. The intramolecular hydrogen bond formed from the hydroxyl groups is the general structural feature in these clusters as has already been shown in the section 3.3.1. Moreover, according to previous computational studies of pure silica clusters, Pereira et al. indicated that the intramolecular hydrogen bonds formed within pure silica clusters stabilise their conformations²⁶. It can also be expected that the intramolecular hydrogen bonds formed in aluminosilicate clusters should have the same effect on stabilising the conformations. Hence, compared with the number of intramolecular hydrogen bonds in tetramers A1 and A2, tetramer A1 has three intramolecular hydrogen bonds whereas tetramer A2 has five, which probably explains why the latter tetramer is more stable.

Table 3.2 Relative energies (kJmol^{-1}) of aluminosilicate isomers: one Al substitution in trimers and tetramers in the gas phase and COSMO solvation.

Trimers	Gas	COSMO sol.	Tetramers	Gas	COSMO sol.
Trimer A1 	0	0	Tetramer A1 	7	19
Trimer A2 	12	3	Tetramer A2 	0	0

3.3.3.2.3 Pentamers

Considering now pentamers in Table 3.3, the order of decreasing stability is: pentamer A2 > pentamer A3 > pentamer A1 in the gas phase as well as COSMO solvation. The result shows that pentamer A2 is more energetically stable than pentamers A3 and A1. As previously, to investigate further, the structural distortion and charge distribution need to be considered. From the geometrical analysis in section 3.3.1.4.1, it is clear that pentamer A3 is the symmetric structure with the average charge distribution and less structural distortion whereas pentamers A1 and A2 are asymmetric structures with the localized charge distribution and large T-O_b-T angle distortion. Our expectation is that pentamer A3 will be the most stable due to its favourable structural condition; however, the calculation show the reverse sequence, i.e. pentamer A2 is the most stable. Hence, it could be that the hydrogen bonds, rather than the structural distortion and charge distribution, control the stability of the pentamers. Indeed, pentamer A2 has the most hydrogen bonds, with five, which can generate the additional hydrogen bond energy to stabilise its structure, but pentamer A3 has three. We, therefore, highlight the role of hydrogen bonds in driving the stability of pentamer A2.

Next, the question of the large structural distortion in pentamer A2 needs addressing, because, in general, the occurrence of the structural distortion in clusters is usually accompanied by the energy penalty which consequently causes the framework to be unstable. Interestingly, the large structural distortion in pentamer A2 seems not to affect its stability. Indeed, the large structural distortion might be interpreted as the formation of the hydrogen bonds, which instead, stabilise the structure.

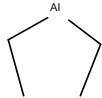
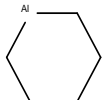
3.3.3.2.4 Hexamers

Finally, in the case of hexamers, their relative stability shows the similar behaviour to pentamers in the gas phase and COSMO solvation, as shown in Table 3.3. When different hydrogen bonds are present in hexamers, the energies decrease in the following order: hexamer A3 > hexamer A2 > hexamer A1 in the gas phase and COSMO solvation. The lowest energy is found in hexamer A3 with seven hydrogen bonds despite the large T-O_b-T angle distortion. The large structural distortion generated can be attributed to the formation of the hydrogen bonds in the framework. Indeed our results suggest that the hydrogen bond plays the critical role in determining the relative stability of these clusters including tetramers, pentamers and

hexamers.

Summarising the energetic analysis of the above open clusters, we find that these open clusters have lower energies when the Al atom is at an interior site of the structures, which has important implications in subsequent condensations; indeed, confirmation that the ends of aluminosilicate chains in COSMO solvation will be siliceous is very significant. With the Al atom located in the interior site, it is possible to form more intramolecular hydrogen bonds that can stabilise the clusters, whose stability seems not to be strongly influenced by the Na⁺ ion, but is greatly influenced by the intramolecular hydrogen bonds.

Table 3.3 Relative energies (kJmol⁻¹) of aluminosilicate isomers: one Al substitution in pentamers and hexamers in the gas phase and COSMO solvation.

Pentamers		Gas	COSMO sol.	Hexamers		Gas	COSMO sol.
Pentamer A1		10	17	Hexamer A1		7	23
Pentamer A2		0	0	Hexamer A2		6	17
Pentamer A3		8	9	Hexamer A3		0	0

3.3.3.3 Two Al substitutions in trimers, tetramers, pentamers and hexamers

We now consider open clusters with two Al atom substitutionals. Before discussing these open clusters, recall that there are two rules both Lowenstein's rule (the Al-O-Al linkages is forbidden) and Dempsey's rule (the Al-Al distance is maximized) to constrain the distribution of aluminum in aluminosilicate zeolite systems. Perhaps the rules control the relative stability of the clusters.

3.3.3.3.1 Trimers

Looking first at the trimers (Table 3.4), the formation energy of tetramers with the

Al-O-Al linkage (trimer B1) and without the Al-O_b-Al linkage (trimer B2) differ from each other by 38-46 kJmol⁻¹ in the gas phase and COSMO solvation; trimer B2 is more stable than trimer B1, which is consistent with Lowenstein's rule. To explain the energy difference between trimers B1 and B2, the consideration of the structural distortion is needed. However, we find that the energy difference is marginally affected by the structural distortion, where the variation of T-O_b-T angle in trimers B1 and B2 is very close, calculated as 129-150° and 128-146°, respectively (section 3.3.1.2.2); and the structural distortion in them seems not to give us any clear explanation of the relative stability. We attribute this energy penalty to the presence of the Al-O_b-Al linkage that produces the double negative charge which would give rise to the unfavourable local charge distribution in the structure.

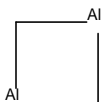
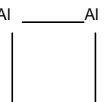
3.3.3.3.2 Tetramers

We next compare the relative energies of four different tetramers, as presented in Table 3.4. For all tetramers studied, the Lowensteinian tetramers (tetramers B1 and B2) have a lower energy over 20 kJmol⁻¹ more stable than non-Lowensteinian ones (tetramers B3 and B4) in the gas phase and COSMO solvation. The higher energy penalty in tetramers B3 and B4 could be attributed to the two factors from the Al-O_b-Al linkage. The first is the presence of the Al-O_b-Al linkage which would result in the unfavourable localized charge distribution; the second is that due to the presence of the Al-O_b-Al linkage, which accompanies the large Al-O_b-Al angle (the Na⁺ ion disorder), the variation of the T-O_b-T angle distortion is significantly larger for tetramers B3 (127-156°) and B4 (125-161°) than for tetramers B1 (129-134°) and B2 (126-132°).

Since tetramers B1 and B2 have satisfied Lowenstein's rule, we need to consider the different siting of the two Al atoms in tetramers B1 and B2 to determine their relative stability. According to our result, the lowest energy is tetramer B2, which is more stable than tetramer B1 by 11-14 kJmol⁻¹. We first consider the result in the context of Dempsey's rule that the Al-Al distance will be maximized is introduced; the relative Al-Al distance of the clusters is presented in Figure 3.11 and 3.12. The Al-Al distance in tetramer B1 is 5.22 Å, whereas the Al-Al distance in tetramer B2 is 5.23 Å. Hence, the Al-Al distance difference does not provide the strong rationalization for the relative stability. Perhaps, a rationale for the relative stability is that the symmetric

distribution of Al atoms, which reflects the highly average charge distribution, would enhance the stability; indeed, tetramer B2, where two Al atoms are arranged in the symmetric position has more stability compared to tetramer B1.

Table 3.4 Relative energies (kJmol^{-1}) of aluminosilicate isomers: two Al substitutions in trimers and tetramers in the gas phase and COSMO solvation.

Trimers	Gas	COSMO sol.	Tetramers	Gas	COSMO sol.
Trimer B1 	46	38	Tetramer B1 	14	11
Trimer B2 	0	0	Tetramer B2 	0	0
			Tetramer B3 	43	35
			Tetramer B4 	47	39

3.3.3.3 Pentamers

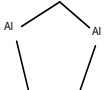
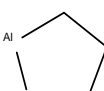
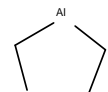
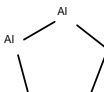
Table 3.5 shows the relative energy of six pentamers. The four most stable pentamers are Lowensteinian structures whereas two least stable pentamers are non-Lowensteinian structures. Similarly, the presence of an $\text{Al-O}_b\text{-Al}$ linkage in pentamers B5 and B6 leads to the unfavourable localized charge distribution and large $\text{T-O}_b\text{-T}$ angle distortion ($127\text{-}165^\circ$ in pentamer B5 and $130\text{-}157^\circ$ in pentamer B6), thus showing less stability.

Here, we only compare the relative stability of the four Lowensteinian structures. In the gas phase, when two Al atoms locate at the outer terminal sites in pentamer B2, it, due to its high symmetry geometry (highly average charge distribution), becomes the most stable structure. However, this result mismatches Dempsey's rule (Figures 3.19-3.21) because the Al-Al distance of pentamer B2 is 5.13 \AA shorter than that of pentamer B3, with 5.66 \AA and pentamer B4, with 5.17 \AA . Our calculation has not

considered the effect of the COSMO solvation on these pentamers and we therefore expect such an effect would cause obvious changes in their energies. Now, the lowest energy value in COSMO solvation are found in pentamers B3 and B4; the relative energies of pentamers B3 and B4 are essentially identical ($<1 \text{ kJmol}^{-1}$), which means that pentamers B3 and B4 very possibly coexist in COSMO solvation. Such an energetic change may arise from the solvation shielding pentamers from their extra-framework Na^+ ions resulting in the Na^+ ions moving away, which consequently impacts on the electrostatic attraction between the clusters and Na^+ ions and the repulsion between the Na^+ ions; in addition, although the interplay between the solvated pentamers and intermolecular hydrogen bonds is not modelled in the COSMO method, in the real system, intermolecular hydrogen bonds may form between clusters to compete with the intramolecular hydrogen bonds in clusters themselves.

This result seems therefore to break the constraint of Dempsey's rule because the Al-Al distances of pentamers B3 and B4 are the most longest and the second longest, respectively. The explanation for such behaviour might be that Dempsey's rule is approved in different types of ring frameworks of zeolites but its validity could be a questionable for open clusters. Nevertheless, Dempsey's rule still provide us the correct guide to understand the distribution of the Al atoms in open clusters.

Table 3.5 Relative energies (kJmol^{-1}) of aluminosilicate isomers: two Al substitutions in pentamers in the gas phase and COSMO solvation.

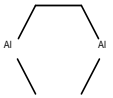
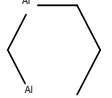
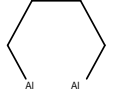
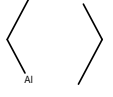
Pentamers	Gas	COSMO sol.	Pentamers	Gas	COSMO sol.
Pentamer B1 	12	18	Pentamer B4 	17	0
Pentamer B2 	0	12	Pentamer B5 	60	38
Pentamer B3 	21	1	Pentamer B6 	51	38

3.3.3.3.4 Hexamers

In the case of hexamers (Table 3.6), six hexamers, which satisfy Lowenstein's rule, have lower energies compared to the other three non-Lowensteinian hexamers in the gas phase and COSMO solvation. Comparing the energies for six Lowensteinian hexamers, we find that in the gas phase, the lowest energy structure is hexamer B1, with the highly symmetry geometry (the highly average charge distribution) and less geometric distortion, but to consider Dempsey's rule (Figures 3.33-3.38), hexamer B1 presents "non-Dempsey" behaviour in that the Al-Al distance of hexamer B1, with 5.52 Å, is shorter than that of hexamer B5, with 5.85 Å and hexamer B3, with 5.72 Å. Considering the inclusion of COSMO solvation, however, the relative energies of hexamers B1, B2 and B5 are very similar to within 3 kJmol⁻¹; the most stable is hexamer B5, which actually follows Dempsey's rule.

From the detailed study for open clusters with two Al atom substitutionals, the results can be summarised as follows (i) The lowest energies of open clusters, which obey Lowenstein's rule can be found in several clusters such as pentamers or hexamers; they may coexist in the gas phase as well as COSMO solvation. (ii) Non-Lowensteinian clusters have an energy penalty of the Al-O_b-Al linkage is 43-60 kJmol⁻¹ in the gas phase as well as 35-65 kJmol⁻¹ in COSMO solvation, which is in agreement with the previous calculation for the short range ordering of Si and Al atoms, as suggested by Catlow et al. (iii) In general, the most stable solvated clusters follow Dempsey's rule.

Table 3.6 Relative energies (kJmol^{-1}) of aluminosilicate isomers: two Al substitutions in hexamers in the gas phase and COSMO solvation.

Hexamers	Gas	COSMO sol.	Hexamers	Gas	COSMO sol.
Hexamer B1 	0	3	Hexamer B6 	28	21
Hexamer B2 	4	2	Hexamer B7 	51	51
Hexamer B3 	5	5	Hexamer B8 	50	44
Hexamer B4 	10	11	Hexamer B9 	58	65
Hexamer B5 	15	0			

3.3.3.4 Three Al substitutions in pentamers and hexamers

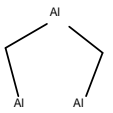
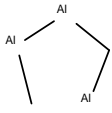
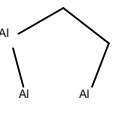
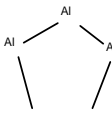
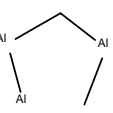
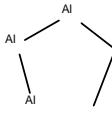
In this section, we examine open clusters with three Al atoms substituted. Only pentamers and hexamers concerning Lowensteinian and non-Lowensteinian structures are compared because more than three Al atoms in trimers or tetramers will be very strong violation of Lowenstein's rule.

3.3.3.4.1 Pentamers

First, the relative energies of the six pentamers are presented in Table 3.7; pentamer C1 is more stable than the other non-Lowensteinian pentamers by 20-79 kJmol^{-1} in the gas phase and by 28-79 kJmol^{-1} in COSMO solvation, being in good agreement with Lowenstein's rule. It is clear that the Al-O_b-Al linkage present in most non-Lowensteinian pentamers gives rise to the structural distortion (the large angle distortion) and unfavourable localized charge distribution, which generate the energy penalty that makes them less stable. Interestingly, the large angular distortion does not occur in pentamer C6, showing the range of 126-132°; the Al-O_b-Al angles are maintained between 126° and 130°. As we have previously mentioned in discussion

trimers B1 and B2, we believe that the stability of these clusters is greatly influenced by the presence of the Al-O_b-Al linkage, but the accompanying large Al-O_b-Al angle distortion is not the essential feature. The similar behaviour can also be observed in hexamers such as hexamers C7 and C8.

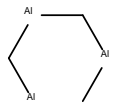
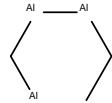
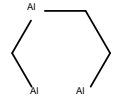
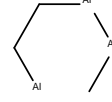
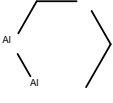
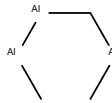
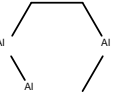
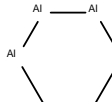
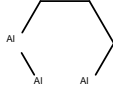
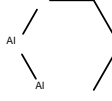
Table 3.7 Relative energies (kJmol⁻¹) of aluminosilicate isomers: three Al substitutions in pentamers in the gas phase and COSMO solvation.

Pentamers	Gas	COSMO sol.		Gas	COSMO sol.
Pentamer C1 	0	0	Pentamer C4 	36	35
Pentamer C2 	20	42	Pentamer C5 	65	65
Pentamer C3 	35	28	Pentamer C6 	79	79

3.3.3.4.2 Hexamers

Turning now to hexamers, ten are presented in Table 3.8. The results, as expected, show that in the gas phase and COSMO solvation, the Lowensteinian hexamers C1 and C2, have lower energies and the most stable is hexamer C1 whereas eight non-Lowensteinian hexamers have higher energy. In particular, hexamers C9 and C10 with two Al-O-Al linkages (the Al-O_b-Al-O_b-Al linkage) are the least stable and energy penalties of hexamers C9 and C10 reach the maximum value of 62 and 70 kJ mol⁻¹ in the gas phase and 58 and 64 kJmol⁻¹ in COSMO solvation. This section has again emphasized that the most stable pentamer and hexamer must have Lowensteinian behaviour.

Table 3.8 Relative energies (kJmol^{-1}) of aluminosilicate isomers: three Al substitutions in hexamers in the gas phase and COSMO solvation.

Hexamers	Gas	COSMO sol.	Hexamers	Gas	COSMO sol.
Hexamer C1 	0	0	Hexamer C6 	27	32
Hexamer C2 	1	4	Hexamer C7 	17	31
Hexamer C3 	8	27	Hexamer C8 	6	16
Hexamer C4 	10	13	Hexamer C9 	62	58
Hexamer C5 	5	18	Hexamer C10 	70	64

3.3.4 Relative energies of rings

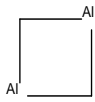
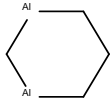
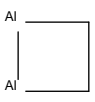
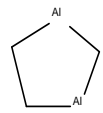
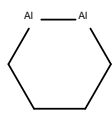
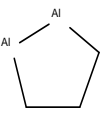
We have studied the energetics of open clusters and found that all the most stable clusters satisfy Lowenstein's rule, but not strictly obey Dempsey's rule. However, such evidence cannot be used to account for what happens in rings because open clusters are merely temporary products in the nucleation processes of zeolites before condensing to various rings. We now consider the energetics of rings. Concentrating on that with two and three Al atoms substituted.

3.3.4.1 Two Al substitutions in the four, five and six rings

Results for structures when two Al atoms substituting for two Si atoms in the four, five and six rings are revealed in Table 3.9. First, for the four and five rings, in the gas phase and COSMO solvation, the most stable rings were found to be four ring B1 and five ring B1, which are Lowensteinian structures, whereas the rings with the Al-O-Al linkage are less stable. Similarly, the result for the six rings shows Lowensteinian behaviour in that six rings B1 and B2 (Figures 3.63-3.64), with the Al-Al separated

distribution are more stable than six ring B3 with the Al-O-Al linkage. On comparing the energy of six ring B1 with that of six ring B2 in the gas phase, there is the little difference, with the former being only 6 kJmol⁻¹ more stable, which is inconsistent with Dempsey's rule as the Al-Al distance of six ring B1 (4.70 Å) is shorter than that of six ring B2 (5.32 Å). Conversely, in COSMO solvation, the situation changes for two the six rings; six ring B1 is less stable than six ring B2 by 6 kJmol⁻¹, corresponding to Dempsey's rule. Indeed, the COSMO solvation, as previously mentioned, plays the significant role in controlling the conformations of clusters.

Table 3.9 Relative energies (kJmol⁻¹) of aluminosilicate isomers: two Al substitutions in the four, five and six rings in the gas phase and COSMO solvation.

Rings		Gas	COSMO	sol.		Gas	COSMO	sol.
4-ring B1		0	0		6-ring B1		0	6
4-ring B2		4	27		6-ring B2		6	0
5-ring B1		0	0		6-ring B3		61	67
5-ring B2		33	49					

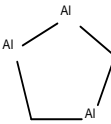
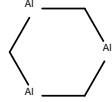
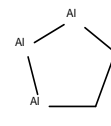
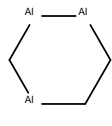
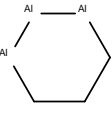
3.3.4.2 Three Al substitutions in the five and six rings

Finally considering the three Al atom substitutionals in the six rings, three the distinct six rings can be compared. The order of stability is: six ring C1 > six ring C2 > six ring C3, with the preference for the formation of six ring C1, in which Al atoms have the alternating ordered distribution. In six rings C2 and C3, the energy is calculated to be higher than six ring C1, owing to the presence of the Al-O-Al linkages.

Indeed, in COSMO solvation, all the most stable rings follow not only Lowenstein's rule but also Dempsey's rule. Indeed, Dempsey's rule, like Lowenstein's rule, may

arise from the stability of the small rings formed during the synthesis of aluminosilicate zeolites.

Table 3.10 Relative energies (kJmol^{-1}) of aluminosilicate isomers: three Al substitutions in the five and six rings in the gas phase and COSMO solvation.

Rings		Gas	COSMO	sol.		Gas	COSMO	sol.
5-ring C1		0	0		6-ring C1		0	0
5-ring C2		60	41		6-ring C2		20	38
					6-ring C3		75	93

3.4 Conclusion

In this chapter, we have analysed key aluminosilicate clusters with regard to both their structures and their relative energies in both gas phase and COSMO solvation. This work reveals that the factors controlling the formation of these calculated clusters are complex because they are directly influenced by the Si/Al distribution and the location of the extra-framework Na^+ ions as well as the formation of intramolecular hydrogen bonds. Such factors, of course, give rise to changes in the bond lengths and angles within the structures, resulting in the structural distortion, which plays an important role in determining the relative stability of the framework.

On the other hand, for the relative stability of aluminosilicate clusters, our result shows that in the gas phase, Lowensteinian clusters are more stable than non-Lowensteinian clusters, except for dimers, and the energies are inconsistent with Dempsey's rule. Moreover, the most stable clusters calculated, especially the open clusters, are found to have the highly symmetrical structures resulting in the favorable charge distribution in their structures. It is worth noting that the competition of the interplay between the Na^+ ions and hydrogen bonds in these clusters can control the

stability of the structures.

In COSMO solvation, we find substantially different results. Some of the most stable clusters, particularly pentamers and hexamers, have the asymmetric structures. Although the interplay between the solvated clusters and intermolecular hydrogen bonds is not modeled in this work, we still propose that when water interacts with these clusters they can form intermolecular hydrogen bonds and consequently better stabilize their structures in the solvent. As expected, in COSMO solvation, all of the most stable clusters follow not only Lowenstein's rule but also Dempsey's rule. In the next chapter, we will further discuss the relative condensation reactions of forming clusters in zeolite synthesis.

References:

1. S. D. Kinrade and T. W. Swaddle, *Inorganic Chemistry* **1989**, 28, 1952
2. O. Ziemens, O. Rademacher and H. Scheler, *Zeitschrift für Chemie* **1989**, 29, 341
3. A. V. McCormick, A. T. Bell and C. J. Radke, *Journal of Physical Chemistry* **1989**, 93, 1741
4. R. F. Mortlock, A. T. Bell and C. J. Radke, *Journal of Physical Chemistry* **1991**, 95, 372
5. R. F. Mortlock, A. T. Bell, A. K. Chakraborty and C. J. Radke, *Journal of Physical Chemistry* **1991**, 95, 4501
6. R. F. Mortlock, A. T. Bell and C. J. Radke, *Journal of Physical Chemistry* **1991**, 95, 7847
7. M. R. North and T. W. Swaddle, *Inorganic Chemistry* **2000**, 39, 2661
8. A. Samadi-Maybodi, N. Goudarzi and H. Naderi-Manesh, *Bulletin of the Chemical Society of Japan* **2006**, 79, 276
9. I. H. Lim, W. Schrader and F. Schüth, *Microporous and Mesoporous Materials* **2012**
10. T. Wakihara, S. Kohara, G. Sankar, S. Saito, M. Sanchez-Sanchez, A. R. Overweg, W. Fan, M. Ogura and T. Okubo, *Physical Chemistry Chemical Physics* **2006**, 8, 224
11. G. Sankar, J. M. Thomas and C. R. A. Catlow, *Topics in Catalysis* **2000**, 10, 255
12. C. R. A. Catlow and G. N. Greaves, in *Applications of Synchrotron Radiation*, Blackie, London, **1990**.
13. P. S. Singh, T. L. Dowling, J. N. Watson and J. W. White, *Physical Chemistry Chemical Physics* **1999**, 1, 4125.
14. W. Fan, M. O'Brien, M. Ogura, M. Sanchez-Sanchez, C. Martin, F. Meneau, K. Kurumada, G. Sankar and T. Okubo, *Physical Chemistry Chemical Physics* **2006**, 8, 1335
15. W. Fan, M. Ogura, G. Sankar and T. Okubo, *Chemistry of Materials* **2007**, 19, 1906
16. C. Baerlocher, W. M. Meier and D. H. Olson, 5th ed., Elsevier-International Zeolite Association, Amsterdam, **2001**, p. 302.
17. J. A. Tossell, *Journal of Physical Chemistry* **1996**, 100, 14828.
18. J. A. Tossell and G. Saghizaboo, *Geochimica Et Cosmochimica Acta* **1997**, 61, 1171.

19. C. R. A. Catlow, A. R. George and C. M. Freeman, *Chemical Communications*, **1996**, 1311.
20. A. R. Leach, *Molecular Modelling Principles and Applications*, 2nd ed., Prentice Hall, Harlow, **2001**.
21. A. Klamt and G. Schuurmann, *Journal of the Chemical Society-Perkin Transactions 2* **1993**, 799
22. K. Baldrige and A. Klamt, *Journal of Chemical Physics* **1997**, *106*, 6622
23. W. Loewenstein, *American Mineralogist* **1954**, *39*, 92
24. W. Dempsey, G. H. Kuhl and D. H. Olson, *Journal of Physical Chemistry* **1969**, *73*, 387
25. Biosym/MSI, *DMol USER GUIDE*, San Diego, 1995.
26. J. C. G. Pereira, C. R. A. Catlow and G. D. Price, *Journal of Physical Chemistry A* **1999**, *103*, 3252
27. M. J. Mora-Fonz, C. R. A. Catlow and D. W. Lewis, in *Molecular Sieves, from Basic Research to Industrial Applications, Parts A and B* **2005**, *158*, pp. 295.
28. S. L. Lawton, W. J. Rohrbaugh, *Science* **1990**, *247*, 1319.
29. H. Robson, *Verified Syntheses of Zeolitic Materials*, 2nd ed., Elsevier - International Zeolite Association, Amsterdam, **2001**.
30. J. D. Gale and A. K. Cheetham, *Zeolites* **1992**, *12*, 674
31. J. J. Pluth and J. V. Smith, *Journal of the American Chemical Society* **1980**, *102*, 4704
32. G. Vitale, C. F. Mellot, L. M. Bull and A. K. Cheetham, *Journal of Physical Chemistry B* **1997**, *101*, 4559
33. B. Tagirov, J. Schott, J. C. Harrichoury and J. Escalier, *Geochimica Et Cosmochimica Acta* **2004**, *68*, 1333.

Chapter 4

Modelling the Polymerisation of Aluminosilicate Clusters

4.1 Introduction

In our previous chapter, molecular simulations employing the DFT/COSMO method were used to investigate the relative structures and energies of several aluminosilicate clusters containing between one and six Si/Al atoms. The main achievement was the successful identification of a series of key aluminosilicate open clusters and rings involved in the prenucleation and subsequent growth processes of aluminosilicate zeolites. As a result, this knowledge can help us to provide a detailed understanding of growth mechanisms of aluminosilicate zeolites. This is a different problem, given that internal and external factors such as pH, reaction time, temperature and various Si/Al ratios have the strong influence over the formation process of zeolites. In particular, the complexity of aluminosilicate zeolites with their variable Si/Al ratios, increases the variety and complexity of the nucleation and growth behaviour.

The aluminosilicate zeolite, whose growth mechanisms have been most widely studied is, zeolite A, composed of the four, six, and double four rings and cages, which have the simple 1:1 Si/Al ratio. In other words, the structure of zeolite A is an assembly of framework's cages; by bridging the cages, zeolite A is formed. Experimental investigations on the formation of zeolite A have been widely reported: NMR¹⁻⁴, high-resolution transmission electron microscopy (HRTEM)⁵⁻⁷, atomic force microscopy (AFM)^{8,9} and Raman spectroscopy¹⁰ supported by X-ray diffraction and NMR have investigated prenucleation and crystal growth. Recently, evidence from *in situ* small angle and wide angle X-ray scattering (SAXS/WAXS)^{11,12} and high-energy X-ray diffraction (HEXRD)¹³ clearly revealed the presence of the small aluminosilicate rings (the four, five and six rings) in the early stages of the nucleation process. Furthermore, UV-Raman spectroscopy combined with XRD¹⁴ or NMR¹⁵ has also been employed to analyse the crystallization of zeolite A and suggested that the four rings or double four rings (D4Rs) are probably the main initial species. Indeed

these studies confirm that the aluminosilicate gel participates in the nucleation of zeolite A that proceeds via small clusters. These questions provoke the primary question of what kinds of key small species such as the $\text{Si}(\text{OH})_4$ or $\text{Al}(\text{OH})_4\text{Na}$ monomers or the $\text{AlSiO}(\text{OH})_6\text{Na}$ dimer are involved in forming these precursor gel species and in facilitating the subsequent development of the nucleation of zeolite A. First, the addition of the $\text{Al}(\text{OH})_4^-$ monomer onto aluminosilicate gel species has been considered as a basic process in the formation of zeolite A by Dutta et al.¹⁰. Additionally, Ciric¹⁶ suggested that in term of the kinetics, possibly the small species: dimers (most likely $(\text{OH})_3\text{AlOSiO}_x(\text{OH})_{3-x}^{(x+1)-}$) or tetramers are the main building units of the formation of zeolite A and Shi et al.³ suggested that from the NMR spectroscopy the silicate and aluminate ions (probably $(\text{OH})_3\text{AlOSiO}_x(\text{OH})_{3-x}^{(x+1)-}$) are incorporated into growing zeolite A crystal. In practice, we are interested in the involvement of the $\text{AlSiO}(\text{OH})_6\text{Na}$ dimer in the nucleation process of zeolite A. Although these studies have provided valuable information regarding the nucleation of zeolite A, only a few studies of the nucleation and growth of zeolite A are investigated by using computational techniques. The subsequent condensation reactions of open aluminosilicate clusters as well as aluminosilicate rings have not yet been investigated; knowledge of these processes is, however, needed if we are to extend our understanding of the overall growth processes.

In this chapter, the same method (DFT/COSMO) is used to simulate polymerisation reactions of the open aluminosilicate clusters and rings in the gas phase and COSMO solvation at 298 and 450K; the characteristic thermodynamical property -Gibbs free energy- for each condensation reaction is presented. Our analysis consists of two basic components: the first is that the main starting reactants are open aluminosilicate clusters between one and four Si/Al atoms which condense with the $\text{Si}(\text{OH})_4$ or $\text{Al}(\text{OH})_4\text{Na}$ monomers or $\text{AlSiO}(\text{OH})_6\text{Na}$ dimer and in the second part, the main starting reactants are aluminosilicate rings including the four, six, double four and double six rings whose compositions are limited to the same Si/Al ratio, which then condense with the $\text{Si}(\text{OH})_4$ or $\text{Al}(\text{OH})_4\text{Na}$ monomers or the $\text{AlSiO}(\text{OH})_6\text{Na}$ dimer. It is worth nothing that in the present study, we consider neutral clusters, which will correspond to less alkaline conditions in which zeolite A has been successfully synthesised¹⁷.

This study therefore attempts to analyse the energetics of the polymerisation reactions of these aluminosilicate open clusters and rings and then to identify not only which pathway is favourable but, of equal importance, which small species regarding the $\text{Si}(\text{OH})_4$ or $\text{Al}(\text{OH})_4\text{Na}$ monomers or the $\text{AlSiO}(\text{OH})_6\text{Na}$ dimer can readily participate in the nucleation and crystal growth processes.

4.2 Methodology

Our previous chapter have modelled a series of key aluminosilicate open clusters and rings with the DFT method. In this chapter, the modelling of a range of large aluminosilicate rings with the limited same Si/Al ratio (Si/Al=1) and the inclusion of sodium ions in the double four and double six rings and the relative fused rings regarding the fused four, six, double four and double six rings are optimised as previously using the DMol³ code¹⁸ based on density functional theory (DFT) with a double numerical basis set plus polarization (DNP) and the BLYP exchange-correlation functional; while the COSMO approach^{19,20} is used to simulate the solvation of the aluminosilicate rings whose geometries are reoptimised.; the techniques used are the same as those detailed in chapter 2. As previously explained, the calculation of the Gibbs free energy with the zero-point energy, and the translational, rotational, and vibrational contributions is achieved by a statistical mechanical approach using the electronic energy from the BLYP/DNP method for two temperatures of 298 and 450 K; for the gas phase and COSMO solvation.

4.3 Results and Discussion

The relative aluminosilicate clusters considered are shown in Figures 4.1-4.9; in addition we refer to our result on monomers, dimers, open clusters and rings including relevant condensation reactions reported in Tables 4.1-4.8. First, we analyse the geometric features of the relative clusters involved in the reactions regarding the double four and double six rings and relative fused rings, which are shown in Figures 4.1-4.9. We are, however, mainly concerned with the mechanism involved in the subsequent condensations onto these clusters. Our investigation of the mechanisms of the condensation reactions has four components. (i) Compared with the free energies of these condensation reactions in different open clusters, the result for the gas phase and COSMO solvation is given in Tables 4.1 and 4.2,

where the Gibbs free energies that involve the condensation reactions of adding the $\text{Si}(\text{OH})_4$ or $\text{Al}(\text{OH})_4\text{Na}$ monomers or $\text{AlSiO}(\text{OH})_6\text{Na}$ dimer are calculated. (ii) The condensation of the $\text{Si}(\text{OH})_4$ or $\text{Al}(\text{OH})_4\text{Na}$ monomers on these starting reactants including the four, six, double four and double six rings, to determine which is the key species in the condensation processes; the calculated Gibbs free energies for various polymerisation reactions are showed in Tables 4.3 and 4.4. (iii) In the light of Lowenstein's rule, further consideration of the Gibbs free energies of the condensation by adding the $\text{Si}(\text{OH})_4$ or $\text{Al}(\text{OH})_4\text{Na}$ monomers or $\text{AlSiO}(\text{OH})_6\text{Na}$ dimer onto the fused rings in order to throw light on the subsequent growth process, as showed in Tables 4.5 and 4.6. (iv) Analysis of the Gibbs free energies for the addition of the $\text{AlSiO}(\text{OH})_6\text{Na}$ dimer condensing with these rings including the four ring, six ring, double four ring and double six ring giving further insight into which the pathway is favoured in the condensation reactions, as showed in Tables 4.7 and 4.8.

4.3.1 Geometry analysis

In the previous chapter, we focused on the detailed analyses of the bond lengths and angles for several open clusters and rings. Hence, in this section, we focus on the geometrical implications on the condensation reactions.

4.3.1.1 Cages: the double four and double six rings

The optimised structures of the double four and double six rings which can be described as the symmetric polyhedra without internal hydrogen bonds and whose structures are rigid with respect to their geometries, are shown in Figure 4.1.

In contrast to the geometry proposed for the double four ring in which each Na^+ ion is located near the centre of one of four face of the cube structure by Tossell²¹, we suggest the structure in which each Na^+ ion is located near the middle of one of four edges of the cube structure and almost equally bonded to the three O atoms forming the highly symmetrical configuration. In the double six ring, the coordination of each Na^+ ion is arranged to bond to the three or four O atoms; each of the two Na^+ ions is near the centre of a hexagon-like plane respectively and the others are arranged in the middle of four edges symmetrically. Regarding the geometric parameters for the double four and double six rings: the range of the T-O bond lengths is 1.68-1.84 Å,

of the T-O_b-T angles is 125-151° and of the Na-O bond lengths is 2.24-2.70 Å.

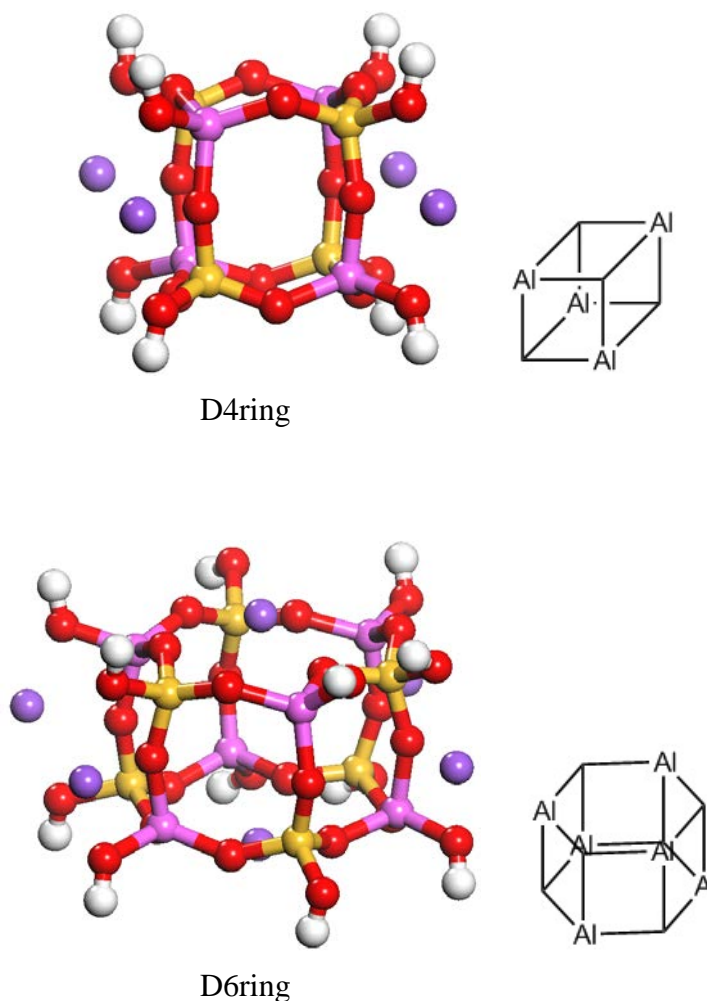


Figure 4.1 Optimised aluminosilicate rings: the double four and double six rings. The abbreviations and line diagrams illustrating connectivity are also shown here. In all Figures, colour coding is as follows: purple Na⁺ ion, yellow Si, pink Al, red O and white H atoms.

4.3.1.2 Ring structures with the “hanging” monomers or dimers

In the nucleation and subsequent growth processes, the stage of the formation of a multitude of multiple rings, which is linked together to be a zeolite crystal nucleus is critical. In general, the conversion from the single aluminosilicate ring to multiple aluminosilicate rings is accomplished by the "hanging" Si(OH)₄ or Al(OH)₄Na monomers or "hanging" AlSiO(OH)₆Na dimer onto the rings. In this

section, we study the structures of the fused four, six, double four and double six rings in which the chain units of the fused rings are the $\text{Si}(\text{OH})_4$ or $\text{Al}(\text{OH})_4\text{Na}$ monomers or $\text{AlSiO}(\text{OH})_6\text{Na}$ dimer.

First let us considered the addition of the $\text{Si}(\text{OH})_4$ or $\text{Al}(\text{OH})_4\text{Na}$ monomers or on the four, six, double four and double six rings. Basically, these rings have two distinct and active sites: the Si and Al atoms, on which the $\text{Si}(\text{OH})_4$ or $\text{Al}(\text{OH})_4\text{Na}$ monomers can be added. There are, therefore, the four possible configurations to be formed for each ring type, abbreviated as the Si-(Si), Si-(Al), Al-(Si), and Al-(Al) fused rings respectively. Here, “(Si)” and “(Al)” denote the active site of the fused ring and “Al” and “Si” refer to the reactants involved i.e. the $\text{Si}(\text{OH})_4$ and $\text{Al}(\text{OH})_4\text{Na}$ monomers. The four possible configurations of the fused four, six, double four and double six rings are illustrated in Figures 4.2-4.5. Similarly, on condensing with the $\text{AlSiO}(\text{OH})_6\text{Na}$ dimer, each type of ring can form four possible fused ring isomers: the Al-Si-(Si), Si-Al-(Si), Al-Si-(Al), and Si-Al-(Al) fused rings. Figures 4.6-4.9 represents four different fused ring isomers regarding fused four, six, double four and double six rings. Moreover, the Al-Al-(Si), Al-Si-Al-(Si) and Si-Al-Al-(Si) fused rings, which have the addition of the $\text{Al}(\text{OH})_4\text{Na}$ monomer or $\text{AlSiO}(\text{OH})_6\text{Na}$ dimer on the Al-(Si) fused four, six, and double four rings are also shown.

We note that while the $\text{Si}(\text{OH})_4$ or $\text{Al}(\text{OH})_4\text{Na}$ monomers or $\text{AlSiO}(\text{OH})_6\text{Na}$ dimer are added on the four, six, double four and double six rings, these additional units, especially the $\text{Al}(\text{OH})_4\text{Na}$ monomers or $\text{AlSiO}(\text{OH})_6\text{Na}$ dimer with the extra Na^+ ion will cause some structural changes of these fused rings, which result from the change of the location of the Na^+ ions associated with additional intramolecular hydrogen bonds generated in the structures comparable to the original rings.

First, for the fused four rings, we find that there are significant structural changes in the fused four rings as seen on comparing the fused six, double four and six rings, due to the influence of the change of the location of the Na^+ ions and formation of several intramolecular hydrogen bonds, which indicates the flexibility of the fused four rings. In contrast, the structural features of the fused six, double four and double six rings are similar to the six, double four and double six rings, even though the addition of the $\text{Si}(\text{OH})_4$ or $\text{Al}(\text{OH})_4\text{Na}$ monomers or $\text{AlSiO}(\text{OH})_6\text{Na}$ dimer on the six, double four

and double six rings has led not only to the slight change of the location of the Na^+ ions, but also to several intramolecular hydrogen bonds that are generated in the structures.

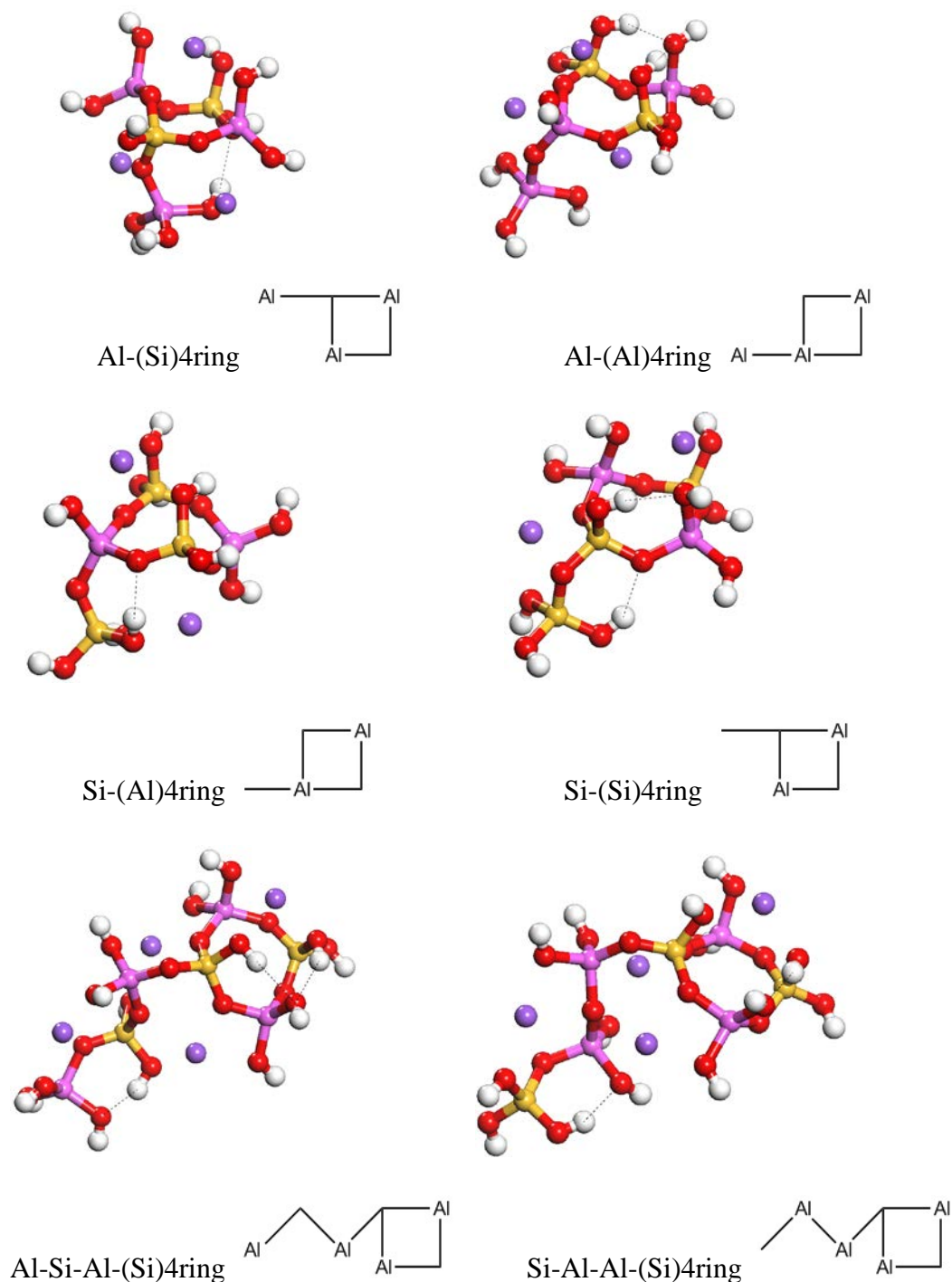


Figure 4.2 Optimised aluminosilicate fused four rings. In the abbreviation, “()” indicates the active atom at which the condensation with other species.

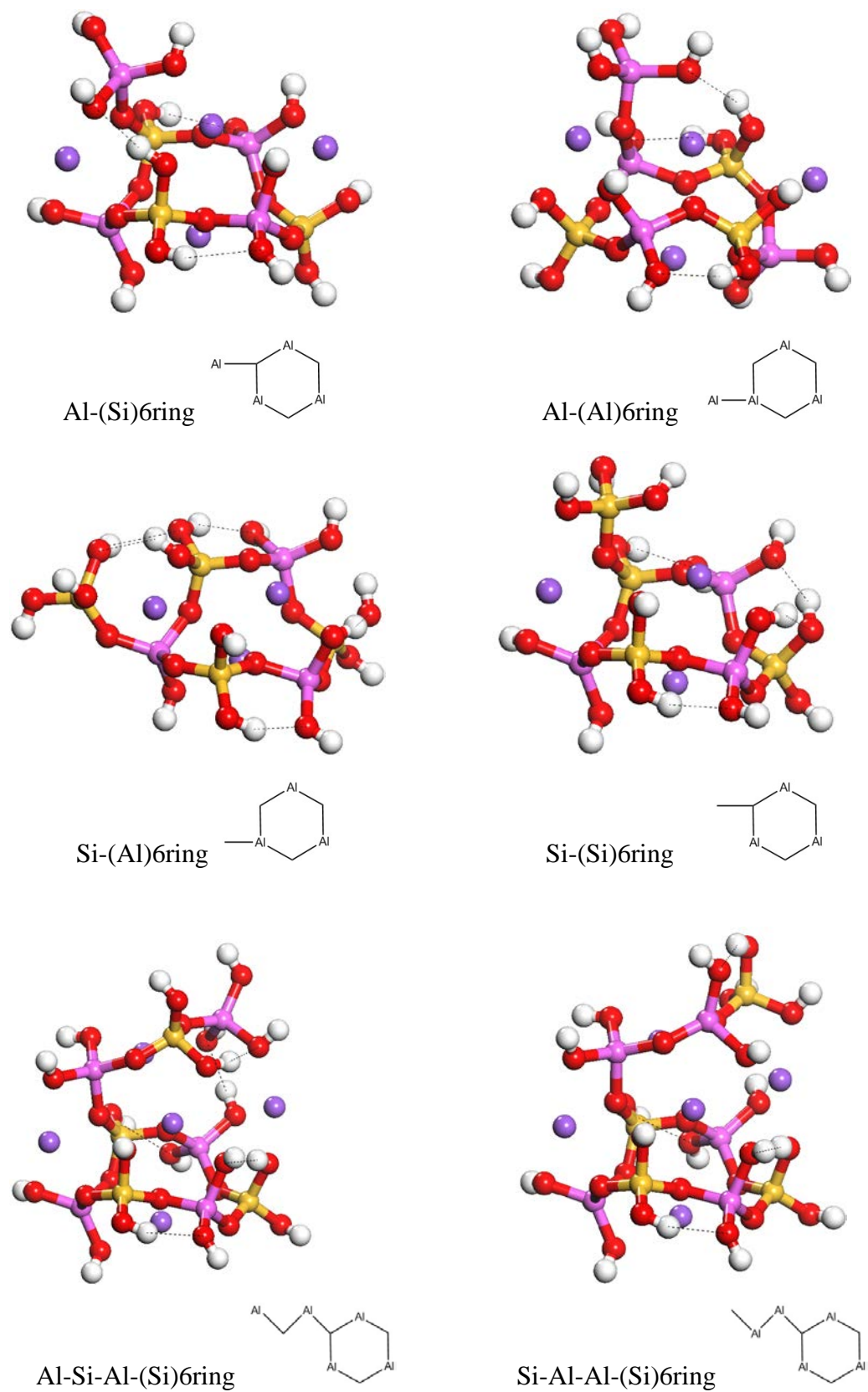


Figure 4.3 Optimised aluminosilicate fused six rings.

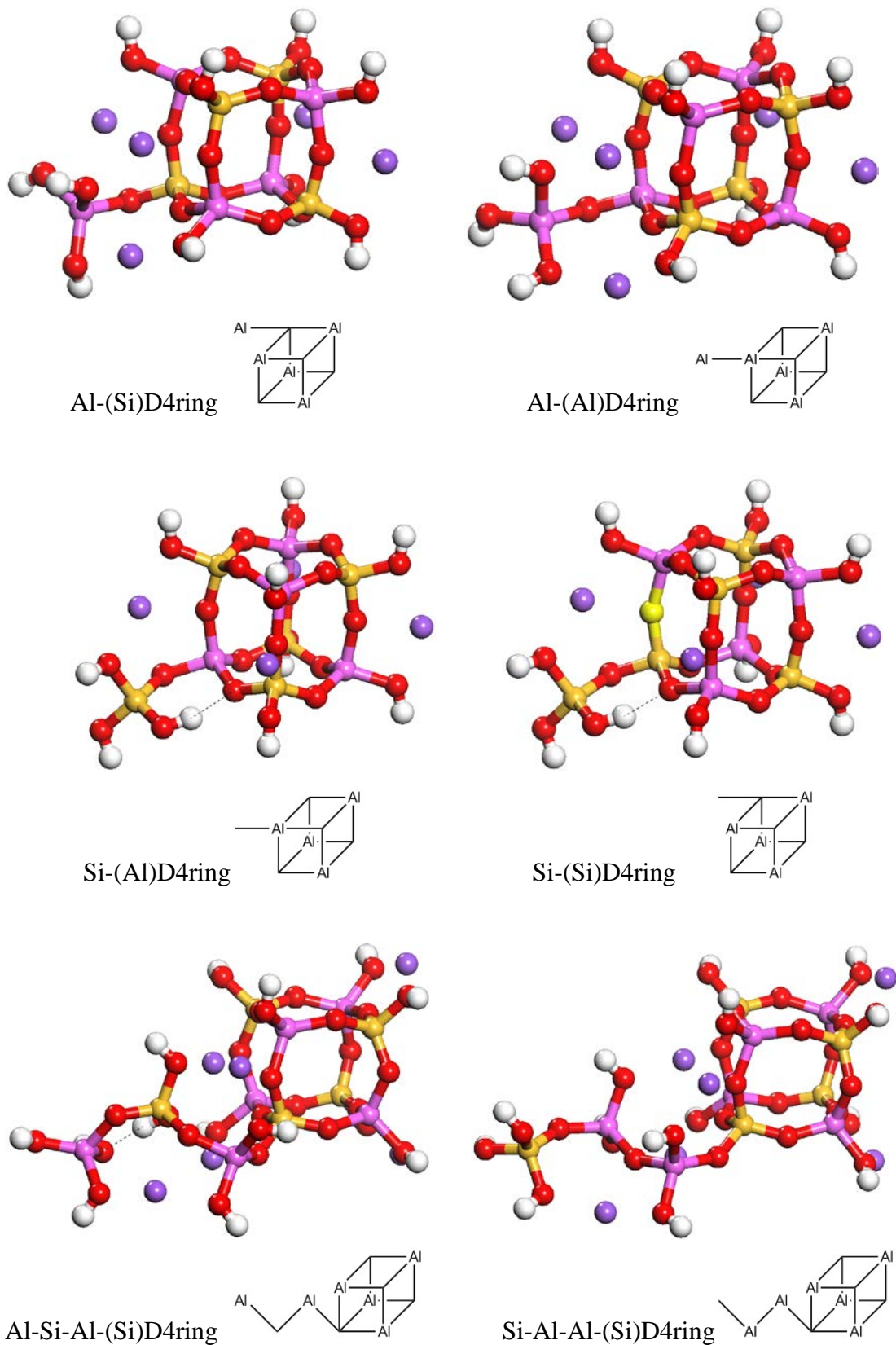
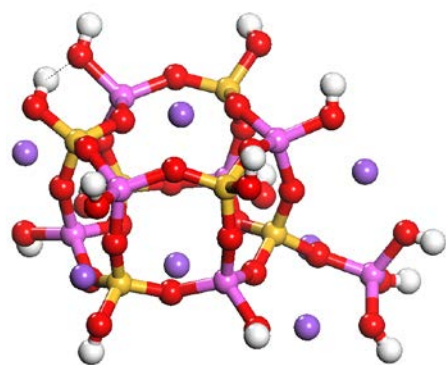
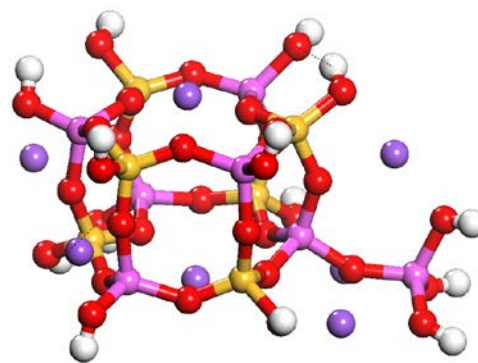
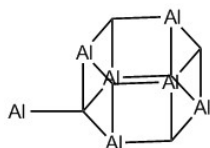


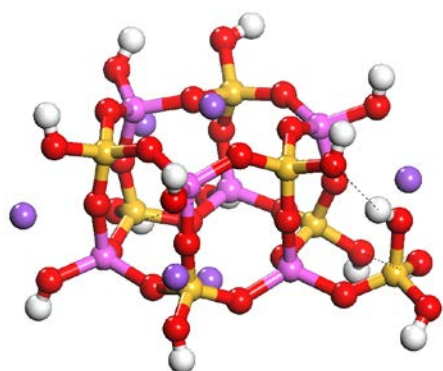
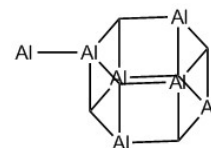
Figure 4.4 Optimised aluminosilicate fused double four rings.



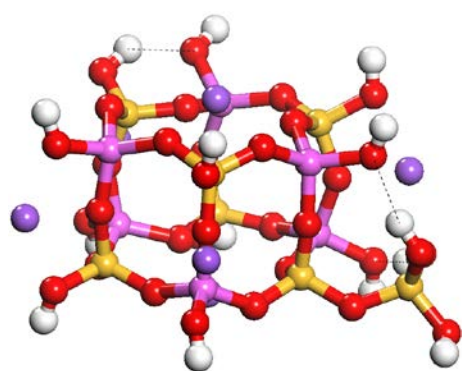
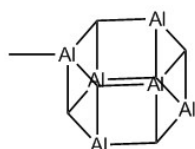
Al-(Si)D6ring



Al-(Al)D6ring



Si-(Al)D6ring



Si-(Si)D6ring

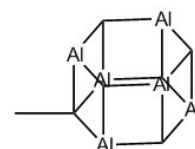


Figure 4.5 Optimised aluminosilicate fused double six rings.

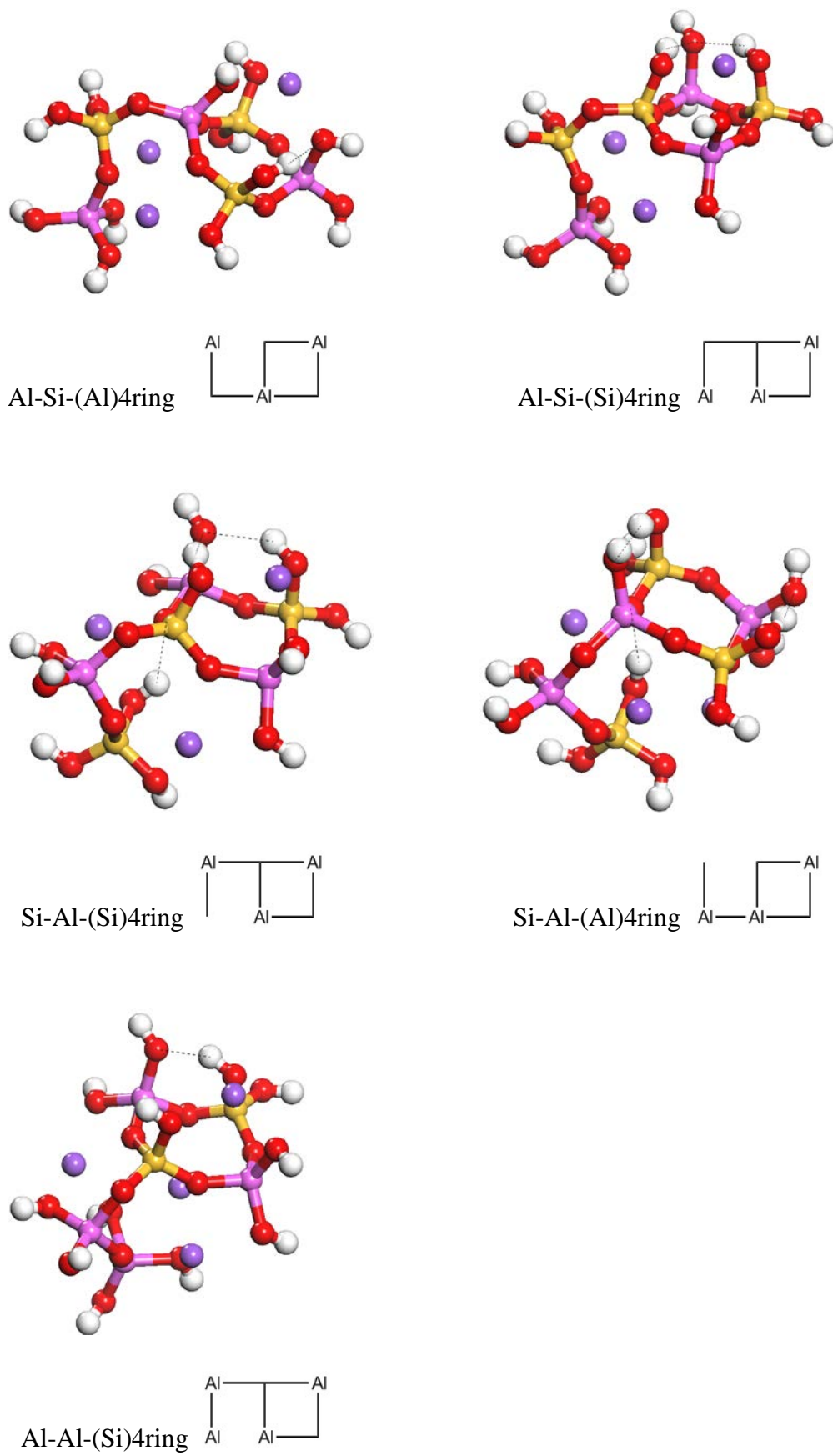


Figure 4.6 Optimised aluminosilicate fused four rings.

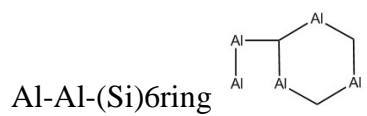
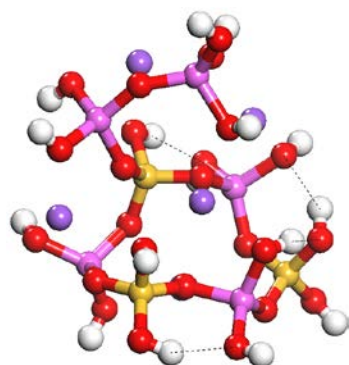
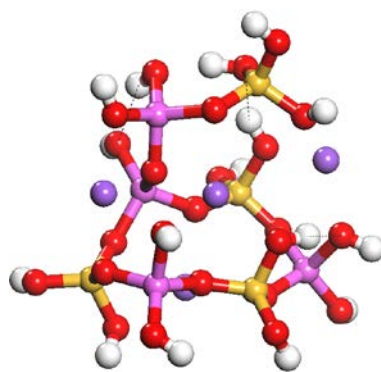
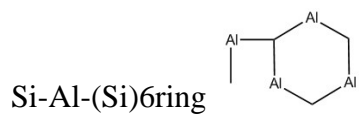
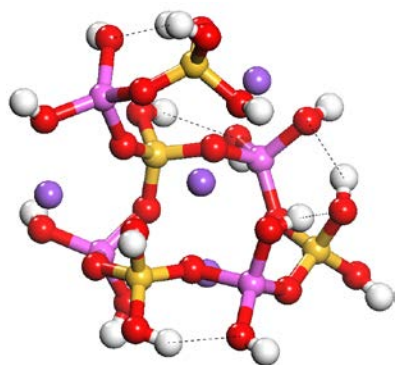
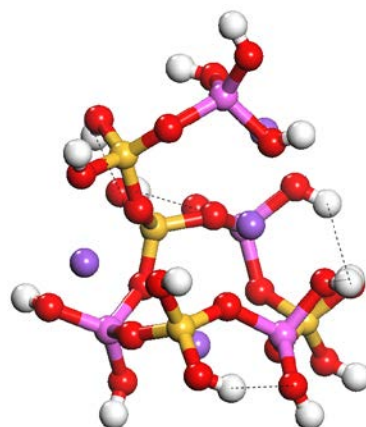
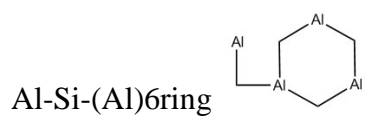
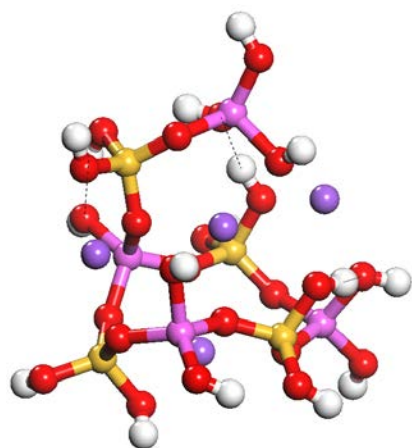
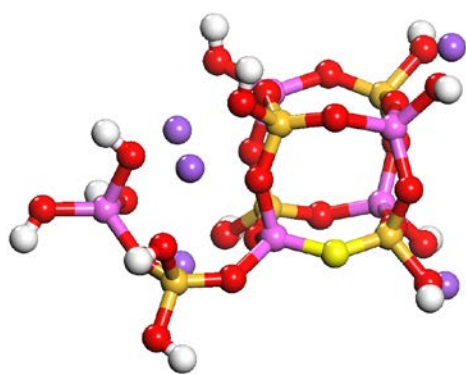
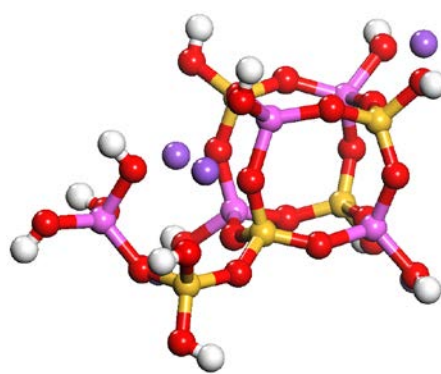
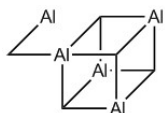


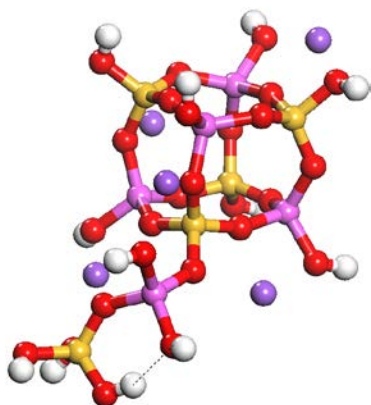
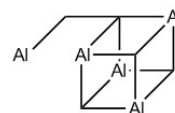
Figure 4.7 Optimised aluminosilicate fused six rings.



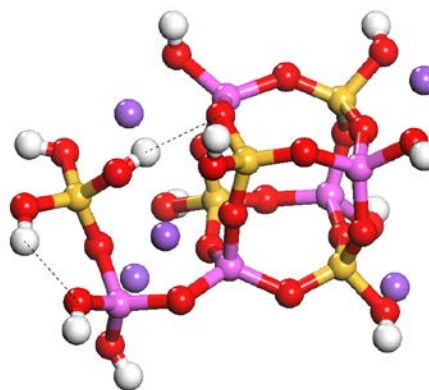
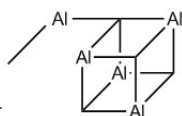
Al-Si-(Al)D4ring



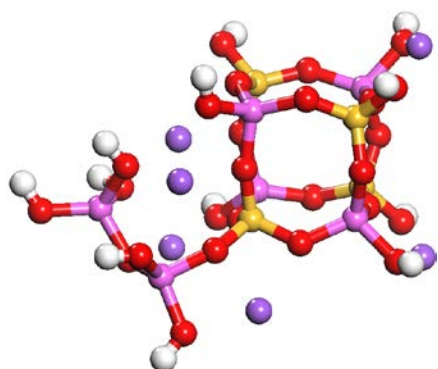
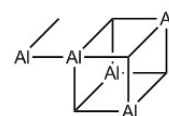
Al-Si-(Si)D4ring



Si-Al-(Si)D4ring



Si-Al-(Al)D4ring



Al-Al-(Si)4ring

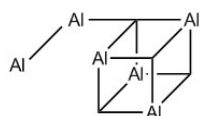


Figure 4.8 Optimised aluminosilicate fused double four rings.

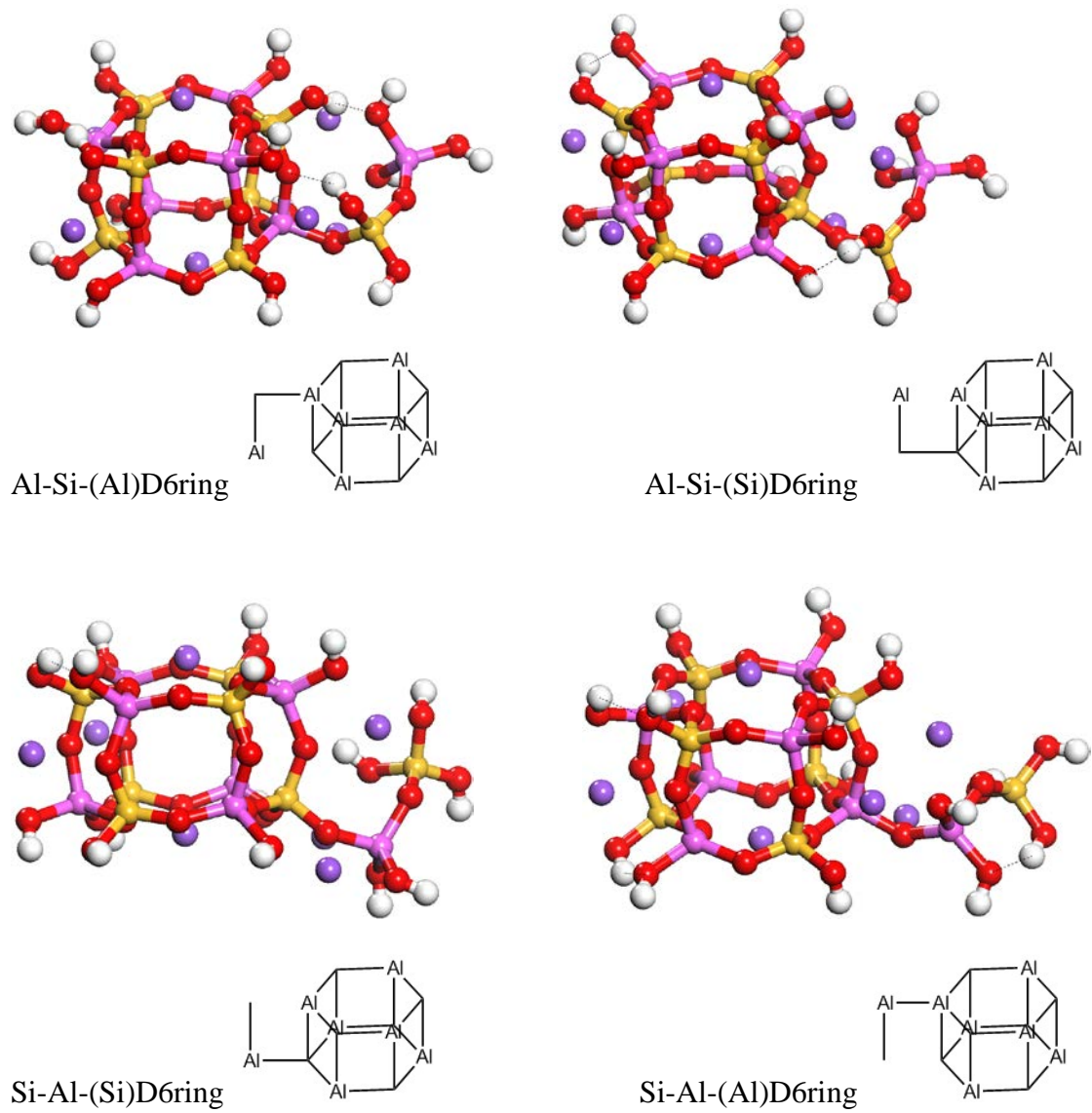


Figure 4.9 Optimised aluminosilicate fused double six rings.

4.3.2 Condensation reactions of open clusters and rings

Following the structures of optimised open clusters and rings in the earlier section, we now study the question of how the condensation reactions of open clusters occur and in particular examine addition of the $\text{Si}(\text{OH})_4$ or $\text{Al}(\text{OH})_4\text{Na}$ monomers or $\text{AlSiO}(\text{OH})_6\text{Na}$ dimer onto the four, six, double four and double six rings with a view to understanding which of these species participate in the nucleation and crystal growth processes.

4.3.2.1 Condensation reactions of open clusters

Before going into a detailed analysis of each condensation reaction of the ring, it is important to understand the condensation reactions of open clusters, which are not only directly related to the formation of the ring, but also provide us with key information on the question of the condensation reactions of aluminosilicate zeolites. The free energies associated with several forms of the condensation reactions of open clusters in both the gas phase and COSMO solvation between 298 and 450K are summarised in Tables 4.1 and 4.2. The first column concerns the reactants involving in the condensation reactions; the second column concerns the products that are produced.

4.3.2.1.1 Trimerisation reactions

The first condensation reactions: dimerisation reactions have been analysed in chapter 3; the result suggests that under the thermodynamical condition, the $\text{AlSiO}(\text{OH})_6\text{Na}$ dimer is preferentially formed in the nucleation of aluminosilicate zeolites in COSMO solvation. As a result, the $\text{AlSiO}(\text{OH})_6\text{Na}$ dimer is chosen to participate in the further condensation reactions. Considering now trimerisation reactions (Table 4.1), the two competing trimerisation reactions considered in the gas phase as well as COSMO solvation involve associating the $\text{AlSiO}(\text{OH})_6\text{Na}$ dimer with the $\text{Si}(\text{OH})_4$ or $\text{Al}(\text{OH})_4\text{Na}$ monomers. In the gas phase, the free energy of the formation of the Si-Al-Si trimer is -32 (298K) and -27 kJmol^{-1} (450K) and that of the Al-Si-Al trimer is -112 (298K) and -110 kJmol^{-1} (450K). Obviously, the formation of the Al-Si-Al trimer is comparatively much more favourable than that of the Si-Al-Si trimer. But we recall that zeolites are synthesized in aqueous media but not in the gas phase. Thus, it is important to have the analysis of the same trimerisation reactions including the COSMO solvation, as also shown in Table 4.1; the free energies of the formation of

the Si-Al-Si trimer are -30 (298K) and -26 kJmol⁻¹ (450K) and that of Al-Si-Al trimer are -48 (298K) and -52 kJmol⁻¹ (450K). Although the effect of solvation causes substantial reduction of the free energy of the formation of the Al-Si-Al trimer the same result can also be observed: the formation of the Al-Si-Al trimer is still more favourable than that of the Si-Al-Si trimer. As a result, it can be note that in trimerisation reactions, the Al(OH)₄Na monomer will preferentially condense with the AlSiO(OH)₆Na dimer rather than the Si(OH)₄ monomer. We can explain this interesting result on the basis of electrostatics, we propose that the Al(OH)₄Na monomer ,which is the intrinsic charged species is more reactive than the neutral Si(OH)₄ monomer.

Table 4.1 Calculated free energy (ΔG , kJmol⁻¹) change in the gas phase and COSMO solvation at 298K and 450K in polymerisations.

reactants		products	Gas		COSMO sol.	
			298K	450K	298K	450K
dimerisations						
Al	Si	Al-Si	-60	-54	-21	-23
Al	Al	Al-Al	-106	-100	-16	-18
trimerisations						
Al-Si	Si	Si-Al-Si	-32	-27	-30	-26
Al-Si	Al	Al-Si-Al	-112	-110	-48	-52

4.3.2.1.2 Tetramerisation reactions

The next condensation reactions considered are the tetramerisation reactions. Owing to the four ring being the simplest and most basic building unit in the frameworks of several zeolites, tetramerisation reactions are thought to be a crucial step. Tetramers can directly form four rings via internal condensation reactions, but here we consider the condensation reactions of the trimers and monomer or of the two dimers. The result for the tetramerisation reactions is shown in Table 4.2; there are seven different condensation reactions of forming tetramers through the two types of trimers (the Si-Al-Si or Al-Si-Al trimers) and two types of monomers (the Si(OH)₄ or Al(OH)₄Na monomers) and of the two AlSiO(OH)₆Na dimer. It is also worth noting that in the tetramerisation reactions, the formation of the Si-Al-Si trimer is calculated to be less favourable than that of the Al-Si-Al trimer, but consideration reaction of the Si-Al-Si

trimer involves in the tetramerisation reaction is to do double check if the $\text{Al(OH)}_4\text{Na}$ monomer is more reactive with other trimers except the Al-Si-Al trimer than the Si(OH)_4 monomer in tetramerisation reactions.

4.3.2.1.2.1 Tetramerisation reactions with the Si(OH)_4 or $\text{Al(OH)}_4\text{Na}$ monomers

First, considering the formations of two tetramers (the Si-Al-Si-Si and Al-Si-Al-Si tetramers) from the Si-Al-Si trimer and Si(OH)_4 or $\text{Al(OH)}_4\text{Na}$ monomers as shown in Table 4.2. Initially, the tetramerisation reactions in the gas phase are considered, the large different free energies between the Si-Al-Si-Si and Al-Si-Al-Si tetramers are found to be -17 (298K) and -18 kJmol^{-1} (450K) and -98 (298K) and -92 kJmol^{-1} (450K), respectively; the formation of the Al-Si-Al-Si tetramer is significantly more thermodynamically feasible than that of the Si-Al-Si-Si tetramer, which, again shows that the tetramerisation reaction that is proceeded via the $\text{Al(OH)}_4\text{Na}$ monomer is more energetically favoured instead of the Si(OH)_4 monomer. Considering now the inclusion of the COSMO solvation, the result shows that the free energy for the Si-Al-Si-Si tetramers becomes the little more favourable (-26 (298K) and -26 kJmol^{-1} (450K)) and on the contrary, the free energy for the Al-Si-Al-Si tetramers become less favourable (-33 (298K) and -48 kJmol^{-1} (450K)), thus according to this result, the $\text{Al(OH)}_4\text{Na}$ monomer is a need to be taken part in the tetramerisation reactions instead of the Si(OH)_4 monomer.

Comparing now the free energies of the two tetramers (the Al-Si-Al-Si and Al-Si-Al-Al tetramers) from the Al-Si-Al trimer and Si(OH)_4 or $\text{Al(OH)}_4\text{Na}$ monomers. In the gas phase, we find that the formation of the Al-Si-Al-Al tetramer (-89 (298K) and -78 kJmol^{-1} (450K)) is more energetically favourable than that of the Al-Si-Al-Si tetramer (-19 (298K) and -9 kJmol^{-1} (450K)). The formation of the Al-Si-Al-Al tetramer, however, would contradict Lowenstein's rule; in other words, such a condensation reaction occurred will preferentially generate a large amount of clusters (the Al-Si-Al-Al tetramer), which would hinder the development of the next condensation reaction. We consider that it is unlikely that this non-Lowensteinian reaction proceeds raising the issue if the $\text{Al(OH)}_4\text{Na}$ monomer indeed participates in the tetramerisation reactions.

After the COSMO solvation is introduced, compared with the free energy of the

Al-Si-Al-Al tetramer with -18 kJmol^{-1} -16 kJmol^{-1} at 298 and 450K, the free energy of the Al-Si-Al-Si tetramer is slightly negative with -7 kJmol^{-1} and -0.2 kJmol^{-1} at 298 and 450K. Although the stabilizing effect of the solvation and charge neutralizing Na^+ ions would reduce the condensation energy, this trend is the same as the gas phase. The formation of the Al-Si-Al-Al tetramer (non-Lowensteinian structure) is more favourable than that of the Al-Si-Al-Si tetramer, again emphasizing the role of the $\text{Al}(\text{OH})_4\text{Na}$ monomer as a promoter of condensation reactions. However, if the $\text{Al}(\text{OH})_4\text{Na}$ monomer is indeed the reactant it would build up zeolites in contradiction to Lowenstein's rule; other species such as the $\text{AlSiO}(\text{OH})_6\text{Na}$ dimer might be proposed instead for condensation reactions. We will also address this question of the $\text{Al}(\text{OH})_4\text{Na}$ monomer in the later studies of the condensation reactions of rings.

4.3.2.1.2.2 Tetramerisation reactions with the $\text{AlSiO}(\text{OH})_6\text{Na}$ dimers

The $\text{AlSiO}(\text{OH})_6\text{Na}$ dimer is the alternative reactant in tetramerisation reactions. The rationale for the hypothesis of the participation of the $\text{AlSiO}(\text{OH})_6\text{Na}$ dimer in reactions first is that as reported in chapter 3, the $\text{AlSiO}(\text{OH})_6\text{Na}$ dimer is more thermodynamically favourable to be formed than the $\text{Al}_2\text{O}(\text{OH})_6\text{Na}_2$ dimer in the dimerisation reactions in COSMO solvation, thus suggesting that the $\text{AlSiO}(\text{OH})_6\text{Na}$ dimer could be the main starting reactant in further condensation reactions; Table 4.2 shows the free energy of the formation of three tetramers via the condensation reactions of two $\text{AlSiO}(\text{OH})_6\text{Na}$ dimers: the Al-Si-Al-Si, Al-Si-Si-Al, and Si-Al-Al-Si tetramers.

In the gas phase, note that the formation of the Al-Si-Si-Al tetramer has more highly negative free energy with -91 kJmol^{-1} (298 K) and -85 kJmol^{-1} (450K) than that of the Al-Si-Al-Si tetramer with -70 kJmol^{-1} (298 K) and -64 kJmol^{-1} (450K); the formation of the Si-Al-Al-Si tetramer is the least favourable, but the calculated free energy is still negative, being -43 kJmol^{-1} at (298 K) and -34 kJmol^{-1} (450K). Hence, the result, as we expected, shows the following trend for decreasing free energy: the Al-Si-Si-Al tetramer > the Al-Si-Al-Si tetramer > the Si-Al-Al-Si tetramer, corresponding to the Lowenstein's rule. Moreover, another important observation concerns the comparison of the formation of the Lowensteinian tetramers from the condensation reactions of the two Si-Al dimers and of the Al-Si-Al trimer and $\text{Si}(\text{OH})_4$ monomer (Tables 4.1 and 4.2); the former reactions are more favourable than the latter. To verify this result,

we must consider the COSMO solvation.

In the presence of the COSMO solvation, we find that at 298 K, the Al-Si-Si-Al and Al-Si-Al-Si tetramer have the free energy within 1 kJmol^{-1} , but interestingly, at 450 K, the formation of the Al-Si-Si-Al tetramer is more favourable than that of the Al-Si-Al-Si tetramer, by 6 kJmol^{-1} . Hence, if we consider the formation of the four ring with the Al-Si-Al-Si sequence (the Lowensteinian structure), which is the key ring to enable the next condensation reaction to be moved on in the nucleation process, from the internal condensation reactions of the Al-Si-Al-Si tetramer, the reaction would be more limited at high temperature (450K) due to its lower thermodynamic stability, but could proceed at room temperature (298K), showing the requisite of low temperature reaction steps. On the other hand, compared with the formation of the Al-Si-Si-Al and Al-Si-Al-Si tetramers, the Si-Al-Al-Si tetramer, which has energetic prohibition with marginal positive value ($+3 \text{ kJmol}^{-1}$ at 298 K and $+5 \text{ kJmol}^{-1}$ at 450K) is the least likely to be formed. Again, in COSMO solvation, this result is in line with Lowenstein's rule as the $\text{AlSiO}(\text{OH})_6\text{Na}$ dimer takes part in the tetramerisation reactions. The formation of the Lowensteinian tetramers from the condensation reactions of the two Si-Al dimers and of the Al-Si-Al trimer and $\text{Si}(\text{OH})_4$ monomer, the similar situation can be observed in COSMO solvation as in the gas phase; the tetramerisation reactions via the condensation reaction of two $\text{AlSiO}(\text{OH})_6\text{Na}$ dimers are more favourable. Such a finding in concert with our hypothesis that the tetramerisation reactions caused by the $\text{AlSiO}(\text{OH})_6\text{Na}$ dimer are the more likely route because the participation of dimer not only satisfies Lowenstein's rule also is the most favoured thermodynamically. To test this suggestion, we next examine how the four, six, double four, and double six rings condense with the $\text{Si}(\text{OH})_4$ or $\text{Al}(\text{OH})_4\text{Na}$ monomers or the $\text{AlSiO}(\text{OH})_6\text{Na}$ dimer.

Considering further the formation of open aluminosilicate clusters, the comparison of the calculated free energy of the gas phase and COSMO solvation shows the large difference in all condensation reactions, which can be attributed to the effect of the solvent. Turning our attention to the effect of temperature, we find that at room temperature, most reactions are exergonic. Thus, increasing temperature seems not to benefit these condensation reactions. Indeed, in the case of zeolite A, it has been synthesized successfully at room temperature. However, we note that the increase in

free energy from the formation of the four rings via the tetramers follow the increase in temperature, an important point to which we return in chapter 5.

Thus, the preliminary conclusion in this section is that in the formation of open aluminosilicate clusters, the $\text{Al}(\text{OH})_4\text{Na}$ monomer is more reactive than the $\text{Si}(\text{OH})_4$ monomer, which the products are inconsistent with the Lowenstein's rule. We therefore suggest that the $\text{AlSiO}(\text{OH})_6\text{Na}$ dimer might be the prevailing reactant which participates in the condensation reactions directly.

Table 4.2 Calculated free energy (ΔG , kJmol^{-1}) change in the gas phase and COSMO solvation at 298 and 450K in polymerisations.

reactants		products	Gas		COSMO sol.	
			298K	450K	298K	450K
tetramerisations						
Si-Al-Si	Si	Si-Al-Si-Si	-17	-18	-26	-26
Si-Al-Si	Al	Al-Si-Al-Si	-98	-92	-33	-48
Al-Si-Al	Si	Al-Si-Al-Si	-19	-9	-7	0
Al-Si-Al	Al	Al-Si-Al-Al	-89	-78	-18	-16
Al-Si	Al-Si	Al-Si-Al-Si	-70	-64	-34	-30
Al-Si	Al-Si	Al-Si-Si-Al	-91	-85	-34	-36
Al-Si	Al-Si	Si-Al-Al-Si	-43	-34	3	5

4.3.2.2 Condensation reactions of the four, six, double four and double six rings

In this section, we start with the rings, which are the basic units in the frameworks of zeolites which have been formed via the internal condensation reactions of open clusters that will be analysed in chapter 5 and consider small oligomers condensing onto the ring which is necessary to form multiple ring structures, which is the key processes in the nucleation of zeolites. Thus, we return to the question of which kind of small clusters including the $\text{Si}(\text{OH})_4$ or $\text{Al}(\text{OH})_4\text{Na}$ monomers or $\text{AlSiO}(\text{OH})_6\text{Na}$ dimer would condense with the ring structures; the four, six, double four and double six rings are taken as the starting rings for the condensation reactions.

4.3.2.2.1 Condensation reactions of the four ring with the Si(OH)₄ or Al(OH)₄Na monomers

First let us consider the condensation reactions of the Si(OH)₄ or of Al(OH)₄Na monomers on the four ring. As mentioned earlier, the four possible configurations of the fused four rings can be formed: the Si-(Si), Si-(Al), Al-(Si), and Al-(Al) fused rings, respectively. Here, we consider the condensation reactions of the four ring with the Si(OH)₄ or Al(OH)₄Na monomers in the gas phase and COSMO solvation at 298 and 450K; the calculated free energy for forming the fused four rings is presented in Table 4.3. We note that the Si(OH)₄ or Al(OH)₄Na monomers can condense with the four ring at the two distinct and active sites: the Si and Al atoms to form four different types of the fused four rings: first those in which the Al(OH)₄Na monomer condenses to form the Al-(Si) and Al-(Al) fused four rings and second those in which the Si(OH)₄ monomer condenses to form the Si-(Al) and Si-(Si) fused four rings.

In the gas phase, the comparison of the condensation energies is reported in Table 4.3; it clearly indicates that the formation of the Al-(Si), Al-(Al), Si-(Al), and Si-(Si) fused four rings are highly favourable. The formation of the Al-(Si) fused four ring through the Al(OH)₄Na monomer has the free energy of -143 (298K) and -133 kJmol⁻¹ (450K) and the next reaction is the formation of the Al-(Al) fused four ring condensing with the Al(OH)₄Na monomer with the free energy of -102 (298K) and -95 kJmol⁻¹ (450K). But, when the Si(OH)₄ monomer is involved in the reactions, the free energy of the formation of the Si-(Al) fused four ring is -54 (298K) and -48 kJmol⁻¹ (450K) and that of the Si-(Si) fused four ring is -46 (298K) and -42 kJmol⁻¹ (450K). The different condensation reactions give rise to large differences in the calculated free energy. The Al-(Si) and Al-(Al) fused four rings are more likely to be formed than the Si-(Si) and Si-(Al) fused four rings by -97 (298K) and -91 kJmol⁻¹ (450K) and -48 (298K) and -47 kJmol⁻¹ (450K), showing that the Al-(Si) and Al-(Al) fused four rings preferentially are formed in the gas phase, when the Al(OH)₄Na monomer is employed. The most favourable reaction is that where the Al(OH)₄Na monomer condenses on the Si site of the four ring and the least favourable is where the Si(OH)₄ monomer condenses on the Si site of the four ring with the following trend for decreasing free energy: the Al-(Si) fused four ring > the Al-(Al) fused four ring > the Si-(Al) fused four ring > the Si-(Si) fused four ring.

Now we consider the effect of the COSMO solvation in these reactions. As shown in the previous sections, understanding the effect of the COSMO solvation in the condensation reactions is of key importance, because most zeolite syntheses proceed in aqueous media. Table 4.3 shows that the trend is similar to those found in the gas phase, but the free energy of the COSMO solvation becomes less favourable because as mentioned previously, the stabilizing effect of the solvation and of the charge-neutralizing Na^+ ions reducing the condensation energies. The formation of the Al-(Si) fused four ring is the most favoured by over -40 kJmol^{-1} (between 298 and 450K), being more energetically favourable than other three the fused four rings. Moving on to the remaining three the fused four rings, we find that their free energy is similar, i.e. within -20 kJmol^{-1} (between 298 and 450K) for the Al-(Al) fused four ring, within -17 kJmol^{-1} (between 298 and 450K) for the Si-(Al) fused four ring, within -15 kJmol^{-1} (between 298 and 450K) for the Si-(Si) fused four ring. According to these results, of course, the Al-(Si) fused four ring should be the predominant product in COSMO solvation. Again, the trend in the free energy is consistent with the gas phase: the Al-(Si) fused four ring > the Al-(Al) fused four ring > the Si-(Al) fused four ring > the Si-(Si) fused four ring. The $\text{Al(OH)}_4\text{Na}$ monomer would preferentially condense to the four ring rather than the Si(OH)_4 monomer, probably because of its negative charge. Moreover, this result, is fully in line with the condensation reactions of open clusters. For the sake of consistency and completeness, the following section still focuses on the six, double four and double six ring condensing with the Si(OH)_4 or $\text{Al(OH)}_4\text{Na}$ monomers.

Table 4.3 Calculated free energy (ΔG , kJmol^{-1}) change in the gas phase and in COSMO solvation at 298 and 450K in polymerisations. The reaction: $\text{R} + \text{M} \rightarrow \text{FR} + \text{H}_2\text{O}$.

reactants		products	Gas		COSMO sol.	
			298K	450K	298K	450K
Al	(Si)4ring	Al-(Si)4ring	-143	-133	-43	-46
Al	(Al)4ring	Al-(Al)4ring	-102	-95	-17	-20
Si	(Al)4ring	Si-(Al)4ring	-54	-48	-15	-17
Si	(Si)4ring	Si-(Si)4ring	-46	-42	-12	-15

Code used: M = Si(OH)_4 or $\text{Al(OH)}_4\text{Na}$, D = $\text{AlSiO(OH)}_6\text{Na}$, R = 4, 6, D4, and D6rings, FR = fused 4, 6, D4, and D6rings.

4.3.2.2.2 Condensation reactions of the six, double four and double six ring with the $\text{Si}(\text{OH})_4$ or $\text{Al}(\text{OH})_4\text{Na}$ monomers

We now extend our analysis to the condensation reactions on six, double four and double six rings. As above, we consider the $\text{Si}(\text{OH})_4$ or $\text{Al}(\text{OH})_4\text{Na}$ monomers and the four possible configurations forming the Si-(Si), Si-(Al), Al-(Si), and Al-(Al) fused ring and calculate the free energies associated with these condensation reactions in the gas phase and COSMO solvation between 298 and 450K; the result is given in Table 4.4. In all cases, they have the similar behaviour to the condensation reaction for the four ring discussed above; the order of decreasing the free energy of the six, double four and double six rings via the $\text{Si}(\text{OH})_4$ or $\text{Al}(\text{OH})_4\text{Na}$ monomers is the Al-(Si) fused ring > the Al-(Al) fused ring > the Si-(Al) fused ring > the Si-(Si) fused ring in the gas phase as well as the COSMO solvation. Further analysis of Table 4.4, again shows that the inclusion of the COSMO solvation in the condensation reactions reduces the free energy, but all reactions are favourable. We also find that the formation of the Al-(Si) fused rings involving the $\text{Al}(\text{OH})_4\text{Na}$ monomer on the Si site of the rings is the most thermodynamically favourable, being the same as the cases of the open clusters and four rings discussed above. In other words, the $\text{Al}(\text{OH})_4\text{Na}$ monomer has the strong tendency to condense with these rings.

However, the question I have sought to address is that according to Lowenstein's rule, the formation of the Al-(Al) fused rings, which would be expected lead into the non-Lowensteinian species, might be expected to be the most unfavourable but actually it is not. In almost all cases the Al-(Al) fused rings are formed as the second thermodynamically favoured products, and would suggest that the Al-(Al) fused ring is still more likely to be formed than the Si-(Al) fused or the Si-(Si) fused rings.

It is also worthy of note that the ends of the chain component of all these fused rings are likely to be aluminous, which means that when these Al-(Si) fused rings continue to grow, if Lowenstein's rule is to be followed, the condensation should be restricted to siliceous or aluminosiliceous species such as the $\text{Si}(\text{OH})_4$ monomer or $\text{AlSiO}(\text{OH})_6\text{Na}$ dimer. We must therefore again question whether the $\text{Al}(\text{OH})_4\text{Na}$ monomer is actually involved in further reactions despite the favorable energies have reported in Tables 4.3 and 4.4. The issue is similar to that raised by our previous observation that the formation of the Al-Si-Al-Al tetramer is favourable, but

contradicts Lowenstein's rule. Thus, in order to clarify this question, we need to consider how the subsequent condensation reactions of these Al-(Si) fused rings might proceed, if as might be expected, the Al(OH)₄Na monomer is still the key reactant. The detailed analysis will be presented in the following sections.

Table 4.4 Calculated free energy (ΔG , kJmol⁻¹) change in the gas phase and COSMO solvation at 298 and 450K in polymerisations.

a.

reactants		products	Gas		COSMO sol.	
			298K	450K	298K	450K
Al	(Si)6ring	Al-(Si)6ring	-126	-118	-64	-63
Al	(Al)6ring	Al-(Al)6ring	-109	-101	-42	-41
Si	(Al)6ring	Si-(Al)6ring	-36	-32	-12	-14
Si	(Si)6ring	Si-(Si)6ring	-31	-26	-9	-8

b.

reactants		products	Gas		COSMO sol.	
			298K	450K	298K	450K
Al	(Si)D4ring	Al-(Si)D4ring	-136	-126	-49	-48
Al	(Al)D4ring	Al-(Al)D4ring	-97	-89	-28	-26
Si	(Al)D4ring	Si-(Al)D4ring	-53	-48	-29	-29
Si	(Si)D4ring	Si-(Si)D4ring	-44	-39	-20	-19

c.

reactants		products	Gas		COSMO sol.	
			298K	450K	298K	450K
Al	(Si)D6ring	Al-(Si)D6ring	-188	-188	-107	-115
Al	(Al)D6ring	Al-(Al)D6ring	-144	-145	-64	-72
Si	(Al)D6ring	Si-(Al)D6ring	-88	-84	-30	-35
Si	(Si)D6ring	Si-(Si)D6ring	-72	-65	-22	-25

4.3.2.3 Condensation reactions of the Al-(Si) fused four, six and double four rings

We now consider the energetics of the $\text{Si}(\text{OH})_4$ or $\text{Al}(\text{OH})_4\text{Na}$ monomers or the $\text{AlSiO}(\text{OH})_6\text{Na}$ dimer condensing on the Al-(Si) fused rings. Taking the Al-(Si) fused rings including the four, six and double four rings as the reactants, the two different condensation routes can be considered for subsequent reactions: one is the condensation reaction between the Al-(Si) fused ring and $\text{Si}(\text{OH})_4$ or $\text{Al}(\text{OH})_4\text{Na}$ monomers and the other is that between the Al-(Si) fused ring and $\text{AlSiO}(\text{OH})_6\text{Na}$ dimer. The relative free energies from these condensation reactions are given in Tables 4.5 and 4.6.

4.3.2.3.1 Condensation reactions of the Al-(Si) fused four rings with the $\text{Si}(\text{OH})_4$ or $\text{Al}(\text{OH})_4\text{Na}$ monomers or the $\text{AlSiO}(\text{OH})_6\text{Na}$ dimer

Table 4.5 shows the formations of four different products (the fused four rings): the Si-Al-(Si), Al-Al-(Si), Al-Si-Al-(Si) and Si-Al-Al-(Si) fused rings via two different types of condensation pathways: the $\text{Si}(\text{OH})_4$ or $\text{Al}(\text{OH})_4\text{Na}$ monomers and $\text{AlSiO}(\text{OH})_6\text{Na}$ dimer respectively. First, we start with the condensation reactions between the Al-(Si) fused rings and $\text{Si}(\text{OH})_4$ or $\text{Al}(\text{OH})_4\text{Na}$ monomers forming the Si-Al-(Si) and Al-Al-(Si) fused four rings respectively. The calculated free energy in the gas phase shows that the formation of the Al-Al-(Si) and Si-Al-(Si) fused four rings is thermodynamically favoured, with the former being more energetically favourable than the latter, calculated as -88 (298K) and -86 kJmol^{-1} (450K) for the $\text{Al}(\text{OH})_4\text{Na}$ monomer and -32 (298K) and -28 kJmol^{-1} (450K) for the $\text{Si}(\text{OH})_4$ monomer. It appears therefore that thermodynamics favors the formation of the of the Al-Al-(Si) fused four ring instead of the Si-Al-(Si) fused four rings and again the $\text{Al}(\text{OH})_4\text{Na}$ monomer is more reactive than the $\text{Si}(\text{OH})_4$ monomer; but interestingly the formation of the Al-Al-(Si) fused four ring which would give the Al-O-Al linkage in contradiction to Lowenstein's rule appears to be favoured. The similar result was obtained previously, and clearly we must examine the effect of COSMO solvation, the result of which, however, is that the $\text{Al}(\text{OH})_4\text{Na}$ monomer is still found to be highly reactive in condensing with the Al-(Si) fused four ring and that the product -the Al-Al-(Si) fused four ring- is calculated to be -16 (298K) and -20 kJmol^{-1} (450K) more energetically favourable to be formed than the Si-Al-(Si) fused one. This behaviour happened is again in clear contradiction to Lowenstein's rule as in the

previous tetramerisation reactions between the Al-Si-Al trimer and Si(OH)₄ or Al(OH)₄Na monomer. As a consequence, the condensation of the AlSiO(OH)₆Na dimer with the Al-(Si) fused four ring must again be examined.

The comparison of Table 4.5 shows that the condensation reactions of the AlSiO(OH)₆Na dimer on the Al-(Si)fused four ring forming the Al-Si-Al-(Si) and Si-Al-Al-(Si) fused rings are all exergonic processes. Considering the free energy change in the gas phase, the formation of the Al-Si-Al-(Si) fused four ring is calculated to be -95 (298K) and -91 kJmol⁻¹(450K) lower in free energy than that for the Si-Al-Al-(Si) fused four ring; the Al-Si-Al-(Si) fused four ring seems to be more likely to be formed and be consistent with Lowenstein's rule. The result, when the COSMO solvation is included, there is the small energy difference between the Al-Si-Al-(Si) and Si-Al-Al-(Si) fused four ring formed as the formation of the Al-Si-Al-(Si) fused four ring is only -4 (298K) and -6 kJ mol⁻¹(450K) more energetically favourable than the Si-Al-Al-(Si) cluster, again satisfying the Lowenstein's rule. As a result, the comparison in the condensation reactions of the Si(OH)₄ or Al(OH)₄Na monomers or AlSiO(OH)₆Na dimer on the Al-(Si) fused rings suggests that the AlSiO(OH)₆Na dimer would be essential in the nucleation processes since as we have noted there is a question over the participation of the Al(OH)₄Na monomer. To examine further this key issue, we will explore the Si(OH)₄ and Al(OH)₄Na monomers or the AlSiO(OH)₆Na dimer condensing on the Al-(Si) fused six, double four rings in the next section.

Table 4.5 Calculated free energy (ΔG , kJmol⁻¹) change in the gas phase and COSMO solvation at 298 and 450K in polymerisations. The reaction: FR + M or D \rightarrow FR + H₂O.

reactants		products	Gas		COSMO sol.	
			298K	450K	298K	450K
Si	Al-(Si)4ring	Si-Al-(Si)4ring	-32	-28	-7	-10
Al	Al-(Si)4ring	Al-Al-(Si)4ring	-88	-86	-23	-30
Al-Si	Al-(Si)4ring	Al-Si-Al-(Si)4ring	-95	-91	-48	-50
Al-Si	Al-(Si)4ring	Si-Al-Al-(Si)4ring	-88	-82	-44	-44

4.3.2.3.2 Condensation reactions of the Al-(Si) fused six, double four rings with the Si(OH)₄ or Al(OH)₄Na monomers or AlSiO(OH)₆Na dimer

As with the previous study for the four ring, taking now the Al-(Si) fused rings including the fused six and double four rings as the reactants, two different types of condensation pathways can be considered for subsequent reactions: one is the condensation reaction between the Al-(Si) fused ring and the Si(OH)₄ or Al(OH)₄Na monomers and the other is that between the Al-(Si) fused ring and AlSiO(OH)₆Na dimer, results for which are shown in Table 4.6.

In all cases, the similar trend can be repeatedly be found as those noted for previous condensation reactions of the fused four ring, including the reduction of the free energy of the condensation reactions due to the solvent effect. We return, however, to the study of the two different types of condensation reactions. First, we start with the condensation reactions between the Al-(Si) fused rings and Si(OH)₄ or Al(OH)₄Na monomers forming the Si-Al-(Si) and Al-Al-(Si) fused rings respectively . As seen in Table 4.6, the formation of all the Al-Al-(Si) fused rings regarding the six and double four rings is more favourable than the Si-Al-(Si) fused rings in the gas phase and COSMO solvation. The formation of the Si-Al-(Si) fused four and six rings is observed to be only slightly favoured thermodynamically, with the free energy of the Si-Al-(Si) fused six ring being -6 (298K) and -3 kJmol⁻¹ (450K) in COSMO solvation (Table 6a). It appears therefore that these Al-(Si) fused rings are likely to condense with the Al(OH)₄Na monomer, which would give the Al-O-Al linkage that is in contradiction to Lowenstein's rule. Thus, given that the Al-Al-(Si) fused rings are prone to being formed, the formation of this type of ring could be considerably higher in COSMO solvation, probably leading to non-Lowensteinian structures. We suggest that this type of non-Lowensteinian aluminosilicate clusters serves as a nutrient and will not have any contribution to the polymerisation reactions and may indeed hinder the processes of the nucleation. Of course, we should consider the kinetic controls of the polymerisation reactions whereas in this thesis, we focus on thermodynamics. It is possible that the formation of the Al-Al-(Si) fused rings is kinetically unfavourable compared to the Si-Al-(Si) fused rings. As mentioned in the previous reaction, the Si(OH)₄ and Al(OH)₄Na monomers perhaps react rapidly to form the AlSiO(OH)₆Na dimer, which probably dominates in subsequent condensations. Hence, despite its reactivity the Al(OH)₄Na monomer is unavailable at the stage of the nucleation.

Let us now therefore consider in more detail the $\text{AlSiO}(\text{OH})_6\text{Na}$ dimer and its condensations with the Al-(Si) fused rings to form the Al-Si-Al-(Si) and Si-Al-Al-(Si) fused rings respectively. Comparing the free energies for the formation of the Al-Si-Al-(Si) fused ring with those of the Si-Al-Al-(Si) fused ring (Table 4.6), we find that in each case, the formation of the Al-Si-Al-(Si) fused ring is more favoured than the Si-Al-Al-(Si) fused ring in the gas phase and COSMO solvation, following Lowenstein's rule. The result supports our contention that the $\text{AlSiO}(\text{OH})_6\text{Na}$ dimer prevails in these condensation reactions instead of the $\text{Al}(\text{OH})_4\text{Na}$ monomer. In the next section, by examining the condensation reactions of the $\text{AlSiO}(\text{OH})_6\text{Na}$ dimer on the four, six, double four and double six rings, we will again be able to examine as assumption of the $\text{AlSiO}(\text{OH})_6\text{Na}$ dimer being the key reactant in the condensation reactions.

Table 4.6 Calculated free energy (ΔG , kJmol^{-1}) change in the gas phase and COSMO solvation at 298 and 450K in polymerisations. The reaction: $\text{FR} + \text{M}$ or $\text{D} \rightarrow \text{FR} + \text{H}_2\text{O}$.

a.

reactants		products	Gas		COSMO sol.	
			298K	450K	298K	450K
Si	Al-(Si)6ring	Si-Al-(Si)6ring	-46	-37	-6	-3
Al	Al-(Si)6ring	Al-Al-(Si)6ring	-100	-19	-19	-20
Al-Si	Al-(Si)6ring	Al-Si-Al-(Si)6ring	-117	-112	-42	-46
Al-Si	Al-(Si)6ring	Si-Al-Al-(Si)6ring	-94	-91	-16	-22

b.

reactants		products	Gas		COSMO sol.	
			298K	450K	298K	450K
Si	Al-(Si)D4ring	Si-Al-(Si)D4ring	-52	-56	-30	-39
Al	Al-(Si)D4ring	Al-Al-(Si)D4ring	-93	-90	-37	-41
Al-Si	Al-(Si)D4ring	Al-Si-Al-(Si)D4ring	-85	-82	-59	-59
Al-Si	Al-(Si)D4ring	Si-Al-Al-(Si)D4ring	-60	-53	-32	-29

4.3.2.4 Condensation reactions of the four, six, double four and double six rings with the $\text{AlSiO}(\text{OH})_6\text{Na}$ dimer

We have already discussed the reason for the involvement of the $\text{AlSiO}(\text{OH})_6\text{Na}$ dimer in the condensation reactions and shown that the Al-Si-Al-(Si) fused ring species are the more stable products. Thus in order to confirm that as findings at applicable to other rings, the $\text{AlSiO}(\text{OH})_6\text{Na}$ dimer is again chosen to condense with additional ring species. The similar rings used: the four, six, double four and six rings are chosen to condense with the $\text{AlSiO}(\text{OH})_6\text{Na}$ dimer and there are four possible fused rings, due to two distinct and active sites: the Si and Al atoms, on which the $\text{AlSiO}(\text{OH})_6\text{Na}$ dimer can be added: the Al-Si-(Al), Al-Si-(Si), Si-Al-(Si), and Si-Al-(Al) fused rings, respectively. The reinvestigation of the $\text{AlSiO}(\text{OH})_6\text{Na}$ dimer condensing on the rings will provide more valuable mechanistic insight into these condensation reactions.

4.3.2.4.1 Condensation reactions of the four ring with the $\text{AlSiO}(\text{OH})_6\text{Na}$ dimer

Table 4.7 gives the calculated free energies for formation of the four isomeric products: the Al-Si-(Al), Al-Si-(Si), Si-Al-(Si), and Si-Al-(Al) fused four rings. According to Table 4.7, in the gas phase, the formation of the Al-Si-(Al), Al-Si-(Si), Si-Al-(Si) and Si-Al-(Al) fused four rings, with the calculated free energies of -136 (298K) and -135 kJmol^{-1} (450K), -141 (298K) and -135 kJmol^{-1} (450K), -115 (298K) and -106 kJmol^{-1} (450K), and -73 (298K) and -63 kJmol^{-1} (450K), respectively, are exergonic; the former three are over -100 kJmol^{-1} more stable than the last one between 298K and 450K. Such a finding shows that the formation of the Si-Al-(Al) fused four ring is the most energetically unfavourable reaction, which accords with Lowenstein's rule. Furthermore, we focus our attention on the formation of the Al-Si-(Al), and Al-Si-(Si) fused four rings; the relative energies of which are similar. The small energy difference in the two sets of condensation reactions shows that the reaction to form the Al-Si-(Si) fused four ring has the small preference at 298K (by -5 kJmol^{-1}), but the free energy change is identical at 450K, which means the two reaction will occur simultaneously. Having studied in detail the condensation reactions in the gas phase, it is clear necessary to examine the results for COSMO solvation to provide the verification of whether the trend is similar. For all condensation reactions, in COSMO solvation, the free energy decreases significantly,

but all reactions are still exergonic.

Indeed the magnitude of the calculated free energies in COSMO solvation quite different; -76 (298K) and -82 kJmol⁻¹(450K) for the Al-Si-(Al) fused four ring, -53 (298K) and -58 kJmol⁻¹(450K) for the Al-Si-(Si) fused four ring, -29 (298K) and -33 kJmol⁻¹(450K) for the Si-Al-(Si) fused four ring and -8 (298K) and -8 kJmol⁻¹(450K) for the Si-Al-(Al) fused four rings, respectively. But the trend is similar to those we found in the gas phase; the formation of the Al-Si-(Al), Al-Si-(Si), Si-Al-(Si) fused four rings are more energetically favourable than that of the Si-Al-(Al) fused four ring, by 21-68 (298K) and 25-74 kJmol⁻¹ (450K). Moreover, the Al-Si-(Al) fused four ring, which is over 20 kJmol⁻¹ lower in energy than Al-Si-(Si) cluster probably is now suggested as the predominant product in the condensation reactions. Hence, the free energies favoring the formation of the fused ring via the AlSiO(OH)₆Na dimer are in order: the Al-Si-(Al) fused four ring > the Al-Si-(Si) fused four ring > the Si-Al-(Si) fused four ring > the Si-Al-(Al) fused four ring. Such a finding is also consistent with Lowenstein's rule, again suggesting that the AlSiO(OH)₆Na dimer will participate in the condensation reactions. To get a further understanding of these condensation reactions via the AlSiO(OH)₆Na dimer, we now examine the six, double four and double six rings.

Table 4.7 Calculated free energy (ΔG , kJmol⁻¹) change in the gas phase and COSMO solvation at 298 and 450K in polymerisations. The reaction: R + D → FR + H₂O.

reactants		products	Gas		COSMO sol.	
			298K	450K	298K	450K
Al-Si	(Al)4ring	Al-Si-(Al)4ring	-136	-135	-76	-82
Al-Si	(Si)4ring	Al-Si-(Si)4ring	-141	-135	-53	-58
Al-Si	(Si)4ring	Si-Al-(Si)4ring	-115	-106	-29	-33
Al-Si	(Al)4ring	Si-Al-(Al)4ring	-73	-63	-8	-8

4.3.2.4.2 Condensation reactions of the six, double four and double six rings with the $\text{AlSiO}(\text{OH})_6\text{Na}$ dimer

Moving on to the $\text{AlSiO}(\text{OH})_6\text{Na}$ dimer condensing with the six, double four and double six rings, on condensing with the $\text{AlSiO}(\text{OH})_6\text{Na}$ dimer, each type of the ring can again form four possible fused ring isomers: the Al-Si-(Al), Al-Si-(Si), Si-Al-(Si), and Si-Al-(Al) fused rings. Table 4.8 shows all the relative free energies for all the rings in the gas phase and COSMO solvation between 298 and 450K. Again, these condensation reactions show the similar behaviour to those above in that the inclusion of the COSMO solvation decreases the free energy of the reactions. Comparing now the calculated condensation free energies, first, it is generally found that in the gas phase, the most stable cluster is the Al-Si-(Si) fused ring, but in COSMO solvation, the most stable Al-Si-(Al) fused ring can be formed. Second, in the gas phase and COSMO solvation, the least favourable reactions are to form the Si-Al-(Al) fused rings, but the calculated free energies are still negative, which is, however, in line with Lowenstein's rule as the formation of the Al-O-Al linkage results in reducing stability of the aluminosilicate clusters. Again, the decrease in the free energies is observed in the following order (the COSMO solvation): the Al-Si-(Al) fused ring > the Al-Si-(Si) fused ring > the Si-Al-(Si) fused ring > the Si-Al-(Al) fused ring. Expected, we can summarise by noting that, the result is not only consistent with Lowenstein's rule, but also with the suggestion put forward both earlier and in experimental studies that the $\text{AlSiO}(\text{OH})_6\text{Na}$ dimer is the key species in nucleation processes.

On the other hand, it should be noted that the ends of the chain component of all the most stable fused rings are likely to be aluminous. Hence, using our proposals that the $\text{AlSiO}(\text{OH})_6\text{Na}$ dimer and the Al-Si-(Al) fused rings are the key species, a detailed mechanism for the nucleation of zeolite A will be explored in chapter 5. It is, however, difficult to give any simple reason why the Al-Si-(Al) fused rings are formed preferentially. The energies cannot also be accounted for by considering the difference in the geometry as the different rings have the similar configurations.

Furthermore, let us consider two other factors: temperature and pH which are thought as of key importance influencing the condensation reactions. In general, increasing temperature and pH has been thought to tend to drive the condensation reactions to be proceeded. However, increasing temperature seems not to result in the significant

change in the free energy of these condensation reactions and even at room temperature, the condensation reactions are thermodynamically favoured, which means that these aluminosilicate clusters are highly reactive. But we should also comment that we have not considered the cyclisation for aluminosilicate clusters, and as shown in chapter 5 temperature causes different trends in cyclisation reactions. As for the effect of pH, the deprotonated species such as: the $\text{Si}(\text{OH})_3\text{O}^-$ cluster that usually produces under high alkaline conditions were not included in this calculations; nevertheless, these condensation reactions are still thermodynamically favoured, indicating that compared with pure silica clusters where condensation reactions proceed under highly alkaline conditions with deprotonated clusters, the aluminosilicate condensation reactions may require less alkaline conditions. Indeed, however, a study of the deprotonated aluminosilicate clusters involved in the condensation reactions will be reported in chapter 6.

Table 4.8 Calculated free energy (ΔG , kJmol^{-1}) change in the gas phase and COSMO solvation at 298 and 450K in polymerisations. The reaction: $R + D \rightarrow FR + H_2O$.

a.

reactants		products	Gas		COSMO sol.	
			298K	450K	298K	450K
Al-Si	(Al)6ring	Al-Si-(Al)6ring	-113	-106	-87	-82
Al-Si	(Si)6ring	Al-Si-(Si)6ring	-120	-114	-52	-54
Al-Si	(Si)6ring	Si-Al-(Si)6ring	-111	-100	-48	-44
Al-Si	(Al)6ring	Si-Al-(Al)6ring	-99	-96	-33	-33

b.

reactants		products	Gas		COSMO sol.	
			298K	450K	298K	450K
Al-Si	(Al)D4ring	Al-Si-(Al)D4ring	-144	-136	-100	-98
Al-Si	(Si)D4ring	Al-Si-(Si)D4ring	-143	-135	-89	-86
Al-Si	(Si)D4ring	Si-Al-(Si)D4ring	-127	-127	-58	-64
Al-Si	(Al)D4ring	Si-Al-(Al)D4ring	-74	-65	-11	-10

v.

reactants		products	Gas		COSMO sol.	
			298K	450K	298K	450K
Al-Si	(Al)D6ring	Al-Si-(Al)D6ring	-143	-140	-80	-83
Al-Si	(Si)D6ring	Al-Si-(Si)D6ring	-155	-153	-69	-75
Al-Si	(Si)D6ring	Si-Al-(Si)D6ring	-140	-134	-70	-70
Al-Si	(Al)D6ring	Si-Al-(Al)D6ring	-116	-116	-48	-53

4.4 Conclusion

The formation of the open cluster and fuse rings has been analysed in this study. First, the formation of the open clusters is via the $\text{AlSiO}(\text{OH})_6\text{Na}$ dimer instead of the $\text{Si}(\text{OH})_4$ or $\text{Al}(\text{OH})_4\text{Na}$ monomers. Second, the result shows that when the condensation reactions of these rings start with the $\text{Si}(\text{OH})_4$ or $\text{Al}(\text{OH})_4\text{Na}$ monomers, the thermodynamically driving force for the formation of these fused rings is in order: the Al-(Si) fused ring > the Al-(Al) fused ring > the Si-(Al) fused ring > the Si-(Si) fused ring, suggesting that the $\text{Al}(\text{OH})_4\text{Na}$ monomer is the most likely species to condense with these rings. But further analysis shows that when the most stable Al-(Si) fused ring condenses with the $\text{Si}(\text{OH})_4$ or $\text{Al}(\text{OH})_4\text{Na}$ monomers the

$\text{Al}(\text{OH})_4\text{Na}$ monomer is again favored over the $\text{Si}(\text{OH})_4$ monomer in the condensation reactions which would result in growth that is inconsistent with Lowenstein's rule; in contrast, the $\text{AlSiO}(\text{OH})_6\text{Na}$ dimer on condensing with the Al-(Si) fused ring shows the energetic preference for forming the Al-Si-Al-(Si) fused ring, leading to them that accord with Lowenstein's rule. As a result, we suggest that the $\text{Al}(\text{OH})_4\text{Na}$ monomer does not play as the active role in the condensation reactions, having, we propose, been consumed in the dimer formation. Another route is via the $\text{AlSiO}(\text{OH})_6\text{Na}$ dimer directly condensing with these key rings. The relative preference for the formation of these fused rings in condensation reactions is in order: the Al-Si-(Al) fused ring > the Al-Si-(Si) fused ring > the Si-Al-(Si) fused ring > the Si-Al-(Al) fused ring. From this trend, we suggest that in the same Si/Al ratio condensation reactions, the $\text{AlSiO}(\text{OH})_6\text{Na}$ dimer is the main and basic reactant in cluster growth. Furthermore, temperature seems to have little impact on the thermodynamics of the condensation reactions and they are still thermodynamically feasible without deprotonation.

References:

1. G. Engelhardt, B. Fahlke, M. Magi and E. Lippmaa, *Zeolites* **1983**, 3, 292.
2. G. Engelhardt, B. Fahlke, M. Magi and E. Lippmaa, *Zeolites* **1985**, 5, 49.
3. J. M. Shi, M. W. Anderson and S. W. Carr, *Chemistry of Materials* **1996**, 8, 369.
4. M. Smaïhi, O. Barida and V. Valtchev, *European Journal of Inorganic Chemistry* **2003**, 4370.
5. V. P. Valtchev and K. N. Bozhilov, *Journal of the American Chemical Society* **2005**, 127, 16171.
6. L. Itani, Y. Liu, W. P. Zhang, K. N. Bozhilov, L. Delmotte and V. Valtchev, *Journal of the American Chemical Society* **2009**, 131, 10127.
7. H. Greer, P. S. Wheatley, S. E. Ashbrook, R. E. Morris and W. Z. Zhou, *Journal of the American Chemical Society* **2009**, 131, 17986.
8. J. R. Agger, N. Pervaiz, A. K. Cheetham and M. W. Anderson, *Journal of the American Chemical Society* **1998**, 120, 10754.
9. S. Sugiyama, S. Yamamoto, O. Matsuoka, H. Nozoye, J. Yu, G. Zhu, S. Qiu and T. I, *Microporous and Mesoporous Materials* **1999**, 28, 1.
10. P. K. Dutta and D. C. Shieh, *Journal of Physical Chemistry* **1986**, 90, 2331
11. W. Fan, M. Ogura, G. Sankar and T. Okubo, *Chemistry of Materials* **2007**, 19, 1906.
12. W. Fan, M. O'Brien, M. Ogura, M. Sanchez-Sanchez, C. Martin, F. Meneau, K. Kurumada, G. Sankar and T. Okubo, *Physical Chemistry Chemical Physics* **2006**, 8, 1335.
13. T. Wakihara, S. Kohara, G. Sankar, S. Saito, M. Sanchez-Sanchez, A. R. Overweg, W. Fan, M. Ogura and T. Okubo, *Physical Chemistry Chemical Physics* **2006**, 8, 224.
14. A. Depla, E. Verheyen, A. Veyfeyken, E. Gobechiya, T. Hartmann, R. Schaefer, J. A. Martens and C. E. A. Kirschhock, *Physical Chemistry Chemical Physics* **2011**, 13, 13730.
15. L. M. Ren, C. J. Li, F. T. Fan, Q. Guo, D. S. Liang, Z. C. Feng, C. Li, S. G. Li and F. S. Xiao, *Chemistry-a European Journal* **2011**, 17, 6162.
16. J. Ciric, *Journal of Colloid and Interface Science* **1968**, 28, 315.
17. B. Feron, J. L. Guth and N. Mimounierddalane, *Zeolites* **1994**, 14, 177.
18. Biosym/MSI, *DMol USER GUIDE*, San Diego, **1995**.
19. A. Klamt and G. Schuurmann, *Journal of the Chemical Society-Perkin*

Transactions **1993**, 2, 799.

20. K. Baldrige and A. Klamt, *Journal of Chemical Physics* **1997**, 106, 6622.

21. J. A. Tossell, *Journal of Physical Chemistry* **1996**, 100, 14828.

Chapter 5

Modelling the Nucleation of Zeolite A

5.1 Introduction

As concluded in chapter 4, the key to the success of the polymerisation reactions of aluminosilicate clusters with the same Si/Al ratio (zeolite A) has been found: the $\text{AlSiO}(\text{OH})_6\text{Na}$ dimer is considered to be responsible for the condensation reactions and the ends of the chain component of all the most stable aluminosilicate fused rings are likely to be aluminous. However, although the previous work has provided valuable information regarding the polymerisation reactions of aluminosilicate clusters, the present problem is that the subsequent condensation reactions of open aluminosilicate clusters as well as aluminosilicate rings have not yet been investigated. If we are to extend our understanding of the overall growth behaviour of zeolite A, knowledge of these processes is needed.

In this chapter, the use of interest gained from chapter 4 to provide insight into the nucleation of zeolite A. Before doing this, the following review of relevant literature will provide the important characteristic features of the formation of zeolite A: a brief description of the key proposed mechanisms of the nucleation and crystal growth of zeolite A is as follows:

- (i) As discussed in chapter 4, our thermodynamic modelling for condensation reactions of the nucleation of zeolite A strongly suggested that the $\text{AlSiO}(\text{OH})_6\text{Na}$ dimer is the key species in cluster growth, as suggested by experimental studies^{1,2}.
- (ii) The observation of the early nucleation stage of zeolite A revealed that the aluminosilicate species, which can produce the crystal nuclei of zeolite A is present in solution; the structural size of the precursor according to the molecular description shows medium-range order, but not long-range order³.

- (iii) UV-Raman spectroscopy combined with XRD or NMR has been employed to analyse the crystallization of zeolite A and suggested that the four rings or double four rings (D4R) are probably the main initial rings; otherwise the appearance of the six ring lines in the spectra is not obvious^{4,5}.
- (iv) The use of atomic force microscopy (AFM), which detected the surface structure of zeolite A found that the external structural units are full of the double four rings (D4R), which are suggested to be the key building unit for crystal growth of zeolite A. Similarly, the modelling of surface structures of zeolite A showed that the double four rings (D4Rs) are stable on the terminated surface of zeolite A^{6,7}.
- (v) In the synthesis of zeolite A, it is usual to add cationic species (Na^+ ions) as templates instead of inorganic templates^{8,9}.

To summarise the above key points from these studies, it appears that understanding the question of how the double four ring (D4R) unit is formed by means of the participation of the $\text{AlSiO}(\text{OH})_6\text{Na}$ dimer or other four ring species is the primary task in the nucleation stage of zeolite A.

In this chapter, we present the DFT/COSMO calculation aimed at answering the question mentioned above. To do this, in addition to employing the most stable aluminosilicate clusters ($\text{Si}/\text{Al}=1$) as predicted in chapters 3 and 4, a series of the proposed ring clusters with hanging dimers/tetramers (with the aluminous end of the chains) and multiple linked rings have been identified in this chapter. Another emphasis of this work is the participation of the $\text{AlSiO}(\text{OH})_6\text{Na}$ dimer that controls the condensation reactions in the polymerisation reactions. In order to elucidate the following discussion in this chapter, the schematic description showing the relations between the proposed clusters is given in Figure 5.1, which can help us navigate to a better understanding of the whole reaction processes. Thus, the concept of the proposed reaction pathways established is important in the study.

This work will focus on a series of two main competing condensation reactions as shown in Figure 5.1; polymerisation and cyclisation reactions aim to identify the critical mechanisms controlling the formation of the double four ring (D4R). Note that the relevant thermodynamical properties (enthalpy, entropy and Gibbs free

energy) for each condensation reaction are presented in this work, which can provide valuable information that accounts for the behaviour of each condensation reaction.

5.2 Methodology

As in the previous two chapters, our calculation has been performed using the DFT method and shown the reliability of the approach for aluminosilicate clusters. In this study several structurally distinct aluminosilicate ring clusters with the same Si/Al ratio (Si/Al=1) and with the inclusion of sodium ions have been modelled. The geometry optimisation of the aluminosilicate rings is carried out by the DMol³ code¹⁰ based on DFT with a double numerical basis set plus polarization (DNP) and the BLYP exchange-correlation functional. The treatment of solvent effect (water) is performed using the COSMO approach^{11,12}, which is a simple and computational inexpensive to estimate solvation energy. The electronic energy at 0K can be obtained after the calculation of the geometry optimisation, without correction for the zero point energy (ZPE). Using the optimised structure obtained from the BLYP/DNP method as a starting point, a standard statistical mechanical method is employed to calculate thermodynamical properties i.e. enthalpy, entropy, and Gibbs free energy between 298 and 450K for the gas phase and COSMO solvation.

5.3 Results and Discussion

In this section, 11 structurally distinct aluminosilicate rings optimised in COSMO solvation containing the rings with hanging dimers/tetramers and multiple linked rings are presented in Figures 5.2 and 5.3. All of the reaction pathways related to a synthesis of the clusters are shown in Figure 5.1. Moreover, each condensation reaction path regarding the polymerisation (the addition of the $\text{AlSiO}(\text{OH})_6\text{Na}$ dimer or four ring) or cyclisation reactions is defined by each arrow whose direction indicates each cluster production (with the formation of water omitted for clarity). A complete account of the evaluation of each pathway is presented in the following sections.

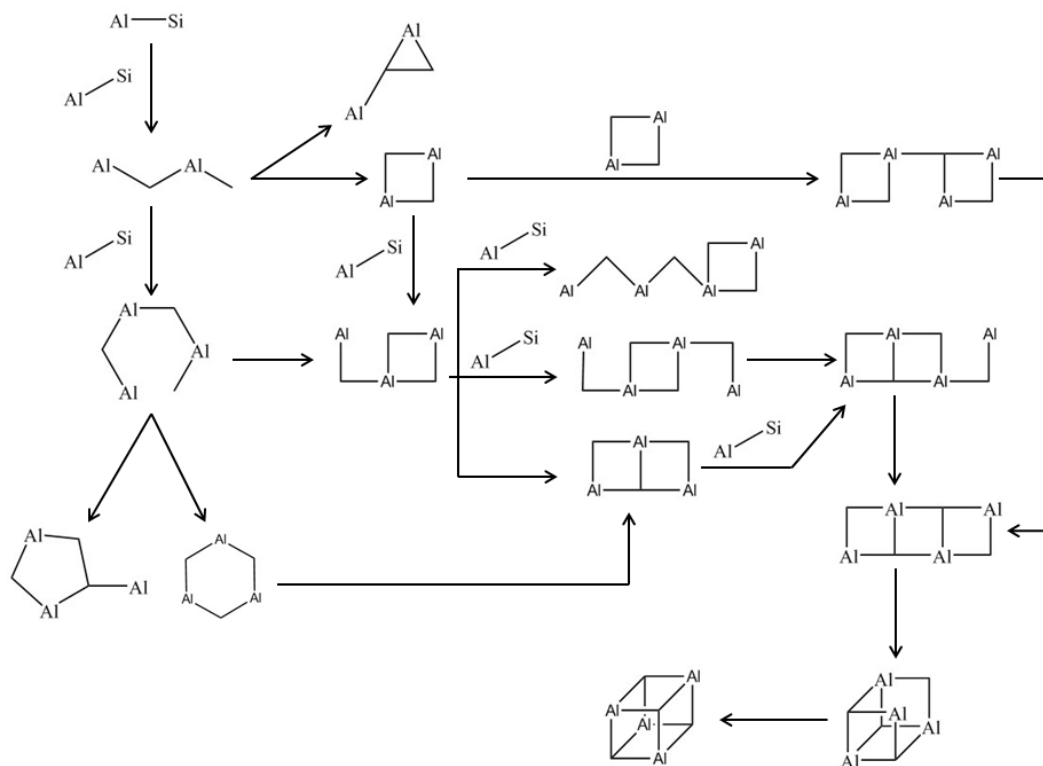


Figure 5.1 Clusters reactions, silicon in each line corner and oxygen in the middle of each line.

The result of this study has two parts. First, the geometric features of the optimised aluminosilicate rings are introduced. Second, we highlight the formation of the double four ring (D4R) that can be predicted in terms of the competing polymerisation and cyclisation reactions in nucleation of zeolites A, with particular emphasis on the change in thermodynamical properties including enthalpy, entropy and Gibbs free energy. In order to clarify general mechanistic aspects of the whole processes, the investigation for the successive condensation reactions can be divided into main two stages: (i) The first linear polymerisation and cyclisation reactions (ii) The subsequent multiple polymerisation and cyclisation reactions. Moreover, we will examine the question whether larger species especially in the multiple rings are formed by the condensation of the dimer or of the larger units (the four rings) in the nucleation stage of zeolite A. The elucidation of these aspects will provide us further insight into the nucleation of this zeolite.

5.3.1 Geometry analysis of the multiple ring structures

As mentioned in chapter 3, the structure of zeolite A contains specific ring units including the four, six, and double four rings and cages. The framework of zeolite A can also be described as the integration of the multiple rings. Most amorphous aluminosilicate gels in solution can lead to formation of multiple rings during the nucleation stage. In addition to the cyclisation reactions, a mechanism for the formation of the multiple rings is determined principally by not only the condensation reaction of rings and small clusters but also that of rings with rings. In chapter 3, we demonstrated reactions of the $\text{Si}(\text{OH})_4$ or $\text{Al}(\text{OH})_4\text{Na}$ monomers or $\text{AlSiO}(\text{OH})_6\text{Na}$ dimer with rings, which is the essential process in the formation of the multiple rings, consequently suggesting the $\text{AlSiO}(\text{OH})_6\text{Na}$ dimer as the simplest model for cluster growth. Hence, due to the presence of the $\text{AlSiO}(\text{OH})_6\text{Na}$ dimer, which restricts the development of the structure of clusters, the formation of various types of the multiple rings has a high probability of having the similar geometric specifications to the prototype of the fused four ring types, which have already found in zeolite A.

Experiments have been reported suggesting that under the nucleation stage of zeolite A, the four ring species are considered as the main and starting reactions in solution. Hence, the four ring is taken as the starting point and the selected multiple rings regarding the bi-four ring, bi-four ring with one dimer, tri-four ring, four-four ring and open double four ring are proposed as representative of modelling the progress in forming the double four ring, as shown in Figures 5.2 and 5.3. Here, the first multiple ring discussed is the bi-four ring, which can arise from two different routes: the internal condensation of the four ring with one dimer and of the six ring. It is worthy of note that the optimised geometry of the structure of the bi-four ring is likely to be the curved, not planar structure due to the Na^+ ions that are bound to three more oxygen atoms of the structure.

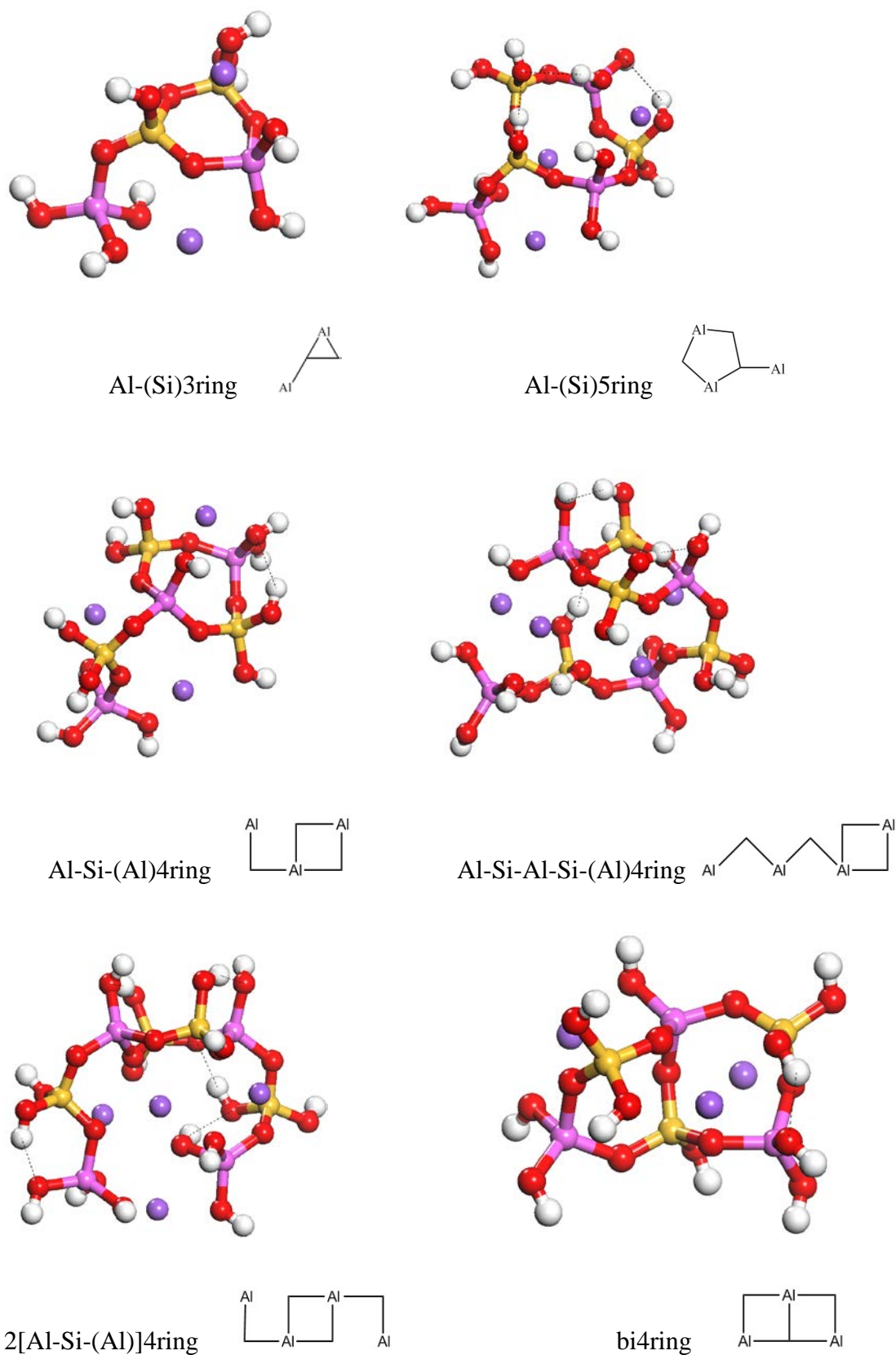


Figure 5.2 Optimised aluminosilicate four ring species. In the abbreviation, “()” indicates the active atom at which the condensation with other species.

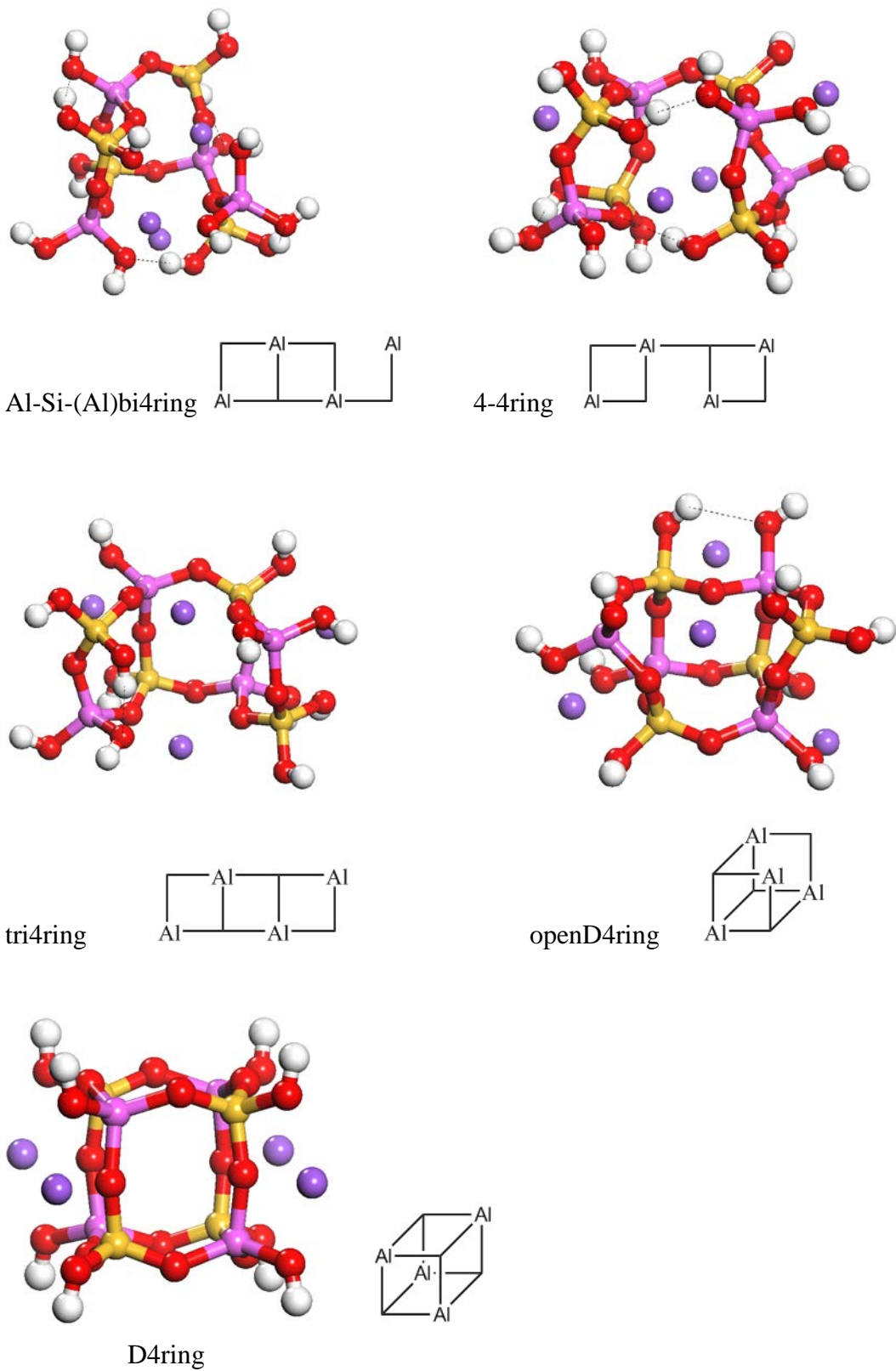


Figure 5.3 Optimised aluminosilicate four ring species.

Note that the bi-four ring owing to its curved structure would be likely to condense itself (by an internal reaction) and then forms the double three ring cage. Indeed, double three rings have been observed in aluminosilicate solution with a range of Si/Al ratios by NMR³, but the double three rings are generally not considered as continuing to the nucleation process. First, any record of the appearance of the double three ring as a building block has not yet been found in aluminosilicate zeolite structures, but the first zeolite structure (ITQ-40: $\text{Ge}_{32.4}\text{Si}_{43.6}\text{O}_{150}(\text{OH})_4$) with the double three ring unit has been successfully synthesized in the Ge/Si zeolite system. Second, the formation of the double three rings would generate the Al-O-Al linkage in its structure hence contradicting Lowenstein's rule. In other words, the strict ordered Si/Al distribution on the structure will restrict the types of multiple rings to be formed. Hence, we suggest that the next step for growth of the bi-four ring, involves the addition of the dimer on the bi-four ring should be a priority, which will favour the formation of the tri-four ring.

For the formation of two types of the tri-four ring, it can be noted that there are two competing side condensation reactions of the bi-four ring with one dimer: one is the chain-shaped (horizontal growth) and the other is the L-shaped (vertical growth). The chain-shaped tri-four ring is more likely to lead to zeolite nucleation because the L-shaped ring is a non-Lowensteinian structure. In addition to the above reactions, as mentioned already, the four ring species is very common in solution. Thus, the tri-four ring (the chain-shaped) could be obtained from the other condensation reaction of the four ring with another four ring, which produces two new Al-O-Si bonds.

As mentioned earlier, due to the electrostatic attraction between the Na^+ ions and four ring structure, the optimised geometry of the tri-four ring (the chain-shaped), as shown in Figure 5.3, is again likely to have the "curved" configuration, which will facilitate the subsequent condensation reactions leading to: (i) the open double four ring that is the key intermediate for the self-assembly of the double four ring (ii) The double four ring that has been supposed as the building unit for crystal growth of zeolite A.

To summarise this section, the geometrical aspects of the multiple rings studied will provide useful insights into the mechanism of self-assembly of the double four ring i.e. the optimised multiple rings are curved, favouring direct condensation reactions into

the double four ring and the formation of the double four ring according to the above analysis can probably be drawn as a simple route: the four ring → the tri-four ring → the double four ring, finally growing the zeolite A crystal. In the next section, on the basis of our preliminary work on the selected rings, we will investigate the detailed mechanism of the whole condensation reactions in forming the double four ring with emphasis on thermodynamic parameters including enthalpy, entropy and Gibbs free energy in order to ascertain which mechanism is favoured.

5.3.2 Polymerisation and cyclisation reactions

In zeolite nucleation, the polymerisation and cyclisation reactions are both essential, which means that the simultaneous occurrence of polymerisation and cyclisation reactions is inevitable. Under this circumstance, the competition between polymerisation and cyclisation reactions will have a large influence on the production of precursors in solution, which can further control the conformational preference of zeolite structures. To our knowledge, the various ring species regarding 4-, 5-, 6-, 8-, 10- and 12- rings are the main constituents of zeolite structures. Hence, it is of vital importance to investigate the competitive position of cyclisation reactions relative to polymerisation reactions in zeolite nucleation. The silicate oligomerisation reactions have been modelled by the DFT method suggesting that the development for the competing reactions of polymerisation and cyclisation reactions of course are primarily dependent on the variation of the silicate species, pH and temperature and the solvent effect.

We now consider the competing reactions of polymerisation and cyclisation reactions regarding aluminosilicate species; the key points highlighted in this work are the role of aluminosilicate species, temperature and the effect of solvent. To begin with, the synthesis is initiated by the condensation reaction of the Si(OH)_4 and Al(OH)_3 monomers and that will produce the $\text{AlSiO(OH)}_6\text{Na}$ dimer, which has been reported to be responsible for the nucleation of zeolite A in chapter 4 as the main trigger in the subsequent reactions. Following the initiation, some reaction processes continue with the step-by-step addition of the $\text{AlSiO(OH)}_6\text{Na}$ dimer; others continue with the addition of large species and the internal reactions. The optimised aluminosilicate clusters and their relationship for our supposed polymerisation and cyclisation pathways have been shown in Figure 5.1.

5.3.3 Polymerisation reactions

5.3.3.1 Dimer

To enter the nucleation process of zeolite A, the dimerisation reactions are the starting reactions; only one of the dimerisation reactions is taken into our consideration, where the $\text{Si}(\text{OH})_4$ monomer first undergoes condensation by the $\text{Al}(\text{OH})_4\text{Na}$ monomer to generate the $\text{AlSiO}(\text{OH})_6\text{Na}$ dimer. The comparison of the dimerisation reactions for three dimers formed has been previously analysed, suggesting that the $\text{AlSiO}(\text{OH})_6\text{Na}$ dimer is more thermodynamically favourable than the other two. In the detailed discussion of the dimerisation reactions or the following polymerisation and cyclisation reactions, the description of the enthalpy and entropy and Gibbs free energy will contribute to a deeper understanding of the relative condensation reactions. The relative energies associated with the relative enthalpy (ΔH), entropy (ΔS) and Gibbs free energy (ΔG) calculated in gas phase and COSMO solvation at 298K and 450K are presented in Table 5.1.

According to the change in the free energy, the $\text{AlSiO}(\text{OH})_6\text{Na}$ dimer has been predicted to be a thermodynamically feasible in the gas phase and COSMO solvation at 298 and 450K in chapter 3. On the basis of its association with the enthalpy and entropy, the analysis of the corresponding enthalpy and entropy of the $\text{AlSiO}(\text{OH})_6\text{Na}$ dimer shows that in the gas phase, the reaction has the large negative enthalpy ($\Delta H = -71$ (298K) and -72 kJmol^{-1} (450K)) and small negative entropy ($T\Delta S = -11$ (298K) and -18 kJmol^{-1} (450K)). On the other hand, compared to the gas phase, in COSMO solvation, the enthalpy is highly reduced to -42 (298K) and -43 kJmol^{-1} (450K) whereas the entropy is slightly increased to -21 (298K) and -20 kJmol^{-1} (450K). Hence, the free energy in the gas phase is 39 (298K) and 31 kJmol^{-1} (450K) higher than in COSMO solvation.

As shown above, the enthalpy change for the $\text{AlSiO}(\text{OH})_6\text{Na}$ dimer is always exothermic in the gas phase and COSMO solvation, with the former being more exothermic, but the latter being less exothermic due to the stabilizing effect of the solvent and of the charge-neutralizing Na^+ ions. Therefore, for the $\text{AlSiO}(\text{OH})_6\text{Na}$ dimer, the exothermicity will favor its spontaneous formation, but the relative entropy must be considered. The entropy change for the $\text{AlSiO}(\text{OH})_6\text{Na}$ dimer is moderately

negative in the gas phase and COSMO solvation, which means that it is unfavourable. However, the entropy contribution to the free energy in the $\text{AlSiO}(\text{OH})_6\text{Na}$ dimer is small in the gas phase, but plays a minor role in COSMO solvation. Moreover, when the $\text{AlSiO}(\text{OH})_6\text{Na}$ dimer is formed, the occurrence of the negative change in the entropy could be attributed to the fact that the stronger electrostatic attraction is generated by the Na^+ ions in the $\text{AlSiO}(\text{OH})_6\text{Na}$ dimer, which probably causes the structural constraint to reduce the degrees of freedom. We note that high temperature slightly increases the negative change in the entropy in the gas phase, but not in COSMO solvation. Such a change seems not to affect the formation of the $\text{AlSiO}(\text{OH})_6\text{Na}$ dimer. In other words, the increased temperature would not facilitate the formation of the $\text{AlSiO}(\text{OH})_6\text{Na}$ dimer.

According to the analysis above, in the dimerisation reaction, the free energy, which is negative (favourable) to form the $\text{AlSiO}(\text{OH})_6\text{Na}$ dimer is the result of the characteristic compensation of the strong favourable enthalpy and small unfavourable entropy contributions; the main parameter determining the ΔG term is the enthalpy. The similar trend can also be observed in the following condensation reaction of large clusters such as tetramer or hexamer.

Table 5.1 Calculated free energy (ΔG , kJmol^{-1}) change, associated with the enthalpy (ΔH) and entropy ($T\Delta S$) change for the formation of dimers in the gas phase and COSMO solvation at 298 and 450K in polymerisations.

Gas phase			ΔE	ΔH	ΔH	$T\Delta S$	$T\Delta S$	ΔG	ΔG
reactants	products		0K	298K	450K	298K	450K	298K	450K
dimerisation									
Al	Si	Al-Si	-73	-71	-72	-11	-18	-60	-54
COSMO sol.									
Al	Si	Al-Si	-44	-42	-43	-21	-20	-21	-23

5.3.3.2 Tetramer

The next polymerisation to be considered is the tetramerisation reaction, as shown in Table 5.2. The main tetramer: the Al-Si-Al-Si tetramer is formed by the condensation reaction of two dimers; the formation of the Al-Si-Al-Si tetramer is crucial due to the fact that it is the direct precursor for the formation of the four ring that is probably the main species involved in for the nucleation of zeolite A.

The formation of the Al-Si-Al-Si tetramer shows the same characteristic as the $\text{AlSiO}(\text{OH})_6\text{Na}$ dimer. It is a thermodynamically feasible process in the gas phase and COSMO solvation. In the gas phase, the Al-Si-Al-Si tetramer formation is connected with the large negative enthalpy of -85 (298K) and -85 kJmol^{-1} (450K) and small negative entropy of -14 (298K) and -21 kJmol^{-1} (450K), giving rise to the large thermodynamical force ($\Delta G = -71$ (298K) and -63 kJ mol^{-1} (450K)). As for t COSMO solvation, the similar situation is found as for the Al-Si-Al-Si tetramer, where the free energy is -34 (298K) and -30 kJmol^{-1} (450K) associated with the moderate negative enthalpy of -41 (298K) and -40 kJmol^{-1} (450K) and smaller entropy of -7 (298K) and -10 kJmol^{-1} (450K).

As with the dimerisation reaction, the enthalpy change for this reaction is negative in the gas phase and COSMO solvation and owing to the effect of solvent, the change in enthalpy in COSMO solvation is greatly reduced by almost a half compared to the gas phase. For the gas phase and COSMO solvation, the higher exothermicity that overcompensates the negative entropy favours the tetramerisation reaction, emphasizing the fact that the enthalpy contribution is particularly important to the free energy in this reaction. Similarly, the negative entropy change produced in the tetramerisation is probably due to the Al-Si-Al-Si tetramer structure being locked by the stronger electrostatic attraction of the Na^+ ions. Moreover, the entropy change has the slight difference between 298 and 450K, while as temperature increases up to 450K, the negative change in the entropy is slightly increased, but will still not inhibit the formation of the Al-Si-Al-Si tetramer. As a result, low temperature has perhaps the most favourable driving force for the tetramerisation reaction.

To summarise this section, the analysis of the calculated free energy of the above polymerisation reactions reveals that the formation of the $\text{AlSiO}(\text{OH})_6\text{Na}$ dimer and Al-Si-Al-Si tetramer is overall an exergonic process and the main factor determining

the favorable ΔG term produced is the enthalpy. Thus, to ascertain the practical feasibility of the formation of the open clusters, which can become the principal pathway to the relevant internal condensation reactions (cyclisations) is an appropriate initial step in the nucleation of zeolite A. In next section, we will consider the hexamerisation reaction and the formation of cyclic clusters from the direct condensation reactions of these open clusters.

Table 5.2 Calculated free energy (ΔG , kJmol^{-1}) change, associated with the enthalpy (ΔH) and entropy ($T\Delta S$) change for the formation of trimers in the gas phase and COSMO solvation at 298 and 450K in polymerisations.

Gas phase			ΔE	ΔH	ΔH	$T\Delta S$	$T\Delta S$	ΔG	ΔG
reactants	products		0K	298K	450K	298K	450K	298K	450K
tetramerisation									
SI-Al	SI-Al	Al-Si-Al-Si	-88	-85	-85	-14	-21	-71	-63
COSMO sol.									
SI-Al	SI-Al	Al-Si-Al-Si	-38	-41	-40	-7	-10	-34	-30

5.3.4 Cyclisation

5.3.4.1 Hexamer, the four ring and three ring with one dangling monomer

We first start with the Al-Si-Al-Si tetramer. Once the Al-Si-Al-Si tetramer forms, it can grow further or condense internally. Here, the internal condensation of the Al-Si-Al-Si tetramer is assisted by its almost circular structure, as mentioned already. Thus, three possible competing condensation reactions can occur involving via the Al-Si-Al-Si tetramer: one is the further polymerisation reaction to produce the Al-Si-Al-Si-Al-Si hexamer and the other two are the intramolecular cyclisations to produce the four ring and the Al-(Si) fused three ring. The Gibb free energy profile for the three condensation reactions is presented in Table 5.3.

Starting with the formation of the Al-Si-Al-Si-Al-Si hexamer, this is formed by the direct condensation reaction of the $\text{AlSiO}(\text{OH})_6\text{Na}$ dimer and Al-Si-Al-Si tetramer. In the hexamerisation reaction, the trend similar to those noted previously

for the $\text{AlSiO}(\text{OH})_6\text{Na}$ dimer and Al-Si-Al-Si tetramer. Particularly important are the observations that the higher enthalpy whose exothermicity favours the forward reaction and smaller negative entropic items due to the loss of the degree of freedom (the electrostatic attraction of the Na^+ ions) can be found in the gas phase and COSMO solvation; the hexamerisation reaction is still exergonic in the gas phase and COSMO solvation, with the former being -41 (298K) and -35 kJmol^{-1} (450K) higher than the latter; again high temperature does not appear to facilitate this reaction thermodynamically and i under low temperature is more favourable.

Table 5.3 Calculated free energy (ΔG , kJmol^{-1}) change, associated with the enthalpy (ΔH) and entropy ($T\Delta S$) change in the gas phase and COSMO solvation at 298 and 450K in polymerisations and cyclisations.

Gas phase		ΔE	ΔH	ΔH	$T\Delta S$	$T\Delta S$	ΔG	ΔG
reactants	products	0K	298K	450K	298K	450K	298K	450K
hexamerisation								
Al-Si-Al-Si	Si-Al Al-Si-Al-Si-Al-Si	-94	-95	-96	-17	-27	-78	-70
4ring cyclisation								
Al-Si-Al-Si	4ring	65	58	57	42	62	16	-5
Al-(Si)3ring cyclisation								
Al-Si-Al-Si	Al-(Si)3ring	67	56	54	44	64	12	-10
COSMO sol.								
hexamerisation								
Al-Si-Al-Si	Al-Si-Al-Si-Al-Si	-71	-67	-68	-30	-33	-37	-35
4ring cyclisation								
Al-Si-Al-Si	4ring	11	9	8	42	56	-33	-48
Al-(Si)3ring cyclisation								
Al-Si-Al-Si	Al-(Si)3ring	18	12	11	42	58	-30	-47

For mechanistic aspects of leading to the basic structural nucleus of zeolite A, the prediction that the formation of the Al-Si-Al-Si-Al-Si hexamer is thermodynamically feasible process is of critical importance because the Al-Si-Al-Si-Al-Si hexamer itself can be directly involved in the relevant intramolecular condensations as the initiator for producing the rings such as the six ring or the three, four, and five rings with

dangling monomers or dimers. The presence of the six ring and the four rings with dangling dimers have more possibility as the building units of zeolite A and these internal condensations from the Al-Si-Al-Si-Al-Si hexamer will be analysed in the following section.

Turning our attention to the cyclisation reactions, the Al-(Si) fused three and four rings are the initial products. We first consider the cyclisation via the Al-Si-Al-Si tetramer which proceeds with the formation of the Al-(Si) fused three ring. In the gas phase, at 298 K, the formation of the Al-(Si) fused three ring is an endergonic process of 12 kJmol^{-1} in the free energy change, associated with the positive enthalpy of 56 kJmol^{-1} and positive entropy of 44 kJmol^{-1} , but at 450 K, it is an exergonic process of -10 kJmol^{-1} with a free energy change at 298 K, associated with a positive enthalpy of 54 kJmol^{-1} and a positive entropy of 64 kJmol^{-1} . Considering now the COSMO solvation, the Al-(Si) fused three ring cyclisation is predicted to be an exergonic process, which is driven by the moderate negative free energy of -30 (298K) and -47 kJmol^{-1} (450K), associated with the smaller enthalpy of 12 (298K) and 11 kJmol^{-1} (450K) and larger positive entropy of 42 (298K) and 58 kJmol^{-1} (450K).

With the observation of the enthalpy change in the Al-(Si) fused three ring cyclisation, we find that the trend in the enthalpy change is in contrast to those for the polymerisation reactions. The change in enthalpy for the gas phase and COSMO solvation is endothermic, which will disfavour the reaction and the occurrence of endothermicity for this reaction that converts the open cluster into the ring could probably be accounted for the generation of ring strain. On the other hand, it can be noted that the enthalpy in COSMO solvation is significantly (-44 (298K) and -43 kJmol^{-1} (450K)) lower than the gas phase due to probably the effect of the solvent that provides the stabilization shell for the reactant and product. As for the entropic item, the entropy change for the Al-(Si) fused three ring cyclisation is largely positive in the gas phase and COSMO solvation; again, the trend in the entropy change contrasts to those for the polymerisation reactions. Moreover, with an increase in temperature, the entropy change becomes more positive; such a change in the entropy will have the significant contribution to the free energy. For example, in the gas phase, the reaction is unfavourable at 298K, but the reaction can be driven at 450K. In other words,

the increase in temperature will have the positive effect on the formation of the Al-(Si) fused three ring. To rationalize the large positive entropy change is due to the fact that the number of particles increases in the reaction.

Consequently, to evaluate the feasibility of the Al-(Si) fused three ring cyclisation, it is particularly important to consider not only that the entropy provides the positive effect on the free energy but also the lower enthalpy induced by the solvation. This indicates the formation of the Al-(Si) fused three ring as being thermodynamically feasible in COSMO solvation. However, if this is the case, there would be a question of whether the Al-(Si) fused three ring can facilitate the nucleation of zeolite A because of the lack of the three ring unit in zeolite A. Hence, this leads us to the consideration that is consistent with the experimental results and analysis of geometry, perhaps the internal condensation of the tetramer to provide the four ring is a more likely process.

Now let us consider the formation of the four ring from the Al-Si-Al-Si tetramer (Table 5.3); this reaction shows the similar trend to those for the Al-(Si) fused three ring in the gas phase and COSMO solvation. In the gas phase, the condensation at 298K is endergonic, inhibited by a thermodynamic force of 16/58/42 $\text{kJmol}^{-1}(\Delta G/\Delta H/T\Delta S)$ whereas the condensation at 450K is slightly exergonic, possibly driven by the thermodynamic force of -5/57/62 $\text{kJmol}^{-1}(\Delta G/\Delta H/T\Delta S)$. However, when the COSMO solvation is employed, the situation is reversed; the production of the four ring is more likely to be a feasible exergonic process, driven by favourable thermodynamic force of -33/9/42 $\text{kJmol}^{-1}(\Delta G/\Delta H/T\Delta S)$ at 298K and -48/8/56 $\text{kJmol}^{-1}(\Delta G/\Delta H/T\Delta S)$ at 450K. Again, this reaction in the gas phase and COSMO solvation has the positive enthalpy change, which is associated with the ring strain and obvious reduction of the positive enthalpy change is found by the treatment of COSMO solvation. In the gas phase and COSMO solvation, the high positive entropy change, which can attributed to an increase of particle numbers is also shown and the increase in the entropy change is directly connected to the increase in temperature. Hence, to do the four ring cyclisation, except of the effect of temperature, the role of the COSMO solvation is more important, which has efficiently lowered the enthalpy penalty from the gas phase, leading to the change in entropy having the significant contribution to the free energy change.

Each of the reactions in the gas phase and COSMO solvation has already been reported in detail. We now consider how the hexamerisation reaction competes with the cyclisation reaction to form the Al-(Si) fused three ring and the four ring. In the gas phase, the formation of the Al-(Si) fused three ring and the four ring do not compete with the hexamerisation reaction; the hexamerisation reaction is the most favourable. This situation will disfavor the cyclisation reaction, especially in the four ring. In other words, the unfavourable cyclisation reaction will hinder the nucleation of zeolite A, because the four ring is the key and basic unit in the framework of zeolite A. The data obtained from the gas phase usually is used as the reference for all the reactions. But, the reactions in COSMO solvation are more significant; and when COSMO solvation is introduced, these two cyclisation reactions become competitive with the hexamerisation reaction. At 298K, the formation of the hexamer is slightly more favourable than the Al-(Si) fused three ring and four ring whereas at 450K, the condensation reactions prefers to form the two ring species rather than continue with the hexamerisation reaction. As a result, changing temperature would result in the change in the relative distribution of rings and hexamer. Of particular note is the very similar free energy of the Al-(Si) fused three ring and the four ring, which means that the Al-(Si) fused three ring cyclisation is as favourable as the four ring cyclisation.

Interestingly, since the framework of zeolite A has no three ring unit and the experimental spectra has no the appearance of the three ring lines, the feasibility of the Al-(Si) fused three ring cyclisation will give rise to this question of what is its role in the nucleation of zeolite A. In other words, given that the Al-(Si) fused three ring really exists in the nucleation process but probably does not involve in the assembly of zeolite A, what is the final fate of this ring? Perhaps due to the formation of the Al-(Si) fused three ring, which encounters the larger ring strain, this will make it unstable, possibly proceeding the further ring-opening polymerisation. Hence, under this assumption, the four ring cyclisation is supposed to be the high possibility leading to the nucleation of zeolite A instead of the Al-(Si) fused three ring cyclisation. this suggestion is also supported by the experimental spectroscopic analysis showing the four ring species are the main initial rings in the nucleation of zeolite A. In addition, to understand how the other relative rings such as the six ring are formed in the nucleation of zeolite A, the Al-Si-Al-Si-Al-Si hexamer representing the alternative precursor for other intramolecular cyclisations is considered in the next section.

5.3.4.2 The six ring, five ring with a dangling monomer and four ring with a dangling dimer

With the Al-Si-Al-Si-Al-Si hexamer formed in the condensation reaction, its intramolecular cyclisation to afford the six ring, five ring with a dangling monomer, the four ring with a dangling dimer or the three ring with monomers/dimer is encountered next, although we do not study all these reactions in this section. The focus here is on the competing formation of the six ring, the Al-(Si) fused five ring, the four ring with a dangling dimer; two of them (the six ring and the four ring with a dangling dimer) are related to the framework of zeolite A. The relative thermodynamic parameters for these cyclisation reactions are shown in Table 5.4.

To begin with the formation of the six ring from the Al-Si-Al-Si-Al-Si hexamer, the six ring cyclisation can be driven by an exergonicity in the gas phase and COSMO solvation ($\Delta G = -12/-32 \text{ kJmol}^{-1}$ (298K/450K) and $\Delta G = -23/-43 \text{ kJmol}^{-1}$ (298K/450K), respectively); the estimated value of the corresponding ΔH is $26/25 \text{ kJmol}^{-1}$ (298K/450K) and $-5/-6 \text{ kJmol}^{-1}$ (298K/450K), respectively and of the corresponding $T\Delta S$ is $38/57 \text{ kJmol}^{-1}$ (298K/450K) and $19/37 \text{ kJmol}^{-1}$ (298K/450K), respectively. According to this data, we find the trend in the enthalpy change is different for the gas phase and COSMO solvation. The moderate positive enthalpy (endothermicity) is found in the gas phase whereas the slightly negative enthalpy (exothermicity) is found in COSMO solvation. Such a change of course shows the more favourable tendency to form the six ring in COSMO solvation. Moreover, the entropy change is always positive in both conditions; high temperature will significantly increase the positive change of the entropy, which has the more positive contribution to the free energy.

The next ring formed is the Al-(Si) fused five ring, which does not appear in the framework of zeolite A. The free energy change has the similar pattern in the gas phase and in COSMO solvation and there is an exergonic process to form this ring. In the gas phase and COSMO solvation, ΔG is predicted to be $-7/-32$ (298/450K) and $-16/-38 \text{ kJmol}^{-1}$ (298/450K), respectively, being associated with ΔH of $42/42$ (298/450K) and $28/28 \text{ kJ mol}^{-1}$ (298/450K), respectively and $T\Delta S$ of $49/74$ (298/450K) and $44/67 \text{ kJmol}^{-1}$ (298/450K), respectively. Following the similar trend to those of previous cyclisation reactions, this cyclisation is also likely to occur at high temperature; the positive enthalpy does not favour this cyclisation reaction, but

the positive entropy is large enough to compensate for the corresponding enthalpy cost.

Table 5.4 Calculated free energy (ΔG , kJmol^{-1}) change, associated with the enthalpy (ΔH) and entropy ($T\Delta S$) change in the gas phase and COSMO solvation at 298 and 450K in polymerisations and cyclisations.

Gas phase		ΔE	ΔH	ΔH	$T\Delta S$	$T\Delta S$	ΔG	ΔG
reactants	products	0K	298K	450K	298K	450K	298K	450K
6ring cyclisation								
Al-Si-Al-Si-Al-Si	6ring	28	26	25	38	57	-12	-32
Al-(Si)5ring cyclisation								
Al-Si-Al-Si-Al-Si	Al-(Si)5ring	46	42	42	49	74	-7	-32
Al-Si-(Al)4ring cyclisation								
Al-Si-Al-Si-Al-Si	Al-Si-(Al)4ring	18	14	15	56	85	-42	-71
COSMO sol.								
6ring cyclisation								
Al-Si-Al-Si-Al-Si	6ring	-3	-5	-6	19	37	-23	-43
Al-(Si)5ring cyclisation								
Al-Si-Al-Si-Al-Si	Al-(Si)5ring	32	28	28	44	67	-16	-38
Al-Si-(Al)4ring cyclisation								
Al-Si-Al-Si-Al-Si	Al-Si-(Al)4ring	8	4	5	77	100	-73	-95

The product leading to the Al-Si-(Al) fused four ring is formed through the intramolecular condensation of the Al-Si-Al-Si-Al-Si hexamer; it is the thermodynamically facile reaction in the gas phase and COSMO solvation. For the gas phase and COSMO solvation, the Al-Si-(Al) fused four ring cyclisation is predicted to be highly exergonic by -42/-71 (298/450K) and -73/-95 kJmol^{-1} (298/450K), respectively and to involve ΔH of 14/15 (298/450K) and 4/5 kJmol^{-1} (298/450K), respectively and $T\Delta S$ of 56/85 (298/450K) and 77/100 kJmol^{-1} (298/450K), respectively. Clearly, the enthalpy contribution to the free energy can be negligible; this cyclisation is entropy-dominated even at room temperature while the entropy has enough driving force to make the Al-Si-(Al) fused four ring proceed.

According to the calculation, the comparison of the three competing reactions shows

that the six ring and Al-(Si) fused five ring cyclisations do not compete with the Al-Si-(Al) fused four ring cyclisation; such a result could result in the low probability for the six ring and Al-(Si) fused five ring and the Al-Si-(Al) fused four ring is predominantly formed. This tendency is in good agreement with the experimental product ratio that the four ring species favour the nucleation of zeolite A. Moreover, it is also worth noting that the direct formation of the six ring from the hexamer has the low probability in the nucleation of zeolite A. How can we explain the existence of the six ring units in the framework of zeolite A? Perhaps the six ring will be produced by other routes such as the condensation of three the four rings that form a larger cluster including the six ring.

Thus overall, we conclude that the four ring species are considered the key to the nucleation of zeolite A. In the latter sections, the reactions take place in all cases through the relative four ring species. Hence, the four ring and the four ring with a dangling dimer are chosen to be the starting structures for the following reactions.

5.3.5 Dimer or the four ring addition to the four ring species

In nucleation of zeolites, the addition of oligomers to rings is commonly considered to be the main reaction (intermediates) in the formation of the multiple rings, which is of key importance in the formation of the zeolite nucleus. In the nucleation of zeolite A, there are two types of cases to be studied. First, the $\text{AlSiO}(\text{OH})_6\text{Na}$ dimer or four ring are added to the four ring; second, one more dimer is added to the four ring with a dangling dimer.

5.3.5.1 The four ring with a dangling dimer and four ring with a dangling four ring

First, in the case of the Al-Si-(Al) fused four ring, the formation of the Al-Si-(Al) fused four ring via the internal condensation of hexamer has been observed. Here the alternative route to form the Al-Si-(Al) fused four ring proceeding through the addition of the $\text{AlSiO}(\text{OH})_6\text{Na}$ dimer to the four ring is considered.

According to Table 5.5, the addition of the $\text{AlSiO}(\text{OH})_6\text{Na}$ dimer to the four ring is a considerably exergonic reaction of $-136/-135 \text{ kJ mol}^{-1}$ (298/450K) in the gas phase and $-76/-82 \text{ kJ mol}^{-1}$ (298/450K) in COSMO solvation. Further inspection of this

reaction reveals that the large negative change in enthalpy is $-139/-138 \text{ kJmol}^{-1}$ (298/450K) in the gas phase and $-72/-71 \text{ kJmol}^{-1}$ (298/450K) in COSMO solvation and the small change in entropy is $-3/-3 \text{ kJmol}^{-1}$ (298/450K) in the gas phase and $4/11 \text{ kJmol}^{-1}$ (298K/450K) in COSMO solvation. Such a finding shows the similar behaviour to the addition of the $\text{AlSiO}(\text{OH})_6\text{Na}$ dimer to the other $\text{AlSiO}(\text{OH})_6\text{Na}$ dimer to form the Al-Si-Al-Si tetramer as shown in section 5.3.3.2. In the presence of the COSMO solvation, enthalpy is reduced significantly, but nonetheless the reaction is still enthalpy-dominated. In contrast, the entropy according to the inclusion of COSMO solvation is reversed, which probably be confirmed by the disordered structure.

In this chapter, there have been several reactions of the dimer adding to form the tetramer, hexamer and four ring with a dangling dimer. A comparison of these reactions will let us get a better understanding of which reaction involving the dimer addition to open clusters or ring is more energetically feasible. We find that the free energy will favour the Al-Si-(Al) fused four ring cyclisation over the tetramerisation or hexamerisation in the gas phase and COSMO solvation. Hence, in light of the predicted preference for the dimer condensing on the four ring rather than the dimer or tetramer, we suggest that the formation of long chain clusters will be unfavourable in the nucleation process.

Since the four ring is the predominant product in the prenucleation stage there should be the higher probability that four rings condenses with each other. Thus, with the exception of the dimer adding to the four ring, we should pose the question: does the four ring grow by the addition of another four ring? Considering this reaction, the similar trend to the dimer addition to the four ring can be found, with the higher energy release of $-158/-146 \text{ kJmol}^{-1}$ (298/450K) and $-51/-74 \text{ kJmol}^{-1}$ (298/450K) in the gas phase and COSMO solvation. For the formation of the four-four ring, the largely negative enthalpy of $-181/-183 \text{ kJmol}^{-1}$ (298/450K) and $-90/-93 \text{ kJmol}^{-1}$ (298/450K) is predicted in the gas phase and COSMO solvation, which significantly contributes to the free energy. As for the entropy, this is relatively unimportant to the free energy, with the smaller negative value of $-23/-37 \text{ kJ mol}^{-1}$ (298/450K) and $-39/-19 \text{ kJmol}^{-1}$ (298K/450K) in the gas phase and COSMO solvation. Additionally, in contrast to the dimer condensing onto the dimer or tetramer in COSMO solvation,

we find that as the temperature increases, there is the significant increase in exoergicity of the reaction. This discrepancy can be attributed to the reduction of the entropy.

On the comparison between the four ring condensation onto the dimer or four ring, the free energy of the former is more favourable in COSMO solvation, being greater by -25 kJmol^{-1} at 298K and -8 kJmol^{-1} at 450K. Based on this calculation, we assume that the Al-Si-(Al) fused four ring is preferentially taken as the main reactant for the forward condensation reactions. Note that the four-four ring cyclisation leading to further other ring species cannot be beyond consideration since the corresponding free energies do not have significant differences especially at high temperatures.

Table 5.5 Calculated free energy (ΔG , kJmol^{-1}) change, associated with the enthalpy (ΔH) and entropy ($T\Delta S$) change in the gas phase and COSMO solvation at 298 and 450K in polymerisations and cyclisations.

Gas phase			ΔE	ΔH	ΔH	$T\Delta S$	$T\Delta S$	ΔG	ΔG
reactants	products		0K	298K	450K	298K	450K	298K	450K
Al-Si-(Al)4ring polymerisation									
4ring	SI-Al	Al-Si-(Al)4ring	-141	-139	-138	-3	-3	-136	-135
4-4ring polymerisation									
4ring	4ring	4-4ring	-186	-181	-183	-23	-37	-158	-146
COSMO sol.									
Al-Si-(Al)4ring polymerisation									
4ring	SI-Al	Al-Si-(Al)4ring	-73	-72	-71	4	11	-76	-82
4-4ring polymerisation									
4ring	4ring	4-4ring	-95	-90	-93	-39	-19	-51	-74

5.3.5.2 The four ring with two dangling dimers and four ring with a dangling tetramer

According to the result in section 5.3.5.1, since the Al-Si-(Al) fused four ring is a predominant product, it is, of course, involved in further growth or internal condensation. Let us first concentrate on cluster growth. As with the similar procedure in the previous section, the second dimer condensing with the Al-Si-(Al) fused four ring forms the two[Al-Si-(Al)] fused four ring and Al-Si-Al-Si-(Al) fused four ring.

From the results in Table 5.6, the similar trend in the energetics of forming the two clusters can be observed. Starting with the gas phase, the two[Al-Si-(Al)] fused four ring and Al-Si-Al-Si-(Al) fused four ring are thermodynamically favourable with -65/-49 (298K/450K) and -60/-47 kJmol⁻¹ (298/450K); the very small preference for the reaction occurring in the latter, being only 5/2 kJmol⁻¹ (298/450K) different. The enthalpy change of the two[Al-Si-(Al)]fused four ring and Al-Si-Al-Si-(Al)fused four ring is largely negative, calculated as -95/-96 kJ (298K/450K) and -86/-87 kJmol⁻¹ (298K/450K), which facilitates the reactions thermodynamically. Such a result also echoes the influence of enthalpy on earlier reactions of the dimer adding to the relative clusters.

In contrast to the gas phase, the addition of the dimer on the Al-Si-(Al) fused four ring is unlikely to occur in COSMO solvation; the free energy change is -7/-3 kJmol⁻¹ (298K/450K) for the two[Al-Si-(Al)] fused four ring reaction and 11/10 kJmol⁻¹ (298K/450K) for the Al-Si-Al-Si-(Al) fused four ring, showing the endergonic and marginally exergonic behaviour, respectively. This result can be attributed to the reduction in enthalpy, calculated as -67/-68 (298/450K) and -49/-50 kJmol⁻¹ (298K/450K) and large entropy penalty, calculated as to -60/-65 kJ mol⁻¹ (298/450K) and -60/-60 kJmol⁻¹ (298/450K) for the two[Al-Si-(Al)] fused four ring and Al-Si-Al-Si-(Al) fused four ring, respectively.

Since the addition of the dimer does not appear to facilitate these reactions thermodynamically, we have to consider other alternative pathways or species to carry out the nucleation. One route is through the internal cyclisation of the Al-Si-(Al)

fused four ring to produce the bi-four ring and the other one is through the internal cyclisation of the four-four ring to produce the tri-four ring; these reactions will be studied in the next section.

Table 5.6 Calculated free energy (ΔG , kJmol^{-1}) change, associated with the enthalpy (ΔH) and entropy ($T\Delta S$) change in the gas phase and COSMO solvation at 298 and 450K in polymerisations.

Gas phase		ΔE	ΔH	ΔH	$T\Delta S$	$T\Delta S$	ΔG	ΔG
reactants	products	0K	298K	450K	298K	450K	298K	450K
2[Al-Si-(Al)]4ring polymerisation								
Al-Si-(Al)4ring	SI-Al 2[Al-Si-(Al)]4ring	-98	-95	-96	-30	-47	-65	-49
Al-Si-Al-Si-(Al)4ring polymerisation								
Al-Si-(Al)4ring	SI-Al Al-Si-Al-Si-(Al)4ring	-89	-86	-87	-25	-40	-60	-47
COSMO sol.								
2[Al-Si-(Al)]4ring polymerisation								
Al-Si-(Al)4ring	SI-Al 2[Al-Si-(Al)]4ring	-70	-67	-68	-60	-65	-7	-3
Al-Si-Al-Si-(Al)4ring polymerisation								
Al-Si-(Al)4ring	SI-Al Al-Si-Al-Si-(Al)4ring	-52	-49	-50	-60	-60	11	10

5.3.5.3 The bi-four and tri-four rings

The free energy profile for the formation of the bi-four and tri-four rings is shown in Table 5.7; the intramolecular Si-O-Al bond formation is the step that determines whether the bi-four and tri-four rings are formed. Commencing with the bi-four ring cyclisation, this is thermodynamically unfavoured (endergonic) by 30/12 kJmol^{-1} (298K/450K) in the gas phase and 5 kJmol^{-1} (298K) in COSMO solvation, with the exception of COSMO solvation at 450K being -11 kJmol^{-1} (less exergonic). The thermodynamics unfavourable formation of the bi-four ring is mainly related to the enthalpy penalty with 66/64 (298/450K) and 23/21 kJmol^{-1} (298/450K) in the gas phase and COSMO solvation. Thus, this reaction is unlikely to occur.

It is also worth mentioning that the six ring can further react internally to produce the bi-four ring, the six ring as the reactant leads to the bi-four ring being thermodynamically feasible, with the free energy of 1/-26 kJmol^{-1} (298/450K) and

-44/-63 kJmol⁻¹ (298K/450K) in the gas phase and COSMO solvation, which is the consequence of the significantly positive entropy of production in COSMO solvation. Hence, given that the bi-four ring can be formed in the nucleation of zeolite A, this reaction pathway is preferentially considered. Moreover, such a route corresponds to the experimental result that the four ring species are the main intermediates rather than the six ring species in the nucleation processes.

Considering now the formation of the tri-four ring, there are two condensation routes: one is from the Al-Si-(Al) fused bi-four ring and the other from the four-four ring. We do not consider the internal condensation of the Al-Si-(Al) fused bi-four ring to produce the tri-four ring, as the two[Al-Si-(Al)] fused four ring and bi-four ring, which are the key reactants to produce the Al-Si-(Al) fused bi-four ring have the unfavourable free energy. In Table 5.7 we find that the route of the internal condensation starting from the four-four ring to afford the tri-four ring is feasible thermodynamically especially with COSMO solvation; the free energy change is calculated as 0/-23 (298/450K) and -39/-39 kJmol⁻¹ (298/450K) in the gas phase and COSMO solvation. Clearly, this reaction in COSMO solvation is entropy-driven with the relatively small enthalpy penalty. Thus, the high probability for this internal condensation reaction is expected from these observations. The tri-four ring (via the four-four ring) could be one of the main intermediates to directly participate in the nucleation of zeolite A.

Table 5.7 Calculated free energy (ΔG , kJmol^{-1}) change, associated with the enthalpy (ΔH) and entropy (TAS) change in the gas phase and COSMO solvation at 298 and 450K in cyclisations.

Gas phase		ΔE	ΔH	ΔH	TAS	TAS	ΔG	ΔG
reactants	products	0K	298K	450K	298K	450K	298K	450K
bi4ring cyclisations								
Al-Si-(Al)4ring	bi4ring	71	66	64	35	51	30	12
6ring	bi4ring	61	53	53	53	80	1	-26
Al-Si-(Al)bi4ring formation								
2[Al-Si-(Al)]4ring	Al-Si-(Al)bi4ring	53	45	42	41	58	4	-16
bi4ring	SI-Al Al-Si-(Al)bi4ring	-116	-116	-118	-25	-40	-91	-77
tri4ring cyclisations								
Al-Si-(Al)bi4ring	tri4ring	28	27	28	44	66	-16	-39
4-4ring	tri4ring	51	47	46	47	69	0	-23
COSMO sol.								
bi4ring cyclisations								
Al-Si-(Al)4ring	bi4ring	28	23	21	18	31	5	-11
6ring	bi4ring	39	31	31	76	94	-44	-63
Al-Si-(Al)bi4ring formation								
2[Al-Si-(Al)]4ring	Al-Si-(Al)bi4ring	21	13	10	42	53	-28	-43
bi4ring	SI-Al Al-Si-(Al)bi4ring	-77	-77	-79	-36	-43	-40	-36
tri4ring cyclisations								
Al-Si-(Al)bi4ring	tri4ring	23	22	22	68	84	-46	-62
4-4ring	tri4ring	23	18	17	57	56	-39	-39

5.3.5.4 The open double four and double four ring

The free energy profile for the formation of the open double four and double four rings is shown in Table 5.8.

Since the tri-four ring is formed, its optimised “curved” structure will be expected to make a direct internal condensation into the open double four ring very likely. However, in the gas phase, the thermodynamic penalty for the open double four ring cyclisation is observed, showing the free energy of 21/-3 kJmol^{-1} (298/450K), which is due to high positive change in enthalpy of 67/66 kJmol^{-1} (298/450K). Considering now the effect of the COSMO solvation, the enthalpy of this reaction

decreases by almost half, to 37/36 kJmol⁻¹ (298/450K) and the resulting free energy change is negative, with -12/-32 kJmol⁻¹ (298/450K). This reaction seems more likely to occur at high temperature and can reasonably be extended to the next condensation reaction.

As mentioned in section 5.1 (Introduction), in the nucleation of zeolite A, the double four ring is supposed to be the main and final product that can further participate in crystal growth. Hence, to determine the formation of the double four ring, the final condensation of the open double four ring to give the closed double four ring is crucial.

Table 5.8 Calculated free energy (ΔG , kJmol⁻¹) change, associated with the enthalpy (ΔH) and entropy ($T\Delta S$) change in the gas phase and COSMO solvation at 298 and 450K in cyclisations.

Gas phase		ΔE	ΔH	ΔH	$T\Delta S$	$T\Delta S$	ΔG	ΔG
reactants	products	0K	298K	450K	298K	450K	298K	450K
openD4ring cyclisation								
tri4ring	openD4ring	73	67	66	46	69	21	-3
D4ring cyclisation								
openD4ring	D4ring	77	73	71	39	57	34	14
COSMO sol.								
openD4ring cyclisation								
tri4ring	openD4ring	43	37	36	49	68	-12	-32
D4ring cyclisation								
openD4ring	D4ring	20	16	15	68	78	-52	-63

It is unlikely that the double four ring is formed by the open double four ring in the gas phase; this can be confirmed by a result of the positive free energy of 34/14 kJ mol⁻¹ (298/450K), which is due to an unfavourable enthalpic factor with the value of 73/71 kJmol⁻¹ (298/450K). When compared to the gas phase, this cyclisation reaction in COSMO solvation is predicted to be exergonic by -52/-63 kJmol⁻¹ (298/450K); such a change can be supported by the large entropic contribution of 68/78 kJmol⁻¹ (298K/450K) that effectively compensates for the enthalpy penalty.

To summarise, in the gas phase, the general trend is shown in the condensation reactions; polymerisation reactions are more feasible than cyclisation reactions. Most cyclisation reactions are impractical (endergonic or less exergonic) especially at room temperature (298K), with some exceptions such as the six ring, the Al-Si-(Al) fused four ring and the Al-(Si) fused five ring. Such a free energy change for the polymerisation and cyclisation reactions can be attributed to the enthalpy, which in the former is exothermic and the latter endothermic. Moreover, temperature has the significant effect on the polymerisation and cyclisation reactions; to increase temperature (to 450K) will effectively make most cyclisation reactions more exergonic, but most polymerisation reactions less exergonic.

When considering the COSMO solvation, polymerisation reactions are less favourable whereas cyclisation reactions become feasible (almost all the reactions are exergonic). Although the enthalpy is reduced due to the solvent effect, the trend for the enthalpy change in COSMO solvation is the same as the gas phase; polymerisation reactions are exothermic and cyclisation reactions are endothermic except for the six ring. Again, when raising temperature to 450K, cyclisation reactions become relatively more favourable, but polymerisation reactions become less exergonic except for the four-four ring. Hence, the effect of temperature will influence which reactions or species are likely to proceed or be formed. Moreover, the interesting finding is that even at room temperature, almost all the reactions in COSMO solvation are thermodynamically favoured, which is corresponding to the experimental result of Smaihi et al.¹³ and Mintova et al.⁸ that synthesizing zeolite A is practical at room temperature.

5.4 Conclusion

In this chapter, the comprehensive computational investigation for the nucleation of zeolite A is presented by means of the DFT/COSMO calculation although the mechanistic scenario is rather complex. To establish the possible nucleation mechanism of zeolite A, we examined and compared the free energy profile for most competitive condensation reactions of polymerisation and cyclisation reactions that are related to the nucleation mechanism. On the basis of our energetic analysis, the highlights of this work can be summarised as below.

(i) Compared with polymerisation reactions, the COSMO solvation is very important in providing the favorable thermodynamic driving force for cyclisation reactions, which means that cyclisation will become competitive with polymerisation reactions. (ii) Enthalpy is the main driving force for polymerisation reactions although the effect of the COSMO solvation reduce the enthalpy change (iii) Entropy is the main driving force for cyclisation reactions. (iv) The formation of longer chain clusters, in COSMO solvation, will be less likely than that of rings. (v) Some condensation reactions are sensitive to temperature for controlling selectivity. (vi) At room temperature, most condensation reactions can proceed successfully, corresponding to the experimental results. (vii) Finally, according to the relative energies of these condensation reactions determined from the COSMO solvation, it can be concluded that the fundamental mechanism of the nucleation of zeolite A is via dimer \rightarrow tetramer \rightarrow the four ring \rightarrow the four-four ring \rightarrow the tri-four ring \rightarrow the open double four ring \rightarrow the double four ring as shown in Figure 5.4. The mechanistic scenario shows the similar behaviour to the experimental results that the four ring species dominate the nucleation of zeolite A.

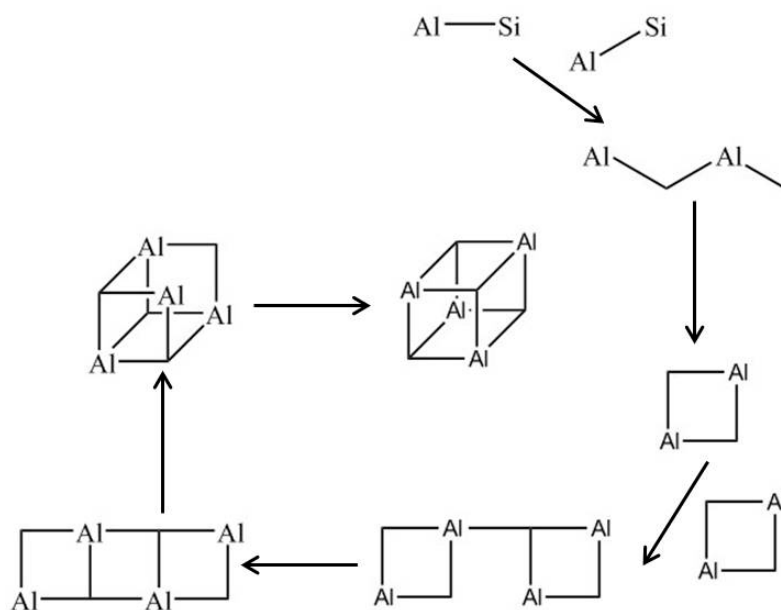


Figure 5.4 A proposed nucleation mechanism for the formation of the double four ring.

References:

1. J. Ciric, *Journal of Colloid and Interface Science* **1968**, 28, 315.
2. J. M. Shi, M. W. Anderson and S. W. Carr, *Chemistry of Materials* **1996**, 8, 369.
3. C. S. Cundy and P. A. Cox, *Microporous and Mesoporous Materials*, **2005**, 82, 1.
4. A. Depla, E. Verheyen, A. Veyfeyken, E. Gobechiya, T. Hartmann, R. Schaefer, J. A. Martens and C. E. A. Kirschhock, *Physical Chemistry Chemical Physics* **2011**, 13, 13730.
5. L. M. Ren, C. J. Li, F. T. Fan, Q. Guo, D. S. Liang, Z. C. Feng, C. Li, S. G. Li and F. S. Xiao, *Chemistry-a European Journal* **2011**, 17, 6162.
6. J. R. Agger, N. Pervaiz, A. K. Cheetham and M. W. Anderson, *Journal of the American Chemical Society* **1998**, 120, 10754.
7. S. Sugiyama, S. Yamamoto, O. Matsuoka, H. Nozoye, J. Yu, G. Zhu, S. Qiu and T. I, *Microporous and Mesoporous Materials* **1999**, 28, 1.
8. S. Mintova, N. H. Olson, V. Valtchev and T. Bein, *Science*, **1999**, 283, 958.
9. S. Mintova, N. H. Olson and T. Bein, *Angewandte Chemie-International Edition*, **1999**, 38, 3201.
10. Biosym/MSI, *DMol USER GUIDE*, San Diego, **1995**.
11. A. Klamt and G. Schuurmann, *Journal of the Chemical Society-Perkin Transactions 2* **1993**, 799.
12. K. Baldridge and A. Klamt, *Journal of Chemical Physics* **1997**, 106, 6622.
13. M. Smaïhi, O. Barida and V. Valtchev, *European Journal of Inorganic Chemistry* **2003**, 4370.

Chapter 6

Modelling the Polymerisation of Aluminosilicate Clusters in Alkali Media

6.1 Introduction

In the previous chapter, to simplify the complexity in the nucleation and crystal growth of zeolites, we investigated only the relative condensation reactions for non-deprotonated clusters and rings. In analysing the results from chapter 4 and 5, our supposition is that the nucleation mechanism of zeolite A, during which the formation of the $\text{AlSiO}(\text{OH})_6\text{Na}$ dimer can be observed, proceeds by the condensation reactions of each of the four ring species. Aside from the effect of alkalinity, the supposed nucleation mechanism scenario for zeolite A indeed corresponds to the experimental results.

It is a fact, however, that most experimental zeolite syntheses including zeolite A typically occur at high pH media (12.6-14); such an alkaline solution can make the starting raw materials (amorphous solid) rapidly dissolve and consequently form soluble active species as the main source for synthesizing zeolites.¹ Experimentally, there has been considerable effort in controlling the relative ratios of the main participants (Si/Al , H_2O , and OH^-) in order to synthesize various types of zeolites, such as zeolite NaY or faujasite at $\text{pH}=11$ and $\text{pH}=12.3-13.8^2$ respectively and the relationship among Si/Al , H_2O , and OH^- concentrations for several zeolite synthesis compositions is shown in Figure 6.1³. The inspection for Figure 6.1 reveals that to synthesize most zeolites, the range of the OH^-/T ratio is between 0.1 and 0.5 in solution. Thus, the alkaline concentration, with the exception of the relative Si/Al ratio, should be considered in the hydrothermal synthesis of zeolites. Moreover, the OH^-/T ratio for synthesizing most zeolites is 0.5, means that about half of the monomer population should be deprotonated. Thus, at the beginning of the nucleation, the neutral and charged silicates/aluminosilicates would both be present in solution.

In general, under an alkaline condition for synthesizing zeolites, the $\text{Si}(\text{OH})_4$ monomer will be deprotonated to form the singly or doubly deprotonated species⁴. The $\text{Si}(\text{OH})_3\text{O}^-$ and $^-\text{OSi}(\text{OH})_2\text{O}^-$ monomers and two deprotonation reactions are

shown below:

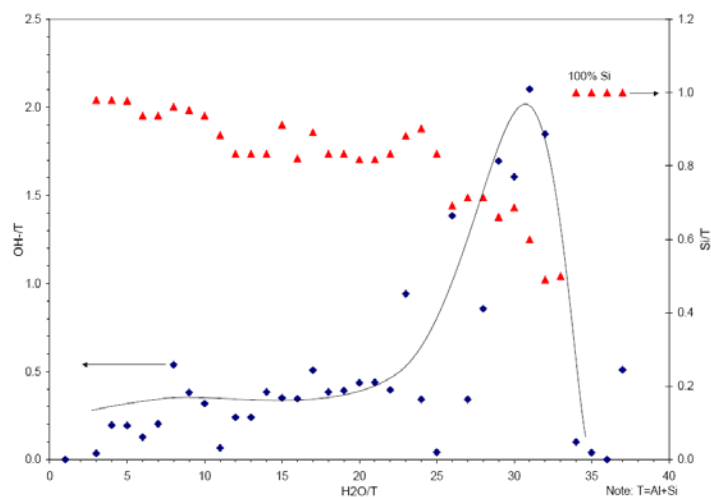


Figure 6.1 The most important participants are shown in each axe in zeolite syntheses. Triangles and diamonds mean the Si/T ratio and the OH^-/T ratio, respectively, where “T” is the sum of Al and Si content. The line is drawn for the OH^-/T ratio^{2,3}.

On the other hand, the Al(OH)_4^- monomer that dominates in the alkaline solution is considered to be involved in the condensation reactions; No evidence has been found that the deprotonated aluminate species such as the $\text{Al(OH)}_3\text{O}_2^-$ monomer exists in high alkaline solution, although other relative aluminate species such as $(\text{OH})_3\text{AlOAl(OH)}_3^{2-}$ or Al(OH)_6^{3-} can be formed at high Al concentration or extreme alkalinity⁴.

As discussed in chapters 4 and 5, the previous theoretical work in simulating polymerisation reactions restricted non-deprotonated open Si/Al clusters and rings to condense with other small species. There is still no well-defined deprotonated model to explain what happened in the condensation reactions under alkali media. Recently, the consideration of the effect of alkalinity (deprotonation) on the modelling of the dimerisation reactions by White et al.⁵ revealed that the $\text{AlSiO(OH)}_6\text{Na}$ dimer would be formed preferentially. However, the effect of alkalinity (deprotonation) on the subsequent condensation reactions regarding other open aluminosilicate clusters as

well as aluminosilicate rings has not yet been studied.

In this chapter, we investigate the relative condensation reactions which proceed through the deprotonated clusters. Following the work in chapter 4, the open Si/Al clusters as well as the deprotonated four rings condensing with the $\text{Si}(\text{OH})_4$, $\text{Si}(\text{OH})_3\text{ONa}$ or $\text{Al}(\text{OH})_4\text{Na}$ monomers and $\text{AlSiO}(\text{OH})_6\text{Na}$ or $\text{AlSiO}_2(\text{OH})_5\text{Na}_2$ dimers are examined by the same method (DFT/COSMO). Our aim is to gain insight into the effect of alkalinity and how it influences on the mechanism of condensation reactions for zeolite syntheses.

6.2 Methodology

In this chapter, the identical approach that discussed in sections 4.2 and 5.2 is employed. We use the DMol³ code⁶ based on density functional theory (DFT) with a double numerical basis set plus polarization (DNP) and the BLYP exchange-correlation functional for all geometry optimisation and total energy calculations (the gas phase) and the solvated clusters with initial gas-phase optimised structures being reoptimised are via the COSMO approach^{7,8}. In the case of deprotonated clusters where the bare oxygen atom bonded on the silicon atom owns the negative charge (-1), the charge is neutralised by adding the sodium counterion. Similarly, the calculation of the Gibbs free energy, which is composed of the zero-point energy and translational, rotational, and vibrational contributions is performed by the standard statistical mechanical methods at 298 and 450K.

6.3 Results and Discussion

In this section, first, we present the result for the deprotonated reactions of the clusters under alkaline conditions, as shown in Tables 6.1 and 6.2. The optimised structures of the deprotonated clusters and their relevant condensation reactions with the Gibbs free energy data are shown in Figures 6.2 and 6.3 and Tables 6.3-6.8. We first describe the geometric features of the relative deprotonated clusters, which are proposed as the main reactants in the condensation reactions. Second, for the mechanisms of the condensation reactions of the deprotonated clusters, there are two components to be examined: (i) Consideration of the formation of different open deprotonated clusters regarding dimers, trimers and tetramers via the $\text{Si}(\text{OH})_4$, $\text{Si}(\text{OH})_3\text{ONa}$ or $\text{Al}(\text{OH})_4\text{Na}$ monomers and $\text{AlSiO}(\text{OH})_6\text{Na}$ or $\text{AlSiO}_2(\text{OH})_5\text{Na}_2$ dimers, the calculated Gibbs free

energy for each condensation reaction is showed in Tables 6.3-6.6. (ii) Consideration of the formation of the deprotonated fused four rings through the condensation reactions of the non-deprotonated/deprotonated four ring and the Si(OH)_4 , $\text{Si(OH)}_3\text{ONa}$ or $\text{Al(OH)}_4\text{Na}$ monomers and $\text{AlSiO(OH)}_6\text{Na}$ or $\text{AlSiO}_2(\text{OH})_5\text{Na}_2$ dimers; the calculated Gibbs free energy for each condensation reaction is showed in Tables 6.7 and 6.8. Mechanisms for the condensation reactions can be given in using the comparison of energetics for these clusters.

6.3.1 Geometric analysis of deprotonated clusters

The detailed description of the geometric parameters for the deprotonated clusters such as bond lengths and angles is not analysed due to the fact that these calculated structures are broadly similar to those for the neutral clusters in chapter 3. All the structures of the deprotonated clusters are the optimised “solvated” clusters as shown in Figures 6.2 and 6.3; the little change in structural geometry is found between the “gas phase” and “solvation” and the inclusion of the additional Na^+ ion is to compensate the negative charge produced of the bare O atom.

In the absence of the proton in each deprotonated cluster, the strong ionic bonds formed between the sodium cation and oxygen anion can be found, resulting in shorter internuclear distance with 2.10-2.20 Å comparable to the non-deprotonated clusters. With respect to the closer anion-cation distance, the presence of the additional Na^+ cation in the deprotonated aluminosilicate clusters would overestimate the calculated binding energies even in COSMO solvation. Such a phenomenon has also been previously shown in the deprotonated silicate clusters. To generate the full description for the “solvated” deprotonated silicate clusters, three explicit water molecules are added to create a solvation shell around the sodium cation and oxygen anion in the deprotonated silicate structures; indeed, such a proper treatment of the “solvated” deprotonated silicate clusters provides the accurate model and value of thermodynamic quantities corresponding to experimental results⁹. However, the complexity of aluminosilicate systems, with the inclusion of several Na^+ ions is computationally expensive and consequently the inclusion of explicit water is not considered in our models. Nevertheless, according to the reliability of the proposed solvation method (the COSMO model without explicit water) used in polymerisation reactions for the deprotonated silicate clusters, this correlation for the deprotonated

aluminosilicate clusters should be acceptable to predict their relative trend in polymerisation reactions.

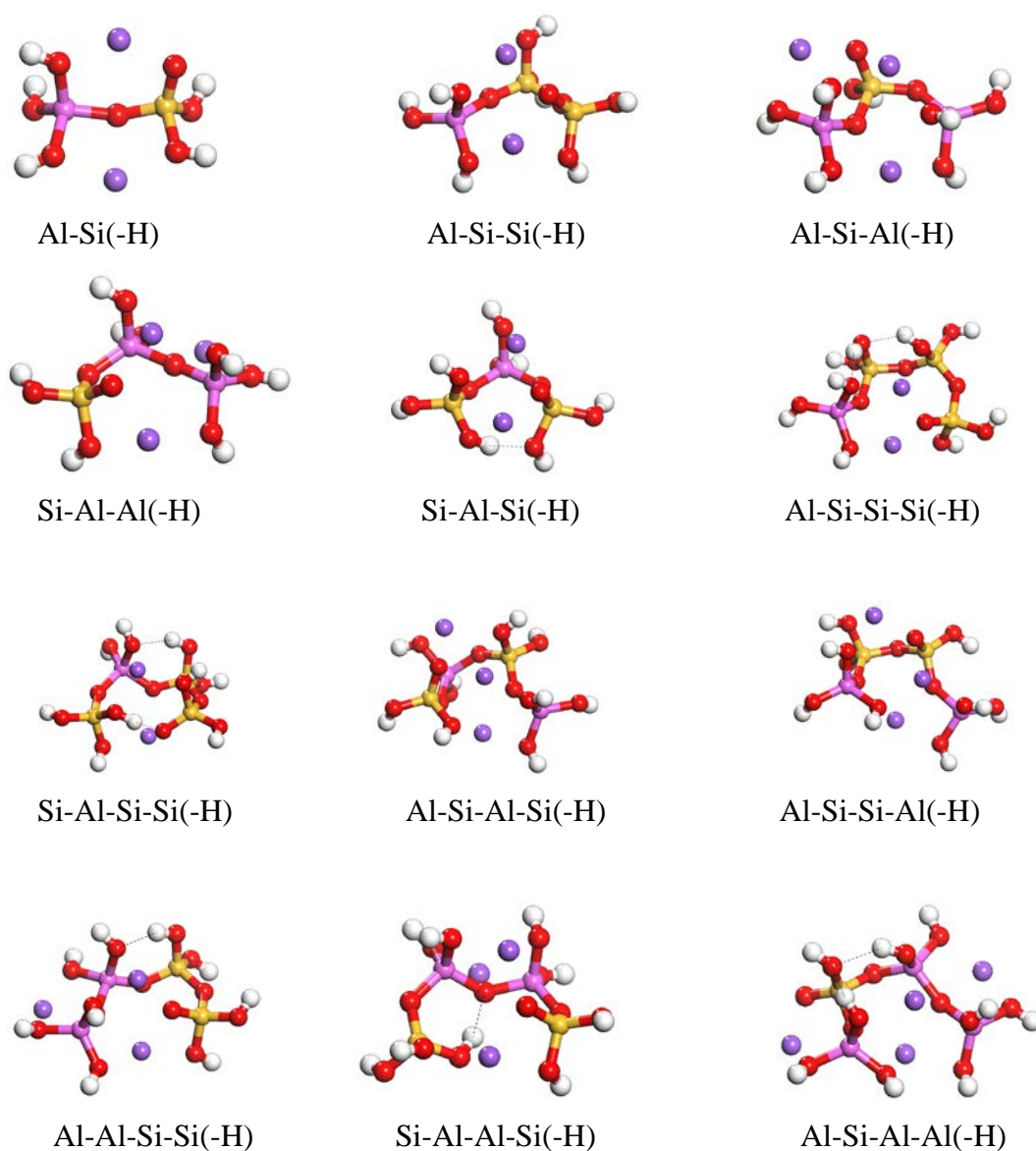


Figure 6.2 Optimised deprotonated aluminosilicate clusters: the open clusters. “(-H)” indicates the singly deprotonated clusters at which the condensation with other species occurs.

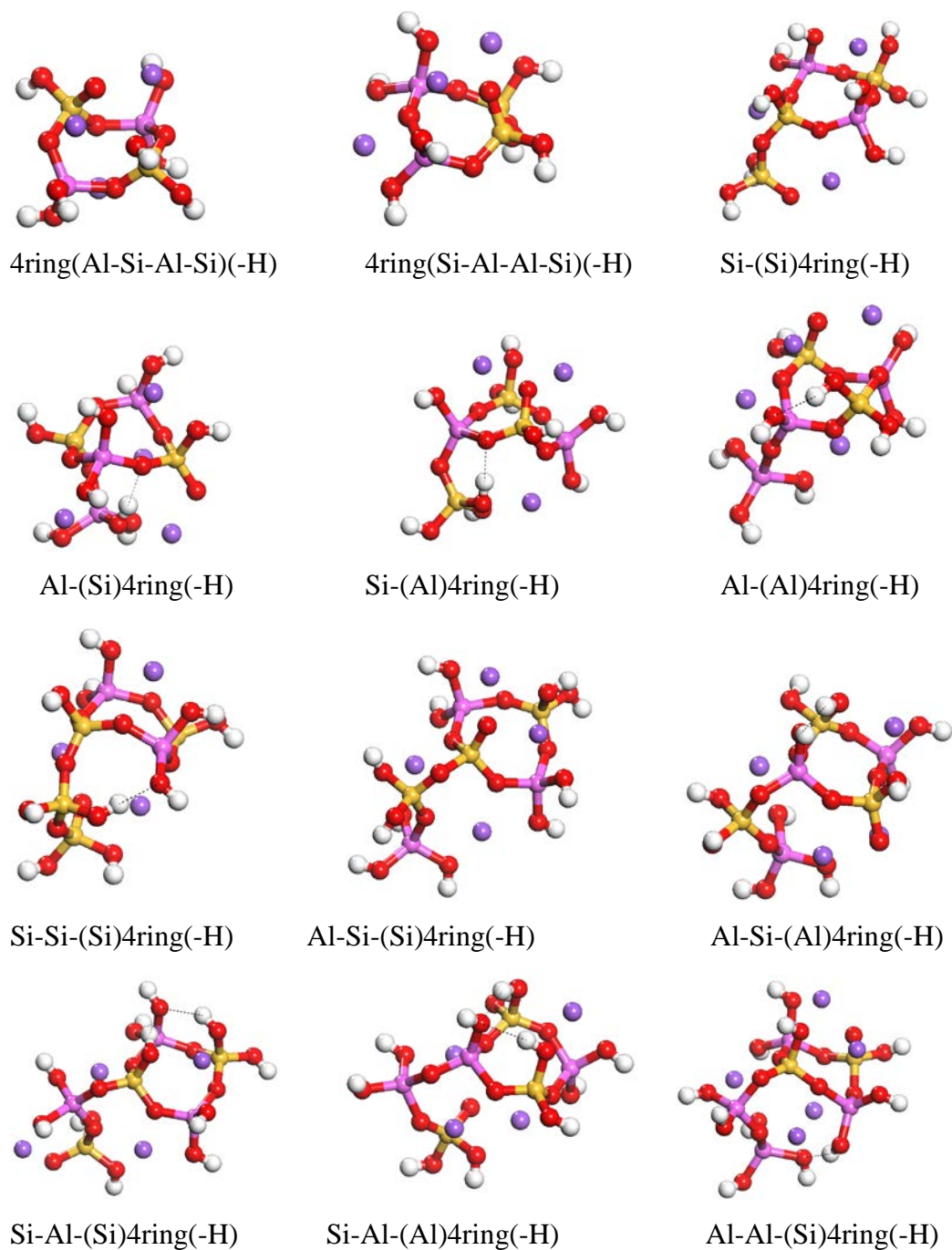


Figure 6.3 Optimised deprotonated aluminosilicate clusters: the four ring species. “(-H)” indicates the singly deprotonated clusters and “()” indicates the active atom at which the condensation with other species occurs.

6.3.2 Deprotonation reactions

As mentioned earlier, silicate or aluminosilicate clusters will be deprotonated to form deprotonated species under alkaline media. Hence, the investigation into energetics of the formation of different deprotonated species via the deprotonation reactions is the basic requirement before analysing the follow-up condensation reactions. The deprotonation energy of a variety of neutral clusters regarding open clusters and four ring species in the gas phase and COSMO solvation are shown in Tables 6.1 and 6.2, where only one proton (H^+ ion) is moved; the non-deprotonated cluster is deprotonated by NaOH and water is produced as the by-product in each deprotonation reaction.

Table 6.1 Calculated free energy (ΔG , kJmol^{-1}) change in the gas phase and COSMO solvation at 298 and 450 K for the deprotonated open clusters. The reaction is $M + OH^- \rightarrow M^- + H_2O$.

reactants		products	Gas		COSMO sol.	
			298K	450K	298K	450K
Si-Al	NaOH	Si-Al(-H)	-137	-120	-61	-52
Si-Si-Al	NaOH	Si-Si-Al(-H)	-185	-183	-58	-71
Si-Al-Si	NaOH	Si-Al-Si(-H)	-131	-126	-39	-48
Si-Al-Al	NaOH	Si-Al-Al(-H)	-191	-188	-86	-96
Al-Si-Al	NaOH	Al-Si-Al(-H)	-117	-109	-34	-38
Al-Si-Al-Si	NaOH	Al-Si-Al-Si(-H)	-182	-184	-83	-98
Al-Si-Al-Al	NaOH	Al-Si-Al-Al(-H)	-102	-97	-30	-34
Si-Al-Si-Si	NaOH	Si-Al-Si-Si(-H)	-191	-185	-124	-127
Si-Si-Si-Al	NaOH	Si-Si-Si-Al(-H)	-195	-188	-84	-92
Al-Si-Si-Al	NaOH	Al-Si-Si-Al(-H)	-159	-158	-77	-85
Si-Si-Al-Al	NaOH	Si-Si-Al-Al(-H)	-197	-195	-99	-109
Si-Al-Al-Si	NaOH	Si-Al-Al-Si(-H)	-205	-203	-109	-119

“(-H)” indicates the singly deprotonated clusters at which the condensation with other species occurs.

Table 6.2 Calculated free energy (ΔG , kJmol^{-1}) change in the gas phase and COSMO solvation at 298 and 450 K for the deprotonated rings. The reaction is $\text{R} + \text{OH}^- \rightarrow \text{R}^- + \text{H}_2\text{O}$.

reactants		products	Gas phase		COSMO sol.	
			298K	450K	298K	450K
4ring	NaOH	4ring(-H)	-168	-165	-56	-67
4ring-(Si)-Si	NaOH	4ring-(Si)-Si(-H)	-191	-189	-93	-103
4ring-(Si)-Al	NaOH	4ring-(Si)-Al(-H)	-119	-116	-42	-49
4ring-(Al)-Al	NaOH	4ring-(Al)-Al(-H)	-160	-157	-53	-63
4ring-(Al)-Si	NaOH	4ring-(Al)-Si(-H)	-158	-154	-62	-71
4ring-(Si)-Si-Si	NaOH	4ring-(Si)-Si-Si(-H)	-203	-203	-105	-117
4ring-(Si)-Si-Al	NaOH	4ring-(Si)-Si-Al(-H)	-147	-146	-60	-70
4ring-(Al)-Si-Al	NaOH	4ring-(Al)-Si-Al(-H)	-135	-126	-36	-40
4ring-(Si)-Si-Al	NaOH	4ring-(Si)-Si-Al(-H)	-147	-146	-60	-70
4ring-(Si)-Al-Si	NaOH	4ring-(Si)-Al-Si(-H)	-168	-163	-89	-95
4ring-(Al)-Al-Si	NaOH	4ring-(Al)-Al-Si(-H)	-191	-187	-79	-89
4ring-(Si)-Al-Al	NaOH	4ring-(Si)-Al-Al(-H)	-126	-115	-42	-43

Considering first the result for the $\text{AlSiO}(\text{OH})_6\text{Na}$ dimer, forming the $\text{AlSiO}_2(\text{OH})_5\text{Na}_2$ dimer in the gas phase, a release of a large amount of free energy is Calculated, with -137 (298K) and -120 kJmol^{-1} (450K). Further analysis of the deprotonation reaction for the $\text{AlSiO}(\text{OH})_6\text{Na}$ dimer in COSMO solvation also shows the negative free energy with -61 kJmol^{-1} at 298 K and -52 kJmol^{-1} at 450K, which still favours this deprotonation reaction, but the solvation deprotonation energy is much less than the gas phase. We find that there is a significant excess of the deprotonation energy for the formation of the $\text{AlSiO}_2(\text{OH})_5\text{Na}_2$ dimer (over > 100 kJmol^{-1}) in the gas phase, which could be accounted for by the shorter Na-O distance associated with the stronger electrostatic interaction. Otherwise, the COSMO solvation can provide the stabilization shell for the deprotonation clusters to lower the electrostatic interaction between the clusters and Na^+ ions, which would be expected to reduce the energy.

The similar situation can be observed in the trimers, tetramers, and four rings (Tables 6.1 and 6.2), where the deprotonation energy calculated for the gas phase has the large negative value, varying from -117 to -191 and -109 to -188 kJmol^{-1} for the trimers, -102 to -205 and -97 to -203 kJmol^{-1} for the tetramers and -126 to -203 and -115 to -203 for the four rings, but for the COSMO solvation has the less negative value, varying from -34 to -86 and -38 to -96 kJmol^{-1} for the trimers, -30 to -124 and -34 to -127 kJmol^{-1} for the tetramers and -36 to -105 and -40 to -117 for the four rings at 298 and 450K, respectively; it is clear that the deprotonation reactions for all clusters will proceed favourably. As expected, the effect of solvation results in the deprotonation energies calculated for the COSMO solvation being much less than that for the gas phase.

Moreover, according to the discussion above, we find the general trend that while the clusters are deprotonated, the larger the cluster size the more the deprotonation reaction is favoured; the order of the energy change decreases: dimer > trimer > tetramer and the four ring > the four ring with a monomer > the four ring with a dimer. In other words, the result mean that which clusters have the relatively high acidity; the order of acidity increases: tetramer > trimer > dimer and the four ring with a dimer > the four ring with a monomer > the four ring. Our conclusion is that the larger clusters will be more acidic (likely be deprotonated by NaOH) than the smaller ones.

6.3.3 Condensation reactions of the open deprotonated clusters and four rings

A portion of the prenucleation species as the building units of zeolite has been shown in Figures 6.2 and 6.3. As mentioned above, these open deprotonated clusters and fused four rings can be formed through the condensation reactions, where the Si(OH)_4 , $\text{Si(OH)}_3\text{ONa}$ or $\text{Al(OH)}_4\text{Na}$ monomers as well as the $\text{AlSiO(OH)}_6\text{Na}$ or $\text{AlSiO}_2(\text{OH})_5\text{Na}_2$ dimers condense with each other or condense on the four rings. As with chapter 4, the quest for understanding the nucleation mechanism of zeolite will be answered by comparing the above different condensation reactions in this section.

6.3.3.1 Condensation reactions of the deprotonated open clusters

The condensation energy of open deprotonated clusters regarding dimers, trimers, and tetramers is summarised in Tables 6.3-6.6. For comparison, we give the result from the previous condensation reactions involving non-deprotonated clusters.

6.3.3.1.1 Dimerisation reactions

Considering now the “gas phase” and “solvated” alkaline condition, where the dominant singly deprotonated species -the $\text{Si}(\text{OH})_3\text{ONa}$ monomer- is formed in the initial stage, similarly, the “gas phase” deprotonated condensation reactions can provide us supportive evidence, but our interest still emphasizes the “solvated” deprotonated condensation reactions under the typical aqueous media.

Table 6.3 Calculated free energy (ΔG , kJmol^{-1}) change in the gas phase and COSMO solvation at 298 and 450 K for polymerisations via deprotonated clusters.

reactants		products	Gas		COSMO sol.	
			298K	450K	298K	450K
dimerisations						
Al	Si	Si-Al	-60	-54	-21	-23
Al	Al	Al-Al	-106	-100	-16	-18
Si(-H)	Al	Si-Al(-H)	-105	-85	-42	-26
Si(-H)	Si	Si-Si(-H)	-35	-31	-16	-15

Let us first focus on the dimerisation reactions. As can be seen in Table 6.3, even under alkaline conditions, the condensation reaction of two $\text{Al}(\text{OH})_4\text{Na}$ monomers to form the $\text{Al}_2\text{O}(\text{OH})_6\text{Na}_2$ dimer is highly favoured in the gas phase, with the free energy of -106 kJmol^{-1} and -100 kJmol^{-1} at 298 and 450K, respectively, which can be attributed to the stronger electrostatic interaction between the cluster and Na^+ ions, which can stabilize its structure. However, when the COSMO solvation is introduced in dimerisation reactions, the condensation reaction of the $\text{Si}(\text{OH})_3\text{ONa}$ and $\text{Al}(\text{OH})_4\text{Na}$ monomers to form the $\text{AlSiO}_2(\text{OH})_5\text{Na}_2$ dimer is more favoured than others, calculated at -42 kJmol^{-1} and -26 kJmol^{-1} at 298 and 450K respectively. Such a result for the gas phase and COSMO solvation can be attributed to the inclusion of the COSMO solvation reducing the free energy change of these dimerisations, which also

is consistent with the observation of the previous dimerisation reactions of the non-deprotonated clusters. The results indicates that the $\text{AlSiO}_2(\text{OH})_5\text{Na}_2$ dimer is most likely to be formed in dimerisation reactions under alkaline conditions. Thus, the $\text{AlSiO}_2(\text{OH})_5\text{Na}_2$ dimer can be preferentially considered as the starting agent for the subsequent polymerisation reactions, i.e. the trimerisation or tetramerisation reactions. On the other hand, compared with the formation of the $\text{AlSiO}(\text{OH})_6\text{Na}$ dimer under the neutral conditions, an increase in pH (adding a base) makes the formation of the $\text{AlSiO}_2(\text{OH})_5\text{Na}_2$ more favourable, especially at lower reaction temperature.

It is also worth noting that the formation of the $\text{AlSiO}_2(\text{OH})_5\text{Na}_2$ dimer is more favourable at 298K than 450K, indicating that lower operating temperature makes it form more easily. Interestingly, in contrast to the formation of the $\text{AlSiO}_2(\text{OH})_5\text{Na}_2$ dimer, high temperature will facilitate the formation of most larger clusters, as will be apparent in the following section. Thus, our result suggests that experimentally, appropriate tuning of the scale of temperature will assist the different polymerisations to be proceeded.

6.3.3.1.2 Trimerisation reactions

The next polymerisation is the trimerisation reaction, where there are four different singly deprotonated trimers for the Si-Si-Al, Si-Al-Si, Al-Si-Al, and Si-Al-Al trimers to be formed by the condensation reaction of two types of dimers: the $\text{AlSiO}(\text{OH})_6\text{Na}$ and $\text{AlSiO}_2(\text{OH})_5\text{Na}_2$ dimer and three types of monomers: the $\text{Si}(\text{OH})_4$, $\text{Si}(\text{OH})_3\text{ONa}$ and $\text{Al}(\text{OH})_4\text{Na}$ monomers as shown in Table 6.4.

In the gas phase, the condensation reaction of the $\text{Si}(\text{OH})_3\text{ONa}$ monomer and $\text{AlSiO}(\text{OH})_6\text{Na}$ dimer to form the singly deprotonated Si-Si-Al trimer is as highly exergonic as that of the $\text{Al}(\text{OH})_4\text{Na}$ monomer and $\text{AlSiO}_2(\text{OH})_5\text{Na}_2$ dimer to form the singly deprotonated Si-Al-Al trimer; the free energy of the former is -117 and -114 kJmol^{-1} and that of the latter is -109 and -116 kJmol^{-1} at 298 and 450K, respectively. However, the formation of the singly deprotonated Si-Al-Al trimer seems to be unlikely due to the contradiction of Lowenstein's rule. Turning our attention to the trimerisation reactions in COSMO solvation, we find that the free energy apparently reduced by the presence of the COSMO solvation; such behaviour also, in part, changes trimers formed in the condensation reactions. The free energy of the singly

deprotonated “solvated” Si-Al-Al trimer is -16 and -34 kJmol⁻¹ at 298 and 450K, showing the relatively low thermodynamic driving force. Instead, the singly deprotonated Si-Si-Al trimer is more feasible in COSMO solvation; there are two reaction routes to form this trimer: the condensation reactions of the Si(OH)₃ONa monomer and AlSiO(OH)₆Na dimer or that of the Si(OH)₄ monomer and AlSiO₂(OH)₅Na₂ dimer, whose free energy is -51 and -54 kJmol⁻¹ for the former and -31 and -51 kJmol⁻¹ for the latter at 298 and 450K, respectively.

Table 6.4 Calculated free energy (ΔG , kJmol⁻¹) change in the gas phase and COSMO solvation at 298 and 450 K for polymerisations via deprotonated clusters

reactants		products	Gas phase		COSMO sol.	
			298K	450K	298K	450K
trimerisations						
Si(-H)	Si-Al	Si-Si-Al(-H)	-117	-114	-51	-54
Si	Si-Al(-H)	Si-Si-Al(-H)	-73	-84	-31	-51
Si(-H)	Si-Al	Si-Al-Si(-H)	-71	-63	-28	-25
Si	Si-Al(-H)	Si-Al-Si(-H)	-27	-33	-8	-22
Al	Si-Al(-H)	Al-Si-Al(-H)	-92	-99	-21	-38
Al	Si-Al(-H)	Si-Al-Al(-H)	-109	-116	-16	-34
Al	Si-Al(-H)	Al-Si-Al(-H)	-92	-99	-21	-38

Although the singly deprotonated Si-Si-Al trimer can be produced from the above two routes, we note that the energetic difference depends on which cluster is deprotonated. Apparently, when the reactant is the deprotonated Si(OH)₃ONa monomer, this reaction releases more energy. However, this statement can be argued. If we consider the option suggested above that the AlSiO₂(OH)₅Na₂ dimer is dominant, we find that the condensation reaction of the AlSiO₂(OH)₅Na₂ dimer and the Si(OH)₄ monomer is possible, but this reaction to produce the singly deprotonated Si-Si-Al trimer is not the lowest energy pathway. To explain this, the protonic transport may occur between different clusters because of the relative acidity. Thus, the preliminary conclusion is that the singly deprotonated Si-Si-Al trimer is the most thermodynamically favourable product in the trimerisation reactions and the most favoured reaction for the singly deprotonated Si-Si-Al trimer would be that where the Si(OH)₃ONa monomer will be

involved in the condensation reactions.

6.3.3.1.3 Tetramerisation reactions

The deprotonated tetramers which could be formed by the condensation reactions of the deprotonated trimer and monomer or that of two dimers are shown in Tables 6.5 and 6.6.

6.3.3.1.3.1 Condensation reactions of the trimer with the Si(OH)₄, Si(OH)₃ONa or Al(OH)₄Na monomers

The free energy for the deprotonated trimer and monomer to form the deprotonated tetramer is summarised in Table 6.5. Considering first the result for all tetramerisation reactions, all condensation reactions of the trimer and monomer are exergonic in the gas phase and COSMO solvation. Similarly, the inclusion of the COSMO solvation, which stabilizes the deprotonated species, decreases the free energy change in tetramerisation reactions.

In the case of tetramerisation reactions, the singly deprotonated Si-Si-Al trimer, which is the most thermodynamically favourable product in the trimerisation reactions is chosen as the important cluster. Thus, the likely route to form the tetramer could be via the condensation reactions of the singly deprotonated Si-Si-Al trimer (or the non-deprotonated trimer) with the Si(OH)₄, Si(OH)₃ONa or Al(OH)₄Na monomers; the comparison of the free energy of the formation of the singly deprotonated Si-Al-Si-Si, Si-Si-Si-Al, Al-Si-Si-Al, and Si-Si-Al-Al tetramers are shown in Table 6.5.

As discussed above, in the gas phase, the most likely tetramer to be formed is the singly deprotonated Si-Si-Si-Al tetramer which forms from the reaction of the Si-Si-Al trimer and Si(OH)₃ONa monomer, being -121 (298K) and -114 kJmol⁻¹ (450K) more energetically favourable than other routes. However, in COSMO solvation, the singly deprotonated Al-Si-Si-Al tetramer formed from the singly deprotonated Si-Si-Al trimer condensing with Al(OH)₄Na monomer, is the most exergonic reaction with the calculated free energy of -41 and -42 kJmol⁻¹ at 298 and 450K. Such a result for tetramerisation reactions shows the difference from the previous trimerisation reactions: the Al(OH)₄Na monomer contrasts favourably to that of trimerisation reactions.

Table 6.5 Calculated free energy (ΔG , kJmol^{-1}) change in the gas phase and COSMO solvation at 298 and 450 K for polymerisations via deprotonated clusters.

reactants		products	Gas phase		COSMO sol.	
			298K	450K	298K	450K
tetramerisations						
Si	Si-Si-Al(-H)	Si-Al-Si-Si(-H)	-21	-10	-18	-12
Si(-H)	Si-Si-Al	Si-Al-Si-Si(-H)	-114	-103	-35	-34
Si(-H)	Si-Si-Al	Si-Si-Si-Al(-H)	-121	-114	-19	-23
Si	Si-Si-Al(-H)	Si-Si-Si-Al(-H)	-29	-21	-2	-1
Al	Si-Si-Al(-H)	Al-Si-Si-Al(-H)	-101	-95	-41	-42
Al	Si-Si-Al(-H)	Si-Si-Al-Al(-H)	-89	-78	-15	-16

In contrast to the result under neutral conditions that the $\text{Al(OH)}_4\text{Na}$ monomer is favoured over the Si(OH)_4 monomer in condensing with other larger clusters and thus results in the non-Lowensteinian clusters formed (chapter 4), we find that under alkaline conditions, the $\text{Si(OH)}_3\text{ONa}$ monomer in the trimerisation reaction can readily condense with the $\text{AlSiO(OH)}_6\text{Na}$ dimer to produce the singly deprotonated Si-Si-Al trimer. The $\text{Al(OH)}_4\text{Na}$ monomer in the tetramerisation reactions shows the energetic preference to condense with the singly deprotonated Si-Si-Al trimer and the singly deprotonated Al-Si-Si-Al tetramer giving structures that accord with Lowenstein's rule. Interestingly, different monomers are involved in different stages of polymerisation reactions under alkaline conditions. But both the $\text{Si(OH)}_3\text{ONa}$ and $\text{Al(OH)}_4\text{Na}$ monomers are highly reactive species. Since the exact reason for this result is not obvious, the kinetic aspects may be of very importance.

Moreover, as mentioned in chapter 5, the four ring is one of the basic species in the framework of zeolite A. Hence, the analysis of the internal reaction of the singly deprotonated tetramer giving the singly deprotonated four ring structure is necessary. The singly deprotonated Al-Si-Si-Al tetramer preferentially may condense internally to form the singly deprotonated non-Lowensteinian four ring (Table 6.6). The value of the free energy reveals that this internal reaction is unfavourable in the gas phase (42 and 27 kJmol^{-1} at 298 and 450K), but is only slightly unfavourable in COSMO

solvation (2 and -9 kJmol⁻¹ at 298 and 450K). Clearly, it is impossible to form the alternate ordered four ring from the internal reaction of the singly deprotonated Al-Si-Si-Al tetramer, which fails to construct the framework of zeolite A. Thus, considering other routes for the formation of the four ring with the Si/Al alternation is very important.

6.3.3.1.3.2 Condensation reactions of the AlSiO(OH)₆Na and AlSiO₂(OH)₅Na₂ dimers

As has been predicted in chapter 4, under neutral condition, the AlSiO(OH)₆Na dimer is more likely to be involved in condensation reactions and directs the open clusters towards the ring structures such as the four or six rings. Hence, in this section, we again hypothesize that under an alkaline condition, the AlSiO(OH)₆Na dimer condensing with the AlSiO₂(OH)₅Na₂ dimer is a possible route for forming the singly deprotonated tetramers.

Considering now the three singly deprotonated tetramers for which results are presented in Table 6.6, the formation of all are exergonic in the gas phase and COSMO solvation and the reduction of the free energy in COSMO solvation is observed. The result indicates that the most likely tetramer formed in these tetramerisation reactions is the singly deprotonated Al-Si-Al-Si tetramer, being -116 and -128 kJmol⁻¹ at 298 and 450K for the gas phase and -57 and -75 kJmol⁻¹ at 298 and 450K for COSMO solvation. Obviously, compared with the condensation reaction of a trimer and monomer, it is even more favourable for the dimers to condense and produce the singly deprotonated Al-Si-Al-Si tetramer. Moreover, the internal condensation reaction for the singly deprotonated Al-Si-Al-Si tetramer can itself produce the Lowensteinian four ring in COSMO solvation, with a free energy -6 and -18 kJmol⁻¹ at 298 and 450K. Thus, such a result indicates once again the importance of the Al/Si dimer addition in the prenucleation stage.

In summary, for all cluster types, the alkaline condition can produce the most reactive species, which can be readily involved in the condensation reactions. Moreover, our calculation suggests that increasing temperature seems not to result in the significant change in the free energy in most of the condensation reactions and even at room temperature, the condensation reactions are thermodynamically favoured.

Table 6.6 Calculated free energy (ΔG , kJmol^{-1}) change in the gas phase and COSMO solvation at 298 and 450 K for polymerisations via deprotonated clusters.

reactants		products	Gas		COSMO sol.	
			298K	450K	298K	450K
tetramerisations						
Si-Al	Si-Al(-H)	Si-Al-Al-Si(-H)	-112	-117	-46	-62
Si-Al	Si-Al(-H)	Al-Si-Si-Al(-H)	-113	-124	-51	-70
Si-Al	Si-Al(-H)	Al-Si-Al-Si(-H)	-116	-128	-57	-75
4ring cyclisations						
Al-Si-Si-Al(-H)		4ring(Al-Si-Si-Al(-H))	42	27	2	-9
Al-Si-Al-Si(-H)		4ring(Al-Si-Al-Si(-H))	30	14	-6	-18

6.3.3.2 Condensation reactions of the deprotonated rings

The addition of monomers or dimers to the ring structure is the likely step in forming nuclei of zeolite. In this section, we consider the non-deprotonated/deprotonated four rings condensing with the $\text{Si}(\text{OH})_4$, $\text{Si}(\text{OH})_3\text{ONa}$ and $\text{Al}(\text{OH})_4\text{Na}$ monomers or the $\text{AlSiO}(\text{OH})_6\text{Na}$ and $\text{AlSiO}_2(\text{OH})_5\text{Na}_2$ dimer.

6.3.3.2.1 Condensation reactions of the four ring with the $\text{Si}(\text{OH})_4$, $\text{Si}(\text{OH})_3\text{ONa}$ and $\text{Al}(\text{OH})_4\text{Na}$ monomers

We consider now the adducts of the four rings and three types of monomers. Table 6.7 shows the free energy with respect to the formation of the four fused rings: the singly deprotonated Si-(Si), Al-(Si), Al-(Al), Si-(Al), Si-Si-(Si) and Al-Si-(Si) fused four rings.

Here we can see that in the formation of the singly deprotonated fused four rings, the free energy for each monomer addition on the four ring is always negative in the gas phase and COSMO solvation. Moreover, the free energy change is reduced as usual when the COSMO solvation is included. First, in the gas phase, the four ring condensing with the $\text{Si}(\text{OH})_3\text{ONa}$ monomer is the most favourable condensation with -144 and -141 kJmol^{-1} at 298 and 450K. Similarly, the result for COSMO solvation reveals that the $\text{Si}(\text{OH})_3\text{ONa}$ monomer reacts more favourably with the four ring compared to other monomers, having value of -64 and -69 kJmol^{-1} for the free energy at 298 and 450K. Thus, the singly deprotonated Si-(Si) fused four ring is the

thermodynamically preference over other three fused four rings in the next condensation reaction.

Table 6.7 Calculated free energy (ΔG , kJmol^{-1}) change in the gas phase and COSMO solvation at 298 and 450 K for polymerisations via deprotonated clusters.

reactants		products	Gas phase		COSMO sol.	
			298K	450K	298K	450K
Si(-H)	4ring	Si-(Si)4ring(-H)	-144	-141	-64	-69
Si	4ring(-H)	Si-(Si)4ring(-H)	-69	-66	-49	-50
Al	4ring(-H)	Al-(Si)4ring(-H)	-95	-84	-30	-28
Al	4ring(-H)	Al-(Al)4ring(-H)	-95	-87	-14	-16
Si(-H)	4ring	Si-(Al)4ring(-H)	-120	-112	-37	-39
Si	4ring(-H)	Si-(Al)4ring(-H)	-45	-38	-21	-21
Si(-H)	(Si)-Si4ring	Si-Si-(Si)4ring(-H)	-147	-142	-67	-72
Si	(Si)-Si4ring (-H)	Si-Si-(Si)4ring(-H)	-48	-42	-15	-18
Al	(Si)-Si4ring (-H)	Al-Si-(Si)4ring(-H)	-112	-104	-30	-34

Since the singly deprotonated Si-(Si) fused four ring is most likely to be formed, it is chosen as the starting structure to condense with one more monomer and thus will produce the four ring with a dangling dimer. Thus, we make the energetic comparison for the formation of two types of fused four rings regarding the singly deprotonated Si-Si-(Si) and Al-Si-(Si) fused four rings via three different routes as shown in Table 6.7.

Comparing the energies of three above reactions, the result for the gas phase reveals that the $\text{Si(OH)}_3\text{ONa}$ monomer condensing with the Si-(Si) fused four rings has more energy released, being -147 and -142 kJmol^{-1} at 298 and 450K, which means the singly deprotonated Si-Si-(Si) fused four ring is more readily formed than the singly deprotonated Al-Si-(Si) fused four ring. In the inclusion of the COSMO solvation, the similar behaviour that the condensation reaction of the $\text{Si(OH)}_3\text{ONa}$ monomer and the Si-(Si) fused four ring with the free energy of -67 and -72 kJmol^{-1} at 298 and 450K is favoured over the other two ones (the Si(OH)_4 monomer + the singly deprotonated

Si-(Si) fused four ring and the $\text{Al}(\text{OH})_4\text{Na}$ monomer + the singly deprotonated Si-(Si) fused four ring). However, the result of Table 6.7 reveals that the singly deprotonated Si-(Si) fused four ring is most likely to be formed, but it which involves in further deprotonated condensation reaction is not the lowest energy pathway as it condenses with one more monomer. Probably, the protonic transport (H^+) also occurs on the singly deprotonated Si-(Si) fused four ring.

To conclude this section, we find that the singly deprotonated Si-Si-(Si) fused four ring formed is energetically more probable as the monomers are involved in this condensation reaction, followed by the $\text{Si}(\text{OH})_3\text{ONa}$ and $\text{Si}(\text{OH})_3\text{ONa}$ monomers. However, we recall that Si and Al sites alternate regularly in the framework of zeolite A. If the singly deprotonated Si-Si-(Si) fused four ring is present, it would be unlikely to produce the ordered alternate four ring species. Again, the question of the role of the monomer is raised; the consideration of the condensation reaction of the four ring joining other clusters to form a ordered alternate four ring species is needed.

6.3.3.2.2 Condensation reactions of the four ring and $\text{AlSiO}(\text{OH})_6\text{Na}$ or $\text{AlSiO}_2(\text{OH})_5\text{Na}_2$ dimer

To gain further insight into the role of the Al/Si dimer condensing with the four ring under alkaline conditions, let us now study the free energy of four different singly deprotonated four rings regarding Al-Si-(Al), Al-Si-(Si), Si-Al-(Si) and Si-Al-(Al) fused four rings.

In Table 6.8, we first find that condensation reactions with the $\text{AlSiO}(\text{OH})_6\text{Na}$ or $\text{AlSiO}_2(\text{OH})_5\text{Na}_2$ dimers to produce all the fused four rings are all exergonic in the gas phase and COSMO solvation. Comparing all “gas phase” condensation reactions, the formation of the singly deprotonated Al-Si-(Si) fused four ring by the $\text{AlSiO}_2(\text{OH})_5\text{Na}_2$ dimer and four ring is more energetically favourable, for which the free energy is calculated to be -152 and -161 kJmol^{-1} at 298 and 450K.

Treatment with COSMO solvation in these condensation reactions, temperature results on the significant change in the relative formation and reaction route of the four fused rings. At 298K, the formation of the singly deprotonated Si-Al-(Si) fused four ring is most likely (-62 kJmol^{-1}) when the $\text{AlSiO}(\text{OH})_6\text{Na}$ dimer and the singly deprotonated four ring are considered; but at 450K, the formation of two different

singly deprotonated fused four rings: the Al-Si-(Si) fused and the Si-Al-(Si) fused four rings, which have the same free energy of -76 kJmol^{-1} , are comparatively more feasible via the condensation reaction between the $\text{AlSiO}_2(\text{OH})_5\text{Na}_2$ dimer and the four ring. Additionally, the comparison of the reactions of the monomer or dimer condensing with the four ring shows that the dimer condensing onto the four ring is energetically more probable.

Hence, the importance of the role of the $\text{AlSiO}_2(\text{OH})_5\text{Na}_2$ dimer is emphasized under alkaline conditions; the presence of the singly deprotonated Si-Al-(Si)fused four ring is expected to itself produce the Lowensteinian four ring species. Incidentally, to probe the nucleation mechanism of zeolite A in the different environments, we find that under neutral conditions, the Al-Si-(Al) fused four ring contributes favourably to the formation of Lowensteinian four ring species whereas under alkaline conditions, the singly deprotonated Si-Al-(Si) fused four ring does.

Table 6.8 Calculated free energy (ΔG , kJmol^{-1}) change in the gas phase and COSMO solvation at 298 and 450 K for polymerisations via deprotonated clusters.

reactants		products	Gas		COSMO sol.	
			298K	450K	298K	450K
Si-Al(-H)	4ring	Al-Si-(Al)4ring(-H)	-135	-142	-51	-70
Si-Al	4ring(-H)	Al-Si-(Al)4ring(-H)	-104	-97	-56	-55
Si-Al(-H)	4ring	Al-Si-(Si)4ring(-H)	-152	-161	-53	-76
Si-Al	4ring(-H)	Al-Si-(Si)4ring(-H)	-121	-116	-58	-61
Si-Al(-H)	4ring	Si-Al-(Si)4ring(-H)	-146	-150	-57	-76
Si-Al	4ring(-H)	Si-Al-(Si)4ring(-H)	-115	-105	-62	-61
Si-Al(-H)	4ring	Si-Al-(Al)4ring(-H)	-127	-130	-26	-45
Si-Al	4ring(-H)	Si-Al-(Al)4ring(-H)	-96	-85	-31	-30

6.4 Conclusion

In this chapter, we have presented the study of the formation mechanism of polymers and fused four rings via the addition of monomers or dimers under alkaline conditions. Our main conclusion is as follows:

For polymerisations, in particular the formation of tetramers, the addition of monomers to produce the singly deprotonated Al-Si-Si-Al tetramer is most likely, which, however, would form non-Lowensteinian four ring species. Moreover, when the $\text{AlSiO}_2(\text{OH})_5\text{Na}_2$ dimer is taken as the starting point, the addition of monomers is followed by the $\text{Si}(\text{OH})_3\text{ONa}$ and $\text{Al}(\text{OH})_4\text{Na}$ monomers, which is different from the result for the neutral condition. To make the comparison with the addition of monomer, the addition of dimers, forming the tetramer, shows that the most likely tetramer formed is the singly deprotonated Al-Si-Al-Si tetramer resulting in the construction of the Lowensteinian four ring being more feasible and hence leading to nucleation of zeolite A.

On the other hand, for condensation reactions of the four ring involving in monomers or dimers, in the addition of monomers, to form the singly deprotonated Si-Si-(Si) fused four ring is energetically favourable, followed by the $\text{Si}(\text{OH})_3\text{ONa}$ monomer and one more $\text{Si}(\text{OH})_3\text{ONa}$ monomer. The singly deprotonated Si-Si-(Si) fused four ring, however, has the low probability for forming the ordered alternate four ring species in nucleation reactions. Another possible route is through the addition of the $\text{AlSiO}_2(\text{OH})_5\text{Na}_2$ dimer on the four ring to produce the singly deprotonated Si-Al-(Si) fused four ring as the most probable product, which is more likely to be the intermediate for forming the Lowensteinian four ring species. Thus, this work suggests that the $\text{AlSiO}_2(\text{OH})_5\text{Na}_2$ dimer would play the key role in proceeding the condensation reactions under alkaline conditions.

References:

1. S. Sugiyama, S. Yamamoto, O. Matsuoka, H. Nozoye, J. Yu, G. Zhu, S. Qiu and T. I, *Microporous and Mesoporous Materials* **1999**, 28, 1.
2. H. Robson, *Verified Syntheses of Zeolitic Materials*, 2nd ed., Elsevier-International Zeolite Association, Amsterdam, **2001**.
3. M. J. Mora-Fonz, *The pre-nucleation of zeolites: a theoretical Approach*, UCL PhD thesis, **2006**.
4. T.W. Swaddle, *Coordination Chemistry Reviews*, **2001**, 219, 665.
5. C. E. White; J. L. Provis,; G. J. Kearley; D. P.Riley; J. S. J. van Deventer, *Dalton transactions*. **2011**, 40, 1348.
6. Biosym/MSI, *DMol USER GUIDE*, San Diego, **1995**.
7. A. Klamt and G. Schuurmann, *Journal of the Chemical Society-Perkin Transactions 2* **1993**, 799.
8. K. Baldrige and A. Klamt, *Journal of Chemical Physics* **1997**, 106, 6622.
9. Mora-Fonz, M. J.; Catlow, C. R. A.; Lewis, D. W. *Journal of Physical Chemistry C* **2007**, 111, 18155.

Chapter 7

Conclusion

In this thesis, the extensive computational study of the structural geometries and nucleation mechanisms of aluminosilicate zeolites has been presented. Our work has been composed principally of four topics: (i) The stability and structures of aluminosilicate clusters (ii) The polymerisation of aluminosilicate clusters (iii) The nucleation mechanism of zeolite A (iv) The polymerisation of aluminosilicate clusters in alkali media. The conclusion is summarised as follows.

7.1 Summary

7.1.1 The stability and structures of aluminosilicate clusters

- A series of key aluminosilicate clusters, which contain dimers, trimers, tetramers, pentamers and hexamers; the three, four, five, and six rings; and the atomic ratio between 1 and 6 Si/Al atoms, with regard to both their structures and their relative energies in the gas phase and COSMO solvation have been analysed by Density Functional Theory (DFT) and the Conductor-like Screening Model (COSMO) approach. We find that the factors controlling the formation of these clusters could be attributed to the Si/Al distribution, location of the extra-framework Na^+ ions, and formation of intramolecular hydrogen bonds.
- In the gas phase, Lowensteinian clusters are more stable than non-Lowensteinian clusters, except for dimers, and the energy is inconsistent with Dempsey's rule. Moreover, the most stable clusters calculated have the high structural symmetry.
- With the inclusion of the COSMO solvation, which is important in stabilizing aluminosilicate clusters, all of the most stable clusters follow not only Lowenstein's rule but also Dempsey's rule.

7.1.2 The polymerisations of aluminosilicate clusters

- For condensation reactions forming open clusters/fused rings, the $\text{Al}(\text{OH})_4\text{Na}$ monomer is favored to react with other open clusters/fused rings over the $\text{Si}(\text{OH})_4$ monomer in condensation reactions, but the product formation is inconsistent with Lowenstein's rule. In contrast, the $\text{AlSiO}(\text{OH})_6\text{Na}$ dimer

condensing with open clusters/fused rings shows the energetic preference to produce Lowensteinian clusters, which means the $\text{AlSiO}(\text{OH})_6\text{Na}$ dimer plays as the active role in condensation reactions for the nucleation of aluminosilicate zeolites.

7.1.3 The nucleation mechanism of zeolite A

- The formation of ring species is more likely than that of longer chain clusters under the COSMO solvation, which suggests that there is the tendency to condense internally to form ring species, rather than continuing to form longer chain clusters.
- Enthalpy is the main driving force for polymerisation reactions; entropy is the main driving force for cyclisation reactions.
- Controlling temperature can selectively allow some reaction routes to be proceeded or prevented in condensation reactions.
- The four ring species formed could be the most likely structure in the nucleation of synthesizing zeolite A and its nucleation mechanism could be by the following reaction route: dimer \rightarrow tetramer \rightarrow the four ring \rightarrow the four-four ring \rightarrow the tri-four ring \rightarrow the open double four ring \rightarrow the double four ring.

7.1.4 The polymerisation of aluminosilicate clusters in alkali

media

- The alkaline condition can favourably drive condensation reactions for open clusters and rings species.
- The most likely products regarding the open clusters or the fused rings are formed through the $\text{AlSiO}_2(\text{OH})_5\text{Na}_2$ dimer instead of monomers. Therefore, the $\text{AlSiO}_2(\text{OH})_5\text{Na}_2$ dimer plays the key role in producing aluminosilicates.

7.1.5 Future work

This thesis has shown that, through computational techniques, evidence of detailed geometric and thermodynamic properties of key species and reactions for aluminosilicates can be obtained. Most of these investigations focused on non-deprotonated aluminosilicates. It is a fact however that the formation of zeolites occurs in high pH media. A more detailed study of the deprotonation reactions of aluminosilicates including the doubly deprotonated species has not been discussed. Hence, for understanding better the complete zeolite nucleation, it is necessary to clarify this process.

Furthermore, in areas where the mere thought of thermodynamics would have several limitations in research of the zeolite nucleation, such as the mechanisms and barriers of condensation reactions, introducing kinetics simulation can provide supplementary and clear information to the zeolite nucleation. In general, molecular dynamics (MD) or Monte Carlo methods are essential tools to predict kinetics behaviour of the zeolite nucleation.